2001

Study of the effect of turbulence on the properties of flocculated mud

Manning, Andrew James

A Study of the Effect of Turbulence on the Properties of Flocculated Mud

by

Andrew James Manning

A thesis submitted to the University of Plymouth
in partial fulfilment for the degree of

Doctor of Philosophy

Institute of Marine Studies
Faculty of Science

July 2001

A Study of the Effect of Turbulence on the Properties of Flocculated Mud

by

Andrew James Manning

Abstract

For the successful management of an estuary, an accurate simulation model predicting sediment transport patterns is a necessity. This requires a knowledge of the vertical mass settling flux (MSF), which is the product of the suspended particulate matter (SPM) concentration and the settling velocity (Ws). However the presence of cohesive sediments (i.e. mud) complicates this description due to the ability of mud particles to flocculate into larger aggregates (flocs) which demonstrate faster settling velocities and lower effective densities (ρ_e) than the component cohesive particles. The generation of turbulent shear stress (TSS) within the water column is regarded as having a controlling influence over the structure of floc populations. A poor understanding of cohesive sediment settling fluxes has existed due to the severe lack of coherent in-situ floc and hydrodynamical data.

Spectra of floc size, settling velocity and effective density were recorded at 10-25 minute intervals using the non-intrusive INSSEV (IN-Situ Settling Velocity) instrument, whilst simultaneous high frequency time series of three-dimensional flow velocity (from which turbulent fluctuations and shear stress could be calculated) and SPM concentration were measured by the POST (Profile Of Sediment Transport) system. Both instruments were mounted together on a specially designed bed frame, and all measurement were made in the near-bed region within an Eulerian reference frame. This combined instrumentation rig was successfully deployed within the upper reaches of the Tamar estuary (SW England, 1998) during neap and spring tidal conditions, and the lower reaches of the Gironde estuary (SW France, 1999) during neap tides. These experiments yielded a total of 125 floc samples. Supplementary floc data was obtained from a series of controlled laboratory studies conducted at the University of Plymouth (UK) and the Laboratoire des Ecoulements Geophysiques et Industriels (LEGI) in Grenoble (France). Aspects of the data are available, for model calibration purposes, at the following internet URL: *http://hydrography.ims.plym.ac.uk/cosinus/.*

A qualitative assessment determined that 160 μm provided the optimum segregation point between the sub-populations of macroflocs (> 160 μm) and microflocs (< 160 μm). A parametric multiple regression statistical technique was used to correlate in-situ hydrodynamic and floc data, and in turn produce a conceptual flocculation model ($_{CM}$). Three

primary equations were generated which could calculate: i) macrofloc and ii) microfloc settling velocities ($Ws_{macroCM}$ and $Ws_{microCM}$, both with units mms^{-1}), and iii) the ratio of macrofloc to microfloc suspended particulate matter content ($SPM_{ratioCM}$, units of gl^{-1}):

i. $Ws_{macroCM} = 0.599 + 0.492\ SPM + 9.33\ TSS - 12.8\ TSS^2$ $\quad R^2 = 0.906$

ii. $Ws_{microCM} = 0.17 + 4.15\ TSS - 4.95\ TSS^2$ $\quad R^2 = 0.723$

iii. $SPM_{ratioCM} = 0.671 + 3.4\ SPM - 0.175\ SPM^2$ $\quad R^2 = 0.761$

The inclusion of both turbulent shear stress and SPM concentration as independent variables produced a highly significant R^2 of 0.906 for $Ws_{macroCM}$, and illustrated the importance of both these factors in controlling macrofloc settling velocity which generally ranged between 1-10 mms^{-1}. The macroflocs typically demonstrated ρ_e ranging from 20-90 kgm^{-3}. $Ws_{macroCM}$ displayed a similar relationship to that proposed by Dyer (1989), with an increase in settling velocity at low shear stresses due to flocculation enhanced by shear, and floc disruption at higher stresses for the same concentration; the transition point being a turbulent shear stress of about 0.36 Nm^{-2}. The $Ws_{microCM}$ was more closely correlated with just the TSS. As with the macroflocs, the microfloc settling velocity rose with increasing shear stress until a limiting TSS of ~0.42 Nm^{-2} was reached. At this point the regression model predicted a peak $Ws_{microCM}$ of ~1 mms^{-1}; this was significantly slower than the comparative macroflocs. The higher limiting shear stress for the microflocs can be attributed to their stronger inter-connective bondings, together with their residence time history; this agreed with the findings of Eisma (1986). Conversely, the $SPM_{ratioCM}$ showed a strong interdependency principally with SPM concentration.

To implement the conceptual model equations into mathematical sediment transport simulation models, the three regression expressions were combined to predict mass settling flux rates (MSF_{CM}) with the units of $g.m^{-2}s^{-1}$:

$$MSF_{CM} = \left[1 - \frac{1}{1+SPM_{ratioCM}} \cdot (SPM \cdot Ws_{macroCM})\right] + \left[\frac{1}{1+SPM_{ratioCM}} \cdot (SPM \cdot Ws_{microCM})\right]$$

This type of expression describes the fundamental aspects of estuarine flocs (i.e. their impact on deposition) throughout the continually changing levels of turbulent mixing and concentration levels, as opposed to a formulation which just has floc settling velocity as the dependent variable. The MSF_{CM} expression predicted MSF rates for 110 floc samples from neap and spring tides with a cumulative error of only +0.9%. In comparison, the use of single settling velocity values of 0.5 mms^{-1} and 5 mms^{-1} were both in error by -85.1% and +48.6%, respectively. Representing mean floc settling velocity by: *a)* a simple SPM concentration power-regression relationship, *b)* the Lick et al. (1993), and *c)* the van Leussen (1994) approaches, all under predicted MSF by ~29%.

Contents

List of Figures

List of Tables

List of Plates

Acknowledgements

The completion of this thesis was only possible with the help and assistance of numerous persons. Primarily, I would like to acknowledge the support and encouragement offered throughout this study by my two supervisors: Prof. Keith Dyer and Dr. Tony Bale. I am grateful for Keith's guidance and advice offered during the various aspects of the study, together with the confidence he showed in my abilities, and particularly his insight into the art of writing scientific papers. I learnt a great deal from Tony's experience and expertise in conducting field experiments during the Tamar estuary experimental programme. His comments and the use of the Lasentec P100 particle sizer was very much appreciated, and I thank him for his support.

I owe a great deal to the many people who contributed to the acquisition of the field data. Both Dr. Malcolm Christie and Paul Turner who's assistance in operating the POST system and with the turbulence data was very much appreciated. Peter Ganderton's electrical expertise kept the field study instrumentation functioning at all times, and together with Malcolm and Paul, vitally assisted in both Tamar and Gironde estuary experiments. Keith and Tony both actively kept everything moving during the COSINUS experiments. The input and good humour of my office mate, Dr. Cyril Mallet, was very welcome at all times, particularly during the SWAMGIR1 experiment.

The IMS technical manager Ron Hill is thanked for his co-operation in allowing me to occupy the IMS workshop for six weeks during the construction of the University of Plymouth research pontoon "*R.P. AMAP-1*". The IMS technician Andy Prideaux, together with Andy Willcox (IT undergradute student) both have a special mention, as without their expertise and dedication, *R.P. AMAP-1* would not have been built and launched on time. Thanks also to my mum who showed an artistic flare to the way she painted *R:P. AMAP-1* in "battleship grey". The professionalism of the crews of PML vessels *Tamaris* (Ron and Pete) and *Sepia* (Mike and Tony) is acknowledged for their instrumental participation in the Tamar estuary experiments, plus the towing of the *R.P. AMAP-1* to the Calstock sampling location.

My inclusion in the EC MAST III COSINUS project, introduced me to a very knowledgeable multi-disciplinary scientific group. The workshops gave me a platform to openly discuss my research, and have it constantly examined by my peers. We also

established a constructive collaboration between UOP and Universite Joseph Fourier throughout COSINUS which culminated in a series of laboratory experiments organised by Nicolas Gratiot and Mathieu Mory. I thank Nicolas for his hard work and hospitality in making the laboratory collaboration at LEGI the success it was. I say thank you to my other COSINUS colleagues: Gwyn Lintern, Lucas Merckelbach, Ankie Bruens, Bill Roberts, Han Winterwerp, and Jens Wyrwa, for many interesting discussions (such as those at "Hotel Merckelbach") and exchanges of ideas.

Prof. David Huntley, Prof. Mike Collins, Prof. Jean-Pierre Tastet, Dr. Laurent Masse, Dr. Robert Lafite and Dr. Jean-Marie Jouanneau are all thanked for their assistance during the planning and coordination of the SWAMGIR1 Gironde estuary experiment. The hospitality provided by Bordeaux, Rouen and Southampton during the various SWAMIEE workshops created an excellent working atmosphere. The crew of the CNRS vessel *Cote D'Aquitaine* are also thanked for excellent marine support.

Data acquisition was a key component of this study, and at times instruments needed repairing. I would like to thank both Tony Moon at Custom Camera Designs of Well, Somerset, U.K., and Valeport Limited, Dartmouth, Devon, who both provided excellent repair services, and thus prevented delays in the experimental time schedule.

My doctoral research would not have been possible without the funding from the European Commission projects: COSINUS (contract No. MAS3-CT97-0082) which funded my studentship, together with SWAMIEE, and INTRMUD. I thank the European Commission for the opportunities they have provided me in contributing to the field of estuarine scientific research.

Finally, I would like to give a big thank you to all members of the Coffee Club, my mum, my late father, my brother Jonathan, and aunt Rose who have all provided so much support over the years.

Author's declaration

At no time during the registration for the degree of Doctor of Philosophy has the author been registered for any other university award.

The author was financed primarily by the EC MAST III COSINUS project (under contract No. MAS3-CT97-0082). The COSINUS funding included the financing of the Tamar estuary flocculation experiments (Task B.1), together with biological analyses of suspended particulate matter composition (Task B.2), and the University of Plymouth (UOP) / Universite Joseph Fourier collaborative laboratory experiments (Task C.1.b). The SWAMGIR1 experiment was funded by the EC TMR SWAMIEE project (under contract No. ERBFMRXCT970111). The production of papers 4# and 6# was also partially funded by the EC MAST III INTRMUD project (under contract No. MAS3-CT95-0022).

Regular contributions were made to both COSINUS newsletters, and the main internet site: http://sun-hydr-01.bwk.kuleuven.ac.be/COSINUS/cosinus.html. Also a UOP COSINUS internet home page was regularly maintained: http://hydrography.ims.plym.ac.uk/cosinus/.

Presentations were made at the following workshops and conferences during the period of study:

- Plymouth Environmental Research Council (PERC) 97/98 research seminar series, April 1998, at UOP where paper 6# was presented.
- COSINUS 1st Mid-year Workshop, 27-28 April 1998, Leibnitzhaus, Hannover, Germany.
- COSINUS Pre-September 98 field experiment – Task B group meeting, May 98, UOP.
- COSINUS 1st Annual General Meeting, 3-4 September 1998, LEGI, Grenoble, France.
- SWAMIEE 5th Cohesive Sediment Workshop, 28-29 January 1999, Bordeaux University (BU), France.
- COSINUS 1st Post Tamar estuary experiment – Task B meeting, 2 March 1999, UOP.
- COSINUS 2nd Mid-year Workshop, 18-19 March 1999, Danish Hydraulics Institute, Copenhagen, Denmark.
- SWAMIEE 6th Cohesive Sediment Workshop, May 1999, Southampton Oceanography Centre (SOC).
- COSINUS 2nd Post Tamar estuary experiment – Task B meeting, 9 August 1999, UOP.
- COSINUS 2nd Annual General Meeting, 1-3 September 1999, St. Catherine's College, University of Oxford.
- Seine-Aval Conference, 17-19 November 1999, University of Rouen, France where a poster illustrating preliminary results from the *SWAMGIR1* experiment was presented.
- SWAMIEE 1st Post-SWAMGIR1 experiment workshop, 20 December 1999, BU, France.
- PERC 99/00 research seminar series, 24 February 2000, UOP, where aspects of the COSINUS and SWAMIEE field experiments were presented.
- COSINUS 3rd Mid-year Workshop, 1-3 March 2000, Laboritoire National Hydraulique (LNH), Paris.
- The VII International Conference on the Oceanography of the Golfe De Gascogne, 4-6 April 2000, Biarritz, France. The conference was organised by IFRERMER, and paper 9# was presented, together with a poster.

- SWAMIEE 2nd Mid-year Progress Workshop, 28 April 2000, SOC.
- COSINUS 3rd Post Tamar estuary experiment – Task B meeting, 27 April 2000, UOP.
- COSINUS Final General Meeting, held in conjunction with the 6th International Conference on Cohesive Sediment Transport (INTERCOH 2000), 4-8 September 2000, Delft Hydraulics, Delft, The Netherlands, where paper 7# was presented.

The author contributed to the following publications during the course of this study:

1. Christie, M.C., Dyer, K.R., Turner, P. and Manning, A.J., (2001). *The effects of density gradients upon water column turbulence within a turbidity maximum* (In preparation).
2. Dyer, K.R., Bale, A.J., Christie, M.C., Feates, N., Jones, S. and Manning, A.J., (2001). *The turbidity maximum in a mesotidal estuary, the Tamar estuary, UK. Part I: Dynamics of suspended sediment.* INTERCOH 2000, Delft (accepted and awaiting publication).
3. Dyer, K.R., Bale, A.J., Christie, M.C., Feates, N., Jones, S. and Manning, A.J., (2001). *The turbidity maximum in a mesotidal estuary, the Tamar estuary, UK. Part II: The floc properties.* INTERCOH 2000, Delft (accepted and awaiting publication).
4. Dyer, K.R. and Manning, A.J., (1998). *Observation of the size, settling velocity and effective density of flocs, and their fractal dimensions.* Journal of Sea Research, 41: 87-95.
5. Manning, A.J., (2001). *The design and fabrication of the University of Plymouth research pontoon "R.P. AMAP-1".* Internal Report for Institute of Marine Studies, University of Plymouth (in preparation).
6. Manning, A.J. and Dyer, K.R., (1999). *A laboratory examination of floc characteristics with regard to turbulent shearing.* Marine Geology, 160: 147-170.
7. Manning, A.J. and Dyer, K.R., (2001). *A comparison of floc properties observed during neap and spring tidal conditions.* INTERCOH 2000. Delft (accepted and awaiting publication).
8. Manning, A.J. and Dyer, K.R., (2001). *The quantification of natural mud floc data and their incorporation within mathematical sediment dynamical models* (In preparation).
9. Manning, A.J., Dyer, K.R. and Christie, M.C., (2001). *Properties of macroflocs in the seaward limit of the Gironde estuary.* Proc. VII Colloque International D'Oceanographie Du Golfe De Gascogne, Biarritz, France, 4-6 April 2000 (in press).
10. Manning, A.J. and Fennessy, M.J., (1997). *INSSEV (In Situ Settling Velocity instrument) - 1.3: Operator Manual.* Internal Report for Institute of Marine Studies, University of Plymouth, 25 pp.
11. Mory, M., Gratiot, N., Manning, A.J. and Michallet, H., (2001). *CBS layers in a diffusive turbulence grid oscillation experiment.* INTERCOH 2000, Delft (accepted and awaiting publication).
12. Peterson, O., Vested, H.J., Manning, A.J., Christie, M.C. and Dyer, K.R., (2001). *Numerical modelling of mud transport in the Tamar Estuary.* INTERCOH 2000, Delft (accepted and awaiting publication).

Signed... A. J. Manning.....

Date... 27th July 2001.....

Chapter One:

Introduction

From an oceanographic perspective, estuaries are typically the areas of interaction between fresh and salt water. The most commonly used descriptive definition for an estuary is that given by Cameron and Pritchard (1963). However, Cameron and Pritchard's definition does not take into account the important influence of the tide. A qualitative definition emphasising the tidal effects in an estuary was offered by Dionne (1963) where: "*An estuary is an inlet of the sea, reaching into the river valley as far as the upper limit of tidal rise, usually being divisible into three sectors: a) a marine or lower estuary, in free connection with the open sea; b) a middle estuary, subject to strong salt and freshwater mixing; and c) an upper or fluvial estuary, characterised by fresh water but subject to daily tidal action*". More detailed estuarine definitions have been given by both Dalrymple et al. (1992) and Perillo (1995). However, the best overall definition is given by Dyer (1997); this is a modified version of the Cameron and Pritchard's definition and states: "*An estuary is a semi-enclosed coastal body of water which has a free connection to the open sea, extending into the river as far as the limit of tidal influence, and within which sea water is measurably diluted with fresh water derived from land drainage*".

Estuaries and their surrounding hinterlands have long provided a haven for shipping traffic, commerce, and industrial activities. As economies grow, so the development of estuaries increase. This development can be in the form of: the reclamation of intertidal flats, the construction of port and harbour infra-structure, coastal protection schemes, and increased accessibility. Ecologically, estuaries also represent important natural areas for floral and faunal propagation. This puts estuaries amongst both the most developed and stressed areas in many countries. Thus, the management of an estuary possess many conflicts of interest, and therefore the managing authorities must weigh the various interests and predict the consequences of implemented measures in a continually changing and increasingly complex regime.

Most estuaries are dominated by cohesive sediments (generally referred to as mud), the transport and fate of which plays a major role in most engineering projects. For example, the accumulation of sediment in navigation channels and berths can often result in the need for expensive dredging operations. Similarly, new developments can cause significant

alterations to the sediment transport patterns, so the ability to be able to predict the probable impact on the sedimentational regime is very desirable. Also, these muds have the potential to adsorb pollutants on to the individual particle surfaces (Delo, 1988), so an engineer would require an indication of how contaminants released into an estuary would mix and disperse. From a long term perspective, a report by the Intergovernmental Panel on Climate Change (Houghton et al., 1990) predicted that the mean global sea level will have risen by ~ 0.6-1 m by the end of this century (approximately the year 2100). This would have a profound effect on both the individual tidal regime and turbulence generated, and in turn the sediment dynamics within an estuary.

Predictive mathematical models of cohesive sediment dynamics are necessary for the optimum management of estuarine locations. Recent advancements in computing hardware development and modelling software (including full three-dimensional codes), have made potentially very powerful tools for such a purpose. However, our present understanding of both the complex physical processes and the mathematical description of natural muddy sediments, is still lagging behind the technology.

1.1 State of the art

Both Kirby (1986) and Van Leussen (1991) concluded that a quantitative understanding of the dynamics of the vertical structure of cohesive sediments in suspensions is essential for an accurate estuarine sedimentation model. This requires an understanding of the physical processes related to the transport, erosion and deposition of mud. Figure 1.1 is a conceptual illustration of these processes describing the interrelationship between a homogeneous suspension and a settled cohesive bed. In reality the whole cycle is particularly complicated, because it does not necessarily have to be closed, and processes are interdependent. For instance, settling does not always lead to deposition, i.e. when entrainment dominates, and the sediment then remains in suspension. Similarly, the consolidation processes within the bed are affected by flocculation processes in the water column, and in turn the erosion processes are governed by the consolidation processes and mediated by the biota (Toorman and Berlamont, 1999).

For the purpose of predicting sediment movement, the determination of the various spatial and temporal mass fluxes are of significant importance. Figure 1.2 shows the vertical movement of sediment and the associated vertical mass fluxes, for idealised profiles of concentration and velocity. One particular area which has caused numerous problems, is the

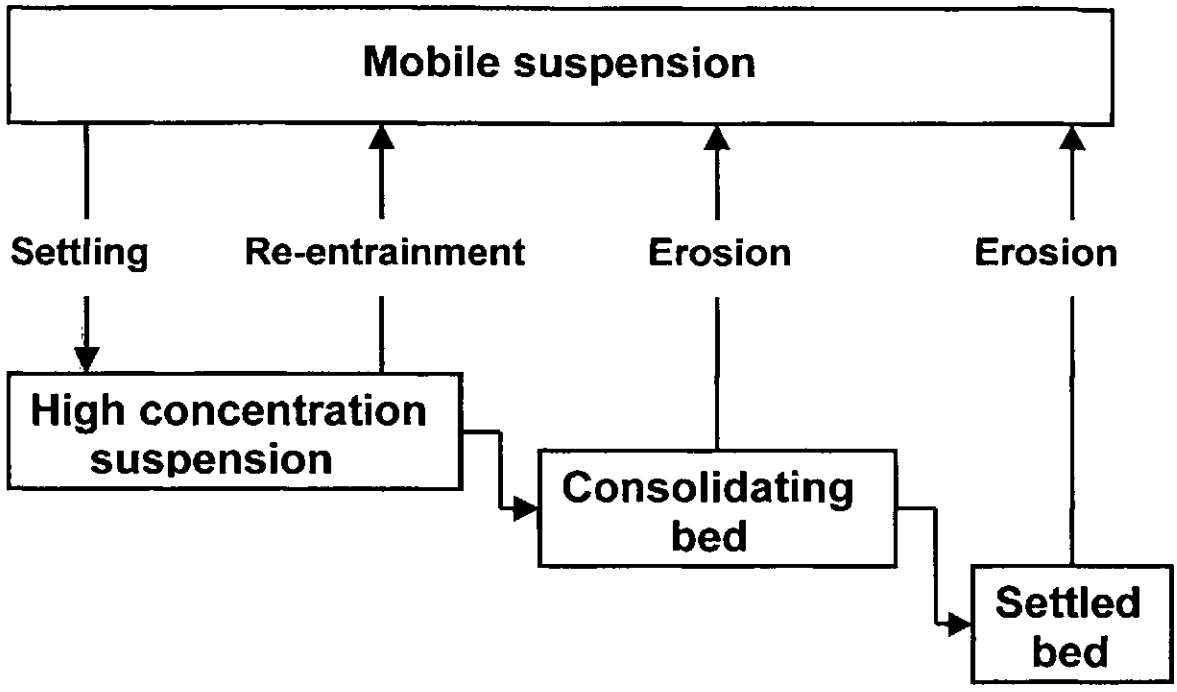

Figure 1.1 The physical states of cohesive sediments in estuarine waters (modified from Parker and Kirby, 1982).

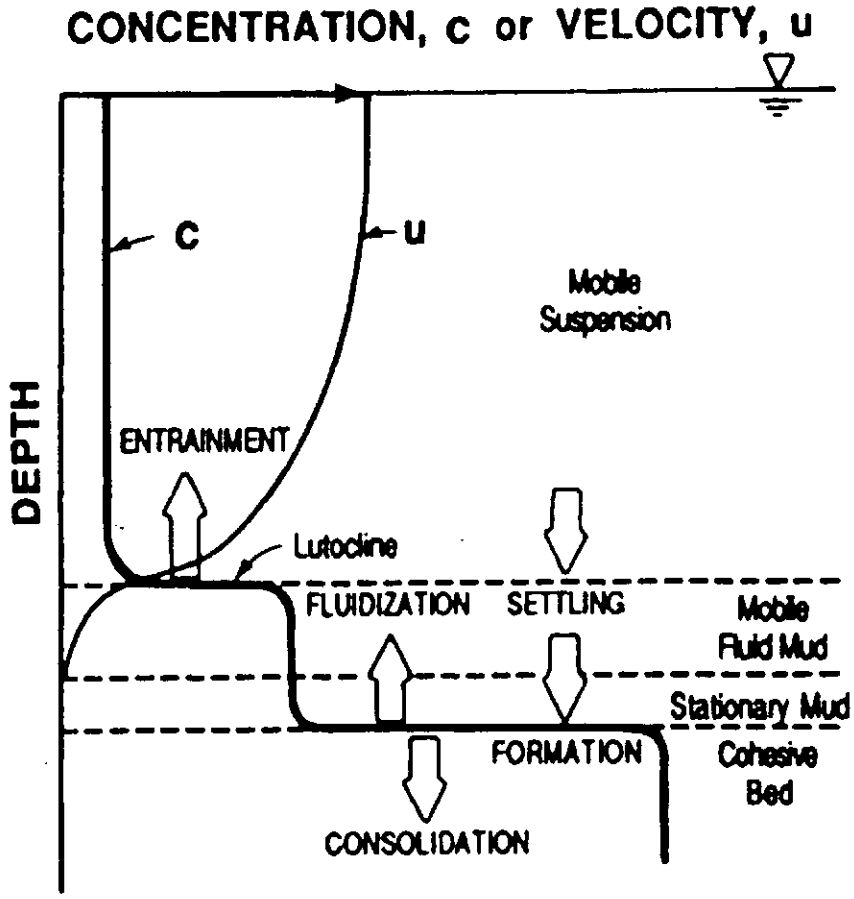

Figure 1.2 Instantaneous vertical concentration and velocity profiles and associated vertical mass fluxes (from Mehta and Dyer, 1990).

modelling and mathematical description of the vertical mass settling flux of sediment, which becomes the depositional flux near to slack water. This is the product of the concentration and the settling velocity. For non-cohesive sediment this is relatively simple as the settling velocity is proportional to the particle size. Whereas muds are also composed partially of different types of biological matter, at various stages of decomposition, and they have the potential to flocculate in to larger aggregates called flocs. These flocs typically demonstrate a lower effective density, but faster settling velocities than the individual cohesive particles. Flocculation is a function of sediment concentration, salinity, mineralogy, chemical composition, organic matter content, and the physical mechanisms which bring the cohesive particles into contact, such as velocity gradients produced in the water column. It is also generally thought that increases in concentration encourage floc growth, however significantly high levels of turbulence which occur during a tidal cycle create disruption and pull the constituent components of a floc apart.

The largest and fastest settling flocs, which tend to contain most of the particulate mass, are very fragile and are easily broken-up upon sampling. This meant that early attempts to accurately sample flocs in-situ with devices such as Owen tubes (Owen, 1976) were not very successful as these instruments were very disruptive, but were better than the laboratory. More studies were devoted to laboratory based analysis, but these were at variance with the Owen tube measurements, being lower in settling velocity, and negate the interrelations which occur in a real estuary. The recent advent of unintrusive in-situ floc sampling devices has provided a tool with which floc size and settling velocities can be measured within a naturally turbulent flow, without causing de-flocculation. Data produced by such sampling devices could provide a much better insight into the interaction of flocs with the turbulent shear stress (generated by the flow) and concentration during the tidal cycle, particularly within the lower layers of the flow where the turbulent shearing is greatest. Site-specific information of floc settling velocity spectra is a prerequisite for accurate process parameterisation for the implementation into modelling applications. There are currently no studies which have quantified these in-situ processes of flocculation, with the specific emphasis of taking effective density variations into account, together with the ambient estuarine conditions of concentration and turbulent shear stress.

1.2 Study objectives

The primary reason for such a poor understanding of cohesive sediment settling fluxes and deposition, is due to the severe lack of information on coherent in-situ floc samples. The

influence of floc density variations are required for accurate settling flux determination. Therefore a key to rectifying this problem is to use a floc sampling system which could directly measure (in-situ) both the simultaneous size and settling velocity of the large fragile estuarine flocs. A similar argument (i.e., the absence of good quality data) can be held for the poor understanding of near bed hydrodynamic processes in an estuary. Existing flocculation relationships are settling velocity against concentration. This needs to be extended to include the effects of shear. For these reasons, the most important objective for this work was the simultaneous collection of high quality floc samples and turbulence and concentration data time series. This required the implementation of two field proven prototype instrumentation systems: INSSEV and POST.

Most of the field study programmes, formed aspects of two major European Commission projects: COSINUS and SWAMIEE, of which the University of Plymouth was a major contributor. The in-situ data, together with newly acquired laboratory data, would be used to assess the trends in flocculation both qualitatively and quantitatively. Time series of hydrodynamical and master variable data would then be used to calibrate mathematical simulation models of cohesive sediment transport. Whilst a newly developed quantitative conceptual flocculation model would be implemented in the parameterisation of mass settling flux for deposition rate prediction.

The main objective of this thesis was to show that turbulent shear stress is an important controlling factor on the process of both in-situ flocculation and disaggregation. This was achieved through the following tasks:

i. To obtain in-situ measurements of floc size, settling velocity, effective density and mass settling flux, together with simultaneous high frequency time series of flow velocity and concentration from two contrasting estuarine locations at different periods of the tidal cycle, and where possible through both spring and neap conditions.

ii. To also obtain comparative floc spectra measurements made from within a controlled laboratory environment.

iii. Define a definitive boundary between the main groups of flocs from the floc data gathered.

iv. To qualitatively assess and compare the general flocculation patterns observed during both the in-situ and laboratory experiments.

v. To produce simple quantitative flocculation expressions from each of the experiments, and use the expressions to identify the relative significance of the different interrelative factors.

vi. To improve the understanding of near bed cohesive sediment flocculation with respect to the changes in the ambient conditions by developing a general quantitative conceptual model which could be integrated into predictive numerical simulation models for sediment transport application.

vii. To test the conceptual model against commonly used modelling parameterisations for flocculation.

1.2.1 EC MAST III COSINUS project

The COSINUS - Prediction of **CO**hesive **S**ediment transport and bed dynamics in estuaries and coastal zones with **I**ntegrated **NU**merical **S**imulation models - project, contributed to the European Commission **MA**rine Science and **T**echnology (MAST) III Research Task B.1.1: Coastal Processes & Morphodynamics. The COSINUS project was coordinated by the Katholieke Universiteit Leuven in Belgium, and the University of Plymouth was a major contractor. The project had a three year duration. COSINUS covered the theoretical, experimental and numerical study of the processes which play a role in flocculation of sediment particles, the interaction between suspended sediment and turbulent flow, the generation of concentrated near bed suspensions (including lutocline formation) and the transition between fluid mud conditions and the formation of the sediment bed (Berlamont and Toorman, 2000).

The main objective of the COSINUS project was to establish well validated physical and mathematical descriptions of the behaviour and fate of concentrated near bed cohesive sediment suspensions and their interaction with the water column and bed. The objectives were met through detailed experimental and theoretical studies on: sediment - turbulence interaction, flocculation, concentrated benthic suspension (CBS) dynamics, and bed dynamics. The findings were parameterised and implemented into current 3-D and 2DH engineering system models. The performance of the improved systems were then assessed.

This thesis contributed to the topic of flocculation (COSINUS Task B). Primarily, a two week long experiment was carried out within the turbidity maximum of the Tamar estuary, UK (COSINUS Task B.1). The collaborative experiment involved participants from: the University of Plymouth (coordinator), Plymouth Marine Laboratory (PML), Hydraulics

Research Wallingford (HR), University of Wales Bangor (UWB), together with observers from Universite Joseph Fourier (Grenoble, France), Katholieke Universiteit Leuven (Belgium), and Universitat Hannover (Germany). The objectives were to quantify the flocculated state of high concentration near bed layers, the size and settling velocity of the flocs, and their relationships to the driving variables. Biological and floc compositional aspects were also examined (COSINUS Task B.2).

To supplement the in-situ results, COSINUS Task C.1.b was concerned with the understanding of the relationship between turbulence and vertical concentration profiles within a controlled laboratory environment. A series of joint experiments was initiated by Universite Joseph Fourier (UJF) and University of Plymouth (UOP), and measurements were made at the Laboratoire des Ecoulements Geophysiques et Industriels (LEGI) in Grenoble, France during July 1999. The UOP made direct measurements of floc size and settling velocity in a laboratory simulated highly concentrated suspension under imposed turbulent shear; these results are also presented in this thesis.

1.2.2 EC TMR SWAMIEE project

The SWAMIEE: Sediment and WAter Movement in Industrialised Estuarine Environments, project was funded by the European Commission Training and Mobility of Researchers (TMR) network scheme for a three year duration from 1998-2000. The main objective of SWAMIEE was in furthering the understanding of water movement and the interaction it has with both cohesive and non-cohesive sediment types, at a variety of time-scales, within specific industrialised and non-industrialised locations. Like COSINUS, SWAMIEE used an interdisciplinary approach which consisted of five separate field experiments, the examination of historical records, and integrated numerical modelling simulations. The contribution reported in this thesis describes the flocculation, suspended concentration and turbulent shear stress results obtained from the first cohesive field experiment, SWAMGIR1, which was undertaken during June 1999 in the lower reaches of the Gironde estuary, France. As well as the University of Plymouth, this experiment included participants from: the University of Bordeaux, University of Oxford, University of Rouen, and the University of Dublin.

1.3 Thesis structure

Chapter 1 introduces the project subject of estuarine cohesive sediment flocculation in turbulent flows, the key limitations in the current knowledge on flocculation, and lists the

study objectives which will improve the understanding of in-situ flocculation. A detailed review of the current literature and theory is provided in Chapter 2. The first two sections of Chapter 3 outline the methodology, instrumentation, and descriptions of the sampling locations for both the Tamar estuary and Gironde estuary field experiment programmes. The remainder of Chapter 3 (sections 3.3 and 3.4) details the protocols used for the UOP laboratory flume experiments, and the collaborative UOP / UJF laboratory experiments conducted at LEGI. The computation techniques used to process the acquired data was presented in Chapter 4. A summary of the various data sets obtained was given in Chapter 5, together with representative figures. The early part of Chapter 6 draws on the experimental results, and points out the most significant patterns demonstrated principally by the floc data. This is followed by a quantitative analysis which identifies significant correlations between the floc, concentration and flow data. Then a new conceptual model for flocculation (developed from the empirical data) is presented, and compared with other floc parameterisations commonly used in numerical sediment transport modelling. Finally, a summary of the main conclusions, and recommended future studies are presented in Chapter 7.

Chapter Two:

Literature Review

The complex ways in which cohesive sediments interact with continually varying hydrodynamic conditions are primary reasons for the current poor level of predictability of sediment movement within estuarine locations. Therefore, in order to put the work conducted for this thesis into context, the following section explains the nature of cohesive sediments. Sections 2.2 and 2.3 review the current research literature on flocculation processes and floc properties, respectively. Estuarine turbulence, with particular emphasis placed on the generation and mathematical representation of current induced turbulent shear stress, is presented in section 2.4. A summary of different flocculation models is given in section 2.5.

2.1 The nature of cohesive sediment

The majority of the particulate matter which accumulates within an estuary is commonly referred to as mud. This mud is typically composed of mineral grains which originate from both fluvial and marine sources, together with biogenic matter - both living and in various stages of decomposition. The underlying mud layers of a mud flat are often dark in colour and emanate a strong odour; this is a result of the anaerobic decomposition of the organic matter. It is the combination of these features that make estuarine muds sticky in nature and for this reason these sediment types are referred to generically as cohesive sediment (Whitehouse et al., 1999).

The primary mineral component of cohesive muds are clay minerals. Clays have a plate-like structure, and generally have a diameter less than 2 μm (see Table 2.1). Their surfaces have ionic charges creating forces comparable to or exceeding the gravitational force, and these cause the clay particles to interact electrostatically. Consequently, the sediment particles do not behave as individual particles, but tend to stick together. This process is known as flocculation, and the aggregates formed are referred to as *flocs*, whose size and settling velocity are much greater than those of the individual particles, but whose overall floc density is less. Figure 2.1 shows an example, offered by McDowell and O'Connor (1977), of the typical sizes and arrangements of clay particles and flocs. However, current studies (including this thesis) show that natural estuarine floc groups can attain much larger sizes (up to several millimetres) than the 200 μm illustrated. The degree of cohesion increases

with the fraction of clay minerals within the sediment, and starts to become significant when the sediment contains more than 5-10% of clay by weight. The most important types of clay minerals are: kaolinite, chlorite, montmorillonite, and illite. The flocculation potential of particles is further enhanced by the addition of the sticky organic matter.

Table 2.1 Grain size (diameters) scales for fine sediments (after Wentworth, 1922).

Description		Phi (ϕ) $\phi = -\log_2$ (mm)	Microns (μm)
SAND	very coarse	-1	2000
	coarse	0	1000
	medium	+1	500
	fine	+2	250
	very fine	+3	125
SILT	coarse	+4	62.5
	medium	+5	31.3
	fine	+6	15.6
	very fine	+7	7.8
CLAY	coarse	+8	3.9
	medium	+9	1.95
	fine	+10	0.98
	very fine	+11	0.49
COLLOIDS		+12	0.24

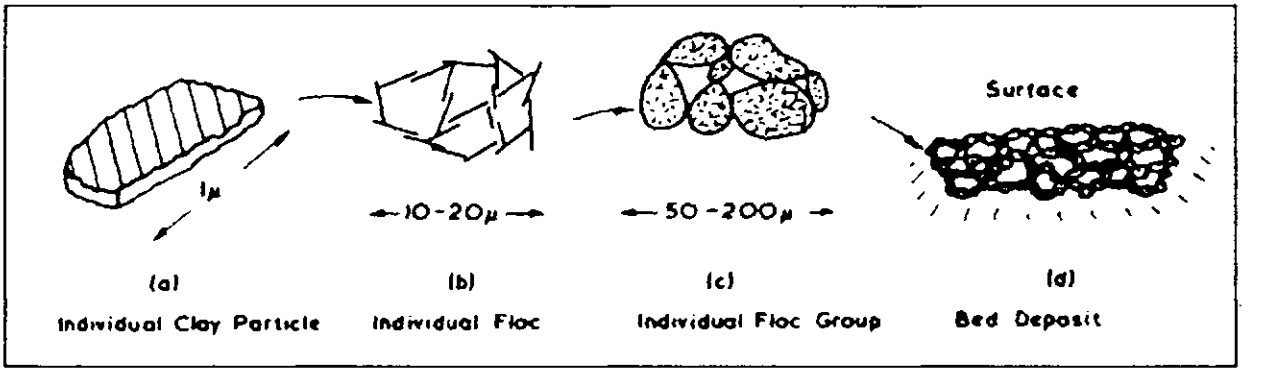

Figure 2.1 Sizes of clay particles, flocs and floc groups (after McDowell and O'Connor, 1977)

A distinct difference exists between cohesive and non-cohesive sediment: for sandy sediment it is the particle size of the bed sediment which controls the mobility, whereas for cohesive sediments it is the bulk properties of the mud admixture which determines the behaviour of the sediment. For this reason the processes of deposition, consolidation and erosion for cohesive sediments are controlled by a complex array of physical, chemical and biological factors. In order to predict sediment transport for cohesive sediments, an accurate description of the hydrodynamical regime must first be made, and then the movement of

water must then be related to the movement of the muddy sediment. This means that the nature of the cohesive sediment throughout its various states (i.e. deposition, erosion or consolidation) needs to be well described. Hayter and Mehta (1982) indicated that seventeen parameters need to be determined in order to fully describe a cohesive sediment type. For this reason most work to date has been more site specific, than fundamental in nature.

There have been many attempts to classify the variety of suspended sediment concentration ranges. For this thesis, the four categories proposed by the EC MAST III project COSINUS will be used. It is based on the gradient Richardson number, Ri_g. The Ri_g is a comparison of the stabilising forces of density stratification to the destabilising influences of velocity shear, i.e. it characterises the turbulence structure of the flow, and is defined as:

$$Ri_g = \frac{-g \cdot \delta\rho / \delta z}{\rho_w (\delta U / \delta z)^2} \qquad (2.1)$$

where g is the acceleration due to gravity, z is the height above the bed (positive upwards), ρ_w is the density of the sediment laden water at height z, and U is the current velocity at height z. Dyer (1997) summarises that when the $Ri_g < 0$ the stratification is unstable, $Ri_g > 0$ the stratification is stable, and when $Ri_g = 0$ it is neutral and the fluid is unstratified between the two depths. Generally, values of $Ri_g < 0.03$ indicate that the production of turbulence by shear greatly exceeds the stabilising effect of the density gradient, and hence flow is fully turbulent. Under these flow conditions, negligible stratification exists. The effect of turbulence damping due to density stratification increases with Ri_g until the value approaches 0.1-0.3 where the density is so strong that the turbulence is damped out and the flow becomes predominantly laminar in structure.

The COSINUS categories are:

1. Dilute Suspension

The concentration is less than 1 gl^{-1}. With a low Ri_g, these suspensions do not significantly effect the turbulent flow field and behave as Newtonian fluids (i.e. they demonstrate a zero shear stress at a zero shearing rate, then show a linear response in shear stress with increasing shear rate, and the effective molecular viscosity remains constant throughout).

2. Concentrated Benthic Suspension (CBS)

This is a suspension typically up to 10 gl^{-1}. The Ri_g are more significant, so there is a significant level of stratification. The sediment is kept in suspension by turbulence, although the CBS layer interacts with the turbulent flow field. It tends to behave in a Newtonian

manner, but with an increased viscosity. A CBS layer behaves as a fluid, and is still transported with the main flow.

3. Fluid Mud

Once the concentration exceeds a critical value of a few 10 gl^{-1}, the particle interactions start to modify the properties of the suspension. The settling flocs are hence affected by hindered settling. To maintain CBS with concentrations beyond the critical value, much more energy is required as turbulence is being damped by buoyancy effects, and by the dissipation of energy due to interparticular collisions and its resulting effect on the floc structure. Therefore, when the energy level is too low to maintain a CBS, the layer collapses and deposits to form a denser fluid mud layer. A fluid mud generally has the rheological classification of a non-Newtonian fluid (Faas, 1984), which possesses a viscosity typically several hundred times larger than that of clear water. The flow is usually laminar. With time the flocs within a fluid mud start to become space-filling, and they can form a network structure called a gel. This process can result in measurable strength building up which resists entrainment, although Toorman (1997) indicates that this takes time.

4. Consolidated Bed

This can be formed either by settling from suspension, or as a transition from a fluid mud. In the latter, once the gel point was exceeded, the flocs formed a continuous network structure and develop effective stresses. This forms a weak saturated soil. At rest, the structure collapses under its self-weight. The interparticular bonds increase in strength and the pore water is slowly expelled, i.e. consolidation.

2.2 Flocculation process

This thesis is primarily concerned with the effects of turbulent hydrodynamical mixing on floc formation for particles in both dilute suspension and in CBS layers. To date, the quantification of estuarine flocculation processes from in-situ observations has not been possible primarily due to instrumentation limitations. Most of the empirical studies were conducted under laboratory conditions, mainly using flumes to simulate hydrodynamical stirring. The early studies of the effects of turbulence on flocculation were conducted by the sanitation industry (Argaman and Kaufman, 1970; Parker et al., 1972). Burban et al. (1989) conducted an investigation on the interactive effects of shear, SPM concentration and salinity, with respect to floc diameter. This was then extended to include settling velocity (Burban et al., 1990). However, these laboratory experiments relied on withdrawing floc samples formed within a flocculator at a constant shear level, and then transplanting them

into a settling tube for measurement. Even so, Tsai et al. (1987) and Burban (1987) both indicated, from laboratory experiments, that the modal floc size was influenced by both the SPM concentration and shear stress. However, laboratory studies can generally only focus on one process (e.g. deposition) in isolation. Although laboratory simulations can instill a sense of control to the examination conditions, high quality in-situ data is required to gain a more complete picture of the many subtle interactions which occur within an actual estuarine water column throughout a tidal cycle.

In order for particles to flocculate into larger aggregates, the particles must be brought into contact with each other and then stick together. The efficiency with which the particles coagulate is a reflection of the stability of the suspended sediment (van Leussen, 1994). A suspension is classified as unstable when it becomes fully flocculated, and is stable when all particles remain as individual entities. The following sections will outline the main mechanisms with regard to both floc growth and break-up, plus particle cohesion.

2.2.1 Particle collisions

In order for aggregation to occur, particles must be brought into contact with each other and then stick together. Particles in suspension collide due to a variety of different mechanisms, and the frequency of contact depends on the mechanism that brings about the contact, as well as on the particle size and the concentration of the particles. There are three principle mechanisms of collision:

1. Brownian motion
2. Differential settling
3. Velocity gradients generated within the suspended fluid (turbulent shear and turbulent inertia)

In the theoretical modelling of flocculation by two body collisions, the collision frequency can be determined by obtaining the product of the number concentrations of interacting particles $n_i n_j$ and a collision frequency function $K(d_i, d_j)$. This is shown as equation 2.2:

$$N_{ij} = K(d_i, d_j)\, n_i\, n_j \qquad \textbf{(2.2)}$$

where N_{ij} is the number of collisions occurring per unit time and per unit volume between two classes of particles of diameters d_i and d_j. The collision frequency functions for three mechanisms are shown in Table 2.2 (from Glasgow and Kim, 1989).

Table 2.2 **Collision frequency functions (from Glasgow and Kim, 1989).**

Collision mechanism	Collision frequency function
Brownian motion	$K_{BM} = \frac{2kT(d_i + d_j)^2}{3\mu d_i d_j}$
Differential settling	$K_{DS} = \frac{\pi \cdot g}{72\nu \cdot \rho_w}(d_i + d_j)^2 (\Delta\rho_i d_i^2 - \Delta\rho_j d_j^2)$
Turbulent shear	$K_{TS} = \frac{1}{6}(d_i + d_j)^3 G$

k = Boltzmann's constant, T = absolute temperature, μ = dynamic viscosity of the liquid, ν = kinematic viscosity of the liquid, ρ_w = water density, ρ_i = density of particle i, $\Delta\rho_i = \rho_i - \rho_{wi}$, and G = turbulence parameter.

It should be noted that the simplified two body collision model assumes no density change with increasing floc diameter (i.e. the collision between two particles forms an aggregate whose volume is equal to the sum of the original two). Also the aggregation process assumes that particles stick together with every collision. This would lead to complete destabilisation of the suspension, and is referred to as rapid flocculation. In reality only a fraction of the collisions are effective and suspensions exist in states of partial stability. Therefore a "collision efficiency" can be employed by modellers to indicate the proportion of collisions which contribute towards constructive aggregation. Very little is known about this efficiency factor α'. Edzwald and O'Melia (1975) conducted experiments with kaolinite, and found that the efficiency was approximately 10% or less. However Alldredge and Silver (1988) indicated that for particulates coated with natural polymers the efficiency could reach 100%. Values of α' generally range from 0.05 to 0.25 for low and highly cohesive sediment, respectively. The aspect of organic coatings will be discussed in section 2.2.3.b.

Particle collisions due to Brownian motion, are the result of the random bombardment by thermally agitated water molecules. Particles which come into contact and stick together as a result of Brownian motion are said to flocculate perikinetically. The number of collisions is a function of temperature, dynamic viscosity and particle size. Van Leussen (1994) found that within typical estuarine conditions this perikinetic mechanism was only effective for particles less than 0.5-2 μm in size. Flocs formed by Brownian motion have a weak composition, are ragged in structure and are easily dispersed by shearing or crushed on deposition.

Particle interaction by differential settling is where larger particles have larger settling velocities, and therefore fall onto relatively smaller particles. As with Brownian motion, there is little stress imposed on the particles during the collision and the result is a poorly bonded floc of low density. Differential settling is only effective under low flow velocity conditions. Many authors such as Van Leussen (1994), and Lick et al. (1993) have attributed the collision mechanism of differential settling as having a major influence on further floc growth. However Stolzenbach and Elimelich (1994) have suggested that differential settling is not an important factor. They conducted experiments in a laboratory settling column and analysed theoretical results presented by Wacholder and Sather (1974). They showed that the probability that a large, but less dense, rapidly falling particle would actually collide with a small, but denser, slowly falling particle was very small, because the smaller particle would be deflected around the larger one.

The velocity gradients which create turbulent mixing within the water column, generate two mechanisms of particle collision. The first is due to the inertia of larger particles responding more slowly to local accelerations than significantly smaller particles. The other mechanism is collision because of shear (laminar or turbulent), which is the result of the presence of a velocity gradient. In a shear flow, particles are brought into contact with each other when an overtaking particle hits or approaches closely to a slower moving particle. This mechanism is affected by the rate of shear and the size of particles.

The relevant importance of the three collision mechanisms was assessed by van Leussen (1988), following Friedlander (1977) and assuming decreasing floc density with increasing diameter according to McCave (1984), for particles d_i of 0.5 μm, 5 μm 50 μm and 500 μm, colliding with particles ranging from 0.01μm to 1 cm. The findings are summarised in Figure 2.2, and it shows that the collision frequency significantly increases with increasing turbulent shear. Although differential settling was also shown to contribute to the collision of larger particles, to reiterate, it may or may not be an effective mechanism, but could only operate at very low turbulent conditions (i.e. slack water). With regards to northern European estuaries, turbulent shear typically ranges from 1-10 s^{-1} in the lower section of the water column throughout a tidal cycle. Hence turbulent shear can be regarded as the most dominant of the three flocculation collision mechanisms. Aggregates formed under this orthokinetic flocculation mechanism are usually relatively strongly bonded.

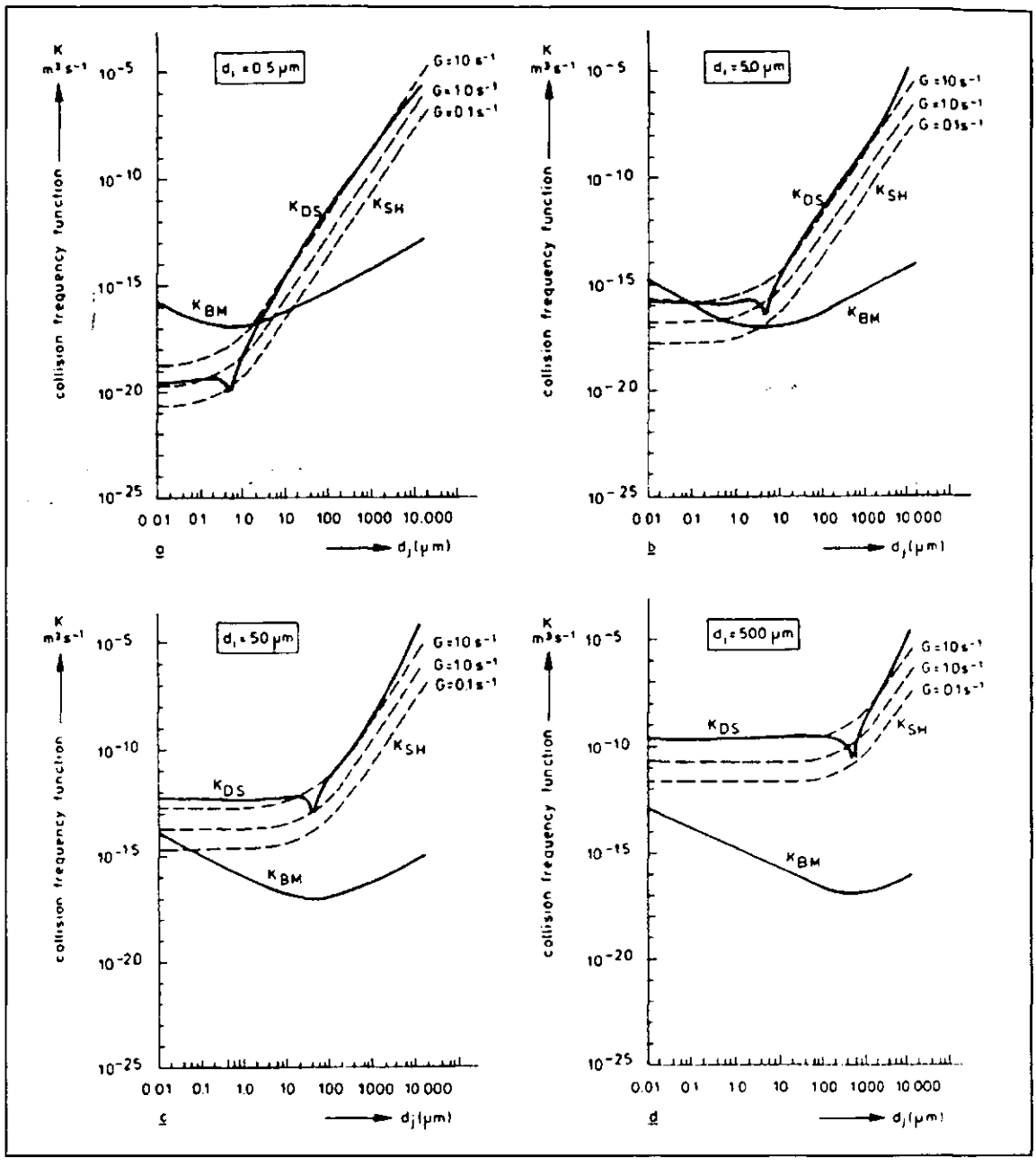

Figure 2.2 Comparison of collision mechanisms: Brownian motion (K_{BM}), differential settling (K_{DS}) and turbulent shear (K_{DS}), for different particle diameters (After Van Leussen, 1994).

2.2.2 Floc break-up

The turbulent shear which was shown to promote floc growth, is also the primary source for creating floc break-up. As turbulence increases - both turbulent pressure differences and turbulent shear stresses in the flow rise. If the floc integrity is less than the ambient turbulent shear stress, the floc will fracture. Hence the turbulent shear stress can impose a maximum floc size restriction on the floc population. This was observed experimentally by Pandya and Spielman (1982), and Tambo and Hozumi (1979) who related the maximum floc size to the turbulent dissipation rate ε and the Kolmogorov microscale of turbulence. Kolmogorov

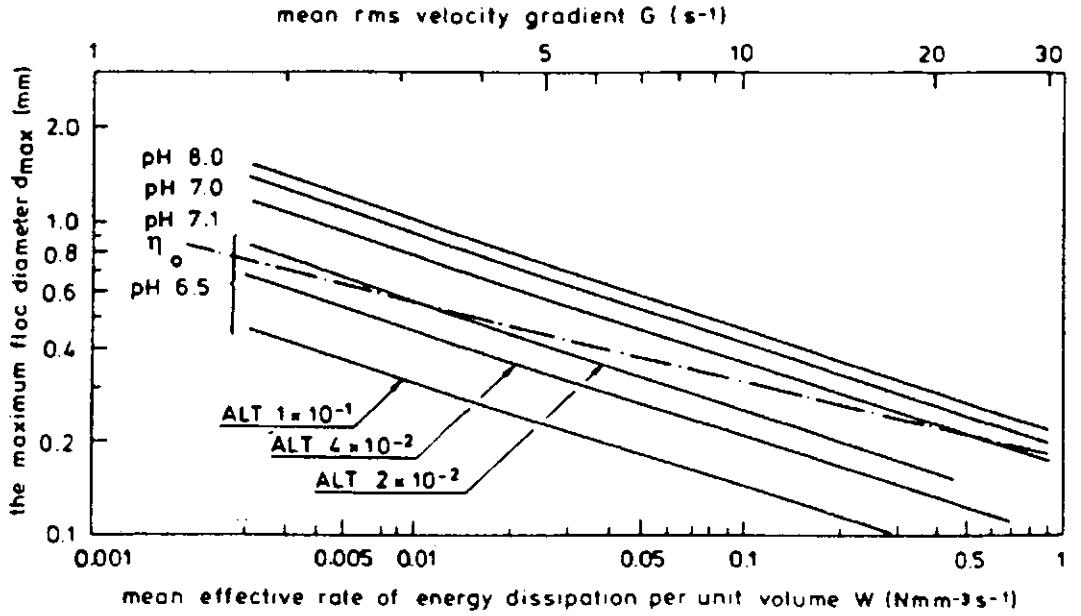

Figure 2.3 Relationship between the maximum floc diameter and the mean effective rate of energy dissipation of clay aluminium flocs (after Tambo and Hozumi, 1979).

(1941) proposed a cascade of turbulent energy from energy-containing eddies down to energy-dissipating eddies; the Kolmogorov microscale is further defined in section 4.2.2. Tambo and Hozumi showed (Figure 2.3) that when the floc diameter was larger than the lengthscale of the energy dissipating eddies, the aggregate will break-up. On a lesser scale, both Argaman and Kaufman (1970) and Parker et al. (1972) suggested that flocs may decrease in size by gradual break-up through surface erosion of the floc by turbulent drag. The rate at which this takes place was proportional to the floc surface area and the surface shearing stress. These processes of floc break-up are more significant at low concentrations.

It must be noted that the act of an aggregate breaking-up causes energy to be removed from the surrounding turbulent shear field. The floc structure model of Van de Ven and Hunter (1977) studied various sources of energy loss due to break-up. It identified that to cause a floc to rupture, energy is dissipated in stretching the internal bonds to the limit of their tensile strength. Also viscous dissipation occurs as a result of the interstitial water moving to accommodate the change in floc shape as it is distorted.

As concentrations increase, the influence of particle collisions can also act as a floc break-up mechanism. Burban et al. (1989) proposed a general formula, based on a paper by Lick and Lick (1988), which described the change in particle size distribution with time. The formula utilised the collision frequency components described in Table 2.2, and was employed to examine the various aspects involved with disaggregation. Their findings are summarised:

If initially it was assumed that floc break-up did not occur and the presence of shear resulted solely in flocculation, the median floc size would be proportional to the square of the particle concentration because the particle collisions increase with concentration. This corresponded with the findings of Eisma et al. (1991), who measured large floc sizes in the bottom water of several estuaries, where particle concentrations were at a higher level. Now if the floc model conditions were altered to allow for aggregate break-up, floc break-up by fluid shear would be seen to be proportional to the concentration, and break-up due to inter-particular collisions would be proportional to the square of the concentration.

Thus, if turbulent shear was the dominant process in the break-up of flocs, the model indicated that the median diameter would also increase with concentration, and if particle collisions due to velocity gradients was the dominant mechanism - the median diameter would remain approximately the same at increasing concentrations. However, if it was assumed that three-particle collisions (as opposed to two-particle collisions) were the dominant process in aggregate break-up, the median floc diameter would decrease with particle concentration. Burban et al. (1989) found from laboratory experiments a marked decrease in the floc size with increasing concentration (at steady state), which indicated that floc break-up by three-particle collisions was the dominant process.

A key factor in floc break-up, due to any of the above mechanisms, is the strength of the floc. As with aggregation, the surface cohesion of the particulates will also have a significant impact on the shear forces required to break down the floc integrity. At present the influence and occurrence of flocculation, as well as floc break-up, on in-situ floc size distributions is largely unknown, apart from the general fact that suspended particulate matter flocculates and flocculation typically dominates over break-up. A conceptual model illustrating expected trends (Figure 2.4), was proposed by Dyer (1989). Still, relatively little quantitative data has been obtained on these inter-relationships.

2.2.3 Cohesion mechanisms

It is the cohesive nature of fine grained particles that allow them to coagulate into larger aggregates. For estuarine sediments, this cohesion can be in the form of either the physio-chemical process of salt flocculation, or the more significant organic enhanced "bioflocculation".

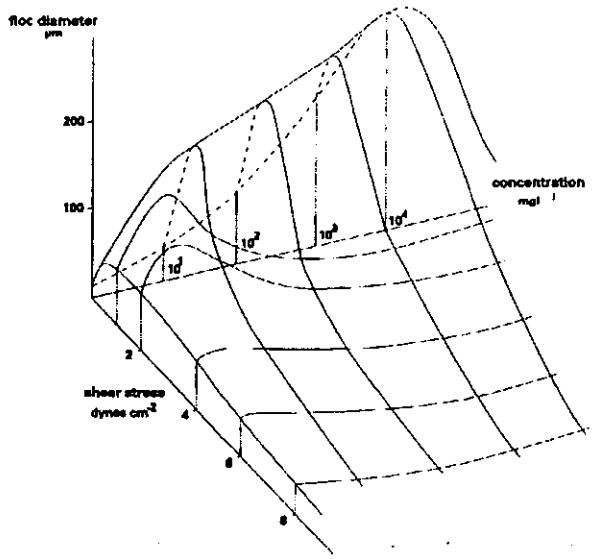

Figure 2.4 Conceptual diagram showing the relationship between floc modal diameter, suspended sediment concentration and shear stress (Dyer, 1989).

2.2.3.a Salt flocculation

Original theories on flocculation regarded the variations in salinity as the main instigator of cohesive sediment flocculation throughout a tidal estuary. The cohesive forces exerted between two clay particles depends both on the mineralogy of the clay, and on the electro-chemical nature of the suspending medium. Most of the individual clay particles, made up from the common clay minerals, have a negative charge on the face of each platelet mainly due to the exposed oxygen atoms in the broken bonds of the crystal lattice. The mutual forces experienced by two or more clay particles in close proximity, are the result of the relative strengths of the repulsive and attractive forces.

The attractive forces (V_A) are known as the London-van de Waals force. This is a gravitational attraction, and is independent of the properties of the fluid. Electrostatic Coulombic forces (V_R) are the repulsive forces, and are due to similar ionic charges repelling each other. Positive ions present in the fluid medium form a closely-held layer of cations on the face of the platelets (by the action of the most negative residual ions), and a more diffuse cloud of hydrated cations. This electrical double layer produces the effect of reducing the magnitude of the negative charge of the clay particle. The result can either be attraction or repulsion between the particles, depending on the relative strengths (i.e. the number of positive ions), and the distance between them. Figure 2.5 illustrates the double layer concept for an idealised model. In summary, at low electrolyte concentrations (Figure 2.5.b) the diffusive double layer is thick, and this means that the repulsive force extends so far away from the particle that the net force (electrical repulsion minus the London-van de Waals attraction) will cause repulsion between particles as they come into the proximity of each

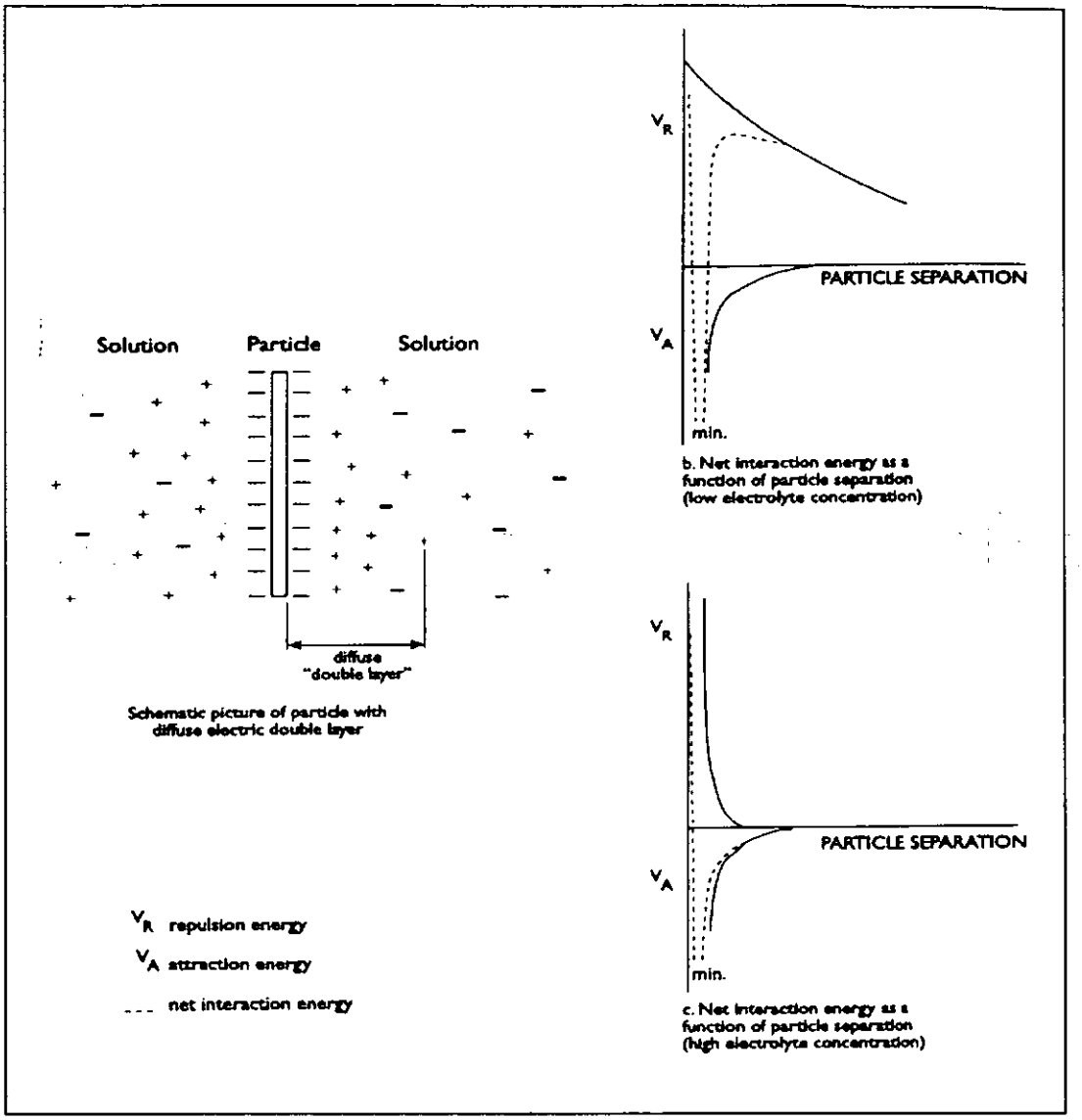

Figure 2.5 Idealised model of particle diffuse electric double layer and interaction (after van Olphen, 1977).

other. Whereas for higher electrolyte concentrations, the double layer becomes thinner (Figure 2.5.c). The electrical repulsion only occurs close to the particle, but once that point is reached the London-van de Waals attraction is already greater than the repulsive force, and under those conditions, two particles approaching each other could flocculate.

Translating these aspects into estuarine conditions means that, in fresh water suspensions (few positive ions), the repulsive forces between the negatively charged particles dominate and the particles will repel each other. In saline water the attractive forces dominate due to the abundance of sodium ions forming a cloud of positive ions (cations) around the negatively charged clay particles resulting in the formation of flocs. It was thought that riverine particles formed flocs when they reached the saline water, and they would then deflocculate when they were returned back into contact with fresh water at the head of the

estuarine salt intrusion. Krone (1963) found that flocculation quickly reaches an equilibrium situation at a salinity of about 5-10, which is much smaller than that of sea water (~35). However, for in-situ flocculation it is now considered that the salinity of the water is of lesser importance.

2.2.3.b Organic coatings

The relevance of salt flocculation in estuaries has increasingly been questioned because of the potential greater influence of organic material present. The electrostatic bonds are very weak, and the presence of large estuarine macroflocs has been observed by in-situ photography (Eisma et al., 1983, 1990; Wells, 1989) in relatively fresh waters. Current research has shown that much of the suspended matter in natural waters generally acquire an organic surface coating. Also, Gibbs (1977) reported the existence of metallic coatings on clay fractions. He postulated that the coatings, with thicknesses ranging from 210 molecular layers on the 0.1 μm size fraction to 4000 molecular layers on the 3.5 μm fraction, would effectively blanket the differing electrostatic properties of the various mineral particles. This means that when a coated particle moves from fresh to saline water, their surface charge not only becomes less negative, but remains negative (Neihof and Leob, 1972, 1974; Leob and Neihof, 1974). Of the two variants, organic coatings are regarded as the most effective for flocculation. Within estuaries, the organic coatings on the particles contain long-chain types of molecules (natural polymers) that stick out through the water mantle around the individual particles. In estuarine waters these polymers are mostly polysaccharides (mucus) produced by mud-dwelling micro-organisms, such as diatoms and bacteria. When particles come close to each other, these chains attract to those on the other particle; this effect is illustrated in Figure 2.6. In this way flocs can be formed in fresh water, as well as in water of a varying saline level. The presence of organic material (biogenic forces) also means that the binding forces increase, and hence the flocs can become larger. In general, flocs held together by polymers are stronger than those held together solely by London-van de Waals forces (Kitchener, 1972).

Figure 2.6 Flocculation and destabilisation by adsorbed polymers (after Gregory, 1978).

However it must be noted that the repulsive energy barrier discussed under salt flocculation (section 2.2.3.a) is not completely eliminated by polymer attributed cohesion. If particles are to be bridged by adsorbed polymers, the later must span the distance over which the double layer repulsion operates. This is called the interparticular bridging model (Ruehrwein and Ward, 1952; La Mer and Healy, 1963), and is show schematically in Figure 2.7.

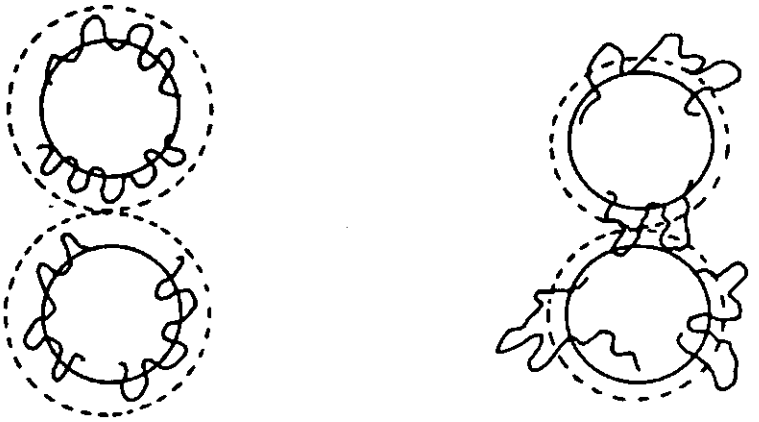

a. Low ionic strength

Bridging prevented by electrical repulsion.

b. High ionic strength

Bridging across the effective repulsion distance.

Figure 2.7 Schematic diagram of polymer bridging and the repulsive energy barrier (dotted line) at the particle surface for: (*a*) low ionic strength and (*b*) high ionic strength (after Gregory, 1978).

Mucus is also produced by diatoms during locomotion. Paterson (1989) related the erodibility of mud beds to the diatom activity at the surface and gave evidence for the bonding of sediment particles by mucillages. Paterson suggests that when the mud flats dried out at low water, the mucillages may degrade and become easier to erode. So rafts of bound microbes, together with sediment, may be lifted off the mud surface by surface tension (Hicks, 1988). These would be easily entrained during the following flood tide. Tsai and Lick (1988) also pointed out that biological bonding of the estuary bed can produce a time dependence to the critical erosion shear stress required (the shear stress which must be exceeded before sediment can be eroded), and this can affect the re-suspension characteristics. Experiments by Kranck (1984) have shown (Figure 2.8) that the flocculation of mineral particles which contained some organic matter, greatly enhanced the settling velocity of the aggregates. Both Cadee (1985), and Kranck and Milligan (1988) reported enhanced flocculation following diatom and coccolith blooms at the entrance of tidal inlets, and coccolithophorids may also act as nuclei around which flocs are created. Jackson (1990) modelled flocculation during a diatom bloom by considering both aggregation processes and

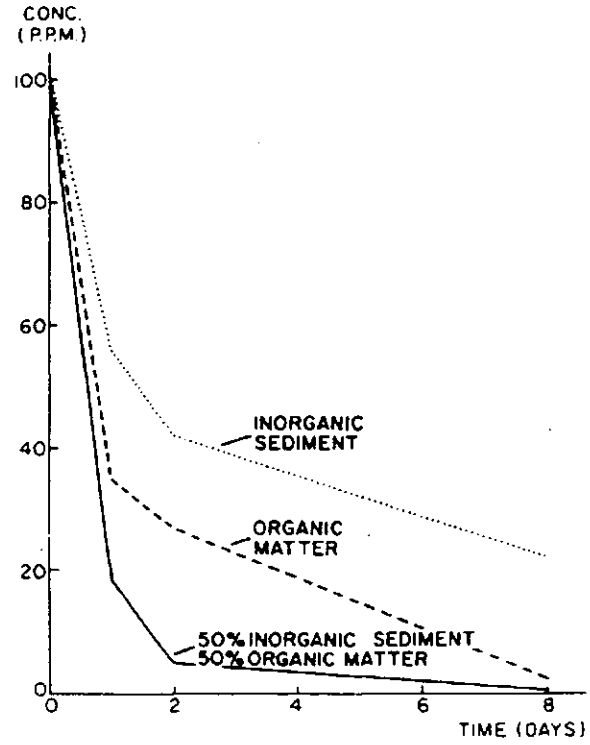

Figure 2.8 Relationship between concentration and time for settling suspensions consisting of inorganic (single mineral) particles, of organic matter, or of flocs consisting of 50% organic matter and 50% mineral particles (after Kranck, 1984).

algal growth. It was concluded that the important parameters were: turbulent shear, the algal (particle) concentration, and the size and stickiness of the algae.

2.3 Floc properties

2.3.1 Floc size, settling velocity and their measurement

Settling velocity is regarded as the basic parameter used in determining suspended particulate matter (SPM) deposition rates in either still or flowing water. Much has been documented on non-cohesive sediments (coarse silts and larger), and it is possible to calculate the settling velocity of low concentrations in suspension, using well defined expressions (e.g. Stokes' Law), from the relative density, size and shape of the particles, since the only forces involved are gravity and the flow resistance of the particle. However, the settling velocity of flocculated, cohesive sediments in estuaries are significantly greater than the constituent particles. An individual floc may constitute up to 10^6 individual particulates. This means that there is the possibility of particles ranging over four orders of magnitude, from individual clay particles of 1 μm to flocs of several centimetres. Also, like the floc size, the settling velocities can range over four orders of magnitude, from 0.01 mms^{-1} up to several centimetres per second (Lick, 1994).

It has been generalised that there are two distinct component groups of flocs: *macroflocs* and *microflocs*. Macroflocs are large, highly porous (> 90%), fast settling aggregates which are typically the same size as the turbulent Kolmogorov microscale, which is defined in section 4.2.2. Although the floc effective density (this aspect will be reviewed in greater detail later in this section) generally decreases as the macroflocs grow larger, the overall settling velocities tend to significantly increase. However, these low effective densities means that the macroflocs become very fragile, and can be progressively broken down in regions of higher turbulent shear stress to form microflocs (Glasgow and Lucke, 1980).

The smaller microflocs are much more resistant to break-up by turbulent shear; they tend to have slower settling velocities, but exhibit a much wider range in effective densities than the macroflocs. Microflocs are formed in a similar way to macroflocs (by inter-particle collisions), but Eisma (1986) attributes the strong bonding of their constituent particles to the biogenic "glues" produced by organisms. The combination of these biological adhesives and particles being brought in contact with each other would produce a very compact microfloc. Eisma (1986) concludes that the limiting factors of a stable microfloc is the binding strength of the organic substances involved in relation to: *1.* the total mass of the mineral particles that are being held together (i.e. the floc), and *2.* the degree of physical disturbance that takes place during the normal procedures of sampling and size analysis.

As shown earlier in section 2.2.1, the particle number concentrations govern the collision frequency of the particles. Therefore it is logical to suppose that floc sizes and settling velocities are strongly dependent on variations in the ambient suspended particulate matter (SPM) concentration. The results of field settling tube experiments conducted in several estuaries are presented in Figure 2.9. It showed a general exponential relationship between median floc settling velocity (W_{50}) and SPM (C) for concentrations ranging up to 10 gl^{-1}, in the form of equation 2.3:

$$W_{50} = k \cdot C^{m} \qquad \textbf{(2.3)}$$

Figure 2.9 shows considerable differences in the exponential relationship between estuaries and Dyer (1989) suggests that these variations are probably a result of floc density variations, and differences in ambient hydrodynamic conditions. Once the concentration reaches a level of 5-10 gl^{-1}, the flocs tend to interact hydrodynamically and the floc growth can be inhibited. A further rise in concentration to beyond 10 gl^{-1} causes the particle interactions to modify the properties of the suspension, whereby the particle interactions lead to a hindered settling flux. The rheological behaviour of these high concentration

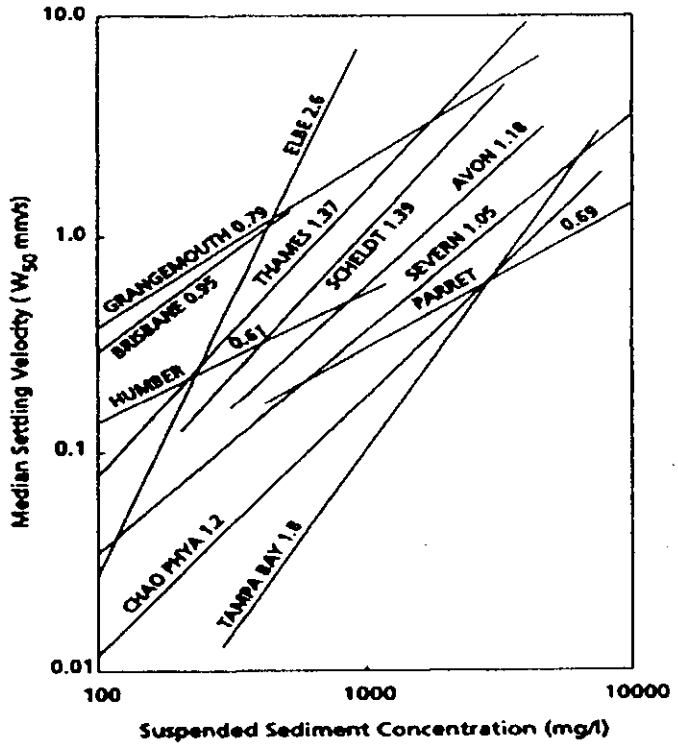

Figure 2.9 The relationship between median settling velocity and concentration for muds of various estuaries. The numbers are the value of the exponent m from equation 2.3 (Dyer, 1989).

suspensions (>10 gl^{-1}) become non-Newtonian. For hindered settling conditions, Maude and Whitmore (1958) found that equation 2.3 had to be modified to the form of

$$W_{50} = W_0 (1 - k_2 \cdot C)^{\beta} \qquad \textbf{(2.4)}$$

where W_0 was the fall velocity of a single grain. An example illustrating the effects of hindered and unhindered settling for mud from Tampa Bay, Florida is shown in Figure 2.10 (after Ross, 1988).

The agglomeration of different types of microflocs, together with single mineral particles, tend to form the basic constituents of the macroflocs. Although organic matter is again used as the principle binding agent which links the microflocs together in a network which forms the macroflocs, the adhesional strength is significantly lower than that which maintains the integrity of the individual microflocs.

Very little is understood about the manner in which the different sized flocs and particles coagulate to form the larger aggregates. Krone (1963) suggested that flocs grew in a progressively hierarchically manner (Figure 2.11). Primary particles glued together form zero order flocs, these in turn combined to form 1st order flocs etc. This was commonly

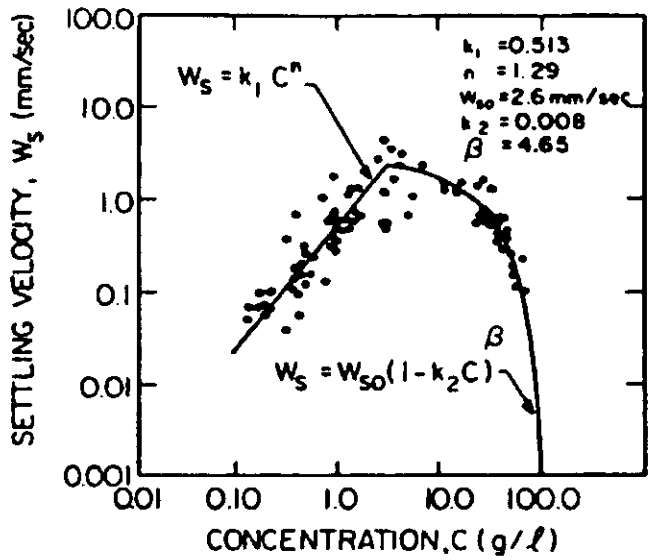

Figure 2.10 Settling velocity and flux variations with suspension concentration using mud from Tampa Bay, Florida (after Ross, 1988).

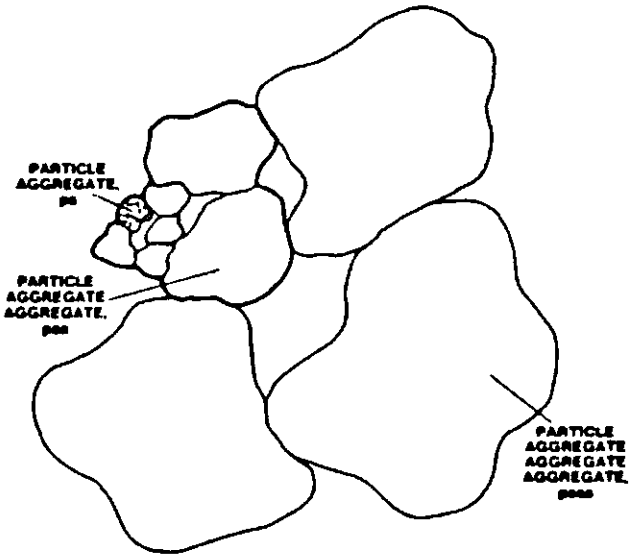

Figure 2.11 A two-dimensional schematic representation of various order aggregates (Krone, 1986).

referred to as Krone's Order of Aggregation theory, and forms the basis of the fractal approach (see section 2.5).

Many authors have offered a wide variety of size divisions for the macroflocs and microflocs, such as Eisma (1986) who suggested 125 μm, but most of these have been assigned on an arbitrary basis. It is an objective of this thesis to determine a definitive division of floc size based on the assessments of a wide spectrum of measured floc characteristics.

Floc size and settling are therefore functions of concentration, shear, biological matter content, and salinity. The ability to be able to predict the particulate mass and fall rate spectra at a specific point (in both time and space) in a tidal cycle is highly desirable, especially from a perspective of mathematical simulation models, which are attempting to predict long term sediment accumulation and morphological changes. With this aim, good quality floc settling velocity data is required. The limiting factor in many previous studies were the sampling devices used. Instruments such as a Niskin bottle (Gibbs and Konwar, 1983) or pipettes, or the Owen Tube (Owen, 1971), are all very disruptive (Gibbs, 1985; Van Leussen, 1988). This could be the reason that previous studies tended to show a much lower floc size range than is now known.

The presence of large estuarine macroflocs was observed by in situ photography (Eisma et al., 1983, 1990), and in situ laser particle sizer measurements (Bale and Morris, 1987), but these techniques still provided no indication of settling velocity. These non-intrusive instruments only measured floc size, and then used Stokes' Law to predict the settling velocity; this required making an assumption of the floc effective density (also known as density contrast, density difference or excess density). However, the settling velocity of a floc is the function of both floc size and the respective effective density. The latter point will be considered in the next section.

The advent of in-situ video camera systems (van Leussen and Cornelisse, 1994; Fennessy et al., 1994a), has made significant progress in the measurement of floc characteristics. A Lagrangian system, VIS, was developed jointly by Rijkswaterstaat and Delft Hydraulics (van Leussen and Cornelisse, 1994), and systems utilising a Braystoke tube to collect the flocs, such as the HR Wallingford video camera system (Dearnaley, 1996), have also been used during recent field sampling campaigns. However these types of instrument have a number of problems related to the type of illumination (creating thermals which influence the settling velocity), the potentially disruptive nature of the floc sampling, and the accurate referencing of the collected flocs to the ambient turbulent conditions.

In contrast, the instrument developed at the University of Plymouth, INSSEV - IN-Situ SEttling Velocity - (Fennessy et al., 1994a) samples the flocs through a decelerator chamber, and then allow the flocs to fall into a settling column underneath. The instrument concept is illustrated in Figure 2.12. The video camera views the flocs through a window in the side of the settling column, and hence the floc size and settling velocity can be obtained. Also, by

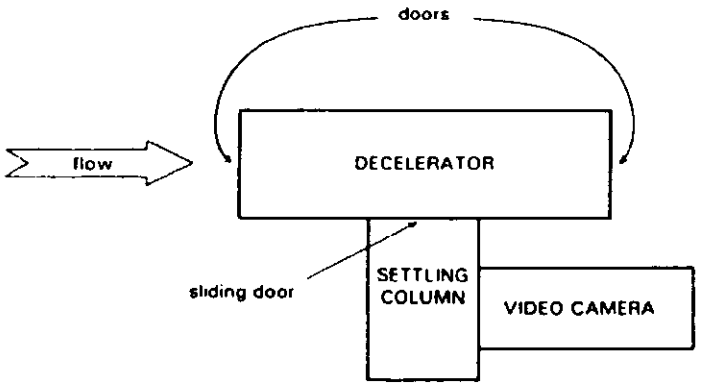

Figure 2.12 INSSEV instrument concept (from Fennessy et al., 1994a)

the use of Stokes' Law, the effective density of the flocs could be calculated (provided the flocs are within the Stokes' range); a combined knowledge of size and settling velocity, together with floc density (all obtained over a range of estuarial conditions), then provides the potential to be able to estimate the mass settling fluxes within that specific estuary. The INSSEV instrument operates within an Eulerian reference frame, and this will be discussed in more depth in section 3.1.3.a.

2.3.2 Effective density

As flocs increase in diameter they become more porous; since the voids are filled with interstitial water, the higher order flocs are less dense than the lower order microflocs. The most practical density value in relation to flocculated aggregates, is that of effective density (ρ_e) . Effective density is the floc bulk density (ρ_f) less the density of the interstitial water (i.e. $\rho_e = \rho_f - \rho_w$). Examples of effective density variations plotted against floc size from different sources are presented in Figure 2.13. A consistent decrease in ρ_e with increasing floc size was observed by each author.

However, very few direct quantitative studies have been conducted on floc effective density variations. Direct analysis by settling flocs in sucrose solutions are suspect, in that, even if the aggregates survive the sampling process, the floc porewater may be replaced by the sucrose solution. As described earlier, the advent of in-situ video camera systems has permitted both floc size and settling velocity to be established simultaneously, with the opportunity to estimate effective density via Stokes' Law.

A knowledge of effective density, ρ_e , is important in the calculation of vertical settling fluxes since the majority of the mass is in the low density, high settling velocity, large flocs

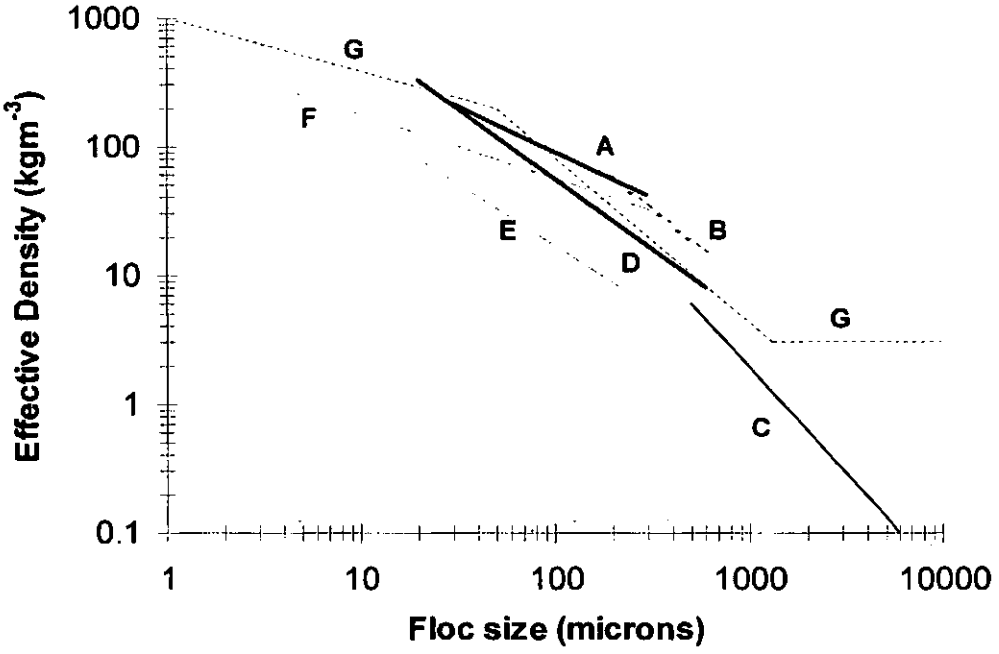

Figure 2.13 Comparative results of effective density against floc size. A = Manning and Dyer (1999), B = Al Ani et al. (1991), C = Alldredge and Gotschalk (1988b), D = Fennessy et al. (1994a), E = Gibbs (1985), F = McCave (1975), and G = McCave (1984) (from Manning and Dyer, 1999).

(Mehta and Lott, 1987). Also the rheological properties of suspended particulate matter are governed by volume concentrations, as opposed to mass concentrations (Dyer, 1989). Fennessy et al. (1996) explains a technique by which the floc population samples obtained by the INSSEV instrument (Fennessy et al., 1994a) could be processed into settling flux spectra. Utilising this spectral technique, a number of field experiments were conducted within the Tamar estuary, South West England (Fennessy, 1994) and the Elbe estuary, North West Germany (Fennessy and Dyer, 1997), and they both identified the larger low density macroflocs containing the majority of the mass flux. This finding concurs with the hypothesis offered by Eisma et al. (1990).

2.3.3 Turbidity maximum

The level of flocculation is highly dependent upon both the SPM concentration and turbulent shear, and both of these parameters can vary quite considerably throughout an estuary. Therefore, the turbidity maximum (TM), which is a feature of many meso- and macro-tidal estuaries (Allen et al., 1980; Postma, 1980; Uncles and Stephens, 1993) is an area where significant levels of flocculation can occur. The conjunction of suspended matter and residual circulation, forms a "sediment trap" in the upper estuary, where the concentrations attain much higher values than either upstream in the river or towards the estuary mouth. The TM at the head of an estuary is a significant feature because it indicates the magnitude

of sediment mobility within the estuary (Dyer, 1989). Dyer (1989) also suggests that the TM encompasses a zone within which the physio-chemical and compositional properties of the water changes rapidly from those of fresh water to those of sea water. It is also a major site in the cycling of chemical and biological reactions between the sediment and water. For example, Anderson (1986) found the abundance of bacteria in the turbidity maximum to be responsible for removal of silicic acid from the riverine water, and its incorporation into diatoms which later reached the sediment.

The primary mechanisms which contribute to the TM formation, are governed by the tidal conditions. During neap tides, when estuaries can become quite well stratified, residual gravitational circulation (due to water density differences) dominates. For the stronger horizontal tidal currents generated by spring tidal conditions, tidal asymmetry is usually the more dominant factor. The bathymetry and topography of an estuary tend to cause a distortion to the tidal curve, i.e. an asymmetry, and this is responsible for the considerable preferential transport of sediment towards the head of the estuary. This residual transport is known as tidal pumping, and is far more significant than residual gravitational circulation. It is the interaction of the tidal pumping with both the sediment settling and re-entrainment during the tide that produces and maintains the TM. The variations of the tidal conditions along the estuary will effect the magnitude of tidal pumping, which typically controls the location of the TM; generally landward of the tip of the salt intrusion (Dyer, 1997). Also, Officer (1981) identified that the sediment dynamics contribute to the occurrence of a TM. As a result of the timescales for the processes of erosion and settling for cohesive sediments, a phase difference can develop between the velocity and concentration variations (i.e. the sediment particles become separated from the flow). Dyer (1995) explains that the phase difference exists in the form of lags (e.g. settling lag, threshold lag, erosion lag, etc.) can produce a residual sediment flux, as long as there is an asymmetry in the tide.

Figure 2.14 shows a schematical representation of the longitudinal residual circulation in a meso-tidal estuary. Sediment is brought into the head of the estuary by the residual downstream transport in the freshwater river. As the seawater enters an estuary, it creates a residual flow which transports suspended solids towards the head. Due to their relative densities, the seawater sinks below the freshwater. In low energy environments (such as those of residual flows) water masses of different density do not readily mix, and a salt-wedge will form. The interface is shown as the dotted-line of Figure 2.14, and represents the level of no net motion. As the sediment transported seaward by the surface residual flow

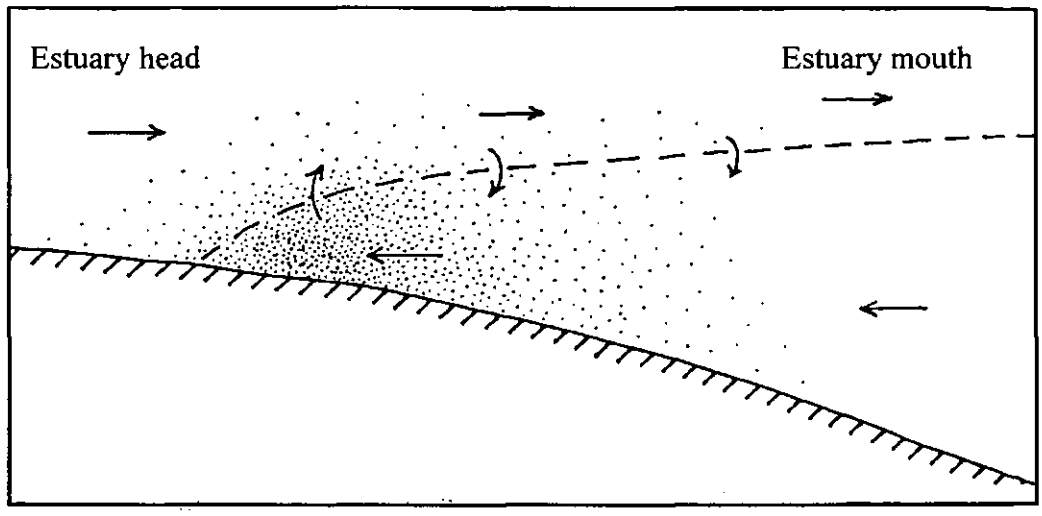

Figure 2.14 A turbidity maximum caused by residual circulation in a partially mixed estuary. Vertical exchanges across the level of no net motion (the dotted line) are illustrated (from Dyer, 1986).

reaches the middle estuary region, it settles into the lower layer (during periods of less vigorous mixing), and joins the landward residual flow. The result is that this suspended particulate matter is then moved with the salt intrusion back to the head of the estuary, where it becomes trapped at the node of the bottom residual flow. Dyer (1986) points out that during a tidal cycle, the concentration of suspended sediment in the TM also varies because of erosion and depositional variability, so it is not simply the residual water circulation that causes the sediment circulation.

2.4 Turbulence theory

Earlier in this chapter, turbulent shear generated within the water column was recognised as having a controlling influence over both the flocculation of fine grained cohesive sediments within estuarine waters, and floc break-up. This section will outline the relevant theory of hydrodynamical turbulence and the methods employed to both measure and represent turbulent characteristics for computational analysis.

2.4.1 Estuarine hydrodynamics

The movement of fine grained sediment in an estuary depends on the hydrodynamic forces caused by currents, waves, pressure gradients (due to both density differences and currents), and gravitational forces on a sloping bed. Estuaries are dominated by tidal processes. The tidal wave progresses up an estuary and then is partially reflected, which results in a quasi standing wave. In idealised conditions (i.e. for a purely sinusoidal tidal curve), the standing wave would cause slack water to occur at times of high and low water. Similarly the times of

maximum flood and ebb currents would correspond to the mid-tide. However in reality the phase difference between the tidal events of high and low water are produced by frictional effects. This produces tidal asymmetry. The circulation patterns are complicated by stratification effects due to inter-mixing of fresh and saline water. Secondary influences on estuarine hydrodynamics are due to the Coriolis effect and surface waves. The Coriolis effect can create cross channel components of flow and water surface slope in wide section of an estuary. Waves in estuaries tend to be small in both height and period (primarily due to the reduced fetch), and only really influence the sedimentation in shallow areas which cover intertidal mud flats (Christie, 1997).

The combination of the tidal regime and river input makes an estuary a high energy flow environment. Fluid dynamics theory categorises flow as either laminar or turbulent. The boundary between them can be defined by the dimensionless Reynolds number which compares the relative importance of inertial (turbulence producing) and viscous (turbulent damping) forces in determining the resistance to flow. The Reynolds number can be determined from equation 2.5:

$$\mathrm{Re} = \frac{u\,D}{\nu} \qquad (2.5)$$

where u is a velocity, D is a depth and ν is the kinematic viscosity. Turbulent conditions can occur as a result of a sufficiently high flow velocity causing an increase in resistance at the channel boundary. The extra resistance being caused because of the energy of the mean flow absorbed in creating the turbulence (Dyer, 1986). Below Re ~ 2000 the flow can be classified as laminar and above approximately 10^5 the flow is most usually fully turbulent (Dyer, 1997). Between the two points the flow is transitional and its character and the point at which it becomes fully turbulent depends largely on the roughness of the estuarine channel walls and bed. Estuarine conditions are dominated by turbulent flows.

Turbulence is an irregular rotational motion whereby eddies are formed. The amount of rotation (i.e. the vorticity of eddies) is proportional to the reciprocal of the time scale. So most of the energy in the flow is associated with the large scale motion, whilst most of the vorticity with the smaller scale motion (Eisma, 1993). In large scale eddies, the viscous forces are significantly smaller in comparison to the inertial forces. For turbulent flow in an estuary, the largest eddies will be in the order of the water depth. These large eddies are stretched by local velocity gradients into smaller eddies. Their energy is dissipated by transfer to progressively smaller and smaller-scaled eddies until a size is reached where the

energy dissipation by molecular viscosity is almost immediate and the energy is transformed into heat (Tennekes and Lumley, 1972; Hinze, 1975). Also, Von Helmholtz (1858) showed that the transfer of kinetic energy from the basic flow through shearing forces or outside forces (e.g. heating) and through larger eddies to progressively smaller eddies, is only possible along a path in three-dimensional flow. Hence turbulent motion is regarded as three-dimensional.

Within an estuary, the large energy containing eddies are influenced in a complex way by features such as: density gradients, tidal regime and the topography. This means that the large eddies are predominantly anisotropic (i.e. demonstrate physical properties that are different in different directions). In contrast, the smaller energy dissipating eddies tend to be isotropic, as the straining action of the larger eddies tends to smooth out the anisotropy at smaller scales. Their scale mainly depends on the energy flux and viscosity.

From a flocculation perspective, individual sediment particles most effectively interact with turbulent eddies of a comparable size. Thus the smallest eddies ranging from 1 μm (equivalent to primary particles) to several millimetres (representative of large low density macroflocs) in size, are the most significant for flocculation processes. Dimensionally, these small eddies are of the same order as the Kolmogorov microscale (Kolmogorov, 1941). The Kolmogorov microscale is the scale defining the limit at which turbulence breaks down to laminar flow; this is further defined in section 4.2.2. The larger eddies are mainly responsible for the general mixing and dispersion of sediment particles in the water column.

2.4.2 Turbulence at the boundary layer

The flow of the riverine input and the tide, creates a frictional drag at the sea bed boundary, which in turn produces turbulent mixing throughout the water column. The turbulence being produced by the flow over and around the roughness elements of the bed. Thus the energy for turbulent mixing is derived from the kinetic energy dissipated by the water flowing across a rigid rough boundary. The frictional force exerted by the flow per unit area of the bed is known as the shear stress (turbulent shear stress during turbulent flow conditions), and is the main hydrodynamic parameter that controls the processes of erosion, entrainment and deposition of mud. In open channel flow, the mean velocity reduces to zero flow at the bed, and zero stress at the water surface. In laminar flow the velocity profile is parabolic, whilst in turbulent flows the parabolic form is modified due to the turbulence transporting momentum vertically.

Van Leussen (1994) identifies two distinct regions of an estuarine water column with regards to turbulent channel flow (Figure 2.15). The first region is adjacent to the bed in which the flow is directly affected by the conditions at the bottom; this is called the wall or inner region. The velocity gradients are largest in the wall region (10-20% of the water column depth), and approximately 80% of the turbulent energy generated by the water flow occurs within this zone. It is here that the strongest lift and shear forces occur, that control the maximum size of the suspended flocs (Mehta and Partheniades, 1975); this is illustrated in Figure 2.16. The second, outer layer is a region where the flow is independent of viscosity and is only affected indirectly by the bottom conditions, although it is highly affected by externally conditions such as variation in mean pressure gradients in the flow direction.

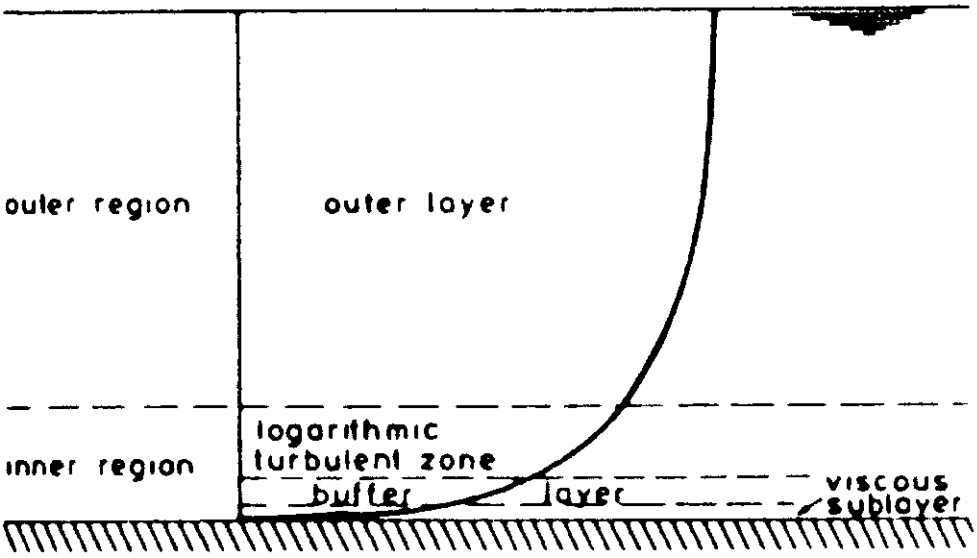

Figure 2.15 A velocity profile illustrating the outer and inner (or wall) regions in turbulent flow above a smooth estuary bed - *not to scale* (from van Leussen, 1994).

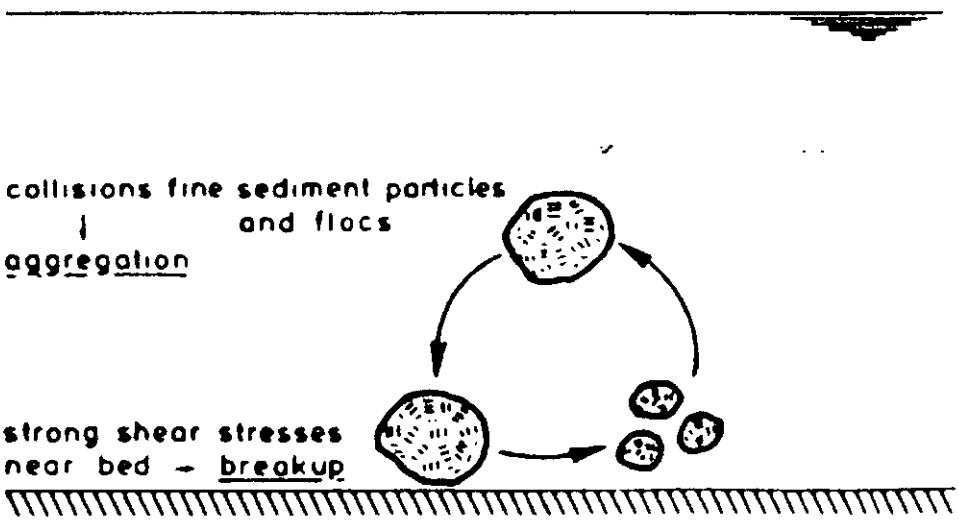

Figure 2.16 Schematic picture of the continuous process of disruption and aggregation of mud flocs in a turbulent flow - *not to scale* (from van Leussen, 1994).

In the wall region the shearing stress is assumed to be constant with height, i.e. it is a constant stress layer. For natural flows, this region can exhibit either smooth or rough turbulent flow. Assuming a unidirectional flow, for the case of smooth turbulent flow, a thin viscous sublayer (typically a few mm thick) forms next to the bed in which mean flow increases linearly with height and which transmits the fluid stress to the bed. For smooth turbulent flow to develop, the bed must be sufficiently smooth that molecular viscosity effects dominate. The thickness of the viscous sublayer varies with current speed, and when the median grain size is less than one-third of the viscous sublayer thickness, the layer remains intact. Above the viscous sublayer, a buffer (or transitional) layer then leads to the over-lying logarithmic layer. This is so termed because of its velocity profile, and within this layer the flow is fully turbulent and is independent of the nature of the bed. The presence of large diameter grains or bedforms can cause the break down of the smooth turbulent flow conditions. This in turn allows the turbulent logarithmic layer to extend towards the bed and interact with the roughness elements. Such rough turbulent flow, has a greater potential to create erosion than smooth turbulent conditions. Rough turbulent flow tends to dominate in estuaries.

However, Gust and Walger (1976) found that the thickness of the viscous sublayer can increase significantly when the concentration of cohesive sediments is high. The consequent reduction in shear transmitted by the layer would reduce the transition to rough turbulent flow. This effect would be of prime importance in a turbidity maximum region of an estuary where it would tend to augment the accumulation of fluid mud by inhibiting erosion and aiding deposition.

In general, within the wall region, the frictional drag at the estuary bed produces a velocity shear, the near bed flow being slowed down progressively relative to that higher up, and turbulence is produced by the flow over and around the rough elements which constitute the bed (Dyer, 1997). Thus the energy for the turbulent mixing is derived from the kinetic energy dissipated by the water flowing across a solid rough boundary. The mean velocity, U, profile for an unstratified flow in the logarithmic layer is given by the classic Von Karman-Prandtl equation:

$$U = \frac{U_*}{\kappa} \ln \frac{z}{z_0} \qquad \textbf{(2.6)}$$

where κ is the Von Karman constant, which is usually taken as 0.4, but McCave (1979) suggests that it may be smaller for high sediment concentrations. The height above the bed is

z, whilst z_0 is the roughness length which is dependent upon the bed characteristics. The frictional velocity, u_*, is related to the bed shear stress (τ_b) and the water density (ρ_w) by:

$$U_* = \left(\frac{\tau_b}{\rho_w} \right)^{0.5} \quad \textbf{(2.7)}$$

However, Dyer (1986) explains that within an actual estuarine water column, the logarithmic profile can easily be altered by flow acceleration and decelerations, salinity stratification, concentration gradients, and other damping effects such as drag reduction (this phenomenon will be explained later in Chapter 6). Turbulence needs to be considered in a stationary frame in order to quantify the exchanges of mass and momentum; the next section will therefore outline how the turbulent properties of the flow can be more accurately represented mathematically, with the emphasis on turbulent shear in the lower water column.

2.4.3 Mathematical representation of turbulence

In order to be able to quantify the exchanges of mass and momentum within a flow, turbulence needs to be considered in a stationary frame. For this purpose, the statistical decomposition of unsteady flow based on the work of Osbourne Reynolds (1895) can be used. Reynolds showed that in an Eulerian reference frame, the flow field could be represented by three orthogonal velocity components: U (streamwise), V (cross-stream) and W (vertical). By removing the tidal flow components (i.e. U_T, V_T, and W_T each equal to zero), the flow can then be decomposed into mean (u, v, w) and fluctuating (u', v', w') components. An example illustrating the decomposition for a streamwise flow velocity time series is shown in Figure 2.17. The mean components are time-averaged over a period that is long relative to the scale of the turbulent disturbances, but short compared to the long-term variations which would not be regarded as part of the turbulent fluctuation of the flow (Duncan et al., 1970), whilst the fluctuating parts represent the turbulent deviations from the mean. The orthogonal components can be written such that:

$$U = u + u' \quad \textbf{(2.8.a)}$$

$$V = v + v' \quad \textbf{(2.8.b)}$$

$$W = w + w' \quad \textbf{(2.8.c)}$$

Although by definition the time average of the fluctuating components is zero, the time average of their squares and mixed products is not. This aspect is further explained in section 2.4.4.a.

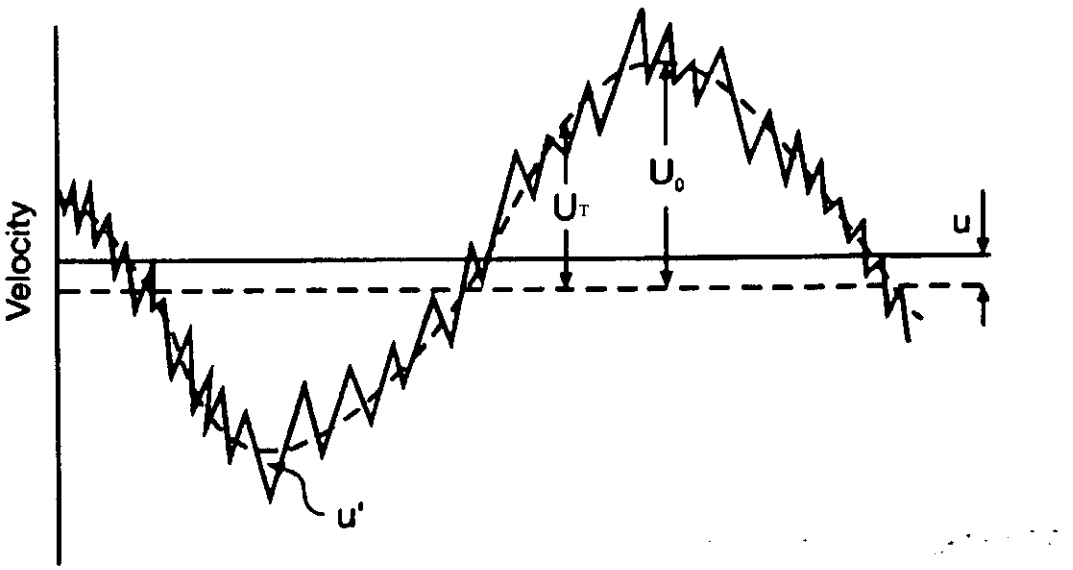

Figure 2.17 Definition sketch for the mean (u), tidal (U_T) and turbulent (u') velocity components from a velocity time series. U_o is the amplitude of tidal oscillation in longitudinal velocity (from Dyer, 1997).

Generally, the motion of a volume of fluid is determined by the forces acting upon each particle, i.e. gravity, and the forces acting on each part of the surface - the pressure and viscous shear stress. Mathematically, these forces are related by the Navier-Stokes equations which describe the conservation of momentum. The non-linearity of the turbulence term means that the equations have to be solved numerically, and for this reason, the mathematical description of turbulent motion varies depending upon the specific nature of the required resolution.

Sediment transport simulation models require a more simplified representation of the turbulent component due to the cost and time of computing power. These types of modelling approaches do not try to represent the chaotic redistribution of the fluid due to turbulence. Instead they allow representation of the average effect of these motions on the mean flow properties by the use of a closure model. These close the time-averaged equations of motion by relating the unknown turbulence correlation to the appropriate averaged variables. Such closure models are a simple eddy viscosity model as derived originally by Boussinesq during the 1870's; a mixing length approach (Prandtl, 1938); or more complex K-ε models (Rodi, 1980). However, these approaches do not represent the actual fluctuating motions and the associated stresses. The application and implementation of these various turbulence parameterisations, have been rigorously assessed as part of tasks A and E during the EC MAST III COSINUS project.

2.4.4 Estimation of the turbulent shear stress

Shear stresses can be estimated from high frequency current velocity measurements and there are a number of methods to achieve this estimate; these are principally: *1.* from a logarithmic profile, *2.* measuring Reynolds stress, and *3.* determining turbulent kinetic energy. As stated earlier, under idealised conditions the wall region would exhibit a logarithmic profile, but when there are large temporal and spatial variations in particulate concentration and water density and when the flow may also be stratified at times, this approach is not feasible. Also the logarithmic profile would require numerous sensors. Therefore, for the work undertaken for this thesis, the two common alternative methods were considered.

2.4.4.a Reynolds stress method

This method utilises Reynolds stochastic turbulence representation method explained earlier. The turbulent Reynolds stresses arise because, although the time-averaged velocity fluctuations are zero, the time average of their squares and mixed products is not. This is because the motions are not symmetrical and the times spent by the vectors in different directions are not equal. Hence, the fluctuating velocities in any two orthogonal planes are assumed to be inversely correlated, i.e. the sign and magnitude of one has an important influence on the sign and magnitude of the other. For example, if we consider fluid particles moving upwards, they carry a momentum deficit into the faster flow above. Conversely, fluid moving downwards carries excess momentum into the slower moving layers below. This momentum exchange creates a retardation in the flow which is of the form of a shear stress (τ) acting on the plane under consideration. If there was no retardation, it would create an acceleration in the fluid. Hence the momentum flux (F) across the horizontal plane parallel to the flow direction is:

$$F = \overline{\rho UW} = \rho uw + \rho\overline{u'v'} + \rho\overline{u'w} + \rho\overline{uw'} \qquad \textbf{(2.9)}$$

The first term is the advective flux on the mean flow, the second the turbulent momentum flux, i.e. the shear stress; the remaining two components are by definition zero. Thus τ is equal to the time average u'w' which is usually negative (negative because of the direction of the coordinate axes), i.e.

$$\tau = -\rho\overline{u'w'} \qquad \textbf{(2.10)}$$

Similarly, there are stresses on two vertical planes due to interactions between the streamwise horizontal (equation 2.11), and the vertical (equation 2.12) fluctuations, with the lateral fluctuations, respectively.

$$\tau = -\rho\overline{v'u'} \qquad \textbf{(2.11)}$$

$$\tau = -\rho \overline{v'w'} \qquad (2.12)$$

These turbulent stresses are called the Reynolds stresses and they are a measure of the flux of momentum at a given height. The Reynolds stresses are responsible for the transfer of energy between the mean flow and the turbulence. Thus the momentum exchange is the shear stress at that height. The structure of the Reynolds stress near a boundary has been examined in the laboratory by Nychas et al. (1973) and Offen and Kline (1975), both using flow visualisation techniques. They found that the production of Reynolds stress was intermittent and it was associated with a sequence of motions collectively called "bursting". Dyer (1996) explains that the Reynolds stresses can be thought of as being produced by a combination of positive and negative fluctuations in the x and z directions, and are hence composed of four contributing events:

1.	an ejection event	$u' < 0, w' > 0$	u'w' -ve
2.	an outward interaction	$u' > 0, w' > 0$	u'w' +ve
3.	a sweep event	$u' > 0, w' < 0$	u'w' -ve
4.	an inward interaction	$u' < 0, w' < 0$	u'w' +ve

A schematic of the quadrant analysis of turbulent fluctuations is shown in Figure 2.18. Situations 1 and 2 represent a movement of fluid away from the boundary, and 3 and 4 a movement towards the boundary (Dyer, 1986). However, a combination of 1 and 3 gives a negative contribution to the value of u'w' and consequently a positive shearing stress. Whereas 2 and 4 combined results in a positive contribution to u'w' and a negative Reynolds stress. Only the ejection and sweep events provide a positive contribution to the Reynolds Stress. It has been estimated that up to 70% of the stress generated may be caused by ejections, even though they exist for only 20% of the time (Dyer, 1986). Furthermore, Heathershaw (1974) observed from field measurements that 57% of the stress is developed in only 7% of the time.

With the Reynolds Stress method it is assumed that the measurements are made within a constant stress layer, and the turbulence is assumed anisotropic. Both Heathershaw (1979) and Soulsby and Humphery (1989) point out that the error in the shear stress estimation due to misalignment of the sensor in the vertical axis may be as much as 156 % per degree of misalignment. Sensor alignment to this level of accuracy is not always possible in a field experiment.

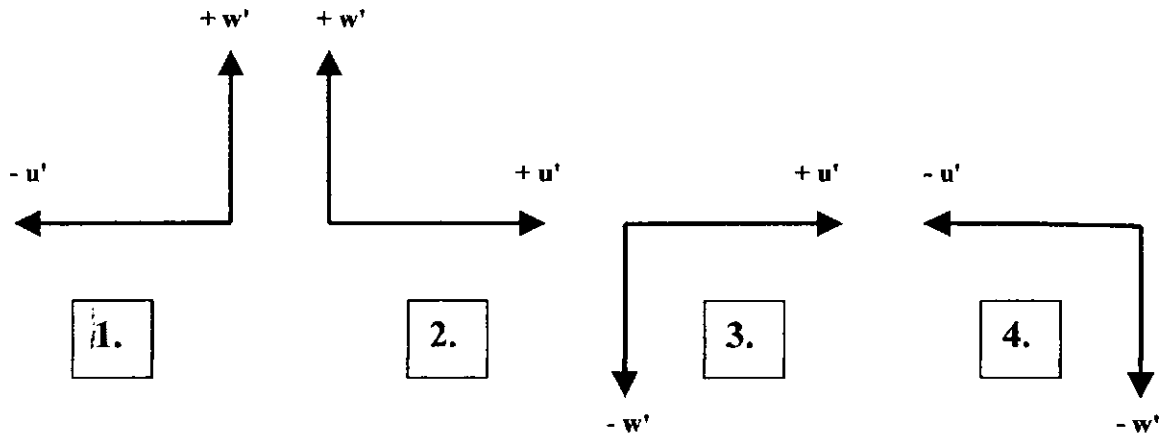

Figure 2.18 Quadrant analysis of turbulent fluctuations contributing to Reynolds stress. The origin is moving at the mean stream velocity. *1)* Ejections, *2)* Outward interaction, *3)* Sweeps, and *4)* Inward interaction (from Dyer, 1986).

2.4.4.b Turbulent kinetic energy (TKE) method

This method is less sensitive to sensor misalignment, as it requires the simultaneous measurement of flow velocity in all three orthogonal planes. The turbulent kinetic energy (Stapleton and Huntley, 1995), E, can be calculated from equation 2.13:

$$E = 0.5\rho_w\left(u'^2 + v'^2 + w'^2\right) \qquad \textbf{(2.13)}$$

Within the wall region, the energy production equals the energy dissipation, so the turbulent shear stress is proportional to the turbulent kinetic energy. Using the constant of proportionality observed over a wide range of flows, Soulsby (1983) suggests the turbulent shear stress τ, can be calculated by:

$$\tau = 0.19\ E \qquad \textbf{(2.14)}$$

Using the TKE method, one could expect to achieve turbulent shear stress accuracies of $\pm$4-5% when utilising high frequency electro-magnetic current meter based systems (assuming reasonable being made during the sensor deployment). For a shear stress of 1 Nm^{-2}, this would translate into a potential error of ± 0.05 Nm^{-2}. This was the main method used for the turbulent shear stress estimation for the flow data obtained during this study.

2.5 Floc mathematical modelling

Various mathematical models of flocculation under turbulent conditions have been put forwards. Early studies by Argaman and Kaufman (1970) and Parker et al. (1972) derived a model that simultaneously examined the flocculation response to turbulence induced growth and break-up. The formulae included many parameters that were difficult to measure, and

Ayesa et al. (1992) later formulated a calibration algorithm for the model, based on experimental results using varying particulate suspension levels. However, this still provided little information about the settling characteristics of the aggregates.

More recently, a number of authors have proposed simple formulae inter-relating a number of floc characteristics which can then be calibrated by empirical study. Such an approach has been used by Van Leussen (1994), who has utilised a formula which modifies the settling velocity in still water, by a growth factor due to turbulence divided by a turbulent disruption factor:

$$Ws = W_{so}\left(\frac{1+aG}{1+bG^2}\right) \qquad \textbf{(2.15)}$$

where Ws is settling velocity, G is the root mean square of the gradient in turbulent velocity fluctuations, a and b are empirically determined constants. G (with the units s^{-1}) is obtained by taking the square root of the turbulent energy dissipation rate ε divided by the kinematic viscosity ν; ε measures the rate at which turbulent energy is dissipated as heat through the action of viscosity. It is worth noting that viscosity is most important at the smallest scales (for which the Reynolds number is small) and it is here that most of the energy is dissipated.

$$G = \left(\frac{\varepsilon}{\nu}\right)^{0.5} \qquad \textbf{(2.16)}$$

The reference settling velocity (taken at zero turbulence), W_{so}, is related to the SPM concentration (C) by:

$$W_{so} = k \cdot C^m \qquad \textbf{(2.17)}$$

where k is an empirical constant, and m is the exponent. Equation 2.15 is a qualitative simplification of the Argaman and Kaufman model, with only a limited number of inter-related parameters, and hence does not provide a complete description of floc characteristics within a particular shear environment.

Lick et al. (1993) similarly derived an empirical relationship where floc diameter (D) was found to vary as a function of the product of the SPM concentration and the turbulence parameter G, where c and d are empirically determined values:

$$D = c(SPM \cdot G)^{-d} \qquad \textbf{(2.18)}$$

A more complex model has been proposed by Winterwerp (1996). This was based on research by Kranenburg (1994) who made the assumption that flocculated mud could be

represented by a self-similar fractal structure. This is similar to the order of aggregation theory, suggested by both Krone (1963, 1986) and Partheniades (1965) and was explained in section 2.3.1. Primary particles of diameter D_p, are related to the floc size D as follows:

$$N \sim \left(\frac{D}{D_p} \right)^{nf} \tag{2.19}$$

where N is the total number of particles in the fractal aggregate, and nf is the fractal dimension.

$$nf = \left(\frac{\ln m_1}{\ln m_2} \right) \tag{2.20}$$

where m_1 is the number of primary particles to form a first order floc; m_2 is a factor by which the floc will increase in size during this hierarchical process. From this, Kranenburg derived that :

$$\rho_e = \rho_f - \rho_w = (\rho_{sed} - \rho_w) \left[\frac{D_p}{D} \right]^{3-nf} \tag{2.21}$$

with ρ_f representing the floc bulk density, ρ_{sed} and ρ_w the sediment and water density, respectively. The fractal dimension is effectively the slope of the curve of size against settling velocity, or effective density.

Substituting equation 2.21 into the classic Stokes' equation, Winterwerp obtained the following relationship:

$$Ws = \alpha' \cdot D_p^{\,3-nf} \frac{(\rho_{sed} - \rho_w) g}{\mu} D^{nf-1} \tag{2.22}$$

Where α' is an empirically derived constant, and μ is molecular viscosity. Equations 2.21 and 2.22 were substituted into a simple aggregation and break-up formula based on G as the turbulence factor, to provide a linear combination of the processes. Values for the fractal dimension generally range between 1.4 (for fragile flocs) and 2.5 (for strong estuarine flocs).

However, in order to make the model solvable analytically, an average nf value has to be used. Using data provided by Van Leussen (1994), Gibbs (1985), and Fennessy et al. (1994a), Winterwerp conducted a linear regression and revealed an average nf of 2. The fractal theory was developed assuming one size and type of primary particle, whereas there may be several constituents of several sizes and densities which may not aggregate in a self-similar fashion.

Another model, proposed by Hill (1996), uses sectional and discrete representations based on the Pandya and Spielman (1982) statistical population-balance approach to floc breakage, which was then incorporated into commonly used particle-aggregation models. Similar to the Winterwerp model, this approach treats the flocs as fractal objects, and hence requires an average fractal dimension value.

However, initial video camera field studies of sediment floc characteristics over a tidal cycle by Fennessy et al. (1994b) revealed significant variations in floc effective density. The applicability of an average fractal dimension, the heuristic van Leussen formula, the empirical approach offered by Lick et al. (1993), together with other commonly employed modelling parameterisations of floc settling velocity will each be examined later in this thesis. They will be compared with new empirical algorithms developed from the experimental results of this thesis.

2.6 Summary

This literature review has shown that estuarine flocculation is an important factor to consider when estimating cohesive sediment behaviour and movement. Hydrodynamical turbulence is known to have an effect on the characteristics of the flocs produced, however very little quantitative data exists on in-situ floc formation. This has principally been due to the absence of specialised instrumentation which could measure simultaneous floc size and settling velocities, together with sensors which could accurately describe the turbulent structure of the water column from which the flocs were sampled. Thus, the next chapters of this thesis will illustrate how two unique instruments, INSSEV and POST, were used to obtain high quality floc and turbulence data in-situ, along with a number of controlled laboratory experiments. This data is then used to qualitatively describe floc spectra at pertinent times in a tidal cycle, and examine the various population sub-groups of flocs which co-exist. The data will also be statistically assessed to find quantitative correlations, with the aim of improving current flocculation parameterisations for the practical implementation into mathematical estuarine cohesive sediment dynamical models.

Chapter Three:

Experimental Methodology

This chapter outlines the strategy and operational conditions of the different experiments conducted to acquire the floc and turbulence data for this study. Sections 3.1 and 3.2 describe the in-situ field experiments which were conducted in the Tamar Estuary and Gironde Estuary, respectively. Locations were specifically chosen in each estuary where current flow was the dominant producer of turbulent shear stress, and surface waves were not deemed significant. The principle instrumentation is also detailed in section 3.1, and was deployed so that detailed in-situ near-bed high frequency measurements of velocity and turbidity could be made, together with the resultant changes in the floc population. Master variable data was also obtained from the larger scale flow patterns.

To further assist the interpretation of the in-situ data, a series of laboratory experiments were conducted at both the University of Plymouth (UOP), and Laboratoire des Ecoulements Geophysiques et Industriels (LEGI) in Grenoble (France). Each series of experiments looked at specific aspects of the flocculation process. The UOP experiments, described in section 3.3 and Appendix I, examined flocculation in low turbidity environments over a wide range of turbulent shear stress. In contrast, the experiments carried out at LEGI, described in section 3.4, employed concentrations ranging up to CBS levels (5-8 gl^{-1}), together with typical moderate to high estuarine turbulent shear stress levels.

3.1 Tamar estuary experiment

A series of three deployments were carried out within the upper Tamar Estuary (Figure 3.1). The aims were to measure the effect of velocity shear and turbulence, salinity, and concentration on the size, settling velocity and effective density of mud flocs. The relationship of these parameters to the concentration and velocity profiles would be tested against theory and the results of laboratory measurements. The results were also used to test and calibrate a new sediment transport model of the Tamar estuary (Peterson et al., 2000).

To meet the experimental aims, it was not deemed crucial to record data continually through out each consecutive tidal cycle. In the first instance this would produce too great a volume of data to process. Secondly, in order to sustain a high quality of data acquisition, the instrumentation required regular servicing in the form of zero off set checks for the EMCMs

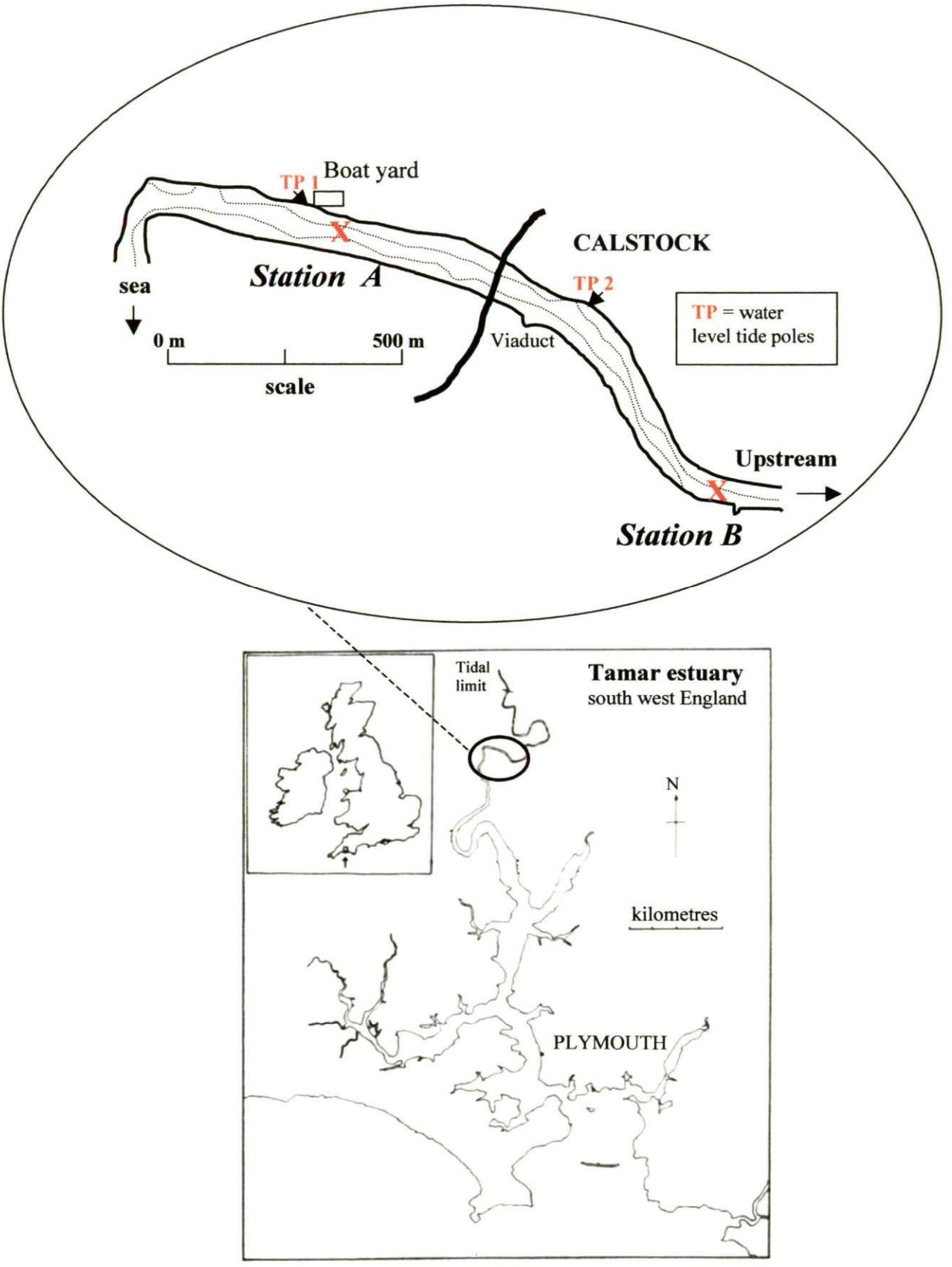

Figure 3.1 Location diagram of the Tamar estuary showing the positions of Station A and B.

and settling column recharging for INSSEV. Also the difficulty and dangers of deploying the rig at night, precluded a continual sampling regime. It was therefore decided to cover more variable conditions over a shorter duration at times when flow conditions were either reasonably steady or gradually changing in order to be able to reliably correlate floc characteristics with flow parameters. This permitted the investigation of detailed processes on a sub-tidal scale.

The general strategy was to deploy both the INSSEV and POST instruments in the mid-channel near bed region. This would permit the acquisition of floc characteristics together with turbulence and suspended solids time series. Two sampling Stations (A and B) were utilised in the upper Tamar estuary; it was anticipated that this would attempt to account for the advection. Regular through depth profiles of salinity and temperature, plus water samples intended for gravimetric and bio-chemical analysis, were collected at both stations during floc / turbulence sampling. Measurements were made during ebb and floods throughout neap and spring tidal conditions. All data presented in this thesis was from Station A unless otherwise stated.

3.1.1 The Tamar estuary

Located on the south-western peninsula of England, the Tamar Estuary provides a natural division between the counties of Devon and Cornwall. Although it is a relatively small estuary, it has been the subject of numerous earlier studies. The Tamar, like many British estuaries is a product of sea level rise which occurred during the Flandrian Transgression of the late Holocene. As a drowned Quaternary drainage channel, the Tamar is topographically dendritic in shape; it has numerous meanders and wide mud flats exposed at low water, and so can be classified as a drowned river valley (i.e. a ria). The estuary drains the high ground of Dartmoor and the surrounding rural farm land predominantly through three fresh water rivers, and eventually discharges into the English Channel at Plymouth Sound. The main contributor is the River Tamar which has a 470 km^2 catchment zone, and from source to estuary mouth it is approximately 75 km in length. However, the tidal influence extends only 31 km inland to Weir Head, near Gunnislake. The annual mean river discharge from River Tamar is approximately 20 m^3s^{-1}. The Rivers Lynher and Tavy, 25 km and 21 km downstream from the head, respectively, provides an additional catchment area of 332 km^2.

3.1.1.a Tidal and bathymetric conditions

The Tamar estuary experiences semi-diurnal tides with mean neap and spring ranges of 2.2 m and 4.7 m respectively. This classifies the Tamar as mesotidal (Davies, 1964). The harmonic constituents of the tide raising forces acting on the Tamar Estuary have been documented by George (1975). Bathymetrically, the lower part of the estuary (known as the Hamoaze) contains deep (18-25 m) navigation channels and has an approximate width of 900 m at the high water mark. In the upper reaches, the estuary channel becomes much narrower (40-200 m) and mean depth also reduces to 1-2 m at low water. These variations in the estuary cross-section and frictional effects produce asymmetry in the tidal curve and a flood current dominance at the head. During spring tides, the ebb can occur up to an hour later at the estuary head, from that of the predicted time at Devonport.

3.1.1.b Sediment characteristics

The majority of the sediment within the Tamar is supplied by river input. Most of this sediment is predominantly cohesive silts, and clay admixtures. Fitzpatrick (1991) found Tamar estuary mud to be generally high in kaolinite (primarily a result of extensive china clay quarrying within the catchment area), together with the presence of both illite and montmorillonite. The tidally enhanced mixing which occurs towards the estuary head, adds a great deal of seasonal mobility to the steep mudbanks of the upper Tamar. The mudbanks have a median particle diameter of 20-30 μm (Uncles and Stephens, 1993). However, the low water channel bed is composed of a sand and gravel mixture, together with some ephemeral cohesive sediment. In contrast, the mudflats in the lower reaches of the estuary are thought to be areas of long term deposition. Measurements by Clifton and Hamilton (1979) reveal that the mudflat near St. Johns Lake were accreting at a rate of 1 cm $year^{-1}$. Mobile bed sediments range from 99% cohesive sediments (where % < 63 μm, by sieve) in the upper regions, and drops to around 60% at the mouth (Bale, 1987), although there is a large amount of local variation. Stephens et al. (1992) found the mean density of the surface layer of these mud deposits to be increasing downstream. Turbidity is typically low in the mid to lower estuary locations, in contrast to upper section where SPM concentrations of the order of several gl^{-1} can be observed.

3.1.1.c Circulation and residual fluxes

Under average run-off conditions, Uncles et al. (1983) found the Tamar Estuary to be generally partially mixed. In the lower section of the estuary salinities are in the range of 20-35. Tidally produced bed stresses in the Tamar increase up-estuary. This is a result of

magnification of the tidal currents due to the decreasing channel cross-section outweighing the frictional tidal energy dissipation. A maximum tidal current velocity (up to 1 ms^{-1} during a spring tide flood), and thus re-suspension, occur in the upper reaches of the Tamar Estuary, where salinity is significantly reduced (0-5). Uncles et al. (1985) explains that this locally enhanced tidal bed stress together with tidal pumping (set up by the tidal asymmetry) are the main contributors to the generation and maintenance of the turbidity maximum (TM). Hence, the upper estuarine zone of accumulation of mobile particles is also subject to locally enhanced tidally controlled resuspension. Together, these processes determine the sharp localisation and high relative magnitude of suspended particle mass in the upper Tamar estuary, and its characteristic variations through semi-diurnal and spring-neap tidal cycles (Bale et al., 1985). Previous surveys conducted at Calstock (McCabe, 1991) found, during average river discharge conditions, that typical nearbed SPM concentrations within the TM varied from 100-500 mgl^{-1} at neap tides to 4-8 gl^{-1} during spring conditions. This mobile stock of bed-source sediment shifts longitudinally in response to seasonal changes in freshwater run-off and tidal range. From December to March, there is a reduction in SPM at the head of the estuary, mainly due to sediment being scoured from the upper estuary by strong ebb currents, enhanced by the high seasonal run-off. Under these conditions the TM is located approximately 14-17 km from Weir Head at Gunnislake. From April to November, as the winter run-off reduces, so the TM relocates to the zone 5-14 km from Weir Head (Uncles et al., 1994).

At the lower end of the estuary, tidal pumping is directed down estuary at both spring and neap tides, so the sediment is flushed out to sea with the fresh water. In the upper reaches, river inputs and Stokes drift account for observed residual currents. The depth averaged residual currents in the upper region of the estuary during spring tides can reach 10 cms^{-1} under average run-off conditions. This decreases to ~2 cms^{-1} at neap tides (Uncles et al., 1985) due to the much smaller frictional dissipation effect of the lower tidal range (Uncles and Jordan, 1980). At the estuary mouth, Stokes drift was typically 0.5 cms^{-1} and 0.1 cms^{-1} at spring and neap tides, respectively.

3.1.2 The Calstock sampling location

An experimental site within the turbidity maximum zone was chosen, because its overall characteristics are fairly well documented (Uncles and Stephens, 1993). In this situation it was expected that there would be considerable settling and erosion of mud from the bed at times during the tidal cycle, and that the suspended sediment dynamics would be dominated

by the bed boundary conditions. Also within this location the water remains predominantly fresh, reducing stratification effects, which would add additional complications to the interpretation of the data. Generally, the concentrations of particles expected on the flood tide are about twice those on the ebb, and those on spring tides range from two to ten times those on neap tides. Similarly, peak current velocities are twice as fast at spring tidal conditions than those at neap tides.

Sampling at this location under different tidal conditions would provide a wide range of turbulence and particle concentration conditions from which the flocculation response could be examined. Deployments were scheduled for the summer and early autumn periods when it was expected that the turbidity maximum would be located between Cotehele and Morwellham (Bale et al., 1987). To minimise the influence of lateral variations on the measurements, a relatively straight section of the estuary was needed. A further consideration was a Queen's Harbour Master (QHM) stipulation that our vessels did not present a potential obstruction or hazard to other marine traffic within the estuary. Taking all the above points into account, the 1.5 km reach at Calstock (see Figure 3.1 page 45, and Plates 3.1 and 3.2), 23 km from the estuary mouth, provided an optimum location. The seaward stretch of the channel up to the town centre slipway is orientated east-south-east, then it changes to a south-east direction. Either side of the 1.5 km stretch are gentle meanders. At low water the flat bottomed main channel has a depth of 1-2 metres and steep mudbanks (~45°) are exposed on both the Devon and Cornish sides.

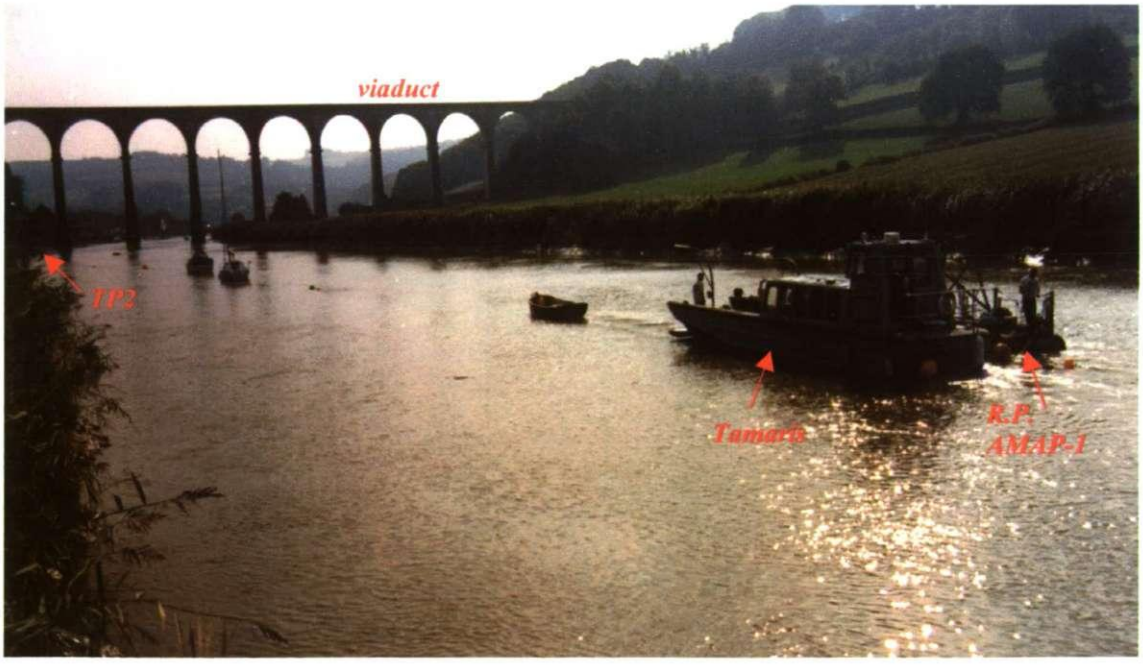

Plate 3.1 Calstock Station A location, looking east towards the viaduct (upstream).

Plate 3.2 Calstock Station A location, looking west (downstream) approaching LW.

The most comprehensive of the three Tamar experiments was experiment 3. This consisted of eight sampling deployments, of approximately three hours duration each, completed during the two-week period of the 14-24th September 1998, covering neap, then spring tide conditions. Experiment 3 formed the principle field measurement campaign for the EC MAST III project COSINUS, and a total of 22 scientists participated throughout the two week period. Two fixed stations were occupied in the Calstock region of the upper Tamar estuary (Figure 3.1). The Plymouth Marine Laboratory (PML) craft, *Tamaris* (a Rotork Sea Truck), and the UOP pontoon, *R.P. AMAP-1*, were both moored 350 metres west of the viaduct at Calstock (Station A: 50° 29.85' N, 04° 12.90' W). A second PML vessel, *Sepia*, was moored 970 metres east of Station A (Station B: 50° 29.57' N, 04° 12.27' W, upstream of Station A). To reiterate, the objective of working two adjacent stations was to try to separate the contribution of advective transport from local processes. UOP and PML worked solely at Station A, with the main portion of the work conducted at Station B being undertaken by Hydraulics Research Wallingford (HRW) and the University of Wales Bangor (UWB). Both vessels were chartered from PML and had 240 volts AC power from on-board generators. Each vessel was positioned in the main navigation channel by fore and aft moorings supplied by Calstock Boat Yard.

Two preliminary Tamar estuary experiments, 1 and 2, were conducted during spring and neap conditions, respectively. Experiment 1 was conducted between 22-25th June 1998, with the second experiment being carried out from 3-6th August 1998. The general aims for 1 and 2, were the same as those for experiment 3. These experiments would provide additional floc and hydrodynamic data which could be compared with the results from the September

deployments. This would provide a better insight into recurring trends in flocculation, and similarly provide a level of redundancy to interrelative algorithms derived from the results. During experiments 1 and 2, measurements were only made at Station A, so no quantification of advection effects could be made. Again, the vessels *Tamaris* and *R.P. AMAP-1* were employed (as earlier described), and sampling protocols were generally the same as for experiment 3. These two initial experiments were undertaken jointly by PML and UOP, and a total of seven individual data sets were obtained.

3.1.3 Instrumentation description.

Both Tamar and Gironde estuary field campaigns deployed instruments that were particular to the respective studies but, throughout both programmes, a core of two instruments were always used. This included the INSSEV instrument, which could obtain high quality floc images and settling rates in-situ, and is generally regarded as a benchmark to which other floc sampling instruments can be compared. The second was the POST system. This was employed to measure high frequency flow velocity and turbidity variations, from which both turbulent shear stress and concentration values were determined. The following sections describe the main instruments used during the field study programmes. The instrumentation utilised during the laboratory studies was less complex and is outlined in the respective methodology sections.

3.1.3.a INSSEV instrument

The INSSEV - IN-Situ SEttling Velocity - instrument was developed at the Institute of Marine Studies, University of Plymouth by Fennessy et al. (1994a). It has the distinct advantage of permitting the simultaneous measurement of both floc size and settling velocity in-situ. The sampling apparatus is a two chamber device (see Figure 3.2), with an integral underwater video camera which views the flocs as they settle within a lower settling chamber. The apparatus requires physical stability in order to both capture a floc sample of good integrity, and to allow the camera to view the flocs precisely. Thus, to prevent any vertical and horizontal motion during a sampling deployment, it is secured to a heavy bed frame, which sits on the estuary bed. This restricts the INSSEV system to making floc measurements within an Eulerian reference frame, and close to the bed.

To initiate a floc sampling cycle, the decelerator is allowed to flush with both flap doors

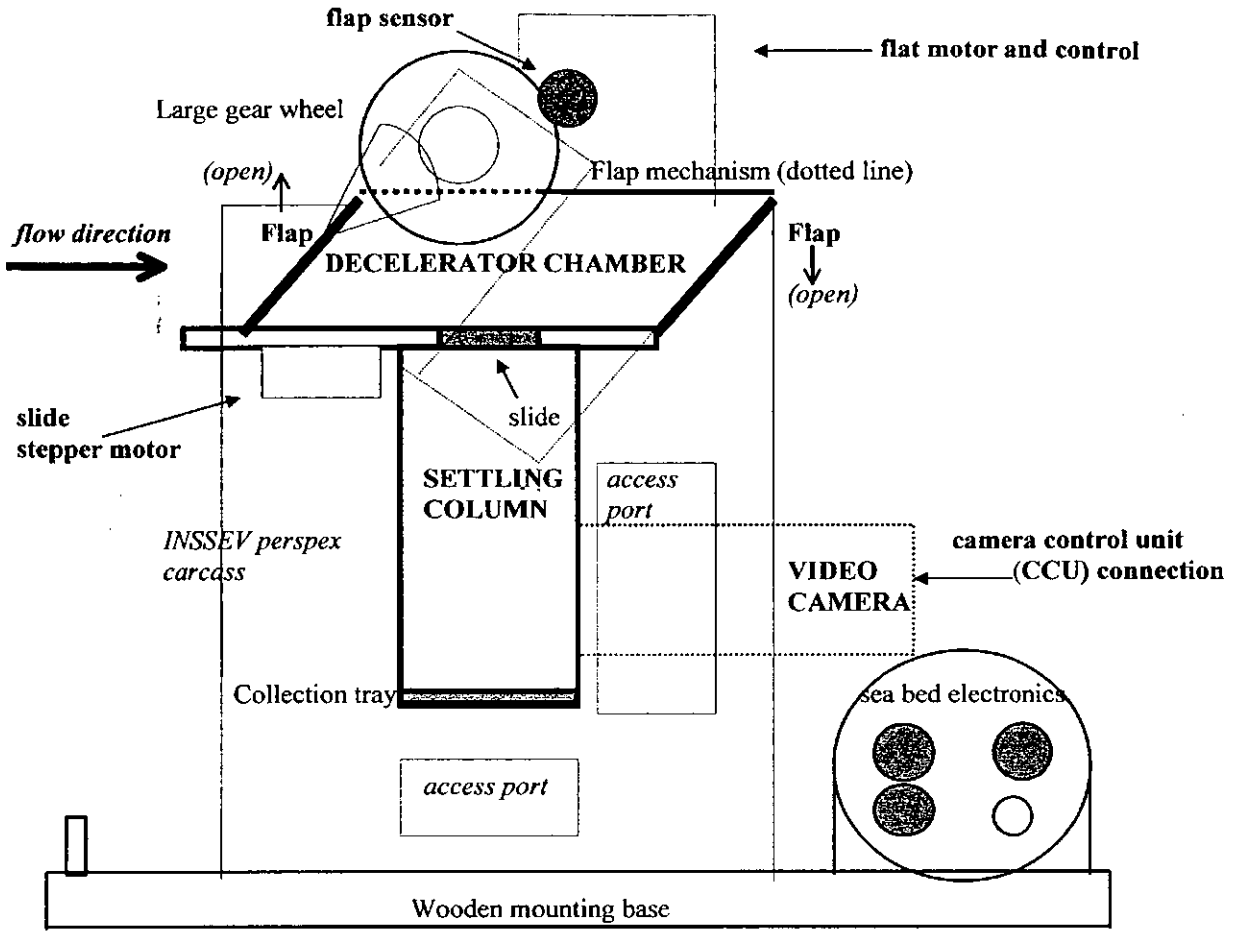

Figure 3.2 A schematic of the INSSEV sampling unit - version 1.3. The side elevation shown with flaps closed (from Manning and Fennessy, 1997).

open and the slide door closed. The flap doors are then closed slowly to isolate ~3 litres of estuary water in the decelerator chamber. Precise alignment of the instrument minimises the occurrence of eddy shearing and potential damage to the sampled flocs. The flaps are programmed by the operator to close at a rate such that the flow velocity in the chamber is reduced to zero, without inducing additional turbulence and causing aggregate break up. The rate of closure is chosen relative to near surface velocity measurements. A period of turbulence decay then commences once the flaps are fully closed. For practical purposes, a nominal period of 20 seconds was used for all of the INSSEV samples obtained for this study. Although a longer period further reduces the turbulence within the collected water sample, a greater percentage of the flocs will potentially settle on to the slide prior to them entering the settling column.

A thin stainless steel slide door in the base of the decelerator chamber is opened to allow some of the flocs present in the decelerator to settle into the 180 mm deep lower settling column. The settling column was pre-filled with filtered water of slightly greater salinity,

and thus density, than in the estuary. This is to minimise the potential transfer of turbulence from the decelerator chamber and the formation of secondary circulations. Charging the column with a positive salinity contrast of approximately 4-6 produces the optimum results of turbulence damping, whilst still permitting low density flocs to settle. Also, this positive density contrast prevents any possible Rayleigh-Taylor instability occurring. Column instability resulting from ambient temperature variations are regarded as low, as temporal temperature changes in estuaries are generally very slow. The sampling apparatus sits on the estuary bed, thus it can be assumed that the water temperature within the column is the same as that of the ambient conditions. Most floc video systems experience temperature problems arising from heating by the camera illumination. This is minimised with INSSEV by the use of LED illumination.

To provide an optimal number of settling flocs in the settling column, the slide door remains open for a duration, T_{sd}, in seconds relative to the ambient water concentration (C) in mgl^{-1}, and was estimated by the following empirical algorithm:

$$T_{sd} = 1860 \cdot C^{-0.8} \qquad \textbf{(3.1)}$$

Operational control of the decelerator chamber flaps and slide door stepper motors was by a microcomputer housed in the surface vessel.

The INSSEV system requires a high resolution imaging system to be able to examine the flocs captured by the sampling apparatus. The complete video camera and recording system were constructed and supplied by Custom Camera Designs Ltd of Wells, Somerset, U.K. The flocs settling within the settling column were viewed by a Puffin model UTC 341 high resolution monochrome all-magnetic Pasecon tube video camera, with built-in integral low heat illumination. It had a 35 mm, F4, macro lens fitted behind a 12 mm thick opal glass faceplate with an anti-reflective coating. The complete camera unit was modified for underwater use by containing all the electrical circuitry within an aluminium outer casing, approximately 260 mm in length and 95 mm in diameter. The camera utilises a back-illumination system (i.e. a silhouetting technique) in which particles appear dark on a light background; this reduces image smearing, and makes the floc structure more clearly visible. This back-illumination is provided by an annulus of six high intensity red LED's (130 mW each) positioned around the camera lens; the camera's electronic circuitry senses the scene reflectivity and adjusts the voltage to the LED's accordingly. The camera is positioned vertically within an aperture in the settling column wall. It viewed all particles in the centre of the column which pass within a 1 mm focal depth of field, 45mm (focal length) from the

camera lens, and at a depth of 110 mm below the slide door. The total image size was 3.3 mm high and 4.7 mm wide.

The video camera was connected to a CCU350WA electronic Camera Control Unit (CCU) by a 20-core STC type 7-2-20C marine cable which enable real-time analogue video images to be displayed on a monitor in the surface vessel. Floc images were recorded by a Super VHS video cassette recorder, which interfaced with the CCU. The CCU provided time referencing information which could be super-imposed onto the recorded video images, and so aid in the processing of the raw floc data. The camera and video recorder combination has a practical lower limit of resolution of 20 μm.

In order to calibrate the video monitor, a scale ruler was placed in front of the camera lens, and both the vertical and horizontal dimensions of the screen were measured. For the auxiliary monitor: 1 mm in real size dimensions produced an on-screen image of 49.36 mm. The alignment of the camera axis to that of the settling chamber was determined by suspending a fine nylon plumbline in front of the camera lens and recording the image. This enabled the relative camera orientation to be made precisely in both vertical and horizontal planes, and the consistency of the image depth of field could be evaluated. A comprehensive review of INSSEV calibrations and operational procedures can be found in Manning and Fennessy (1997).

3.1.3.b POST system

High frequency near-bed measurements of the flow field and concentration gradients were made using the POST - Profile Of Sediment Transport - system. POST was originally developed by Christie (1997) for shallow water measurements on inter-tidal mudflats. The system consists of velocity and turbidity sensor units, with the respective seabed electronics being housed within two stainless steel pressure casings.

Flow velocity sensors

High frequency near-bed measurements of the flow field were made by using four 2 cm diameter discoidal electromagnetic current meters (EMCM). An example of a sensor is shown in Plate 3.3. These sensors are dependent on Faraday's law of electromagnetic induction. When an electrically conductive fluid moves through a magnetic field, an electromotive force is induced in a direction normal to both the motion of the fluid and the magnetic field. The EMCMs measure the voltage produced as the flow modifies the

magnetic field produced by an electromagnet energised by a square-wave direct current from within the sensor head. The induced voltage, detected by electrodes, is a linear function of flow velocity. Each head has two pairs of electrodes spaced 1 cm apart, allowing two orthogonal flow components to be measured. The volume of the flow sensed is taken to be a sphere of diameter equal to twice the electrode spacing.

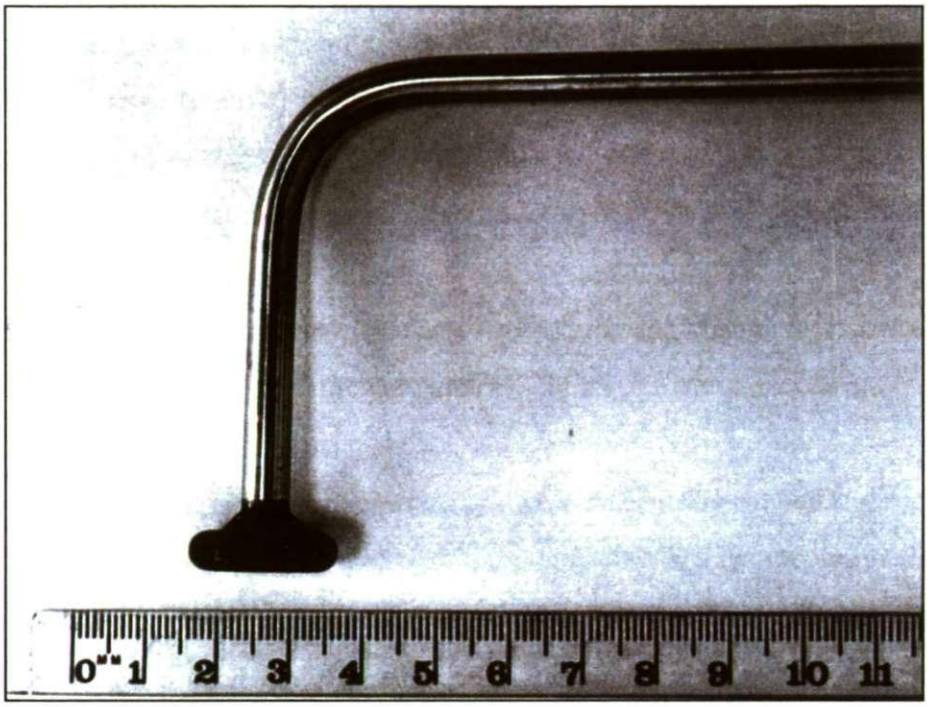

Plate 3.3 Side view of EMCM sensor comprising 2 cm discoidal head (from Christie, 1997).

In order to obtain flow velocity values, the sensors were calibrated by Christie (1997) using a laboratory annular flume. The sensors had a quasi-linear response to the flow velocity, with nominal noise levels of the order of 0.05 ms^{-1} at a flow velocity of 1 ms^{-1} (the maximum flow velocity which can be measured by the EMCM sensors). The calibration equation to obtain flow velocity, u (in ms^{-1}), is of the form:

$$u = a(V_{out} - V_{off}) \qquad \textbf{(3.2)}$$

where V_{out} is the digital voltage output from the sensor, V_{off} is the zero offset, and a is the calibration coefficient which varied for each sensor as follows:

EMCM1: $a = 0.000577\ ms^{-1}\ V^{-1}$ **(3.3.a)**

EMCM2: $a = 0.000496\ ms^{-1}\ V^{-1}$ **(3.3.b)**

EMCM3: $a = 0.000536\ ms^{-1}\ V^{-1}$ **(3.3.c)**

EMCM4: $a = 0.000527\ ms^{-1}\ V^{-1}$ **(3.3.d)**

EMCM5: $a = 0.000510\ ms^{-1}\ V^{-1}$ (Gironde estuary experiment only) **(3.3.e)**

Although EMCMs were not calibrated prior to each experiment (due to the annular flume facility not being available), previous experience has shown that it was the sensor zero offsets, rather than their sensitivity, that changed most between deployments. Thus, the electrical offsets of EMCM sensors vary appreciably with time. Therefore, zero flow offsets were recorded before and after a deployment. Christie et al. (1997), also examined the cumulative effects of increasing concentration on the response of the EMCMs. They concluded that taking into account the experimental error, suspended concentrations of up to 15 gl^{-1} did not significantly alter the sensor calibration. An example of an EMCM sensor calibration is given in Appendix V.

Turbidity sensors

The POST system utilised miniature optical backscatter sensors (OBS) to measure variations in the suspended particulate matter (SPM) concentration (Plate 3.4). These OBSs measure infrared radiation backscattered by particles in water at angles between 140° - 165°. An individual OBS consisted of a phototransistor and an infrared LED with a peak wavelength of 960 nm, mounted beside each other and both facing out towards the water column under observation. The received light is affected by the type and amount of suspended solids, and calibration permits a conversion of the backscattered intensity into a SPM concentration (Downing and Beach, 1989).

Each OBS was calibrated simultaneously on-site at intervals throughout each field study. Sediment from the sampling location was diluted into 12–20 homogeneous slurries of known concentration. The sensors were immersed in the stirred fluid and the sensor output for each OBS was recorded. The sensor output voltage ranges were optimised prior to calibration for each particular sampling location, so as to use more of the measurable scale (and provide a greater resolution) by adjusting the sensitivity of each OBS. An example of an OBS calibration is illustrated in Appendix V.

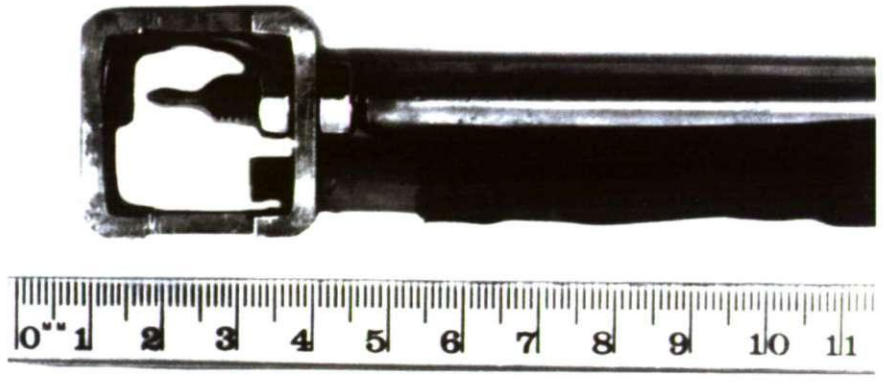

Plate 3.4 Side view of OBS sensor (from Christie, 1997).

POST control and filtering electronics

All data was recorded on a PC located on the surface vessel. In order to be confident that digital EMCM data was of a sufficient accuracy, Shannon (1949) stated that the Nyquist, or sampling, rate of the sensor must be at least twice that of the Nyquist frequency. This enables the usable flow or turbidity data to be separated from the instrumentation noise. The Nyquist frequency is the maximum frequency that can be reconstructed from discrete output and which the sensor will detect. The POST sensors have a Nyquist (sampling) rate of 18 Hz, and therefore a Nyquist frequency of 9 Hz. During data acquisition, aliasing problems can occur, whereby spurious high frequency components (above the Nyquist frequency) which are typically instrument noise, may be comparable with fluctuations in the flow being measured, and take on the identity of lower frequency components in the digital record. These aliasing errors can not be negated by post-processing filtering, and must be removed during the sampling procedure. Therefore, as suggested by Bishop (1991), the POST system has a low pass filter with a pass band of 5 Hz positioned at the front end of the analogue to digital (A/D) converter to counter the aliasing effects. Hence, data filtered at 5 Hz would provide sufficient resolution to meet the requirements of this study, and prevent aliasing.

The OBSs and EMCMs each had their own 8 channel A/D converters. Each A/D converter was 12 bits, with a full scale range of 5 V. This gives a voltage resolution of 1.22 mV. With regards to the OBS sensors, for nominal concentrations of up to 10 gl^{-1}, this translates into a digital resolution of 4.88 mgl^{-1}, but could be increased by altering the output gains for lower concentration scenarios (e.g. neap tide conditions). For the EMCMs, the digital resolution was 0.6 mms^{-1}, with a velocity measurable to an accuracy of $\pm$3%.

3.1.3.c Master variables

A SBE 19 SEACAT Profiler (from Sea-Bird Electronics Inc, Washington, USA) was used to measure the master variables, temperature, salinity, and pressure (depth) throughout the depth profile. The data was recorded at a logging rate of 2 Hz, and stored within a 128K byte internal memory. Temperature and conductivity accuracy was of the order of $\pm$0.01°C (full range: -5 to +35°C) and $\pm$0.001 Siemens per m (full range: 0 to 7 Sm^{-1}), respectively. Pressure data had an accuracy of $\pm$0.25% of the full scale range, which was 150 psi. All sensors were calibrated to the stated accuracies by the manufacturer. As the conductivity cell can be prone to error due to long term salt and organic contamination, a check on the conductivity sensor was made using filtered water samples of various salinities. A comparison showed the SEACAT sensor to be functioning within the stated accuracy.

An NBA DNC-3 impeller type current meter (NBA Controls Ltd., Hampshire) provided a direct readout of mean current speed and direction during the various field deployments, predominantly near to the water surface. Direction was accurate to $\pm 10^{o}$, and speeds up to 2.5 ms^{-1} were accurate to $\pm 2\%$. Manual recording from analogue dials meant that the recording resolution of the current speed was to the nearest 0.01 ms^{-1}. This instrument gave a real time current velocity value from which the INSSEV flap closing speed could be determined, and also provided a useful check for the calibrated POST EMCMs flow data.

3.1.3.d Ancillary instruments

A number of additional specialised instruments were employed throughout the Tamar estuary field work programme to provide either additional data, or aid in the data acquisition process. The two most relevant to the work presented in this thesis are reviewed in this sub-section.

Lasentec P100

This was a commercially available Par-tec 100 (Lasentec Inc., Redmond, WA 98052) laser reflectance instrument, which had been modified at PML and UWB for use underwater. The Lasentec P100 (Figure 3.3) was deployed periodically throughout the Tamar estuary experiment series to obtain profiles of floc size distribution. Using a rapidly scanning laser light focused to a point 0.2 x 0.8 μm (i.e. smaller than the flocs under observation), the instrument then measures the period of the backscattered pulse generated each time the focal point scans a floc in suspension. This sensor arrangement allows the Lasentec P100 to operate in turbid estuarine waters, whilst creating a minimal physical disturbance to fragile macroflocs. A minimum of 1000 counts is required for a measurement, and only flocs with a sufficiently coherent reflected signal that could be separated from background noise are registered. A correction algorithm is applied so as to produce a spherically equivalent diameter. The device is capable of sensing particulate matter within the size range 2-1000 μm, and bins them in 38 approximately logarithmic size intervals. The software can generate size distributions as either percentages of the total number of flocs or of the total volume. More details on the Lasentec P100 are given in Law et al. (1997).

Pontoon "R.P. AMAP-1"

The precise alignment, plus safe handling of the heavy (approximately 250 kg in air) bed frame containing the principle instrumentation, was the cornerstone to the proposed

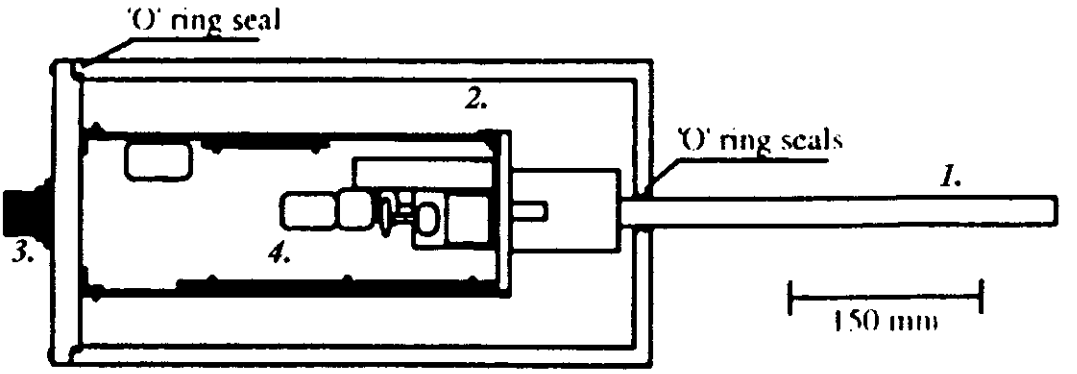

Figure 3.3 Schematic of the adapted Lasentec Par-tec 100 probe unit showing: *1.* the light guide, scanning mechanism and focusing lens, *2.* the PVC cylinder, *3.* watertight cable termination, and *4.* electronic circuitry and power supplies (from Law et al., 1997).

experimental measurements. With no suitable vessels available to meet the required deployment criteria, a nine week project to design and construct a lifting vessel commenced in January 1998. The final design produced a catamaran style pontoon, with a length of 7.0 metres and a beam of 4.3 metres (Plate 3.5). A combination of bolted and welded mild steel cold rolled angle sections formed the skeleton of the pontoon, with each hull being 1.25 metres wide by 0.6 metres deep. Plastic industrial 210 litre drums were utilised as the pontoon's floatation units; they were placed, in pairs, within the steel box-sections of each of the hulls. A total of 14 drums were used for each hull, providing a total combined displacement buoyancy of approximately six tonnes and a resultant net draught of 0.3 m. A 3.2 m high four-poster lifting derrick was positioned over a centred "moon-pool" 1.8 m wide by 2.6 m long. The derrick had a SWL lift capacity of 500 kg certified by Marlift of Plymouth. Dynamic stability tests were conducted, and this led to a safety certificate being issued. The pontoon called *R.P. AMAP-1*, currently a registered UOP vessel, was designed by A.J. Manning (thesis author), and fabricated jointly by A.J. Manning and A.J. Prideaux (Institute of Marine Studies technician). Manning (2001) provides a complete schematic of each stage of the pontoon's design and testing.

3.1.4 Instrumentation set-up and deployment protocols

The division of measurements for experiment 3 can be summarised as follows:

- UOP - deployed INSSEV and POST in a near bed region at Station A. This enabled simultaneous floc size and settling velocity spectra to be collected in-situ, together with complimentary high frequency flow and turbidity profiles. Master variable profiles and gravimetric samples were also collected at Station A. Also UOP made water surface slope measurements.

Plate 3.5 Views of the UOP research pontoon *R.P. AMAP-1* during: (1) fabrication at Queen Anne's Battery Marina, (2) prepared for its maiden launch from a mobile cradle, and (3) being moved to a berthing awaiting towage to Calstock (note the shallow draught of the pontoon).

- PML - measured in-situ floc size distributions with the Lasentec P100 at Station A.
- HRW - collected floc characteristic data via their HR video camera system (Dearnaley, 1996), predominantly at Station B. The SedErode instrument (Mitchener et al., 1996) and shear vanes measured the critical erosion shear stress of the surrounding exposed mudflats. Surface scrapes of the bed were also taken for compositional analysis.
- UWB - used the QUISSET settling tubes (Jones and Jago, 1996) to obtain floc information. Multi-corer samples were also collected at the end of the field study, plus matter variables throughout deployments at Station B.

During experiments 1 and 2, only the UOP and PML aspects were carried out (except for the water slope measurements).

Both the INSSEV sampler and the POST EMCMs required an uninterrupted flow reaching them in order to obtain a sample which was representative of the natural conditions. With this in mind, the POST flow and turbidity sensors were positioned on a vertical aluminium pole laterally off-set from the INSSEV sampler, both of which were at the very front of the

steel bed frame. The electronics casings were located to the rear of the frame, with all loose cables secured so as not to promote any excessive vibrations. The total weight of the frame and instrumentation was approximately 250 kg in air.

The INSSEV decelerator chamber collected floc samples at a mean height of 0.5 metres above the bed (Plate 3.6). The four EMCMs were arranged in pairs typically at heights 0.25 metres and 0.80 metres above the base of the frame (Plate 3.7). This configuration allowed one pair of flow sensors to measure the cross channel velocity V (y-axis), and vertical velocity W (z-axis), with the along channel component U (x-axis) being measured twice. This permitted three-dimensional flow velocities to be calculated both above and below the level sampled by the INSSEV instrument. This arrangement was used for all Tamar Estuary deployments with the exception of the 16 September (ebb tide) and 22 September (flood tide) deployments, when all flow sensors were arranged in a logarithmic profile which only measured cross stream and along channel flow components. All eight OBS probes were available for the Tamar field experiments, and these were arranged approximately logarithmically through the bottom 1.2 metres above the bed. A pressure transducer was attached to the frame and provided a continual record of the water depth during sampling. The exact sensor positions were recorded each day, and a summary of the sensor heights is summarised in Table 3.1.

The PML Rotork Sea Truck *Tamaris* was tied-up along side *R.P. AMAP-1*, and housed the surface electronics. Both vessels were located in the main channel throughout sampling, and their position maintained by fore and aft moorings (Plate 3.8). The predicted water column depth was not expected to exceed 7 metres at high water during spring tides. The bed frame was lowered through a "moon-pool" to the estuary bed by an electric winch from the UOP pontoon *R.P. AMAP-1*, with the sensors looking into the along channel flow (Plate 3.9). Deployment generally commenced at relatively low flow velocities at the start of the ebb or flood, with bed frame orientation controlled by ropes. Once on the bed, both the sensor cables and alignment ropes were tied up to minimise drag on the frame. If the rig was deployed at low water, a careful watch ensured that the flooding tide did not cause the rig to lift off the bed and rotate.

The NBA current meter recorded the flow velocity and direction at 0.25 metres below the water surface. Once the current velocity measurements had been input into the BBC computer memory, a floc sample could be obtained by activating the sampling sequence.

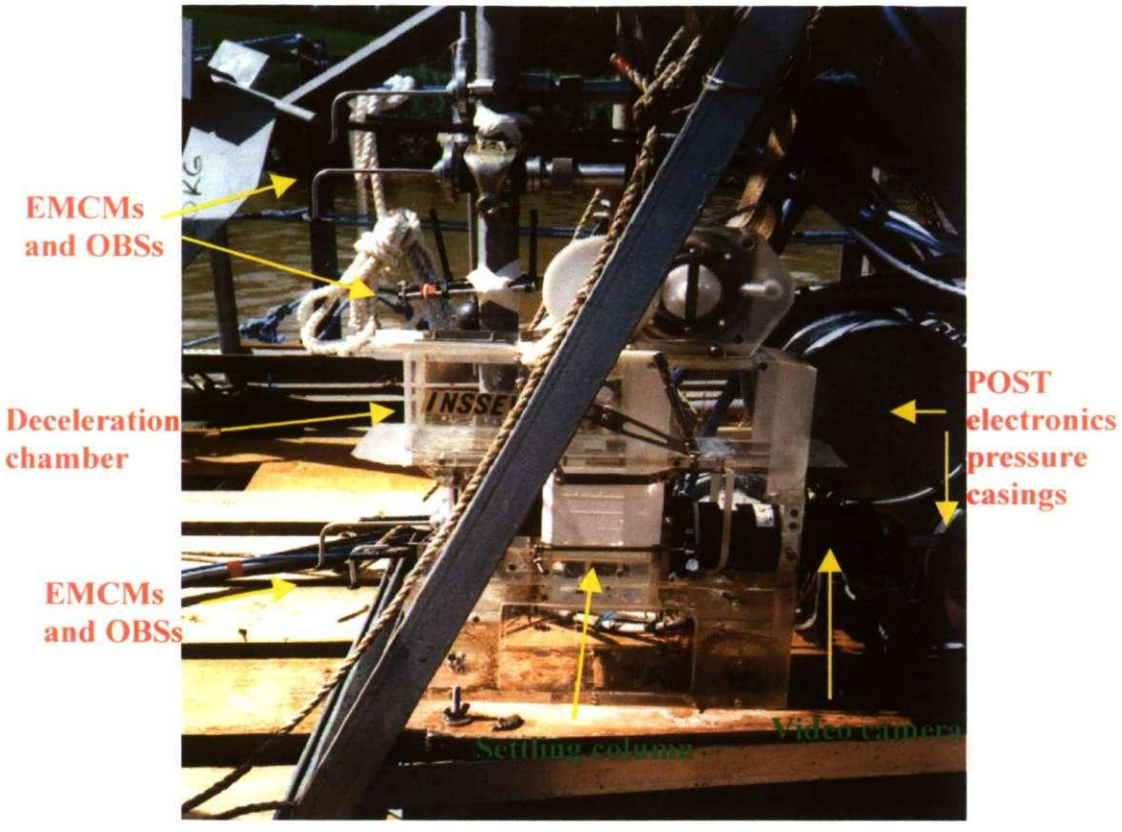

Plate 3.6 INSSEV sampling unit on estuarine bed frame - side view, with POST sensors in the background.

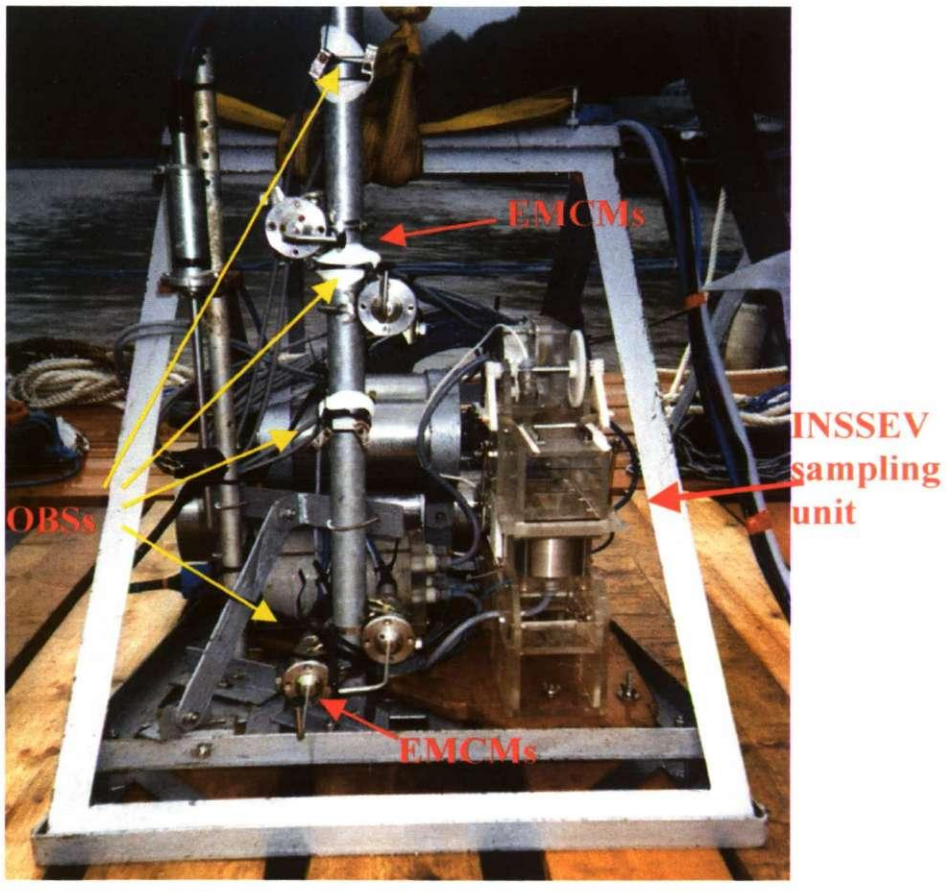

Plate 3.7 INSSEV and POST sensors mounted on the estuarine bed frame - front view.

Plate 3.8 Downstream view of the *Tamaris / R.P. AMAP-1* arrangement employed at Station A (this image was taken during experiment 3).

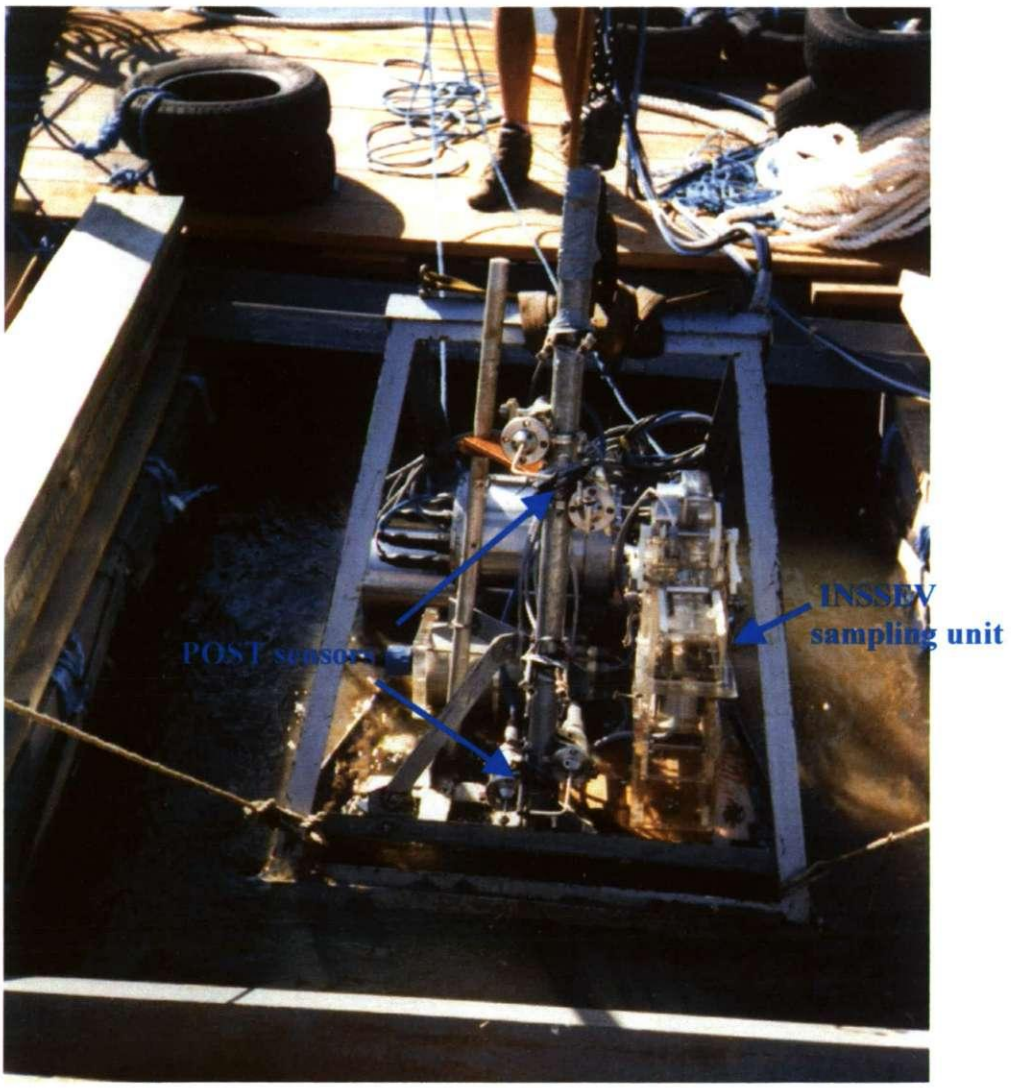

Plate 3.9 Instrumentation rig deployment from Station A at Calstock during spring tide conditions of experiment 3 (September 1998).

Table 3.1 **POST sensor heights for Tamar estuary experiments 1-3 for deployments at Station A, Calstock.**

Date	OBS probe	OBS heights above bed frame base (cm)	EMCM probe	EMCM heights above bed frame base (cm)	EMCM discus orientation
24/06/98	3	22	1	25	face up
	4	59	2	25	vertical
	6, 8	102	3	80	face up
			4	80	vertical
04/08/98	2	23.5	1	25	face up
05/08/98	3	48	2	25	vertical
06/08/98	4	76	3	79	face up
	6	87	4	79	vertical
15/09/98	1	15	1	25	face up
16/09/98	2	23.5	2	25	vertical
(morning	3	52	3	79	face up
flood run)	4	105.5	4	79	vertical
	6	104			
	7	87			
16/09/98	2	24	1	25	face up
(afternoon	4	105.5	2	28	face down
ebb run)	7	40	3	65	face down
			4	111	face down
17/09/98	1	15	1	25	face up
21/09/98	3	48	2	25	vertical
22/09/98	4	76	3	79	face up
(morning	6	87	4	79	vertical
ebb run)					
22/09/98	3	58	1	22	face up
(afternoon	4	104	2	34	face down
flood run)	6	119	3	65	face down
	7	47	4	107	face down
23/09/98	1	15	1	25	face up
	2	24	2	25	vertical
	3	59	3	83	face up
	6	90	4	83	vertical
	8	80			

The collected aggregates, as observed by the video camera, could be viewed in real time settling in the settling column; this provided an indication to the attitude of the bed frame. A new sample was not taken until there were no more flocs seen to be settling in the column. The INSSEV sampling rate, therefore, varied from 4 to 14 minutes, depending on floc settling velocities. Once the first INSSEV sample was taken, the VCR would remain recording throughout that particular deployment.

A typical three hour sampling deployment would see the UOP rig deployed at Station A, and profiles taken nearby with the Lasentec P100 (PML). Simultaneously at Station B, the HR

video floc system would collect the first floc sample from mid-water depth, and UWB sampled with their QUISSET tubes. Marine band VHF radio communication initiated the synchronised deployments. At both stations master variable profiles were taken every 20 minutes using Seacat profilers. Bottle samples of 500 ml were collected at 0.5 metres above the bed (the INSSEV sampling height) at 30 minute intervals (15 minute intervals at Station A in order to calibrate the INSSEV concentrations), and mid-water depth Owen tube type samples taken at an interval of one hour. All water samples were filtered on site using pre-ashed and weighed 55 mm diameter GF/F filter circles, and then transferred to frozen storage.

A number of samples were taken for bio-chemical analysis; these were analysed for chlorophyll-a levels, total carbohydrate content, and the relative proportions of carbon/hydrogen/nitrogen (C/H/N). Samples were taken to represent the full range of tidal conditions, in order to obtain a representation for each of the main tidal conditions. The pigment of chlorophyll-a is regarded as a coarse measurement of the biomass of phytoplankton (Joint, 1983). Total carbohydrate is a measure of the total amount of sugars contained within the suspended matter. These sugars mainly constitute organic polymers, principally polysaccharides produced by micro-organisms, which are important floc bonding agents. From the C/H/N analysis, the particulate carbon (defined as the fraction retained by a 0.45 μm filter pore) is representative of the living organisms (e.g. marine phytoplankton, bacteria and animals) and non-living particles (detritus, i.e. all types of biogenic matter in various stages of decomposition).

All instrument settings and deployment details were individually recorded in log books as a back-up to other self-logging features. To be able to compare data between different systems, all computer clocks and personnel watches were regularly synchronised with the vessel's GPS clock and then converted to local time. Water surface slopes were measured during some experimental deployments from visual water levels at two positions within the experimental reach. At 45 minute intervals, the water level was measured at datum *TP1* (see Figure 3.1 for datum locations), then one minute later it was measured at *TP2*, then re-measured at *TP1* again. An Avon inflatable boat was used to access both datum's points; both datum points were accurately surveyed into benchmarks with a closure error of less than 0.01 m.

The zero offsets of each EMCM were observed prior to deployment and immediately on recovery by placing the sensor heads in small containers of still water. The INSSEV settling column was charged with a clear filtered saline solution with a salinity value greater than that of the maximum expected to be encountered during a specific deployment. Both the pre- and post-deployment column salinities was measured with a WTW LF 196 salinometer. The POST OBSs were calibrated a number of times on-site using natural sediment samples mixed to varying concentrations. The OBS gains were pre-set to measure a maximum expected concentration of ~10 gl^{-1}.

3.2 Gironde estuary experiment

The second set of field deployments took place during June 1999 within the Le Verdon region of the Gironde Estuary, France (Figure 3.4). This work was part of the EC TMR SWAMIEE programme. The experiment, referred to as SWAMGIR1, was the main cohesive sediment field experiment for SWAMIEE. From the UOP perspective, the experimental aims were similar to those of the Tamar estuary programme: to obtain simultaneous floc, hydrodynamic, and concentration data sets. The Gironde data would be used to generate flocculation algorithms and for engineering model calibration, whilst also being compared and integrated with the Tamar estuary results.

A multi-discipinary approach was adopted for this study involving 17 scientists from seven European institutions. The following measurements were made during SWAMGIR1:

- In-situ floc size & settling velocity
- High frequency near-bed flow and turbidity characteristics
- Temperature, salinity and suspended solids profiles
- Velocity profile structure
- Suspended solids by gravimetry
- Field settling "Owen" tube style samples
- Seabed pore water pressure
- Tidal measurements
- Sediment grain size analysis

3.2.1 The Gironde estuary

Draining the 81,000 km^2 sedimentary Aquitaine basin, and possessing a tidal area of 625 km^2, the Gironde estuary is the largest estuary in France. The estuary is situated at the northern extremity of the Landes plain, in the Southwest of France. In the north it rests on chalk cliffs of the Saintonge and forms a deep indentation in the straight Landes coastline. The Gironde designates that part of the estuary between the Bec d'Ambres, which forms the confluence of the rivers Garonne and Dordogne, and the Atlantic Ocean. The River Garonne provides a catchment area of 55,000 km^2 (Latouche, 1971) stretching from the Pyrenees to the Atlantic, and with a total riverine length of 580 km it is regarded as the most important input. The second, the River Dordogne, has a 16,000 km^2 catchment area which lies west of the Massif Central and east of the Aquitaine Basin. The annually-averaged river discharge is 760 m^3s^{-1}. Seasonal variations in river flow occur with maximum values, usually in January (1500 m^3s^{-1}) and minimum values in August (200 m^3s^{-1}).

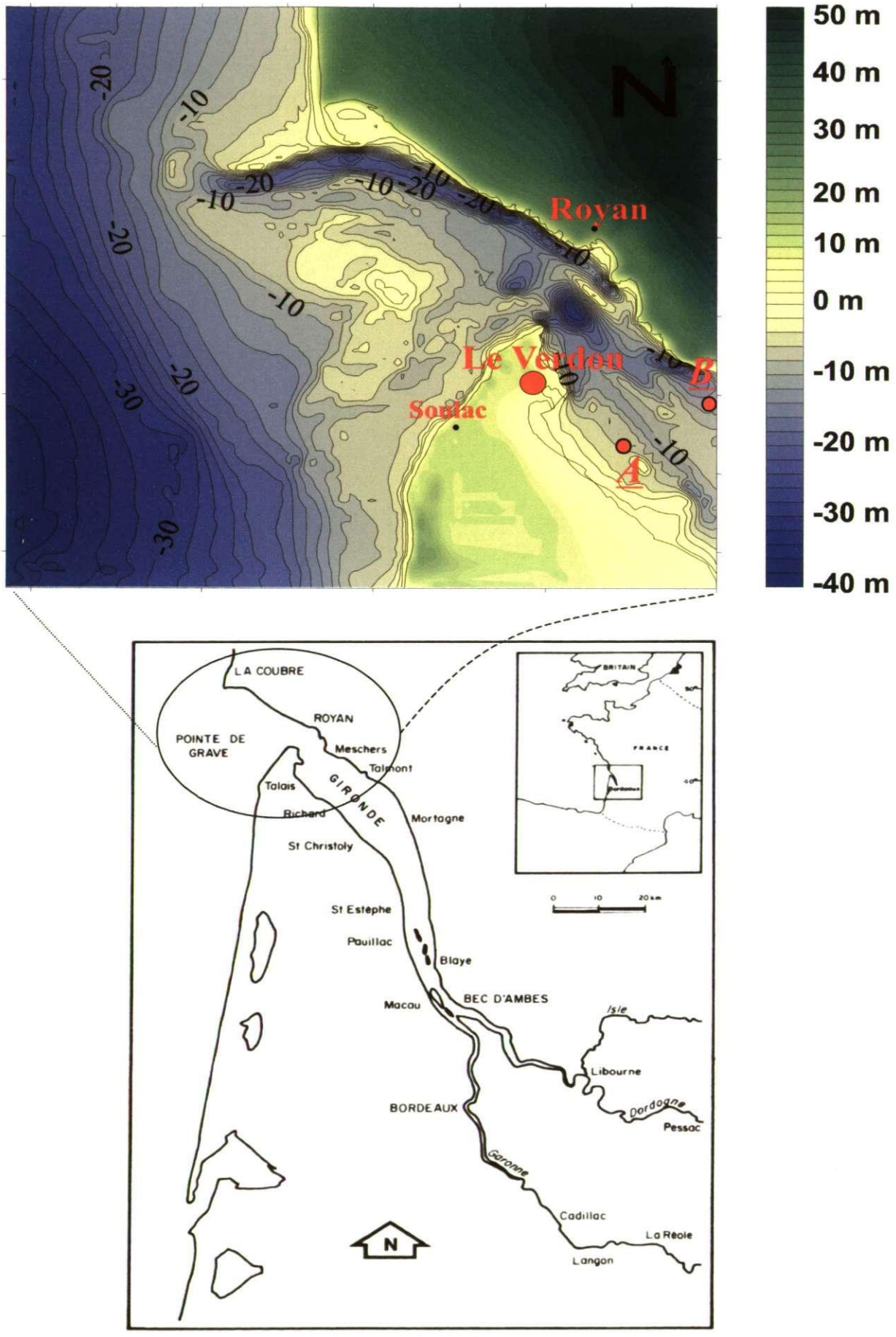

Figure 3.4 Location diagram of the Gironde estuary showing the positions of sampling stations at Le Verdon (*A*) and Talmont (*B*).

3.2.1.a Tidal and bathymetric conditions

The shape of the estuary is very regular and the principle morphological parameters vary exponentially from the mouth of the estuary to the limit of the tidal influence, situated more than 50 km upstream from Bordeaux. Upstream from the Bec d'Ambres, in the tidal zone, the Garonne and Dordogne rivers present all the traits of meandering rivers. The principle features include a single thalweg winding between a succession of meander embankments. Natural levees are set up on some banks behind which develop marshy areas. The morphology of the estuary, from Bordeaux to Pauillac, is relatively complicated by a system of secondary braided channels separated by tidal bars and islands such as the Ile Verte. Geometrically, the water-surface width is about 2-3 km and the depth 6-8 m in the main navigation channel which generally follows the left bank. Down estuary from Pauillac, the morphology simplifies with the main channel and the lesser Saintonge channel (which follows the right bank) being separated by a succession of elongated tidal bars. Here the width varies from 4 km to a maximum of 14 km at Richard, where the depth of the navigation channel is 10 m. From Richard to the mouth of the estuary, depth increases from 10 m to 30 m over a distance of 10 km.

The Gironde estuary is classified as a well mixed, macrotidal estuary. It is has a semi-diurnal tidal regime, with a 12 hours 25 minutes tidal lunar period and 1.5 to 5 m tidal amplitude at the mouth. In the upstream region of the estuary, the tidal range can attain 5.5 m at spring tides. The tidal prism at the mouth (volume of sea water introduced by the flood tide flow into the estuary) is approximately 2×10^9 m^3 during spring tides, reducing to 1×10^9 m^3 during neap conditions. Upstream, this volume decreases exponentially and at Bordeaux the water volume introduced does not exceed 5.2×10^7 m^3 at spring tides (as tidal effects are felt up to 150 km above the mouth during periods of low river discharge), whilst the upper limit of the salinity intrusion is about 75 km above the estuary mouth for low river discharge, and 40 km for high river discharge.

Allen (1972) found that the tidal curves were symmetric at the estuary mouth, but further upstream they became clearly asymmetric; the fall in water level taking longer than the rise. Allen (1972) reported that this phenomenon was particularly noticeable in the upper estuary and at spring tides. At Bordeaux, during spring tides, the ebb typically lasts 8 hours, whilst the flood occurs in only 4.5 hours. Maximum velocities are attained on a spring tide flood with speeds of 1.5 ms^{-1} at 0.6 m above the bed and velocities known to exceed 2.8 ms^{-1} at

the surface. At lower tides, there is a significant reduction in the flow speeds, which are typically of the order of 0.5 ms^{-1} (Migniot, 1971).

3.2.1.b Sediment characteristics

The annually-averaged solid discharge to the estuary was estimated by Migniot (1969) to be about 2.17 million tonnes, two-thirds of which are contributed by the Garonne river. Utilising stations throughout the estuary over a two year observational period, Etcheber (1978) calculated a mean SPM concentration of 1000 mgl^{-1}. The sedimentological structure of the bottom varies from the mouth to the upstream boundaries of the Garonne and Dordogne rivers: at the mouth of the estuary, the bottom is covered by sand. Then from the Talais region to Bordeaux, a fluid mud layer, constituted by silt and mostly by clay minerals, covers the bottom in patches mainly in the navigation channel. These patches are mostly 10 to 20 km long, with a thickness of up to 2-3 meters. They are close to Bordeaux when the river flow is low, but they move seaward to Richard when the river flow is high. From Bordeaux to the upstream boundary and for part of the Dordogne river, the river bed is made of non-consolidated soft mud with patches of sand.

3.2.1.c Circulation and residual fluxes

The vertical mixing processes in an estuary are reflected by the vertical salinity gradient, and the maximum vertical gradient tends to occur in the deep navigation channels, which comprise the principle path of penetration for the seawater. The gradient varies with fluvial discharge, and during periods of heavy river discharge, the mixture of freshwater / salt water is less marked; the salt stratification is more apparent and the vertical gradient is more pronounced. The residual currents are produced by advection linked to the vertical gradients of density resulting from the poor mixture of freshwater with salt water. Depending on river discharge conditions, the maximum vertical gradient occupies a zone around St. Christoly (at lowest water) to Saintonge (in spate).

The river suspended solids discharge combined with the macro-tidal residual circulations, causes the formation of a well-developed turbidity maximum in the nodal point zone of the upper estuary (Glangeaud, 1939; Bonnefille, 1971). During low river flow the TM extends a considerable distance inland from the saline limit (typically located at Bec d'Ambres) and attains the limit of tidal currents (a further 40-50 km further landward). Higher river discharges push the TM to a location ~30km from the mouth where it straddles the limit of the saline intrusion. Using radioactive tracers, Allen et al. (1974) estimated the total mass of

this system (during neap tides) was of the order of 4-6 million tonnes (close to that of the annual solid river discharge). The division is generally 2-3 million tonnes being placed in suspension in the water column, whilst 2-3 million tonnes exist as fluid mud. The turbidity maximum, which has a maximum mean concentration of 3,330 mgl^{-1} (Etcheber, 1978) and the fluid mud concentration varying between 100-350 gl^{-1} (Jouanneau, 1979) are located in the same area of the estuary, and can be considered as a coupled system. They both undergo a yearly migration in response to seasonal river outflow and a cycle of erosion and accumulation, related to the cycle of tidal ranges (Allen, 1971). Bed load transport is the cause of a yearly accumulation of more than 1 million m^3 of sand in the lower estuary (Jouanneau and Latouche, 1981). There is a distinct transverse gradient of salinity in the estuary with fresh water on the right bank in relation to the left. This phenomena is the result of the combined actions of both the Coriolis and centrifugal force, together with the morphology of the estuary banks; this identifies that the Saintonge channel as the preferential fluvial water outlet (Jouanneau and Latouche, 1981). Typical residual current velocities are around 10-15 cms^{-1} at 0.5 m above the bed, and are more than 40 cms^{-1} near the surface (Allen, 1972).

3.2.2 Sampling locations

The sampling limitations of the various instruments governed the experimental site location. The use of a predictive computer model (Bordeaux University) indicated that the turbidity maximum would travel downstream as far as the Pauillac-St.Christoly region. However, because of limitations of high current velocities and high particle concentrations on use of the instruments, two sites were chosen near the mouth in the Le Verdon and Talmont regions (see Figure 3.4, page 68). These sites were located on localised mud deposits with a flat bed bathymetry, and being in the fluvial limit zone, suspended concentrations were not expected to exceed 500 mgl^{-1}. The neap tide conditions of the sampling period also guaranteed that the water column depth (at these sites) would not exceed 14 m at high water, and the flow velocity would stay well within the 1 ms^{-1} acceptable for INSSEV deployments.

3.2.3 Instrumentation set-up and deployment

Both INSSEV and POST were deployed throughout SWAMGIR1. The set-up was generally the same as that used for the Tamar experiments, but with a few modifications. Because the rig would be deployed in faster flow conditions and a much deeper water column than that of the Tamar, a new bed frame was constructed from a larger gauge of angle steel and the overall frame dimensions were increased by 33%. All of the instrumentation sat on an

internal steel lattice tray, and this gave INSSEV a mean sampling height of 0.6 metres above the frame base. This additional space at the bottom of the bed frame was needed to accommodate the University of Oxford (UO) piezometer system and ballast weights. The POST flow and turbidity probes were again mounted on a vertical scaffold pole laterally off-set to the right of the INSSEV sampling unit. The new frame together with instruments weighed 450 kg in air. Plate 3.10 shows the complete rig set up. Because of sensor failures, 3-D flow velocity could only be measured at the INSSEV sampling height using EMCMs 2 and 3. Two components of flow were measured at positions above and below the 3-D sampling position. All instrument heights are summarised in Table 3.2.

Table 3.2 POST sensor heights for SWAMGIR1 experiments (21st -24th June 1999).

Date	OBS probe	OBS heights above bed frame base (cm)	EMCM probe	EMCM heights above bed frame base (cm)	EMCM discus orientation
21/06/99	1	32	1	36	vertical
22/06/99	2	38	2	70	face up
23/06/99	3	71	3	70	vertical
24/06/99	6	78	5	98	face down
	7	133			

The experiment was conducted aboard the CNRS research vessel Cote D'Aquitaine. This was a full displacement-hull type vessel of steel construction, with an overall length of 19 metres and a 6 metre beam. The vessel was berthed at Le Verdon marina each night, and then cruised to the site at the start of a day. Cote D'Aquitaine used it's own fore and aft anchors to maintain position during sampling. A diesel powered crane with a hydraulically controlled telescopic jib facilitated the rig deployment. For practical launch and retrieval purposes, the rig was deployed over the stern (Plate 3.11). With the water depth negating the use of control ropes, instrumentation alignment was achieved by the addition of a 1.5 x 1.2 metre high marine plywood fin attached to the rear of the bed frame.

No visible checks on frame alignment were possible due to the Gironde Estuary sampling locations having water depths in excess of 10 metres. Therefore, in order to provide a frame of reference for the POST EM flow sensors, a fluxgate compass and an electronic 2-axis tilt sensor was borrowed from BLISS - Boundary Layer Intelligent Sensor System - rigs used in North Sea sediment transport research (Blewett, 1998). Both units required a total of 3 output channels, and were housed inside the stainless steel POST optical pressure casing, after removing 3 OBS units. This meant that only five of the eight POST optical probes could be used during *SWAMGIR1*. The output from the fluxgate compass and tilt sensor was

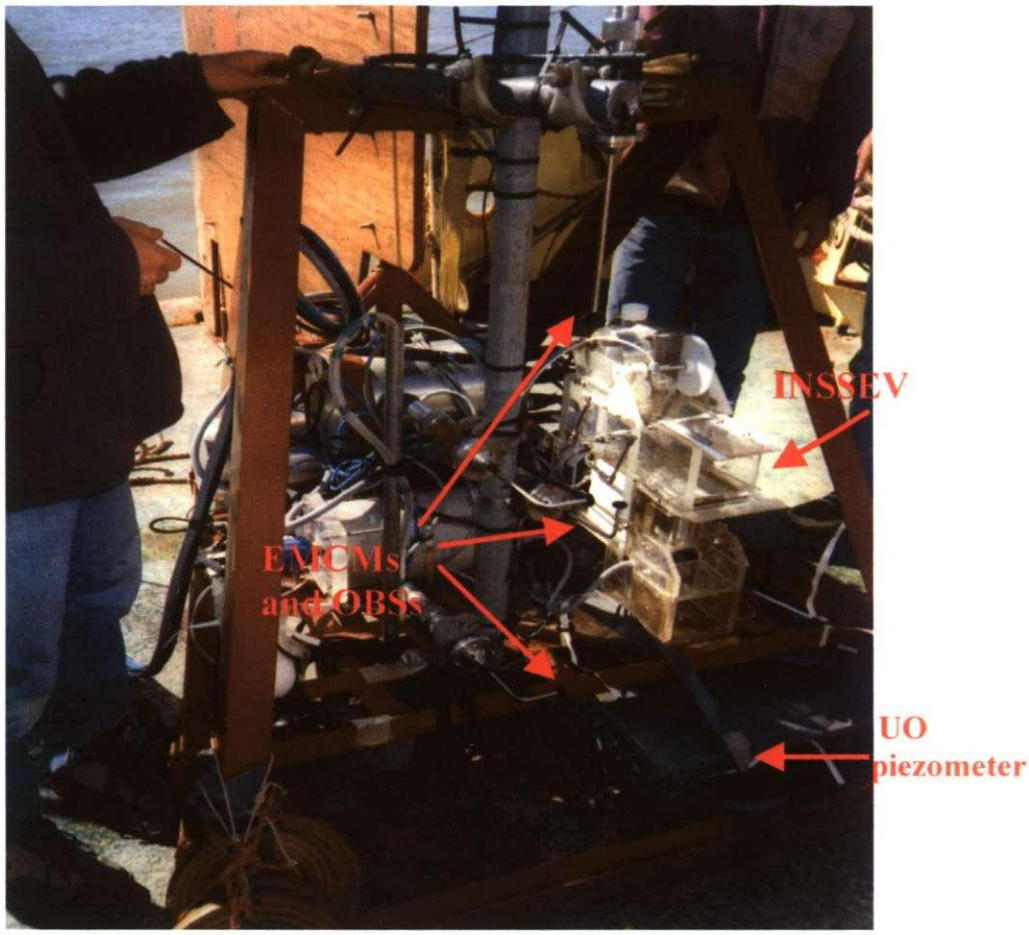

Plate 3.10 INSSEV and POST mounted on the estuarine bed frame used during the SWAMGIR1 experiments on the Gironde estuary (July 1999).

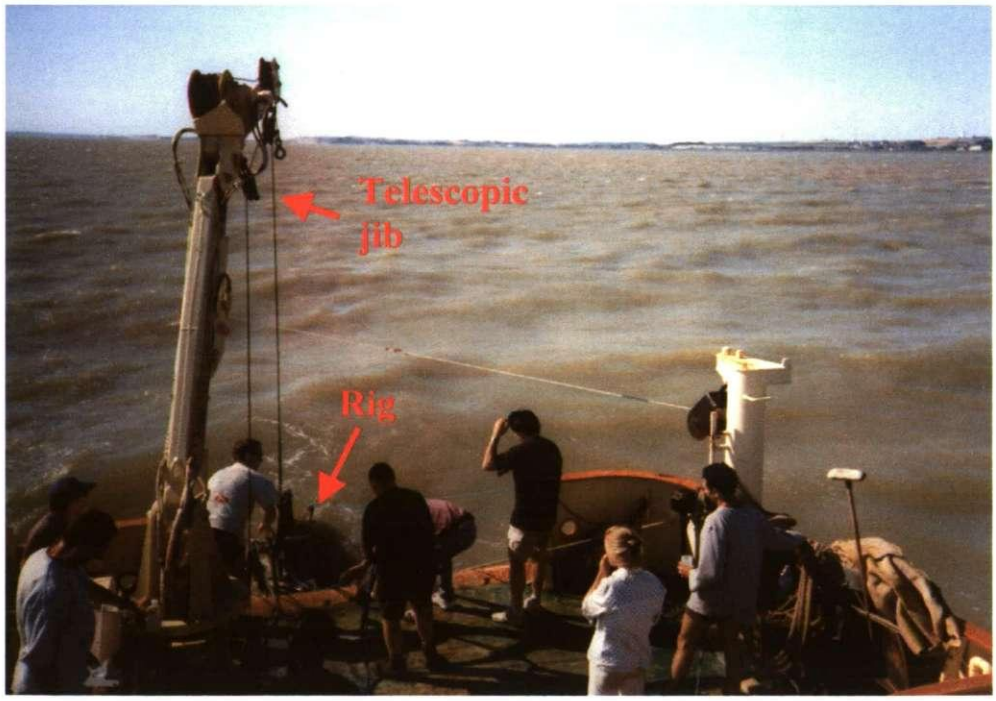

Plate 3.11 Instrumentation rig recovery from the stern of *Cote D'Aquitaine* during the SWAMGIR1 experiments (image taken from site 1 near Le Verdon). Note the distance of the sampling site from the shore line.

recorded on the POST control computer. Calibration of the digital output from the 2.5 V tilt sensor resulted in 57 bits per 2 degrees of tilt (i.e. 35 mV per degree), which gave a maximum measurable inclination of 71.8° on any one axis. The fluxgate compass measured between 0.1 and 1.9 volts, and this translated in to an analogue resolution of 5 mV per degree. The POST cylinders were secured to the rear of the bed frame so that the heading and the tilt of the frame could be zeroed. Then both INSSEV and the POST sensors were bolted to the bed frame and their orientation relative to the integral alignment sensors could be determined prior to each deployment. Output from previous oceanographic surveys indicated that a maximum concentration of approximately 1.5 gl^{-1} would be encountered, so all OBS gains were set to optimise the digital logging resolutions for these conditions.

A daily sampling schedule, similar to that used during the Tamar experiments, was adopted for the SWAMGIR1 series. Once the INSSEV/POST rig together with the UO piezometer system had been deployed satisfactorily (Plate 3.12), master variable profiles and Niskin bottle water samples were made every quarter of an hour. NBA profiles of current velocity variation were conducted at 30 minute intervals (using one metre depth increments). University of Rouen (UR) made current velocity profile measurements with their acoustic Doppler current profiler (ADCP) mounted on the starboard side of the ship's hull. Additional floc measurements were taken at the INSSEV sampling height by UR's video-in-lab (VIL) instrument. Position and time synchronisation was again established from the ship's DGPS units. All floc and water samples were collected at the height above the bed of the INSSEV decelerator chamber. Filtration and optical calibrations were both undertaken on deck.

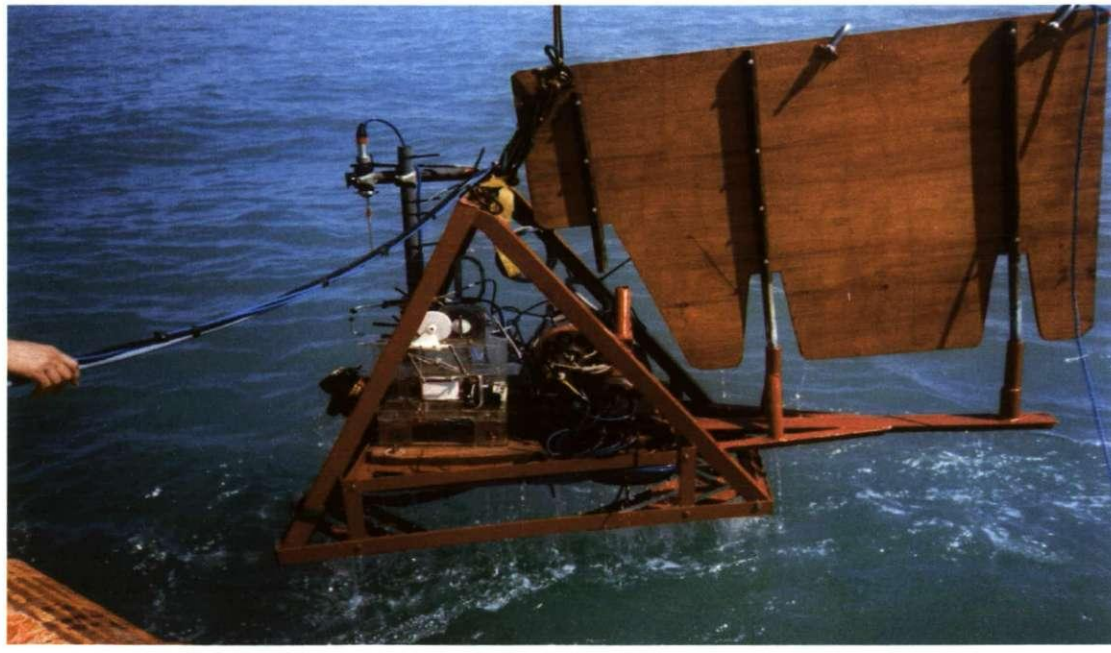

Plate 3.12 Instrumentation rig deployment from the stern of *Cote D'Aquitaine* during the SWAMGIR1 experiment (image taken from site 1 near Le Verdon).

3.3 University of Plymouth (UOP) laboratory experiments

The aim of this study was to use present day non-intrusive video camera technology in a laboratory flume, under varying controlled levels of both SPM concentrations and turbulent shear, to determine flocculated aggregate characteristics. The main part of this study was an MSc project, but it was extended to further complement the field measurements. For the purpose of this thesis, the data from these UOP laboratory experiments would be processed so that they could provide a greater insight into the interpretation of the in-situ experimental results.

Two experiments were carried out in the Institute of Marine Studies *Ocean Science laboratory* (OSL) using an annular flume to shear various concentrations of cohesive sediment within the turbulent shear stress range 0-0.6 Nm^{-2}. The maximum concentration of solids studied was 200 mgl^{-1}; the experimental set-up is illustrated in Plate 3.13. The floc size and settling velocities were measured by the INSSEV system video camera mounted in a viewing port on the flume channel wall. A preliminary investigation of the system was carried out during July 1996 which indicated that it was possible to obtain good quality floc data that was comparable to flocs sampled in the field. The instrument development and experiment 1 are described by Manning (1996). Again using the annular flume, a supplementary experiment (2) was carried out in December 1996 / January 1997 in the OSL to provide additional floc / turbulence data, to complement the data set obtained for experiment 1. Details of the instrumentation and methodology can be found in sections 3-5 of Appendix I which is a re-print of Manning and Dyer (1999).

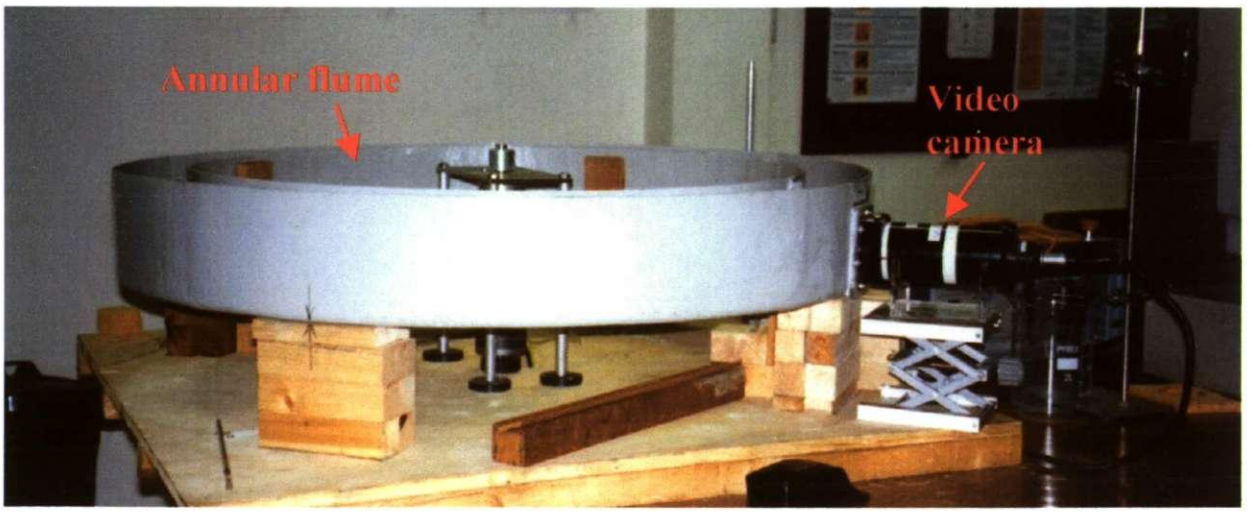

Plate 3.13 UOP annular flume (with rotating roof section removed) with the video camera inset into the flume wall.

3.4 LEGI laboratory experiments

As part of the COSINUS project (task B.3), a joint study on the properties of flocs formed in both dilute suspension and CBS layers was initiated by the UOP and the Universite Joseph Fourier (UJF). For the COSINUS project UJF had the general aims of improving the understanding of the relationship between turbulence and vertical concentration profiles. The culmination of this collaboration was a series of laboratory experiments conducted at the Laboratoire des Ecoulements Geophysiques et Industriels (LEGI) in Grenoble, France between the 12-16th July 1999. For their main contribution to COSINUS, UJF undertook to determine the conditions required to generate a CBS layer as a function of turbulent hydrodynamical conditions. UOP collaborated in measuring the floc sizes, settling velocities and effective densities.

For these experiments, suspensions with concentrations ranging from 0.2-5 gl^{-1} were sheared using an oscillating grid, and then the flocs were examined by the INSSEV video camera utilised for the UOP laboratory experiments. As it was not possible for the camera to view in concentrations in excess of 210 mgl^{-1} (Manning, 1996), and fitting the camera to the grid tank was not practical, it was decided to extract the flocs formed within the turbulent water column to a clear water settling column where the video camera would be situated in the column wall. Making the floc measurements in this manner meant that higher concentration conditions could be studied, and a direct comparison could be made to INSSEV obtained estuarine floc samples.

3.4.1 Instrumentation

3.4.1.a Turbulence grid tank

The apparatus consisted of a cuboidal tank constructed from transparent Plexiglas with a 530 mm wide square base, and a height of 900 mm (Plate 3.14). A horizontal grid was placed inside the tank and was oscillated vertically with a sinusoidal displacement in time, at a selectable frequency and amplitude. The frequency was calibrated by a hand held strobe light. The grid was suspended in the tank by a 5 mm diameter centrally connecting steel shaft, which in turn was attached to a stepper motor positioned on a steel frame directly above the tank. This motor produced the grid vertical motion, and the grid amplitude could be increased by moving the grid to a point further up the connecting shaft. The grid was constructed 15 mm thick square bars, with a mesh spacing of 75 mm (centre to centre). The porosity of the grid, defined as the ratio of surface of the holes to the surface of the grid, was 64%. Previous work conducted by Hopfinger and Toly (1976) at LEGI on turbulent mixing

across a density interface, indicated that grid porosity is an important parameter to consider when assessing the generation of mean secondary flows. A porosity of 64% produces only minimal mean flow inside the tank. The tank was filled from above with slurries of concentration 200 mgl^{-1} to 5 gl^{-1}, and concentration profiles were obtained by taking out slurry sub-samples. The tank was emptied by a valve in the side wall (250 mm above the bottom) and in the base of the tank. The complete schematics of the grid tank induced hydrodynamics is reported by Gratiot (2000).

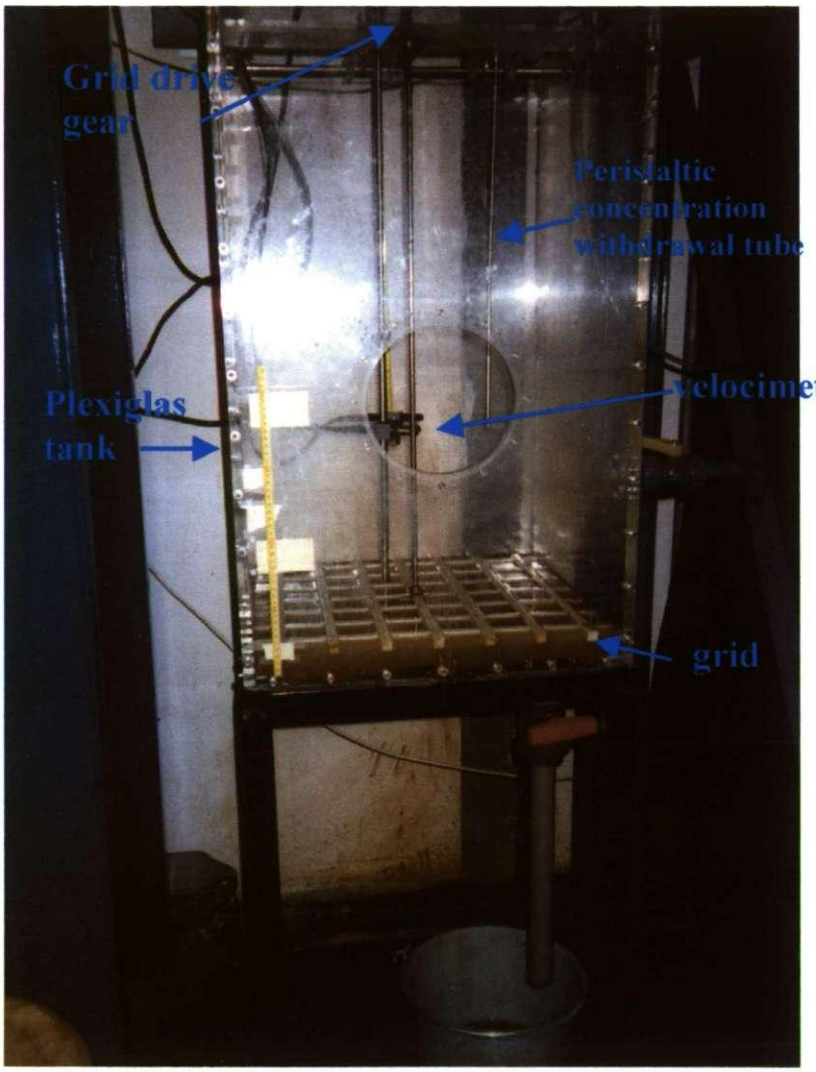

Plate 3.14 LEGI grid tank. The height adjustable peristaltic withdrawal tube and velocimeter are located in the centre of the tank.

3.4.1.b Turbulence measurements

Profiles of turbulent velocity were made within the grid tank by an acoustic Doppler velocimeter (ADV) developed at LEGI. The instrument determined the velocity from the changes in the time shift of pulse to pulse back-scattered signals. A detailed study was conducted by Gratiot et al. (2000) who examined the performance of the ADV to measure turbulent fluctuations within dilute suspensions and CBS layers. They found that within

concentrated mud suspensions of up to 50 gl^{-1} the ADV could measure instantaneous velocities with a data rate of 70 data points per second. The rms turbulent velocity was computed from a time series of 4000 measurements. The ADV could also measure simultaneously the velocity component parallel to the beam axis at 16 positions. The distance between two successive measured volumes was 3 mm. The integral lengthscale l was deduced from the computation of the correlation function of the velocity measurements made simultaneously at the different positions.

The turbulence structure could be described by the root mean square of the gradient in the turbulent velocity fluctuations (G) with the units of s^{-1}. G was computed at distances z above the grid from equation 3.4:

$$G(z) = \left(\frac{u_*^3}{(\nu \cdot l)} \right)^{0.5} \qquad (3.4)$$

where u_* was the turbulent velocity component measured by the velocimeter, and ν was the kinematic viscosity. All velocity measurements and G value calculations were made by Gratiot (2000).

3.4.1.c Floc property measurements

For the floc size and settling velocity measurements, flocs were extracted from the grid tank by a 0.4 m long glass pipette with an internal diameter of 4 mm. A volume of mud suspension was collected in the pipette whilst it was held in a vertical position, at the required depth from within the tank. Flocs were removed from the grid tank and introduced into a 190 mm high, 100 mm square Perspex settling column, filled with water of an equal salinity to than that contained within the grid tank. Similar operational protocols were employed to maintain consistency between the laboratory data and floc samples collected in-situ. The pipette was filled to a produce a fluid head of 100 mm which was the same height as the INSSEV decelerator chamber. For INSSEV the slide door permitted less flocs to enter the settling chamber as the ambient concentration rose. Thus, for the LEGI experiments the pipette was held in contact with the settling column water surface for a duration (T_{sd}) determined by equation 3.1. The flocs passed from the pipette into the settling column without any mechanical assistance; just by the gravitational force. The pipette remained vertical as it was put in contact with the water column surface. Transit time from withdrawal to the commencement of the transplantation to the settling column did not exceed five seconds. This would minimise any flocculation occurring within the pipette. As with the UOP laboratory experiments, the settling flocs were viewed by the INSSEV high resolution

video camera (Manning and Fennessy, 1997) and all observations were recorded by a S-VHS video recorder. The camera was positioned in the side wall of the settling column at a height 75 mm above the base. Again, the video images were pre-calibrated by using a scale ruler and the lower resolution limit was 20 μm.

3.4.2 Sampling protocols

Three experiments were carried out; the first utilised natural mud from the Tamar estuary which was collected from the surface of the mud banks at Calstock boat yard whilst they were exposed at low water. This was close to Station A from where most of the earlier reported INSSEV measurements were made (see section 3.1.2). The second experiment was conducted using mud obtained during the SWAMGIR1 experiment by Shipek grab sampler, (see section 3.2.2) from the seabed near Le Verdon in the Gironde estuary. Both muds used for the first two experiments were stored in tightly sealed plastic containers in a cool environment, so as to preserve the organic matter content. The third experiment used Gironde estuary sediment which was chemically pre-treated so as to remove all organic matter. Each mud was pre-sieved at 100 μm to remove any coarse particles, and mixed into separate mud slurries with nominal concentrations of 200 mgl^{-1}, 600 mgl^{-1}, 1 gl^{-1} (1.8 gl^{-1} for Gironde estuary natural mud), and 5 gl^{-1} (Tamar mud only).

Figure 3.5 shows a schematic of the experimental set up. For a typical experiment, 112 litres of a given suspension was decanted into the LEGI grid tank as a homogeneous slurry. This gave a water column height of 0.4 m. The grid was then oscillated at a frequency of 4 Hz. Profiles of the variations in turbulent shear stress during the experiments were measured with the ADV probe. The flocculation time T_F was calculated by using equation 3.5 (Van Leussen, 1994):

$$T_F = \frac{2.306 \cdot \pi}{4 \cdot \alpha \cdot \phi (10 + G)} \qquad (3.5)$$

where α is a cohesion collision efficiency factor and ϕ is the total volume of sediment per unit volume. Van Leussen defines the flocculation time (T_F) as the time over which the number of particles in a suspension diminish to 10% because of flocculation. Examples of calculated flocculation time with various combinations of G and SPM concentration are shown in Figure 3.6. From research by Gibbs (1983) a nominal α value of 0.18 was estimated for both the Tamar and Gironde estuary mud suspensions with organic content. Thus the longest sample to obtain equilibrium would be the for the lowest G-value ~ 5.5 s^{-1} and SPM = 200 mgl^{-1}. This resulted in a flocculation time of approximately 2 minutes.

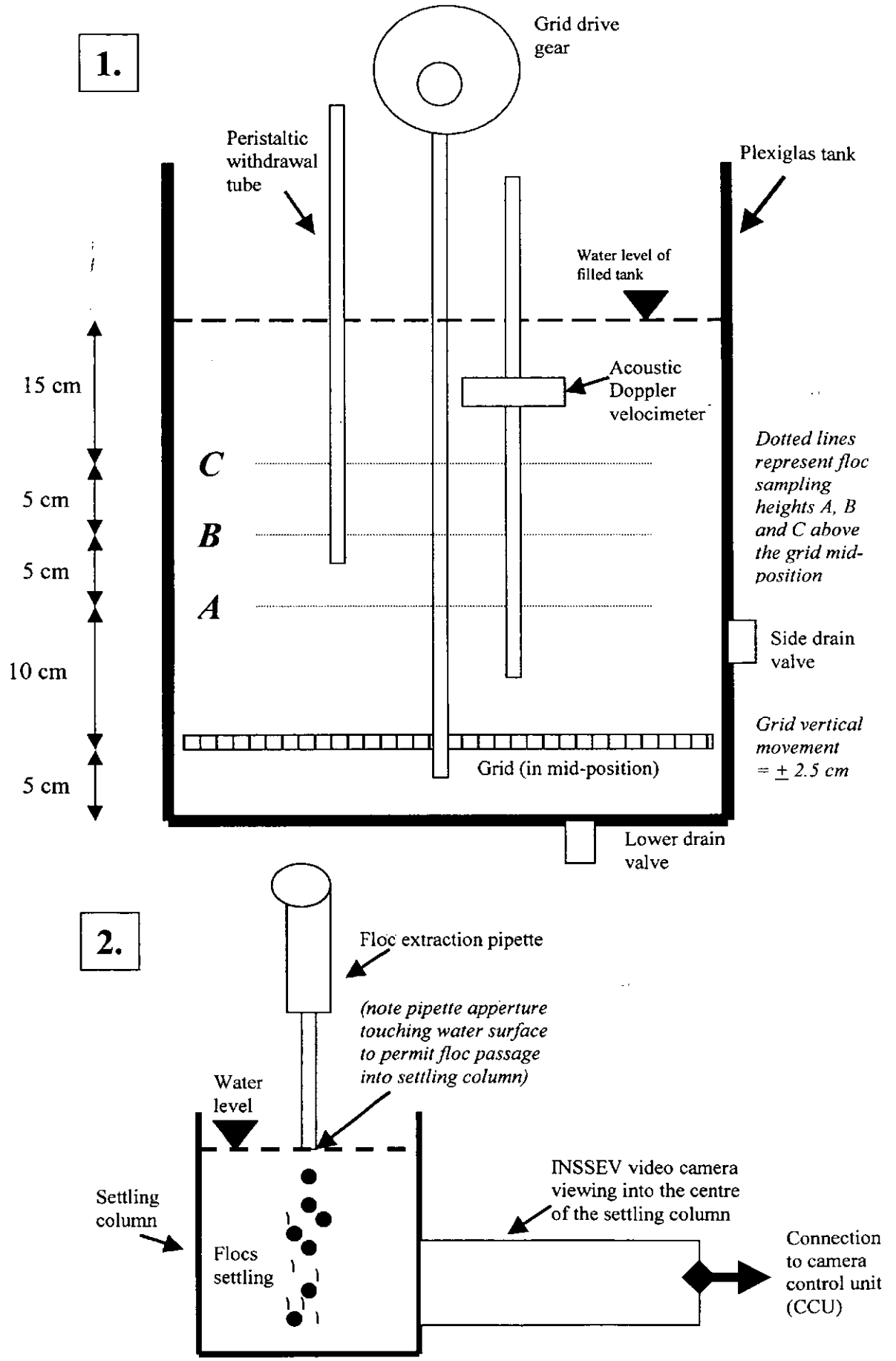

Figure 3.5 Schematics of the LEGI experimental set-up illustrating the grid tank (**1**) and floc settling column (**2**, the drawings are not to scale).

Therefore, all samples were sheared for a nominal 40 minute duration in the grid tank, and the flocs produced were deemed to be in equilibrium with the resultant turbulent environment.

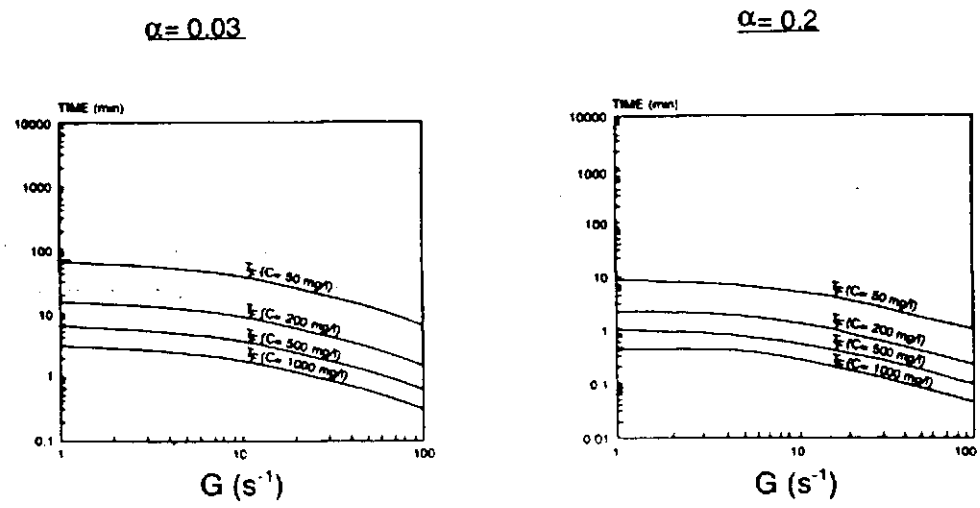

Figure 3.6 A comparison of flocculation time (T_F) against the turbulence parameter G with increasing levels of suspended concentration (C), for $\alpha = 0.03$ and $\alpha = 0.2$. The break-up efficiency factor was kept constant at 0.03 (modified from van Leussen, 1994).

After the initial 40 minutes of agitation, flocs were withdrawn from the water column by the pipette. They were extracted at three different depths: A, B and C, with respective heights of: 10 cm, 15 cm and 20 cm, above the grid when it was at mid-stroke (i.e. 5 cm above the tank base). The flocs were then quickly transferred to the settling column where they could pass from the pipette into a clear saline solution (with a salinity equal to that used in the grid tank), and be observed by the high resolution underwater video camera. The grid continued to oscillate during and between floc extractions. The floc images were recorded by an S-VHS video cassette recorder. A total of 30 flocs samples were obtained: 12 samples with natural Tamar mud, and 9 samples for both natural Gironde muds and Gironde mud with the organic matter removed. Although only a limited number of floc samples were collected, the wide experimental range employed in both the shear and SPM concentration, meant that an intercomparison of the resultant floc data sets could be regarded as statistically valid. The x- and y-axis floc size components, together with settling velocities were measured directly from the video monitor display (manually). Every individual floc from a separate floc population was measured. In order to calculate the floc mass, simultaneous complementary gravimetric samples were collected at the floc sampling heights via a peristaltic withdrawal pump.

Chapter Four:

Data Processing & Analysis

4.1 INSSEV floc data

This section outlines the analysis techniques used to process the floc data obtained using the INSSEV video camera system. Both the in-situ INSSEV and laboratory LEGI experiments employed a sampling technique which had the ability to control the numbers of flocs viewed by the camera during an individual settling experiment; this meant that all recorded aggregate images were analysed. The processing of the floc data obtained from the UOP annular flume experiment is outlined in section 6 of Appendix I.

4.1.1 Floc size, settling velocity and effective density

Floc sizes and settling velocities were both measured directly from the video monitor display (manually) and these were then converted into absolute dimensions using the initial video image calibration. The floc dimensions were measured along the axis in the direction of settling (D_Y), and along the axis normal to it (D_X), from which a height:width ratio could be determined. It is assumed that the floc depth dimension D_Z was equal to D_X. A spherical equivalent floc diameter was then calculated from:

$$D = (Dx \cdot Dy)^{0.5} \qquad \textbf{(4.1)}$$

Settling velocity was obtained as the vertical component of the resultant velocity, the time being provided by the frame counter which was recorded on the video tape (one frame = 0.04 seconds). These values gave raw settling column values ($W_{S\ column}$) and required a number of corrections (Fennessy, 1994). For this purpose, a Stokes' Law relationship was employed to determine the ambient settling velocity (W_S). Primarily, the raw settling values were multiplied by a factor of 1.03 (Allen, 1975), to compensate for the drag due to the walls of the settling column.

$$\rho_{e\ column} = \rho_f - \rho_{w\ column} = \frac{18\mu\left(Ws_{column} \cdot 1.03\right)}{D^2 g} \qquad \textbf{(4.2)}$$

Where $\rho_{e\ column}$ was floc effective density; the difference between the floc bulk density (ρ_f), and the column water density ($\rho_{w\ column}$). Water density was calculated from the measured salinity and water temperature values using the International Equation of State of Sea Water, 1980 (Millero and Poisson, 1981) and from this the dynamic molecular viscosity, μ, could be obtained. Secondly, the water density difference, $\rho_{w\ difference}$, due to the higher salinity in the

settling column compared with the ambient salinity (ρ_w) was applied to produce the corrected ambient floc effective density (ρ_e):

$$\rho_e = \rho_{e\,column} + \rho_{w\,difference} \quad (4.3)$$

and the ambient settling velocity (Ws) was then obtained by recalculating from Stokes equation:

$$Ws = \frac{D^2 \cdot \rho_e \cdot g}{18\mu} \quad (4.4)$$

Stokes settling only occurs when the Reynolds number, R_e, < 1.

$$R_e = \frac{\rho_e \cdot Ws \cdot D}{\mu} \quad (4.5)$$

Many authors such as Ten Brinke (1993) have suggested the use of the Oseen modification (Oseen, 1927) to allow for the increased inertia when $R_e > 0.5$. A correction factor, based on the R_e value, was applied (when $R_e > 0.5$) which had the effect of increasing the calculated ambient effective density (and subsequent computed parameters) values by the following amount:

$$\rho_{e\,Oseen} = \rho_e \cdot \frac{1}{(1 + 0.1875 R_e)} \quad (4.6)$$

where $\rho_{e\ Oseen}$ is the Oseen modified ambient effective density. After any required corrections were applied to the effective density, the resultant effective densities (ambient or Oseen modified) were referred to as ρ_e.

Finally, as we were concerned with examining floc characteristics, all particles which possessed a ρ_e value exceeding 1600 kgm^{-3} were removed as this is the effective density of a quartz particle. The interstitial water (V_{iw}) contained within each floc was calculated by:

$$V_{iw} = 1 - \frac{\rho_e}{\rho_{e\,np}} \cdot V_f \quad (4.7)$$

where $\rho_{e\,np} = \rho_{mo} - \rho_w$; ρ_{mo} is the mean dry density of the primary particles, and $\rho_{e\,np}$ is the mean effective density for solid (non-porous) aggregates. An estimate of ρ_{mo} was made by assuming that the mineral dry density was 2600 kgm^{-3}, and the organic matter had a dry density of 1030 kgm^{-3} and the mineral to organic ratio was obtained from gravimetric loss on ashing. Then floc porosity (P_f), which provides an indication of the level of compactness of the floc, was evaluated by taking the ratio of the volume of the floc interstitial water to that of the total floc volume:

$$P_f = \frac{V_{iw}}{V_f} \cdot 100 \qquad (4.8)$$

Assuming the interstitial fluid density to be equal to ρ_w, the dry mass of an individual floc ($M_{f\,dry}$) can be calculated by:

$$M_{f\,dry} = V_f \frac{\rho_e \cdot \rho_{mo}}{(\rho_{mo} - \rho_w)} \qquad (4.9)$$

4.1.2 Concentration referencing

As a result of measuring all visible aggregates within an individual INSSEV sample, it was possible to transform the observed floc population into estimates of concentration and settling flux spectra. To aid in this the flocs were segregated into bands of varying floc size (Table 4.1). This transformation was also possible with the LEGI experiments, which employed a complementary sampling technique. It was assumed that the flocs originated from a constant sample volume of water within the decelerator chamber (or pipette for LEGI) of 400 mm^3. This comprised a nominal 4 mm screen width, 1 mm depth of field, and a 100 mm decelerator height (or pipette sample height for LEGI laboratory experiments, Figure 4.1). A correction (explained in Fennessy et al., 1997) was applied to the dry mass computed by equation 4.9, to produce $M_{f\,dry\,c}$. This was to compensate for the combined effects of primary losses (flocs prematurely settling to decelerator floor before the slide opens) and secondary losses (slow settling flocs failing to enter the stilling column) from the total sample volume.

Table 4.1 **INSSEV size bands**

Size Band (SB)	Floc size (μm)
1	20-40
2	40-80
3	80-120
4	120-160
5	160-200
6	200-240
7	240-320
8	320-400
9	400-480
10	480-560
11	560-640
12	>640

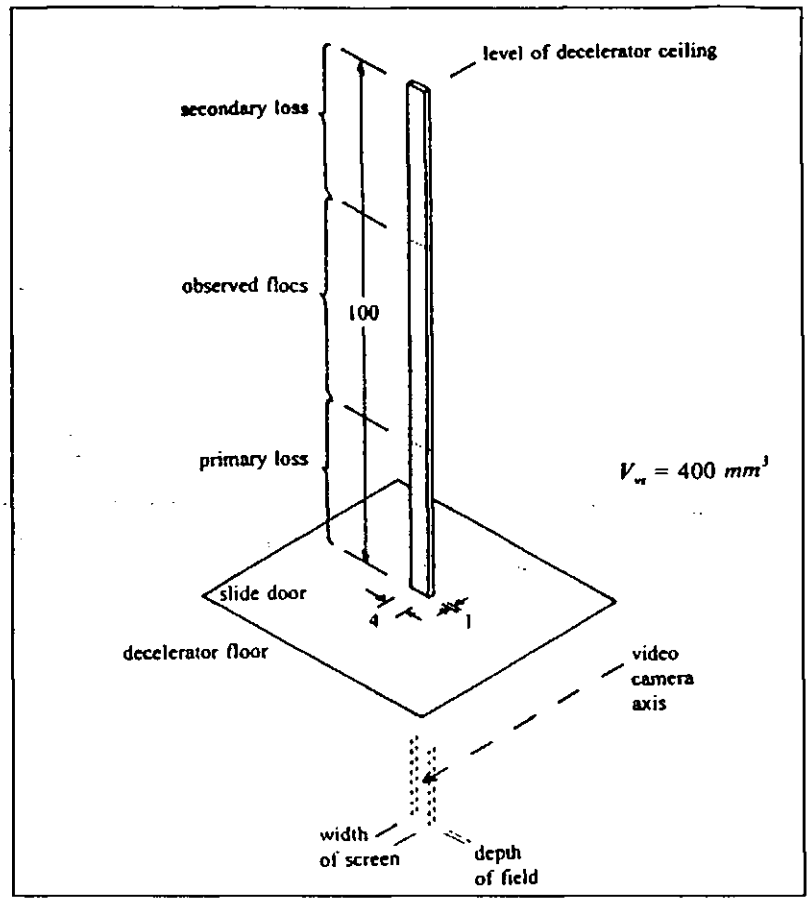

Figure 4.1 Illustration of the INSSEV video object plane sample volume, V_{vs}, and the primary and secondary losses (from Fennessy et al., 1997).

All of the $M_{f\,dry\,c}$ values for an individual sample were summed to produce the total dry mass ($\Sigma M_{f\,dry\,c}$) within the 400 mm^3 sampling volume. This was then multiplied by 2.5 x 10^9 which converts the total dry mass into an SPM concentration, C_{INSSEV}. The INSSEV concentration was then compared with the filtered concentration ($C_{filtered}$) obtained during the respective sampling deployment.

$$Q_c = \frac{C_{INSSEV}}{C_{filtered}} \qquad (4.10)$$

This quality factor, Q_c, provides an indication of how accurately the INSSEV sampling procedure has managed to measure the ambient SPM population. The Q_c values assume that the filtered SPM concentration is the correct SPM value, and is hence comparable to the floc sample collected by INSSEV. A separate filtered SPM sample is obtained because it is not practical to collect the SPM deposited within the INSSEV instrument, and the mass of material sampled by INSSEV is general too small to use for gravimetric analysis (e.g. fifteen INSSEV samples collected through periods of high SPM concentrations during spring tides, typically only produces 1 or 2 mm of deposition on the settling column floor). A value above or below unity highlights an over- or under-estimate of the concentration, respectively. The

reciprocal of equation 4.10, is then used to calibrate the computed INSSEV concentration component of a particular banding scheme, and produce $C_{INSSEVcal}$. The mass settling flux of a component band division can then be calculated by multiplying the $C_{INSSEVcal}$ by the mean settling velocity of the respective band. Thus spectral estimates of mass settling flux can be made.

4.1.3 Fractal dimension (nf)

An estimation of the fractal dimension, nf, was made using equation 2.22 with the assumption that the primary particle diameter (D_P) was 4μm, and the empirical coefficient (α') was taken as 0.18, primarily based on mineralogy (see page 79 for the determination of the collision efficiency factor). The same α' was assumed for the flocs which were composed of Gironde estuary sediment.

4.2 POST flow and turbidity data

4.2.1 Initial signal processing

This data processing was conducted by M. Christie and P. Turner (both University of Plymouth). The analogue signal output from each sensor was amplified, filtered and digitised as defined in section 3.1.3.b. The digital output from all 24 channels was recorded in real-time in binary format on a laptop hard disk using the Valeport Ltd. software ETSU. Each channel recorded 4096 data points at a sampling frequency of 18 Hz, which translates in to a file duration of 3 minutes 47.55 seconds. Time stamps were attributed by the PC internal clock. A Microsoft DOS program (*TRAN.EXE*) was then used to convert the binary files into a comma delimited ASCII format, which facilitated importing into Microsoft Excel.

The next stage was to examine each file structure and calibrate the digitised data. It was observed during some of the Tamar experimental work that there were intermittent data transmission errors. Thus checks were made for the integrity of the data of each file, and corrections were applied where necessary by linear interpolation. The data was then calibrated using the respective sensor's algorithm.

In order to be able to use the EMCM flow data for the examination of the turbulent structure in the water column, it was necessary to separate and consequently remove any undesirable "noise" from the turbulent fluctuations. For this study "noise" was classified as data points which were greater than four times the standard deviation of the data. These points were removed from the time series and then replaced by an interpolated value equal to the mean of

the two adjacent data points. The data was then de-trended for the effects of the tide. Each EMCM and OBS file was then plotted and a visual quality inspection was then conducted, to check for potential sensor fouling. A mean flow velocity, flow direction, and concentration was obtained for each 3 minute 47.55 second file.

4.2.2 Turbulent shear stress

The three components of flow measured by the EMCMs enabled values of turbulent shear stress (TSS), τ, to be calculated at each sensor group height using the Turbulent Kinetic Energy method (Soulsby, 1983). As explained in section 2.4.4, this method was preferred to the logarithmic profile, or Reynolds stress approaches, as the TKE method was the least sensitive to sensor misalignment.

$$\tau = 0.19 \left[0.5 \rho_w \left(u'^2 + v'^2 + w'^2\right)\right] \quad \textbf{(4.11)}$$

where ρ_w is the ambient water density and u', v', w' are the three turbulent Reynolds components (see section 2.4.3 for explanations of the various Reynolds terms). A TSS could then be computed for each 3 minute 47.55 second duration file.

For inter-comparison purposes, the TSS values were also computed into two commonly used alternative measures of turbulent shearing. The first was in the format of G, which is the root mean square of the gradient in the turbulent velocity fluctuations with the unit s^{-1}. The rate of turbulent energy production per unit mass P by turbulent shear stresses is given by

$$P = \frac{\tau}{\rho_w} \frac{\delta u}{\delta z} \quad \textbf{(4.12)}$$

and for a logarithmic profile, as defined in the Von Karman-Prandtl equation (2.6), equation 4.12 becomes:

$$P = \frac{U_*^3}{\kappa \cdot z} \quad \textbf{(4.13)}$$

Nakagawa and Nezu (1975) examined the structure of turbulence in open channel flow, and a selection of their results are shown in Figure 4.2. They found that in the state of fully developed turbulent flow, the turbulent energy production and turbulent energy dissipation (ε) were nearly in balance with each other. Within the wall region P is generally larger than ε, however, Hinze (1975) suggests that this difference is compensated for by the transfer of turbulence by diffusion.

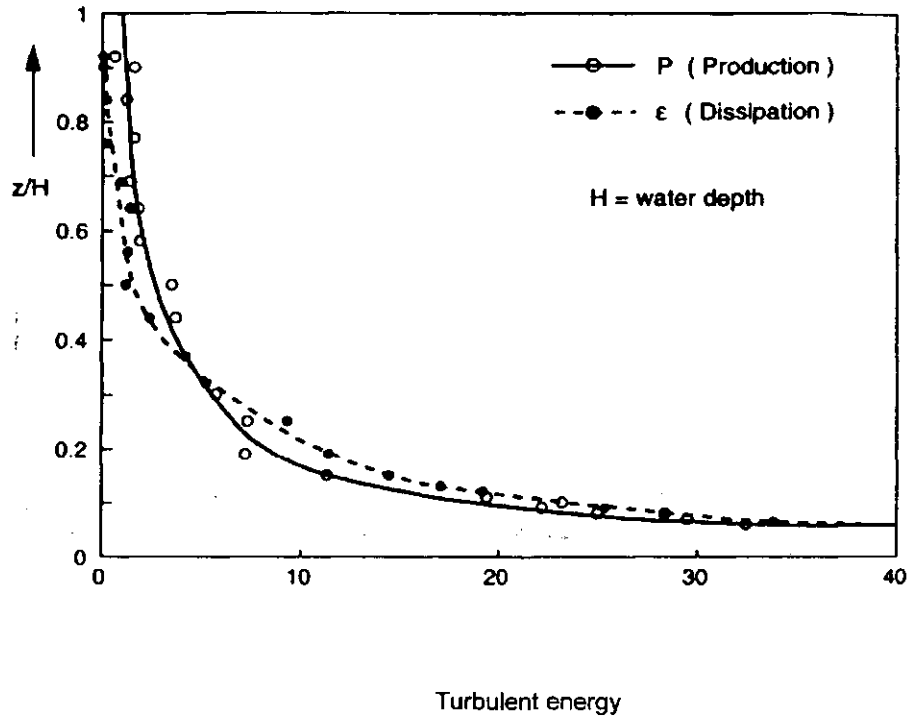

Figure 4.2 Distribution of turbulent energy production and dissipation in flowing water along a smooth wall (Nakagawa and Nezu, 1975).

Generally G can be defined as:

$$G = \left(\frac{\varepsilon}{\nu}\right)^{0.5} \tag{2.16}$$

where ν is the kinematic viscosity (molecular viscosity divided by the density of water). So assuming P = ε, G can be defined as:

$$G = \left[\frac{U_*^3}{(\kappa \cdot \nu \cdot z)}\right]^{0.5} \tag{4.14}$$

where κ is the Von Karmon constant, and z is the distance above the estuary bed.

The second alternative approach classifies the turbulence level by the size of the dissipating eddies in a turbulent flow as defined by Kolmogorov (1941), and is referred to as the microscale of turbulence, η (units are metres):

$$\eta = \left(\frac{\nu^3}{\varepsilon}\right)^{0.25} = \left(\frac{\nu}{G}\right)^{0.5} \tag{4.15}$$

Turbulence parameters were calculated at the INSSEV sampling height by a simple linear interpolation between the two pairs of EMCMs for the Tamar estuary experiments. TSS was measured at the INSSEV height during SWAMGIR1, so no interpolation was required.

For the measurements made on the 16th September 1998 (ebb tide) and 22nd September 1998 (flood tide) deployments, all flow sensors were arranged in a logarithmic profile which only measured the along channel (U) and vertical (W) flow components. In order to use the TKE method to obtain TSS, the cross-stream turbulent component (v') was calculated from the following relationship given by Bowen (1964):

$$0.51 = \frac{v'}{u'} \qquad \textbf{(4.16)}$$

4.3 CTD Seacat profiler

The recorded data was transferred from the profiler's internal memory to a notebook PC hard disk via an RS-232 connector. Communication was through Sea-Bird Electronics' *Seasoft* version 4.2156, using the terminal program *TERM19.EXE*. Each individually recorded cast, formed a separate file in the *.HEX* format. The Seasoft *DATCNV.EXE* program was then used to convert the *.HEX* files in to a *.CNV* format which could be imported into Microsoft Excel, Matlab, and other software packages. Each sensor output was in standard SI units, calibrated using the *2068.CON* file which contains the Seacat instrument calibration coefficients and configuration information.

Negative depth data points (from instrument deployments and recovery) were removed from each data set. The salinity data was presented as profile time series. The software *Surfer for Windows version 6.03* (Golden Software, Inc.) was used to contour the profiles with Kriging interpolation griding employed to determine the contours.

4.4 Gravimetric samples

4.4.1 General processing

Samples of the ambient suspended particle concentration were collected during the field study campaigns at the same sampling height as INSSEV by either simple water sampling units (Tamar estuary) or Niskin bottles (Gironde estuary). These samples were collected simultaneously with each INSSEV floc sample and provided the SPM data from which the floc population concentration referencing could be obtained. Also, between 12-20 samples of progressively increasing concentration were collected after each experiment, so that the OBS sensors could be calibrated.

Known volumes of the samples were vacuum filtered through Whatman™ GF/F 55 mm diameter glass fibre filter circles which had a nominal pore size of 0.45 μm. All filters were

pre-ashed at 450°C, then weighed by a five-figure electronic balance, and stored in individual air-tights plastic wallets. Filtration was conducted on-site, and the filters were stored in a deep freeze until required for further analysis. To obtain SPM concentrations, filters and solids were dried in a thermostatically controlled cabinet for 24 hours and then re-weighed and compared to the original filter dry weight. Organic content was determined by loss on ignition at 450°C for a 6 hour duration.

4.4.2 Bio-chemical composition tests

The Marine Chemistry Research Unit at UOP conducted three bio-chemical tests on suspended particulate matter samples acquired during the Tamar Estuary COSINUS experiment. The SPM samples used were filtered replicates extracted from the water bottle samples used to concentration reference the INSSEV floc samples. Each filter was split so as to produce three sediment loaded sub-samples for each analysis procedure. This permitted an average *content* value to be calculated (for each filter sample) for each bio-chemical test. The laboratory procedures used to obtain: chlorophyll-a levels, total carbohydrate content, and relative proportions of carbon/hydrogen/nitrogen (C/H/N), will be explained in turn.

4.4.2.a Chlorophyll-*a* analysis

The absorption of blue light by chlorophylls and phaeopigments produce emissions of red light. In a sample, the fraction of light transformed is proportional to the amount of pigment. Thus by measuring the absorption of light of specific wavelengths, it is possible to estimate the concentration of these pigments in the sample. This method is detailed in MacKinney (1941). Each filter paper loaded with its frozen SPM was transferred to a centrifuge tube to which 20 ml of methanol was added. The tubes were sealed and the contents warmed in a hot water bath maintained at a temperature of 65°C (boiling point of methanol), the stopper being periodically removed to release pressure inside the tube. When the methanol had boiled for 10 seconds, the tubes were removed, sealed and kept in the dark for approximately 5 minutes. The filter paper was carefully removed and squeezed to maximise solvent removal. The solvent was then centrifuged at 3500 rpm for 7 minutes to remove particles. The contents of each tube, a very faint green colour, was then decanted into a glass cuvette having a path length of 4 cm. The absorbence of the solution was then determined at 665 nm and 750 nm in a Philips Pu8720 Series UV/Vis Scanning Spectrophotometer zeroed on pure methanol. The difference between the two absorbencies was used in the following equation to calculate the Chlorophyll-a concentration (μgl^{-1}):

$$\text{Chlorophyll - } a = \frac{13.9 \cdot A \cdot v_{meth}}{d \cdot V_{filtrate}} \quad (4.17)$$

Where A = absorbence (units) = $A_{665nm} - A_{750nm}$, v_{meth} = volume of methanol (ml), $V_{filtrate}$ = volume of filtrate (l) and d = cell path length (cm). The constant value (13.9) was obtained during the calibration with the standard. The Scanning Spectrophotometer was calibrated from a chlorophyll-a standard stock prepared from commercially-available chlorophyll-a SIGMA^{TM}. The calibration procedure is detailed in Strickland and Parsons (1972).

4.4.2.b Total carbohydrate analysis

This parameter was measured using the phenol-sulphuric acid assay (Underwood et al., 1995). The section of filter paper was placed into a test tube and the total sediment carbohydrate was extracted by adding 2 ml of Milli-Q water, followed by 1 ml of 5% aqueous phenol (wt/vol) and 5 ml of concentrated H_2SO_4. The mixture was then centrifuged at 3000 rpm for 15 minutes and the absorbence of the liquid then measured at 485 nm on a Philips Pu8720 Series UV/Vis Scanning Spectrophotometer. Calibration was achieved by making up a standard curve of glucose concentration versus absorption to give concentration results in glucose equivalents made up in the phenol-sulphuric acid matrix described above.

4.4.2.c Carbon/Hydrogen/Nitrogen (C/H/N) analysis

From each section of filter paper, two discs (approximately 10 mm in diameter) with uniformly distributed SPM were removed with the use of a sharpened apple corer. The discs were placed into small tin cups and their weight determined. The cups were then crushed using tweezers, careful not to loose any sample, to await analysis. A Carlo Erba EA1110 CHNS analyser (CE Instruments) was used for the detection of carbon, hydrogen and nitrogen compounds evolved during analysis. The samples underwent dry combustion at 1000°C (Kramer et al., 1992) and the gas chromatograph (GC) column maintained separation at 60°C. Two blank filter samples were also combusted and yielded none of the above compounds giving no measurable contribution to the sample concentrations. A calibration was performed every 12 samples by placing an unweighed standard (Acetanilide: C = 71.09%, H = 6.71%, N = 10.36% and O = 11.84%), a blank and three weighed standards (approximately 1.5 mg each) into the carousel. This allowed the precision of the instrument to be assessed before commencing a deployment.

Chapter Five:

Experimental Results

The field experimental programmes were designed so that there would be a large amount of repetitive sampling during consecutive tides. This would permit a check on the repeatability of the instrumentation, whilst also incorporating a degree of redundancy into the analysis. This resulted in the compilation of a very comprehensive database of simultaneous floc, flow, concentration and master variable data. A selection of the processed data is available for model calibration at the following internet *URL*: *http://hydrography.ims.plym.ac.uk/cosinus/*. For this reason only the most representative time series and floc samples are presented in this chapter. The COSINUS experiment (3) results are presented in sections 5.1 and 5.2. Sections 5.3 and 5.4 present the data obtained from the preliminary Tamar estuary experiments (1 and 2) during spring and neap conditions, respectively. The results from the SWAMIEE experiment (SWAMGIR1) conducted during June 1999 in the Gironde estuary, are described in section 5.5. The results from the University of Plymouth laboratory flume experiments (5.6) are given in Appendix I. The final section, 5.7, gives the results of the LEGI laboratory grid tank experiments. For illustrative purposes, a selection of INSSEV floc images (from the data sets presented in this chapter of the thesis) are provided in Appendix VII.

5.1 Tamar estuary September 1998 - NEAP TIDES

The data collected between the 15-17th September from four separate deployments (two flood and two ebb) comprised the first half of experiment 3, which was also the COSINUS project field experiment. Throughout these neap tide deployments the river flow was at the annual mean rate of ~20 m^3s^{-1}, and the weather was very mild. Table 5.1 summarises the data acquisition for this set of field experiments. Most deployments were no longer than 3.5 hours in duration as the periods of high near bed turbulent shear stress coupled with steadily increasing or decreasing particulate concentration were of prime interest for this study. Table 5.2 shows the predicted tidal ranges for Devonport, for the experimental days. Maximum surface current velocities did not exceed 0.6 ms^{-1}, whilst near bed SPM concentration was typically 150-400 mgl^{-1} at the time of the turbidity maximum at Station A.

Table 5.1 Deployment summary for the Tamar estuary September 1998 experiment 3 during neap tides.

Date	Time - BST (hrs) run start	run end	INSSEV sample reference numbers	Total floc samples	Description of run
15/09/98	14:30	18:00	15-1 to 15-9	9	ebb tide - afternoon
16/09/98	11:00	14:30	16-2 to 16-11	10	flood tide - late morning
16/09/98	16:10	17:45	16-12 to 16-19	8	ebb tide - afternoon
17/09/98	13:10	15:30	17-1 to 17-10	10	flood tide - early afternoon

Table 5.2 Predicted tides at Devonport for the Tamar estuary September 1998 experiment 3 during neap tides.

Date	Time (hrs BST)	Height (m)
15/09/98	07:45	2.2
	14:12	4.4
16/09/98	09:26	2
	15:28	4.6
17/09/98	10:31	1.7
	16:30	4.9

5.1.1 Ebb Tide - Master Variables

Figure 5.1.A shows the variations in salinity during the ebb tide on 15th September at Station A. Just after high water at 14:30hr, the near bed salinity had reached a maximum of 10, with a halocline forming at about 2m above the bed, and freshwater at the surface. The level of the halocline progressively reduced as the surface freshwater ebb flow gained speed. However, the bottom layer salinity did not fall below 5 until 16:20hr. Thereafter the water column became predominantly fresh. The convoluted form of the halocline may be the result of the contouring package (*Surfer for Windows*), but could suggest considerable interfacial instability occurred during its retreat.

The flow velocity time series is shown in Figure 5.1.B. The first part of the record (15:45hr) shows that the surface current was ebbing at 0.3 ms^{-1}, whereas the lower 1 m of the water column was still flooding at a rate of ~0.1 ms^{-1}. This, albeit slow, flooding of the salt intrusion, coupled with the overlying fast ebbing surface current, had the potential to create a high level of turbulent induced mixing at the halocline interface. The bottom layer did not start to ebb until 16:10hr; this was 1 hour 30 minutes after predicted high water at Calstock. The ebbing bottom layer then rapidly accelerated to an initial peak velocity of 0.33 ms^{-1}, at 0.79 m above the bed, occurring at 16:30hr. Up to this point in the tidal cycle, the suspended particulate matter concentration (Figure 5.1.C) in the bottom layer had not exceeded 30 mgl^{-1}; a result of the underlying saline water preventing bed erosion. A decrease in velocity then occurred at both the 79 cm level and at the surface, where the current speed at the former level fell to 0.24 ms^{-1}. The SPM started to increase rapidly at 16:50hr, which coincided with the occurrence of a second current acceleration at the 79 cm level. These twin velocity peaks will be discussed in section 5.1.3.

A peak SPM value of 650 mgl^{-1} was measured 24 cm above the bed at 17:10hr. Interestingly the turbidity then declined quickly, even though the surface current velocity was still flowing at a rate of 0.5 ms^{-1}. This suggests the possibility that the particulate matter comprising the

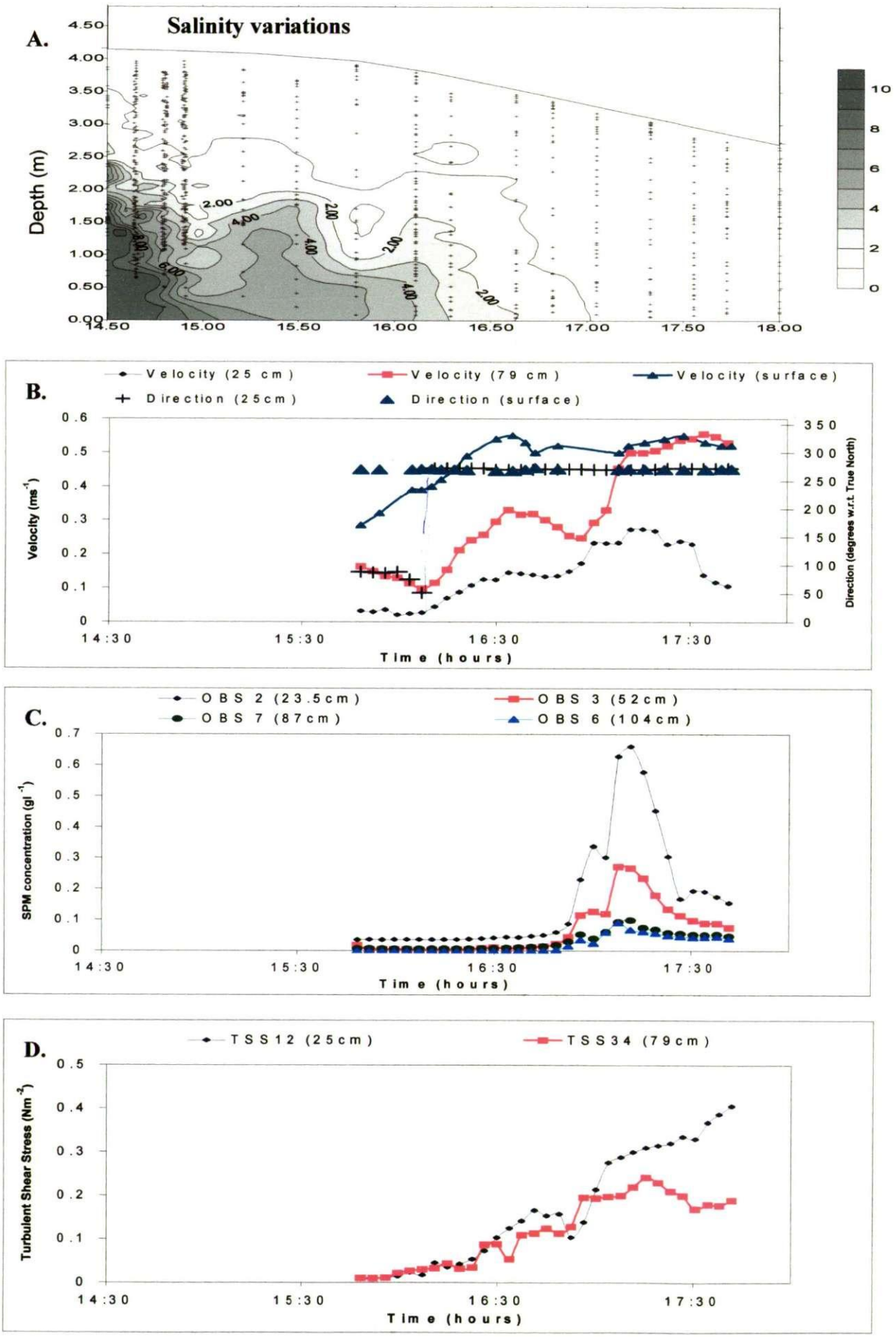

Figure 5.1. Time series of variations in: ***A.*** salinity, ***B.*** velocity, ***C.*** suspended particulate matter concentration, and ***D.*** turbulent shear stress for the neap tide on the 15th September 1998.

turbidity maximum was from a locally eroded source. Extrapolation from the record of calculated turbulent shear stress (figure 5.1.D) suggests that it had a critical erosion shear stress of ~0.17 Nm^{-2}. Although the soft top layer of the bed was easily eroded, there was probably not enough energy in the flow to remove any of the more compact sediment below, hence limiting the amount of material in suspension. A maximum turbulent shear stress (TSS) of 0.4 Nm^{-2} was measured at 25 cm above the bed, at the termination of this deployment at 17:40hr. This translates to a Kolmogorov eddy size of 475 μm, using equation 4.15.

Four gravimetric samples collected at: 15:56hr, 16:11hr, 16:41hr, and 17:31hr from 0.5 m above the bed were bio-chemically analysed (see Table 5.3). Early in the deployment, when the salt wedge was still present at Station A, the low amount of particulates in suspension was composed of 28% organic matter, most of which was particulate carbon. The chlorophyll-a content was approximately 0.44 μgl^{-1} and the total carbohydrate content was 37 mg/g SPM. As the concentration gradient increased, so the level of the organic matter and particulate carbon both reduced to ~13%. Similarly, at the occurrence of the highest concentrations the carbohydrate content had fallen to 12 mg/g SPM, whereas the chlorophyll-a content peaked at 1.04 μgl^{-1}. Laboratory analysis revealed that it was not possible for the C/H/N instrumentation to determine nitrogen or hydrogen levels for samples with concentrations under 1 gl^{-1} due to the lack of material retained on the filters.

Table 5.3 Bio-chemical composition of suspended particulate matter from samples obtain 0.5 m above the bed during Tamar estuary neap tides from experiment 3 (X denotes where no characteristic analysis was possible).

Date	Time (hrs)	Filter number	Ambient SPM (mgl^{-1})	Chlorophyll-a (μgl^{-1})	Total carbohydrate mass (mg/g SPM)	Total carbohydrate concentration (mgl^{-1})	Carbon (%)	Hydrogen (%)	Nitrogen (%)
150998	15:56	597	16	0.33	35.4	0.57	X	X	X
150998	16:11	598	17	0.44	36.9	0.63	X	X	X
150998	16:41	599	32	0.10	25.8	0.83	28.0	X	X
150998	17:31	600	80	1.04	12.1	0.97	12.8	X	X
170998	13:20	35	498	0.33	11.1	5.53	22.2	X	X
170998	13:50	320	588	0.83	6.3	3.70	6.5	X	X
170998	14:42	312	82	0.60	7.2	0.59	5.5	X	X
170998	15:24	316	40	0.41	16.8	0.67	11.6	X	X

5.1.2 Ebb Tide - Flocs

Nine INSSEV samples were collected during the ebb tide on the 15th September. The low ambient solids concentration limited the floc numbers to a maximum population of 148 aggregates sampled at the occurrence of the TM, at which time individual flocs sizes of up to 950 μm were recorded. The most identifiable feature from this series of floc measurements was the variations in floc effective density. Prior to 16:05hr, the floc effective density values were generally very high (500-1000 kgm^{-3}), as the record for INSSEV sample 15-1 (Figure 5.2) shows. Consequently, with the exception of size band (SB) 2 (40-80 μm), porosities were in the region of 23-65%, and fractal dimensions 2.45-2.9. This categorised these aggregates as strong flocs possessing a compact, mineral-like composition. A number of the aggregates captured by INSSEV in the sub-120 μm size range had settling velocities of 20-25 mms^{-1}, and consequently demonstrated effective densities 4-6 times greater than an equivalent quartz particle. The possible origin of these dense aggregates will be examined in the next chapter.

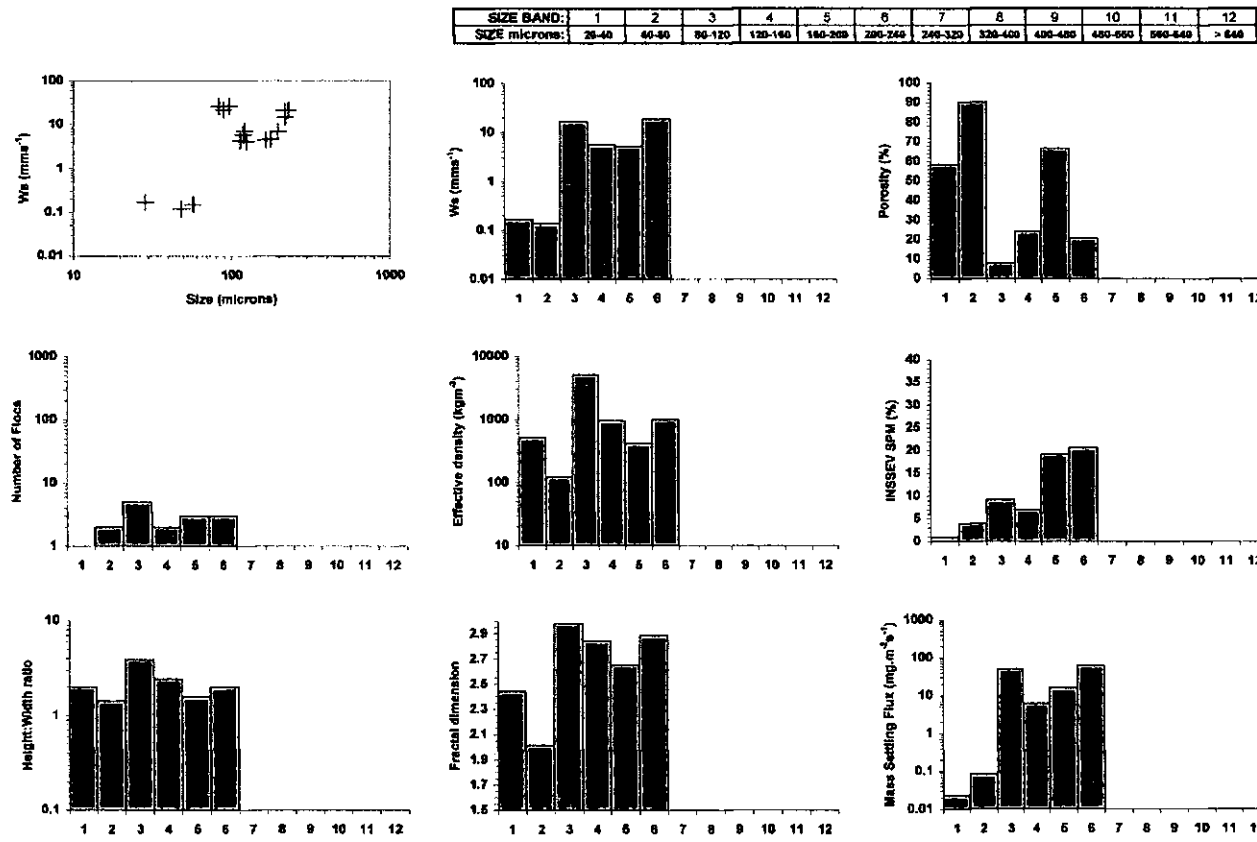

Figure 5.2 Floc characteristics for INSSEV sample 15-1 collected at 15:48hr.

As the salt wedge began to recede and fell below the INSSEV sampling height, the size spectra increased towards the larger sizes with the increasing SPM concentration. Sample 15-6 (Figure 5.3), taken at 16:41hr (HW+2:03), had two flocs in the 320-400 μm size range (SB 8), and these constituted 13% of the overall ambient SPM content (which was 32 mgl^{-1}). By now

the low turbulent (~0.14 Nm^{-2}; G = 2.8 s^{-1}) conditions permitted the more organic-rich, cohesive particles to flocculate, and this is reflected in the flocs throughout size bands 3-8, by a generally high porosity, and effective densities all under 105 kgm^{-3}. The SB 1-4 (20-160 μm) flocs which had settling velocities of 0.2-0.3 mms^{-1}, and fractal dimensions of 1.85-1.95, indicates that these were poorly bonded flocs and very susceptible to disaggregation under increased turbulent shear. Although the flocs greater than 160 μm in diameter sampled from 16:30hr onwards tended to have settling velocities predominantly in the 1-3 mms^{-1} range, a greater portion of the particulate mass was seen to move towards the macrofloc population. This was demonstrated by 52% of the SPM being contained by the flocs exceeding 160 μm in size, observed at 16:55hr (sample 15-7), when the TSS and SPM were 0.17 Nm^{-2} (G = 3.3 s^{-1}) and 115 mgl^{-1}, respectively.

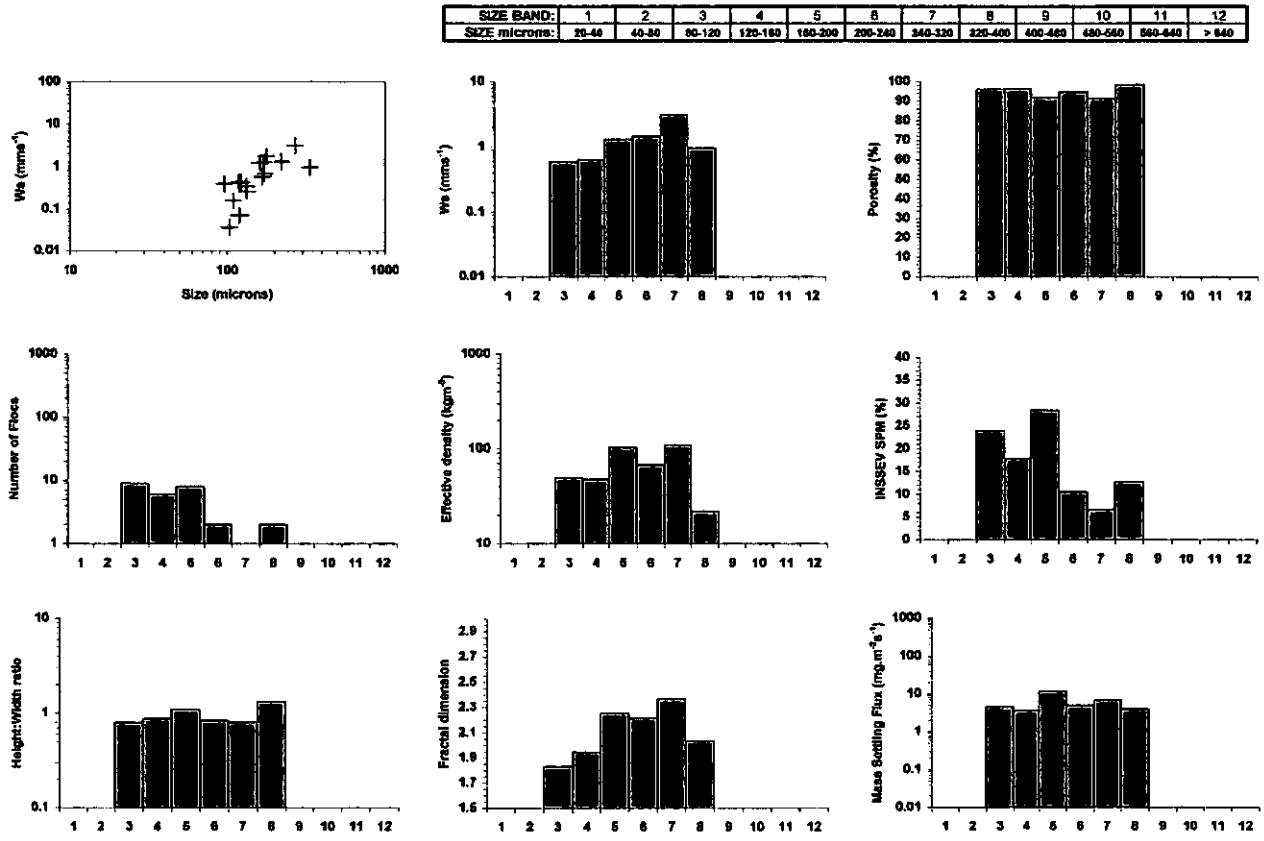

Figure 5.3 Floc characteristics for INSSEV sample 15-6 collected at 16:41hr.

By 17:08hr both the TSS and SPM had risen to values of 0.27 Nm^{-2} and 271 mgl^{-1}, respectively. Examination of INSSEV sample 15-8 (Figure 5.4), which was collected at 17:08hr, showed that the amount of suspended matter constituting the floc sub-population greater than 160 μm had increased to 77.4%. This suggests that the combined rise in particle abundance and turbulent shear stimulated floc growth. As the concentration fell to 80 mgl^{-1}, but the TSS level remained constant, so the proportion of particulate matter represented as

macroflocs reduced to 67.3%. In terms of mass settling flux (MSF, for sample 15-8), the flocs > 160 μm contributed 92.5% of the total MSF, only 1.6% more than the earlier sample (15-7). This was due to 47.5% of the MSF of sample 15-7 being contained by three lower density (~30 kgm^{-3}) flocs between 750-950 μm in diameter, with settling velocities of up to 9.7 mms^{-1}. For sample 15-9, the absence of fast settling flocs greater than 420 μm in diameter, reduced the MSF of the portion > 160 μm to 82.3%.

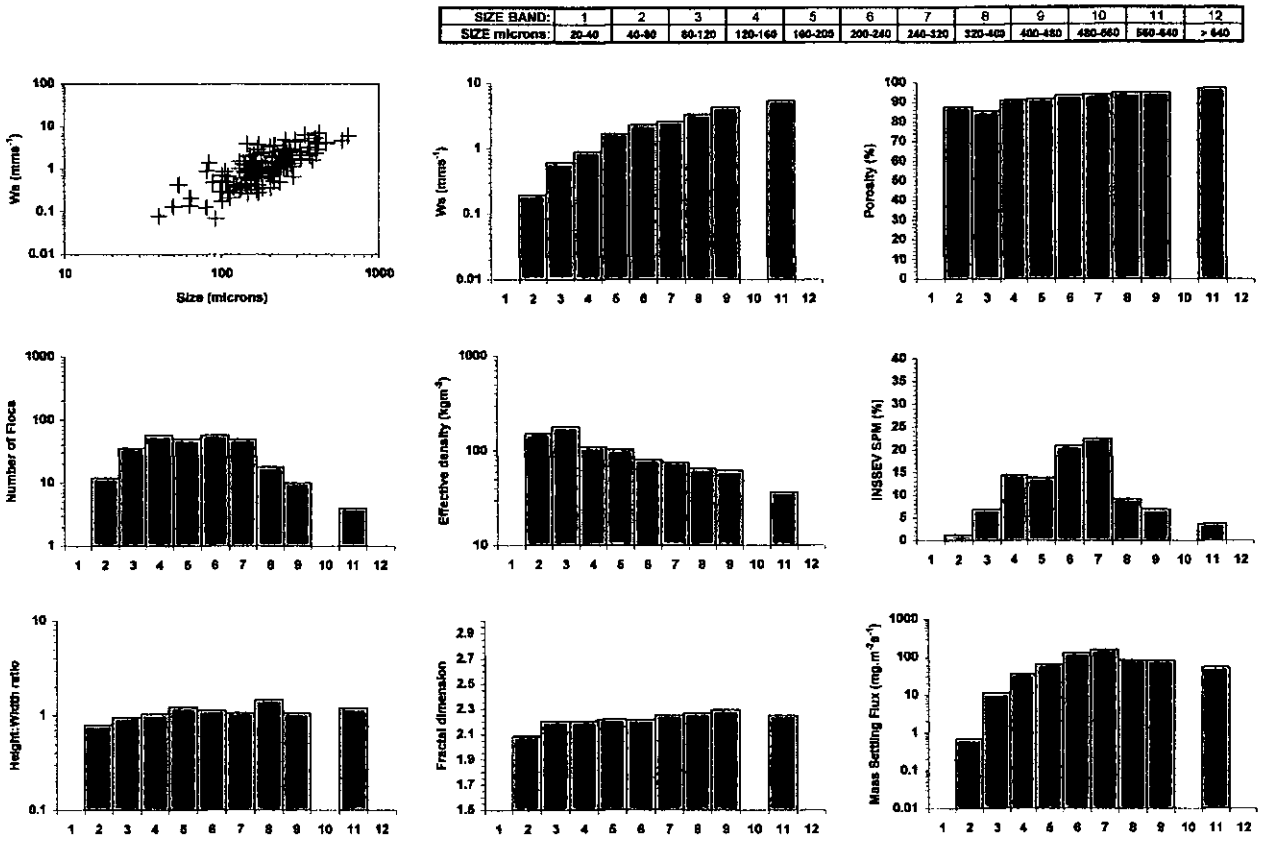

Figure 5.4 Floc characteristics for INSSEV sample 15-8 collected at 17:08hr.

5.1.3 Flood Tide - Master Variables

The first flood tide to be examined was on the 16th September and commenced at 11:00hr, which was 80 minutes after low water at Calstock. At this time the water column was composed entirely of freshwater as the salinity time series shows (see Figure 5.5.A). The salt intrusion arrived at Station A as a well mixed vertical wall at 12:30hr with a salinity of 2. By 14:30hr the near bed salinity had increased to 8.5, reducing in the upper one metre, to a salinity of 3. The flood water advancement in the upper estuary had the appearance of a constant thickness saline layer pushing under a wedge of fresher water. The surface current velocity (Figure 5.5.B) showed the flow speed increasing linearly with the growing water depth. The velocity peaked at a rate of 0.4 ms^{-1} at 12:00hr, then proceeded to decrease to 0.2 ms^{-1}. Examination of the SPM time series (Figure 5.5.C) shows that the initial current increase

$$+ UU_x = -g S_x$$

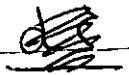

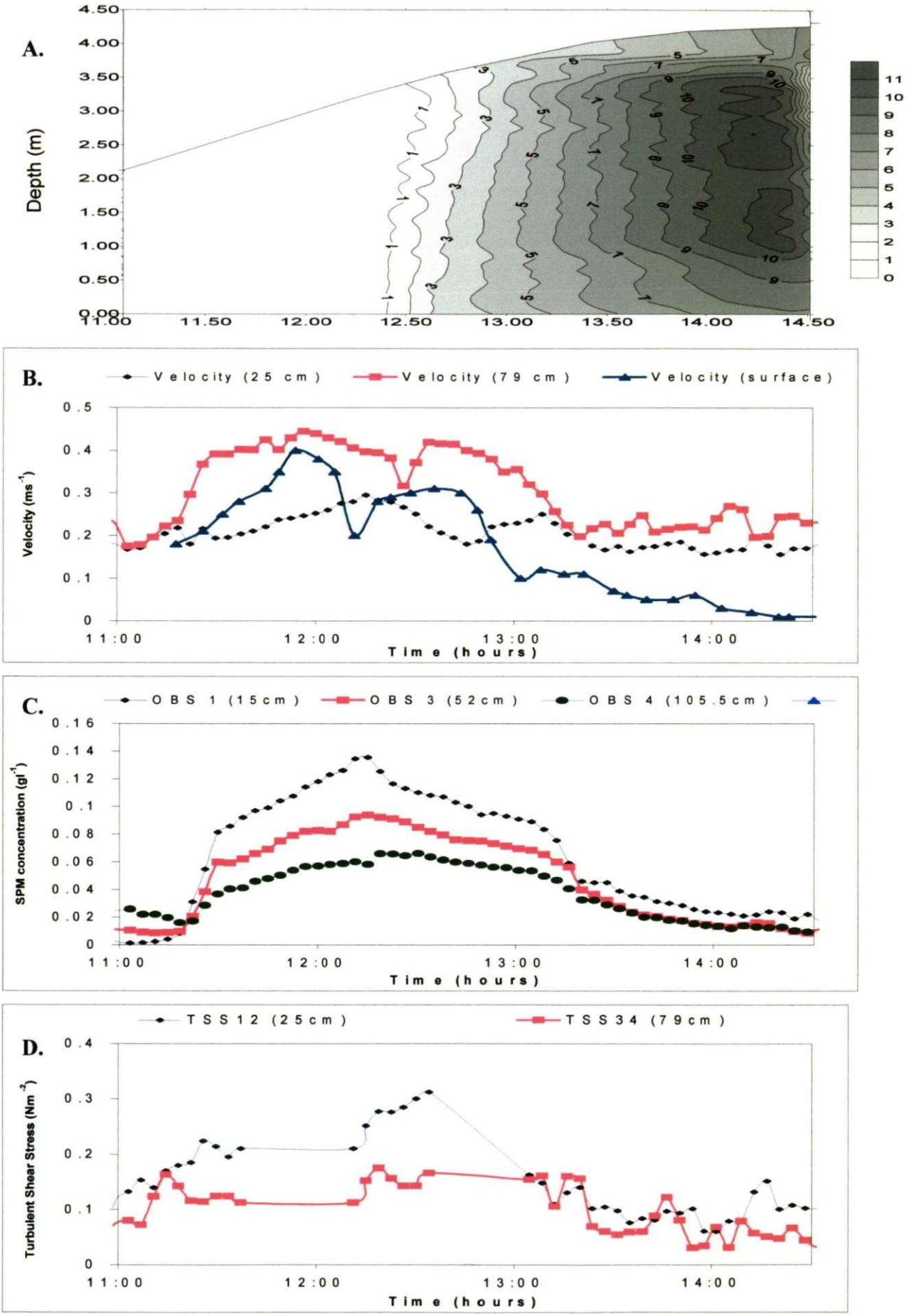

Figure 5.5. Time series of variations in: ***A.*** salinity, ***B.*** velocity, ***C.*** suspended particulate matter concentration, and ***D.*** turbulent shear stress for the neap tide on the 16th September 1998.

corresponds with the increasing concentration gradient. A maximum near-bed concentration of 138 mgl^{-1} occurred at 12:20hr. This event corresponded with the dip in surface current after the first peak, and was also just prior to the saline water reaching Station A. This indicates that the TM was on the upstream side of the salt intrusion on both neap ebb and flood tides.

Both the surface current velocity and the TSS 25 cm above the bed (Figure 5.5.D) continued to increase as the SPM content reduced. A second peak in surface current velocity occurred at 12:45hr with a rate of 0.3 ms^{-1}, and the near bed TSS reached a maximum value of 0.31 Nm^{-2}. The observation that the SPM concentration fell as the current speed continued to increase, suggested that the formation of a neap tidal TM in the upper estuary, on both the flood and ebb, was principally by erosion of a soft upper layer of the bed.

The observation of the double velocity peaks can be explained by changes in the water slope. A series of water level measurements were conducted at intervals during the neap tide deployment on the 16th September (see Figure 5.6). The errors in the measured slopes were $\pm 0.5 \times 10^{-5}$, so the findings were regarded as significant. The water level rise on the 16th flood tide was approximately 2 mhr^{-1}, but the slope was not monotonic. Up to the occurrence of the first velocity peak at 12:00hr, the water was seen to slope downwards towards the sea (a positive slope). After this peak the water slope then abruptly decreased, and was virtually horizontal by 12:30hr. As the second velocity peak developed at 12:45hr, the strong positive water slope returned. Dyer et al. (2000a) describes this as a "bow-wave" phenomenon whereby a bulge in the water surface precedes the saline intrusion moving upstream on the flood tide. The bulge causes a temporary reduction in the water slope, and consequently the reduction in flow velocity. A similar effect was also observed during the ebb tide on the 16th September, as the salt intrusion receded seaward. It was suggested that the presence of this feature controlled the separation of the salt intrusion from the turbidity maximum, at this time.

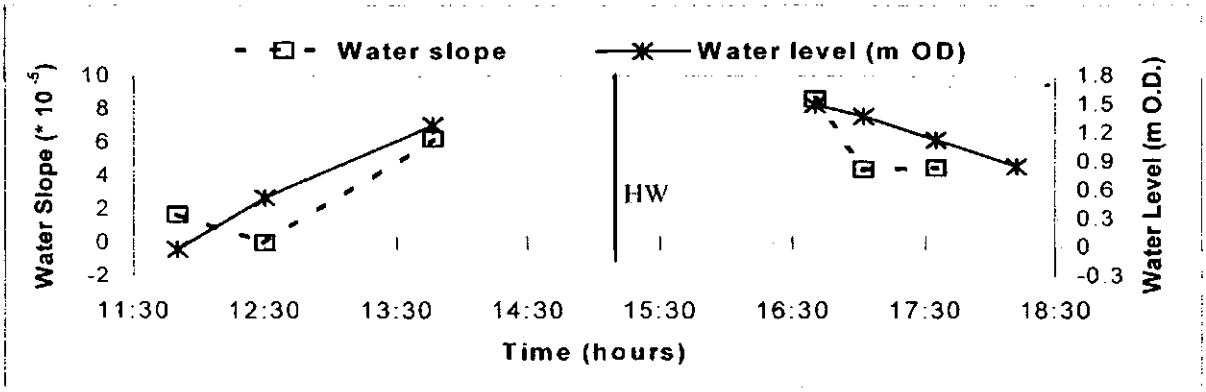

Figure 5.6 Water slopes between the lower and upper measuring positions on the neap tide of the 16th September 1998, and the water level at the lower position. Water levels are shown relative to Ordnance Datum. Slopes are positive when water slopes downwards towards the sea (from Dyer et al., 2000a).

The second neap flood tide results which will be presented, are those from the 17th September. During the early stages of the flood, the salinity (Figure 5.7.A) at 13:15hr was only 0.1 at Station A, whilst the surface current (Figure 5.7.B) was flooding at 0.48 ms^{-1}. The SPM concentration (Figure 5.7.C) at this stage in the flood tide was 0.78 gl^{-1} and 0.48 gl^{-1} at the 15 cm and 48 cm levels above the bed, respectively. The suspended matter in the early part of the record (13:20) was highly organic, with a particulate carbon content of 22.2%. This corresponded to chlorophyll-a and total carbohydrate contents of 0.33μgl^{-1} and 11.1 mg/g SPM, respectively. A marked increase in tidal range from the 16th to the 17th September, produced a greater amount of turbulent energy within the water column, as the initial TSS value (see Figure 5.7.D) of 0.55 Nm^{-2} indicated. This had the net result of suspending a higher amount of sediment.

A maximum turbidity gradient of 1.5 kgm^{-4} developed in the bottom region at 13:50hr, where the SPM concentration 15 cm above the bed peaked at 1.27 gl^{-1}. The particulate carbon percentage had dropped to 6.5%, indicating a marked reduction in organic matter. At this point in the tide, the chlorophyll-a content was 0.83 μgl^{-1}; this was a reduction of 20% from the particulates sampled during the occurrence of the TM at Calstock during the ebb on the 15th September. Similarly there was a 50% reduction in total carbohydrate, when compared with the 15th September, down to 6.3 mg/g SPM, however, the increased mass of particulates translated the total carbohydrate concentration to 3.7 mgl^{-1}. When this was compared to a total carbohydrate concentration of ~1 mgl^{-1} during the 15th September, the overall difference was significant. Close examination showed that the particle concentration continued to increase at least 45 minutes after the current velocity started to decrease. This signifies a combination of settling increasing the near bed concentration, together with a proportion of the matter in suspension probably due to advection. A dip in the surface current velocity coincided with the TM peak concentration at 13:50hr. The passing of the TM was followed by the vertically well mixed saline intrusion. The surface current steadily reduced to slack conditions by 15:30hr, where the salinity had risen to a maximum of 10 in the lower half of the water column.

5.1.4 Flood Tide - Flocs

A different flocculation pattern emerged for the flood period of the 16th September, when compared to the neap tide ebb. For the ebb tide, most of the flocculation occurred when particulate entrainment from the bed was at its highest, whereas during the flood tide of the 16th September, larger flocs were observed at the tail-end of the TM. This point is illustrated by Figure 5.8, which shows the INSSEV record for sample 16-4. These flocs were observed at

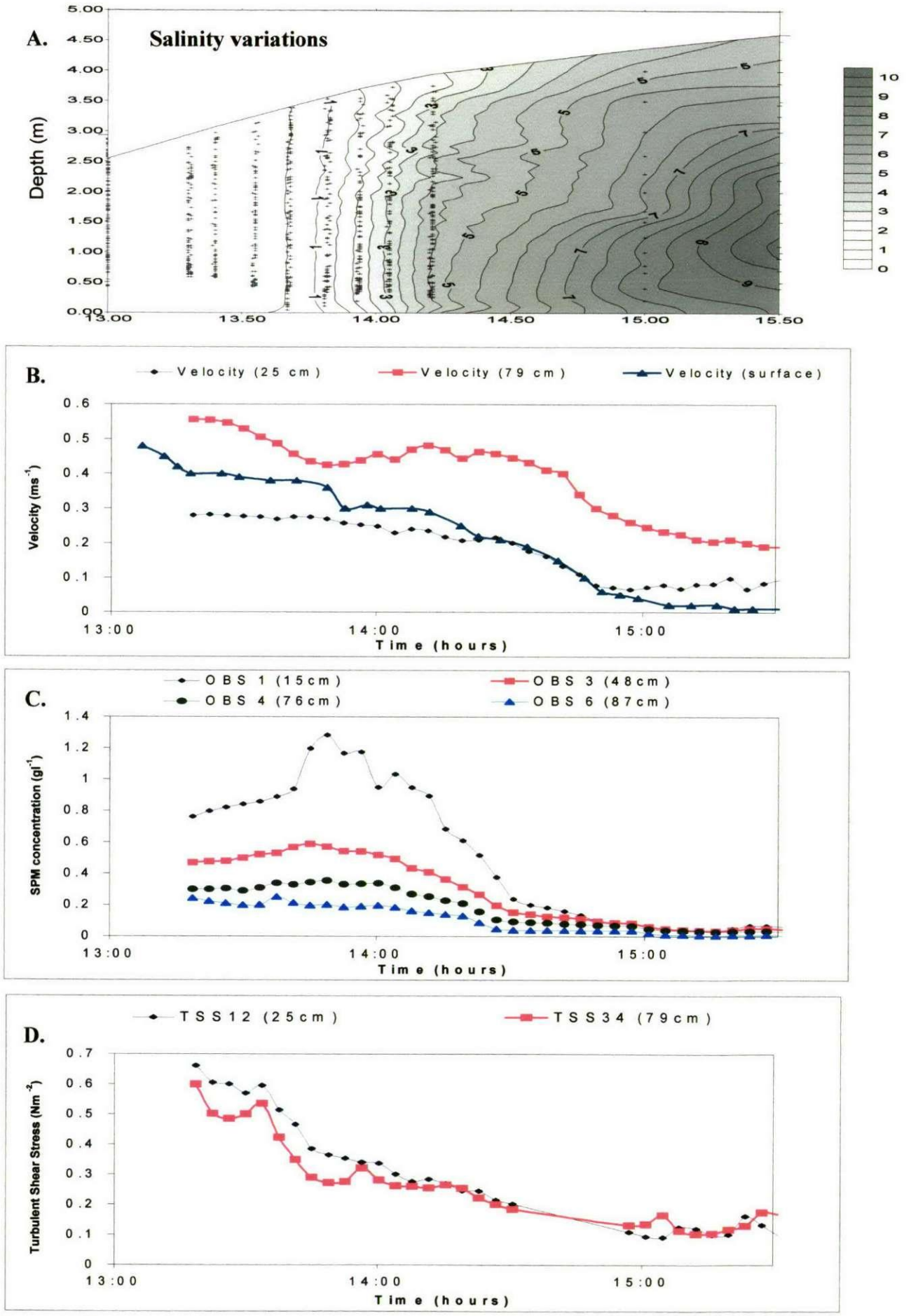

Figure 5.7. Time series of variations in: ***A.*** salinity, ***B.*** velocity, ***C.*** suspended particulate matter concentration, and ***D.*** turbulent shear stress for the neap tide on the 17th September 1998.

$$\frac{d}{dx}\left[(H+\zeta)u\right] = 0$$

12:15hr, when the TM had reached a peak concentration of 94 mgl^{-1}, together with a TSS of 0.2 Nm^{-2} (G = 3.7 s^{-1}), at the INSSEV sampling height of 0.5 m. These conditions limited the floc size to a maximum of 256 μm, and only 27% of the population were greater than 160 μm in size. The maximum settling velocity for the largest flocs was 2.3 mms^{-1}, whilst the mean settling rate for the latter floc group (> 160 μm) was 1.75 mms^{-1}.

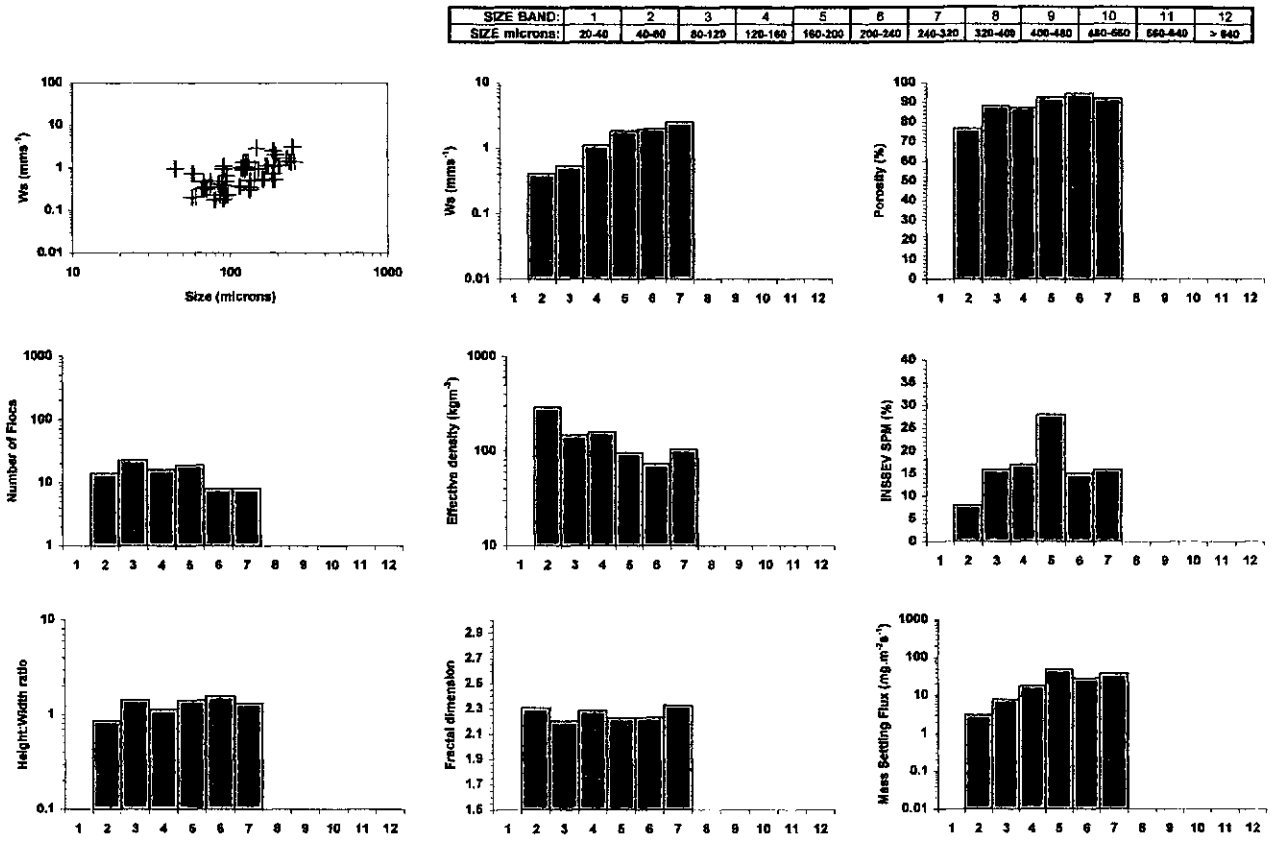

Figure 5.8 Floc characteristics for INSSEV sample 16-4 collected at 12:15hr.

Sample 16-5 (Figure 5.9) was taken 50 minutes later in the tide (than sample 16-4) where the ambient turbidity was still relatively high (~70 mgl^{-1}), but the TSS had fallen to 0.16 Nm^{-2} (G = 3.7 s^{-1}). At this time 54.2% of the flocs were over 160 μm, and the spherical equivalent size ranging between 24-560 μm. The larger fraction (SB10) of this floc population was "comet-shaped", very porous (98.2%), and had an effective density of around 23 kgm^{-3}. At the other extreme, the 24 μm microflocs were much more compact (porosity of 49%) and demonstrated an effective density of 634 kgm^{-3}. Comparatively the settling velocity of the respective size fractions were 2.79 mms^{-1} and 0.15 mms^{-1}, respectively.

As the turbidity gradient began to disperse at the tail-end of the TM, a more bi-modal floc distribution developed. The majority of the flocs were in the 20-200 μm size range (SB 1-5), with a limited number in the four highest size bands. This was a result of the larger flocs

formed earlier at higher SPM, settling out as the turbulent shear reduced to 0.1 Nm^{-2} (G = 2.2 s^{-1}) in the near bed region. Consequently, with a complementary decrease in the ambient turbidity levels (< 40 mgl^{-1}), the relative inter-particular contact frequency was significantly reduced.

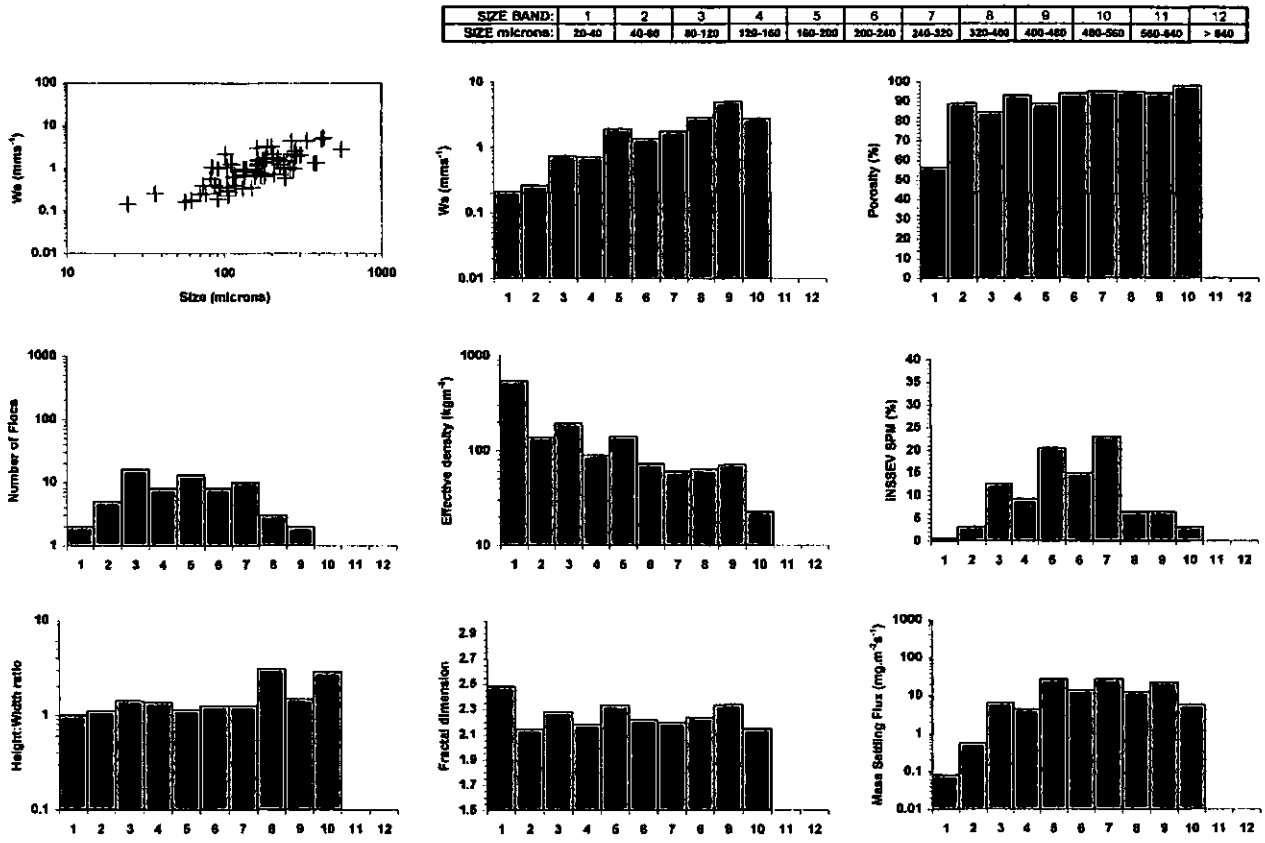

Figure 5.9 Floc characteristics for INSSEV sample 16-5 collected at 13:05hr.

The higher ambient current velocities experienced at Station A during the flood tide on the 17th September produced a much greater particulate concentration level during the TM formation, when compared to the earlier neap tidal deployments. This had a marked effect on both floc size and settling velocity. Figure 5.10 shows the floc characteristics of sample 17-1 which was recorded at 13:21hr. This was when the upstream section of the TM was at Station A, and the very turbulent flow conditions (TSS = 0.66 Nm^{-2}; G = 9 s^{-1}) had eroded a large amount of material from the bed producing a concentration of 498 mgl^{-1} at 0.5 m above the bed. Of the 289 individual flocs measured, only 110 flocs were larger than 160 μm in diameter. Although the SPM division was virtually equal between the two sub-groups separated at 160 μm, a third of the suspended matter mass was contained within 80-120 μm (SB3). These facts, together with a mean size of only 170 μm (for the larger fraction), indicated that the resultant high collision frequency created by the ambient conditions was not very productive from a flocculation perspective.

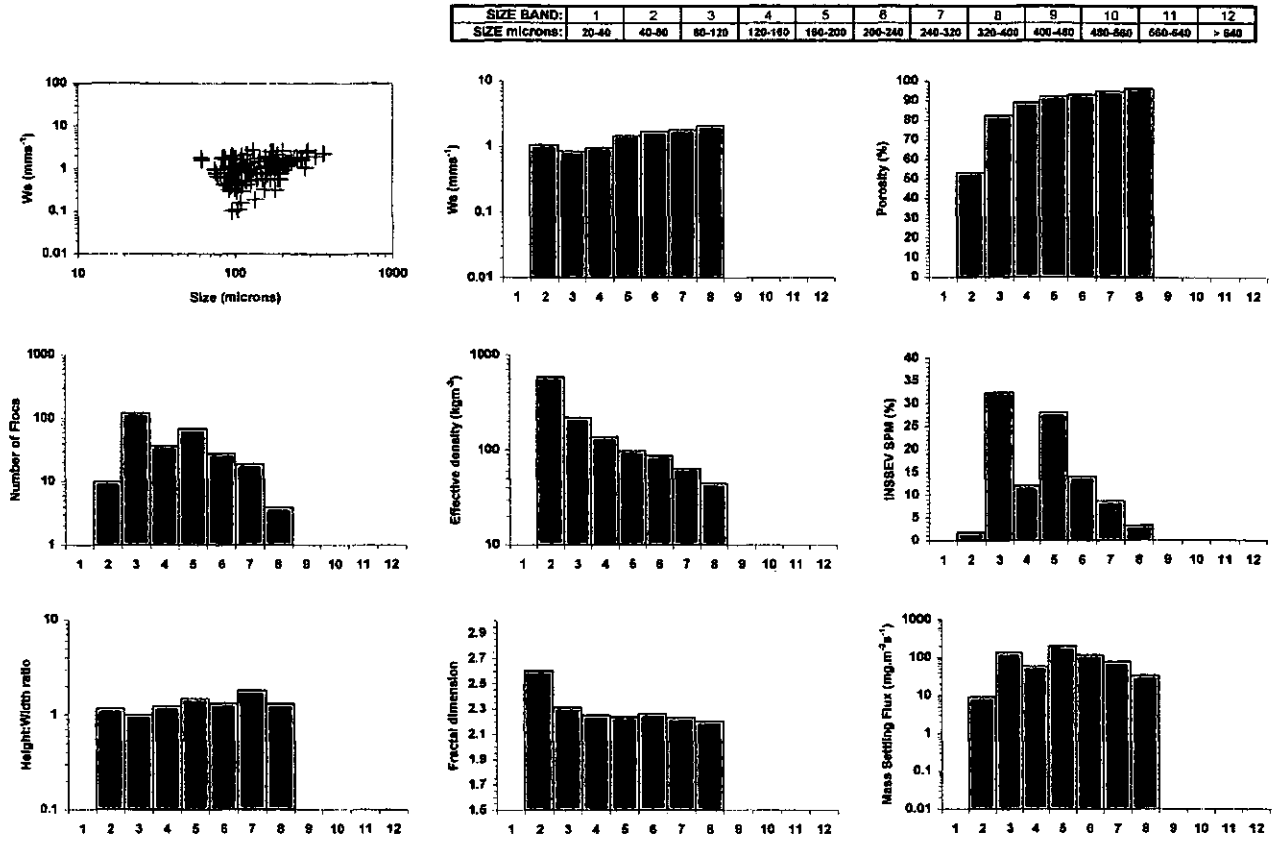

Figure 5.10 Floc characteristics for INSSEV sample 17-1 collected at 13:21hr.

By 13:45hr, the main body of the TM was in the Calstock location. The near-linear reduction in TSS, with increasing water depth, to a rate 0.34 Nm^{-2} (G = 5.5 s^{-1}) allowed more of the particles to coagulate as sample 17-3 (Figure 5.11) shows. A very distinctly bi-modal distribution was demonstrated by the observed floc population, consisting of 323 individual aggregates. The first sub-population comprised 148 small flocs with sizes ranging between 40-120 μm, and settling rates of less than 0.4 mms^{-1}. These microflocs had significantly higher effective density values than those of the larger flocs, suggesting they were lower order flocs from which the larger macroflocs were primarily constructed, as the order of aggregation theory suggests (Krone, 1963; 1986). The remaining flocs had significantly faster settling velocities ranging from 1.4 to 6.8 mms^{-1}. The size range had increased by 144 μm when compared to sample 17-1, giving a maximal floc size of 490 μm. The particulate matter was generally distributed more evenly through the floc size ranges, with the exception of SB5 (160-200 μm) which was a primary mode containing 27.5% of the SPM.

Once the tail-end of the TM had arrived at Station A (14:08hr), the reduction in both TSS and SPM to respective values of 0.27 Nm^{-2} (G = 4.6 s^{-1}) and 434 mgl^{-1}, brought about a further evolution in the flocculation cycle. At this point in the flood tide, the total carbohydrate

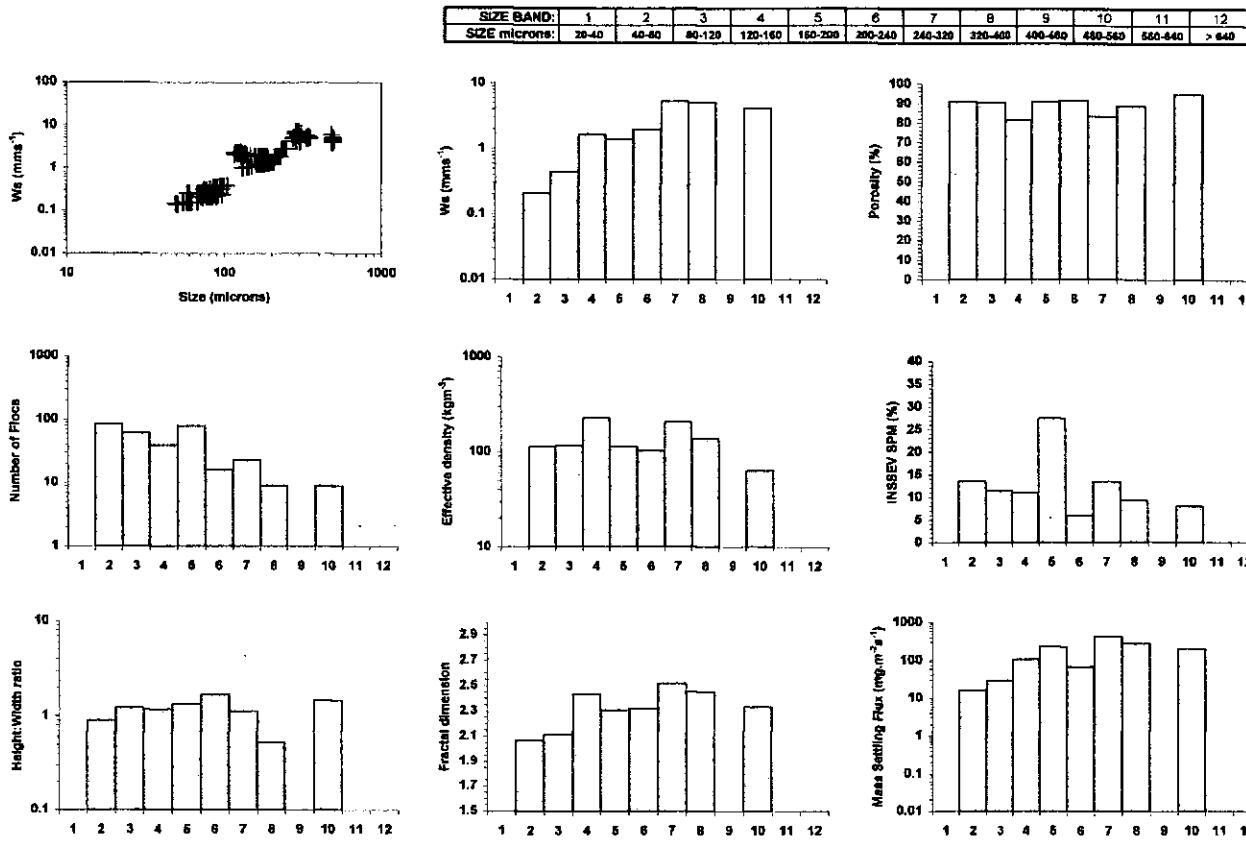

Figure 5.11 Floc characteristics for INSSEV sample 17-3 collected at 13:45hr.

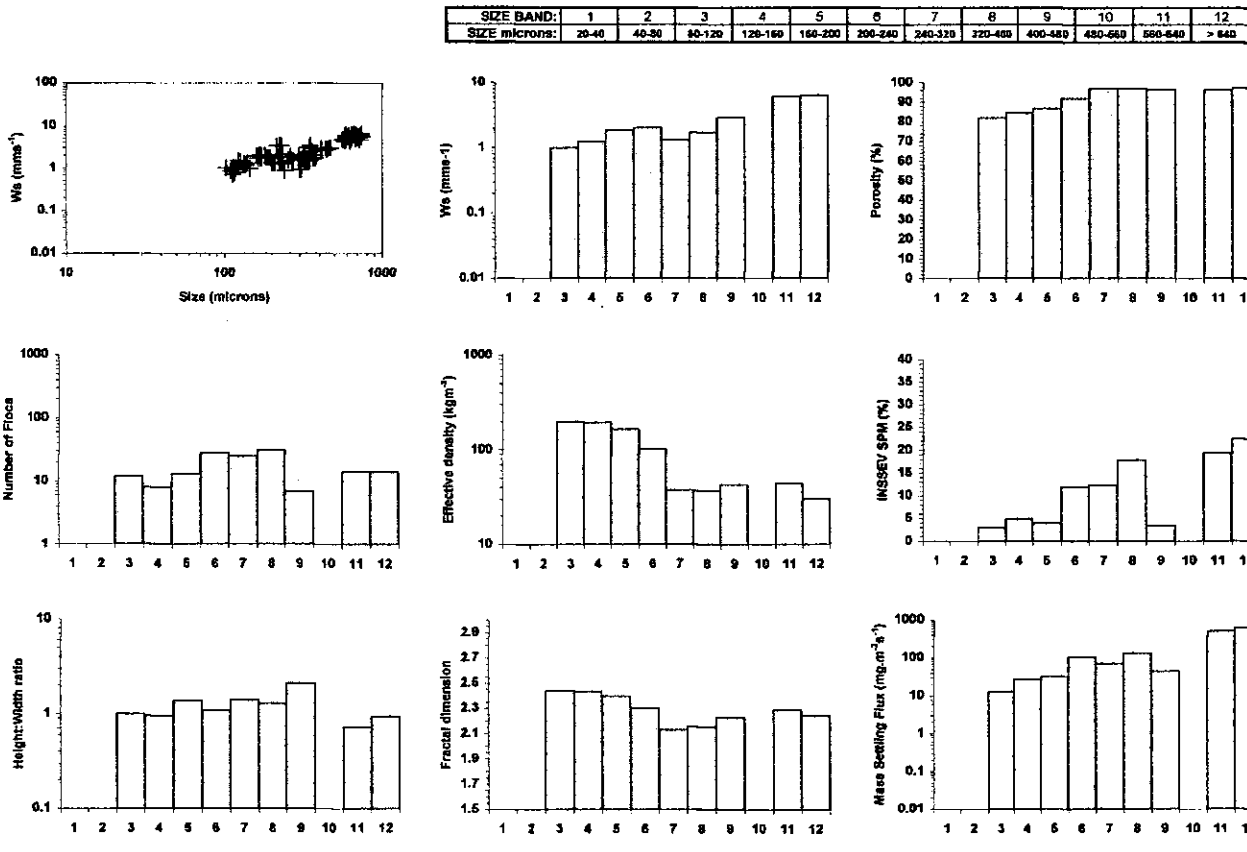

Figure 5.12 Floc characteristics for INSSEV sample 17-5 collected at 14:08hr.

concentration was at its peak (2.52 mgl^{-1}). Thus, the combined interaction between the hydro-dynamical mixing and the "stickier" particulate mater, resulted in optimal flocculated aggregate growth as sample 17-5 indicated (Figure 5.12). There were only 20 flocs less than 160 μm in size, the largest flocs measured 740 μm in diameter, and the whole population was composed of only 152 individual aggregates. The two largest size band flocs had settling velocities of ~7 mms^{-1}, with the remainder having settling rates of between 1-3 mms^{-1}, but all of the flocs over 240 μm in size were of very low density ($\rho_e < 45$ kgm^{-3}). The very low effective density of these flocs, was a result of the low turbulent shear creating more numerous low-impact inter-particular collisions which gave the larger flocs a more ragged appearance, and consequently a greater number of voids.

$$u_t + uu_x = -g\zeta_x$$

5.2 Tamar estuary September 1998 - SPRING TIDES

The second half of the COSINUS experiment (experiment 3) was conducted during the spring tides of the 21st-23rd September and the same stations were utilised. A total of 29 INSSEV samples were obtained (Table 5.4). Most flocs samples were from dilute suspension concentrations of 0.5-3 gl^{-1}, however six samples were obtained from within CBS layers possessing SPM concentrations of up to 8.5 gl^{-1}. The tidal range (Table 5.5) was much higher than the preceding week's neap tides, and contributed to current velocities nearing 1 ms^{-1}. The river flow remained unchanged at the annual mean flow rate.

Table 5.4 Deployment summary for the Tamar estuary September 1998 experiment 3 during spring tides.

Date	Time - BST (hrs)		INSSEV sample	Total floc samples	Description of run
	run start	run end	reference numbers		
21/09/98	12:00	13:45	21-1 to 21-4	4	ebb tide - early afternoon
21/09/98	15:00	16:48	21-5 to 21-7	3	flood tide - afternoon
22/09/98	11:00	12:45	22-1 to 22-6	6	ebb tide - late morning
22/09/98	16:10	18:20	22-7 to 22-14	8	flood tide - afternoon
23/0998	10:40	13:25	23-1 to 23-8	8	ebb tide - afternoon

Table 5.5 Predicted tides at Devonport for the Tamar estuary September 1998 experiment 3 during spring tides.

Date	Time (hrs BST)	Height (m)
21/09/98	07:00	5.3
	13:23	0.8
	19:10	5.4
22/09/98	07:32	5.3
	13:55	0.8
	19:42	5.4
23/09/98	08:02	5.3
	14:23	0.9
	20:13	5.3

5.2.1 Ebb Tide - Master Variables

The spring ebb run on 21st September concentrated on a 2 hour 40 minute period prior to low water (at Calstock), which was around 14:00hr. The water column was fresh throughout for the latter stages of the ebb. The surface flow (Figure 5.13.A), which had a velocity of 1 ms^{-1} at 11:10hr, linearly decreased in speed in response to the water level reduction, and reached a minimum speed of 0.16 ms^{-1} at low water, Devonport (local LW occurring later). The near bed SPM concentration (Figure 5.13.B) was 4 gl^{-1} at 12:25hr, a marked increase when compared to the preceding neap tides. This created a concentration gradient of 2.78 kgm^{-4} immediately above the bed.

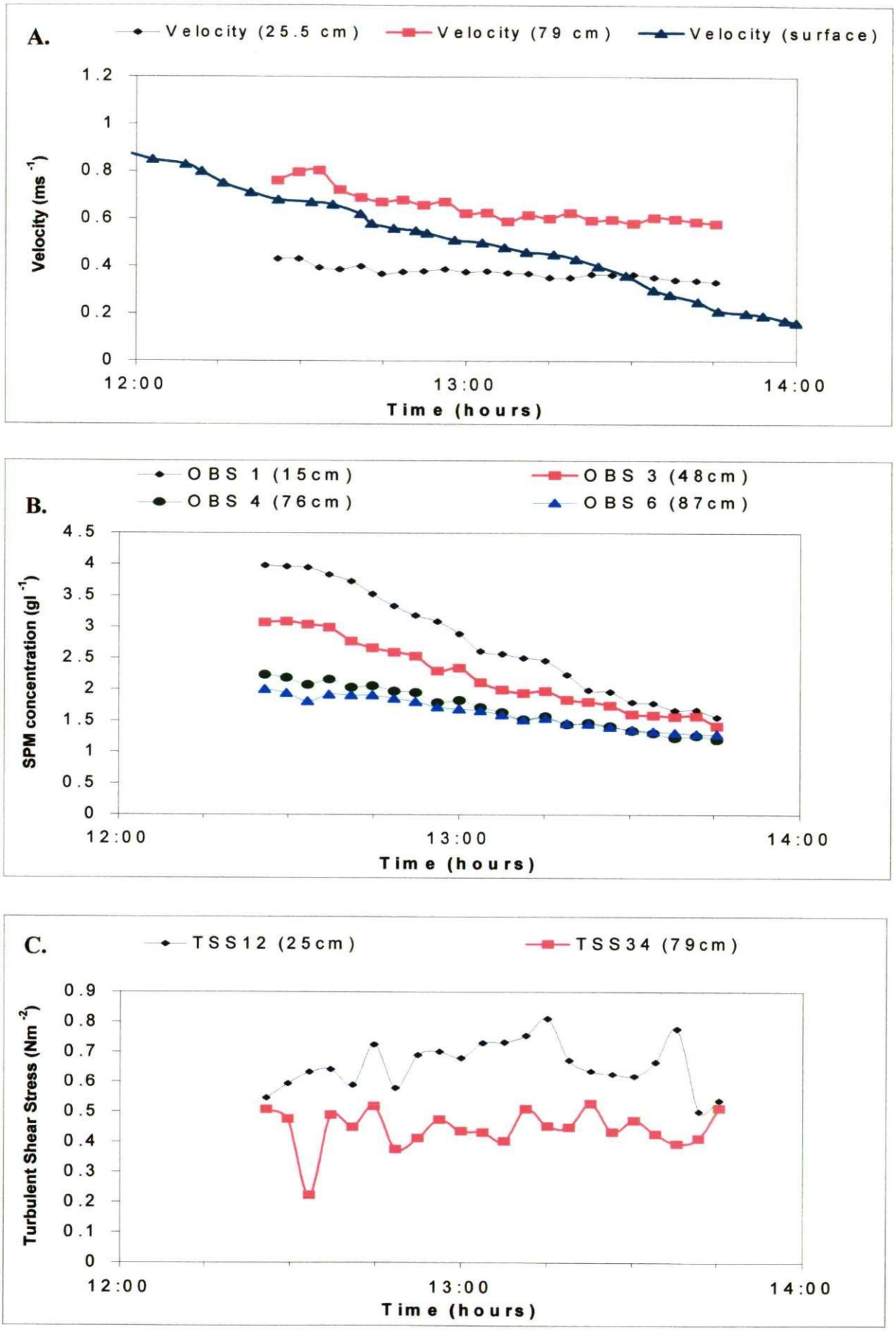

Figure 5.13. Time series of variations in: ***A.*** velocity, ***B.*** suspended particulate matter concentration, and ***C.*** turbulent shear stress for the spring tide on the 21st September 1998.

The carbon content of the particulate matter throughout the 90 minutes leading to low water was much less than measured under neap conditions, with the carbon content remaining at 5.3% through this ebb run. Measurements of total carbohydrate (two samples during this ebb run), indicated that the mass per gramme of sediment had significantly reduced during this spring tide ebb, the content not exceeding 5.2 mg/g SPM (see Table 5.6). The hydrogen and nitrogen levels were 1% and 0.46% respectively at 12:20hr, and reduced to 0.7% and 0.25%, respectively, by low water. Over the same period the chlorophyll-a level halved, from an initial value of 0.32 μgl^{-1}. Although the velocity recorded for this period seems relatively smooth, the turbulent shear stress (Figure 5.13.C) displayed far more variation in response to the concentration changes. At 25 cm above the bed the TSS had an intensity of 0.54 Nm^{-2} at 12:25hr.

By 13:15hr the SPM concentration (at the 25 cm level) had fallen to 2.5 gl^{-1}, and even though the near bed current velocity at the same height had remained virtually constant throughout during this period, the TSS at 25 cm had increased to 0.8 Nm^{-2}. This indicates that the high initial density gradient (due to concentration) was probably affecting the turbulence. This is supported by a gradient Richardson number Ri_g of 0.05 calculated (using equation 2.1) for the region between 0.25-0.79 m above the bed at 12:25hr.

Table 5.6 Bio-chemical composition of suspended particulate matter from samples obtained 0.5 m above the bed during Tamar estuary spring tides from experiment 3 (X denotes where no characteristic analysis was possible).

Date	Time (hrs)	Filter number	Ambient SPM (mgl^{-1})	Chlorophyll-a (μgl^{-1})	Total carbohydrate mass (mg/g SPM)	Total carbohydrate concentration (mgl^{-1})	Carbon (%)	Hydrogen (%)	Nitrogen (%)
210998	12:20	201	2771	0.32	3.7	10.3	5.3	1.00	0.46
210998	13:15	209	1974	0.18	5.2	10.3	5.3	0.70	0.25
210998	14:59	215	1142	0.07	6.4	7.3	4.6	0.60	0.22
210998	15:54	221	4270	0.28	1.1	4.7	4.4	0.66	0.38
210998	16:54	229	4992	0.19	3.4	17.0	7.3	0.74	0.64
230998	10:54	515	448	0.15	7.1	3.2	6.5	X	X
230998	11:56	523	1910	0.27	5.1	9.7	5.6	0.40	0.21
230998	12:42	517	3085	0.20	3.7	11.4	5.2	0.90	0.33
230998	13:18	519	2934	0.21	4.1	12.0	5.2	0.81	0.30

5.2.2 Ebb Tide - Flocs

Figure 5.14 shows the record for INSSEV sample 21-1 which was collected on the 21st September at 12:26hr. The ambient concentration was just over 3 gl^{-1}, and the TSS was 0.53 Nm^{-2} (G = 7.6 s^{-1}) - both at the INSSEV sampling height of 0.5 m above the bed. Sample 21-1 constituted a total population of 973 individual flocs. There was a negative skewing of the population distribution across the size spectra, with most aggregates having a near-spherical shape. Settling velocity distributions showed a very linear increase in settling rate, with each larger size band sub-group. The population was dominated by an abundance of macroflocs, with 77.6% of the mass contained by flocs in excess of 200 μm in size. The aggregates composing this section of the floc population became progressively less dense and more porous structurally as their size increased. This was shown by the respective values of effective density and porosity being 82 kgm^{-3} and 93.4% for the SB6 flocs. In comparison the flocs over 640 μm in diameter, the size band mean effective density had reduced to 33 kgm^{-3}, whilst the porosity had risen to 97.3%. Furthermore, the size spectra showed that nearly half of the particulate mass was represented by flocs over 320 μm in diameter. It may also be hypothesised that the addition of a total carbohydrate concentration of 9.6 mgl^{-1} (which was 3.8 times higher than experienced during neap tides), could have had a significant effect by assisting with inter-particular bonding as a result of the high collision frequency. Although the spectra showed a predominantly unimodal distribution of the SPM%, with the primary mode (20.2%) occurring at SB8 (320-400 μm), a much higher mass settling flux existed in the higher size bands despite their individually lower total mass content. For example, the largest size fraction (> 640 μm) had a sub-population of 14 flocs and this constituted 4% of the total particulate mass in suspension; but with the aggregates possessing a mean settling velocity of 6.1 mms^{-1}, a resultant MSF of 770 $mg.m^{-2}s^{-1}$ was achieved (for SB12). Comparing this to SB8 which had a MSF of 2760 $mg.m^{-2}s^{-1}$, 3.58 times that created by the higher size band (12) flocs. However this was achieved by SB8 having nearly 9.5 times as many aggregates composing its sub-population. The total mass settling flux for this sample was 10.4 $g.m^{-2}s^{-1}$. To put this into context, this MSF value was 6.7 times greater than the value computed by the use of an estimated settling velocity of 0.5 mms^{-1}; a typical parameterised Ws value used in numerical model simulation of sediment transport.

INSSEV sample 21-4 was obtained 49 minutes later at 13:15hr, and the floc characteristics are shown in Figure 5.15. The increase in TSS to a run peak of 0.68 Nm^{-2} (G = 9.2 s^{-1}), together with a 50% reduction in the ambient SPM to ~2 gl^{-1} (both at the INSSEV sampling height), had the subsequent effect of restricting floc growth to a single maximum floc with a

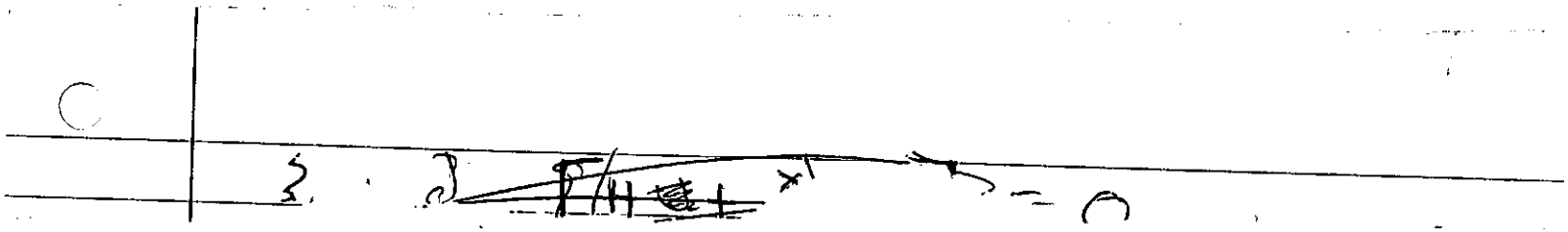

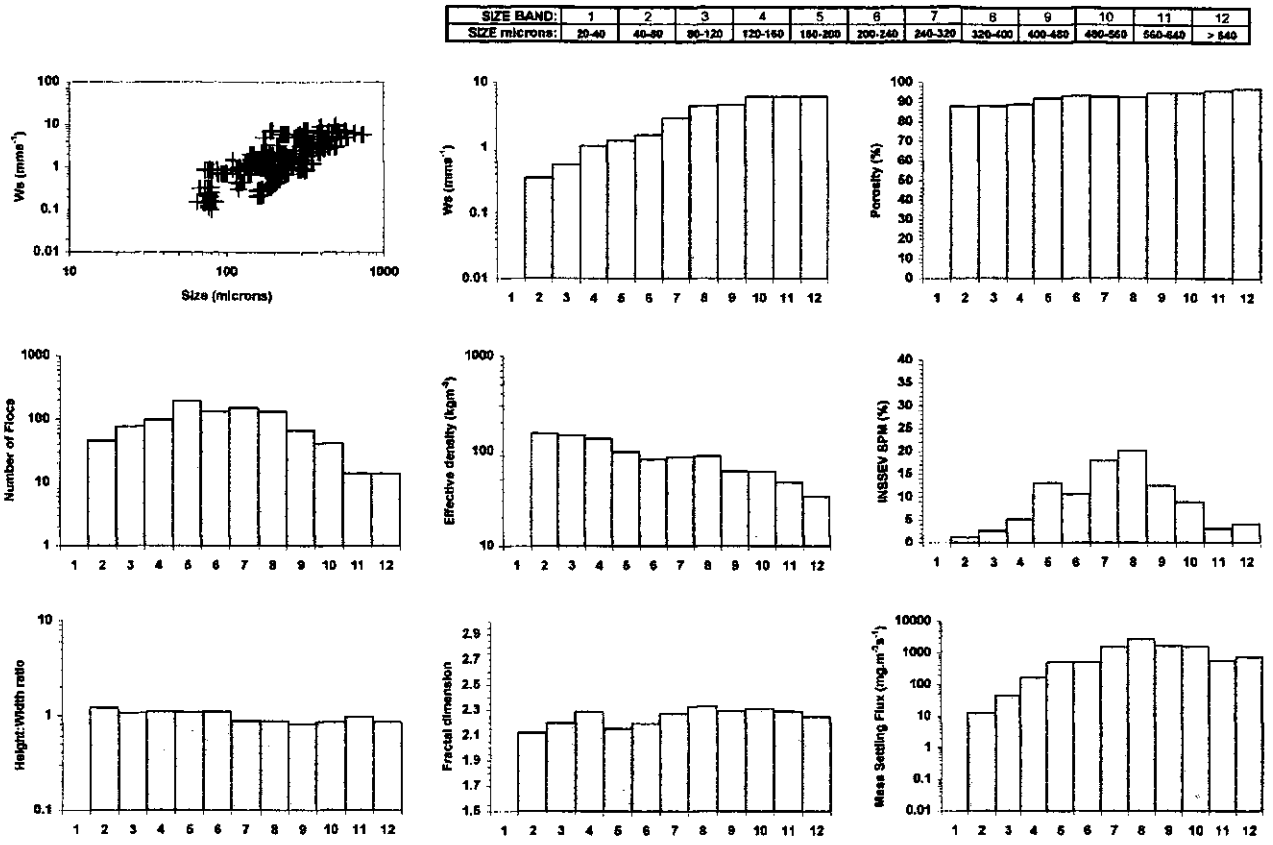

Figure 5.14 Floc characteristics for INSSEV sample 21-1 collected at 12:26hr.

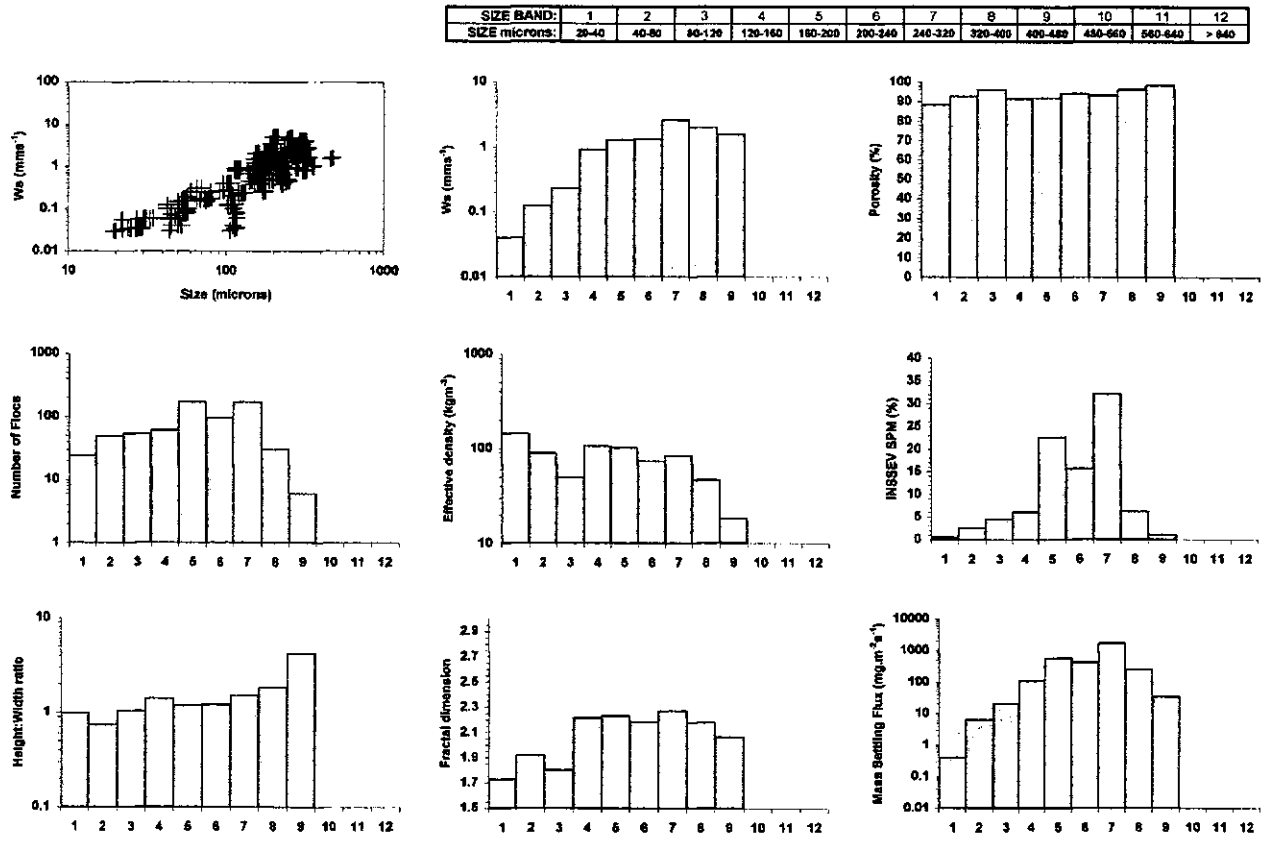

Figure 5.15 Floc characteristics for INSSEV sample 21-4 collected at 13:15hr.

diameter of 458 μm. With a size restriction imposed on the floc population, this had the result of shifting the primary modal size band from SB8 down to SB7 (240-320 μm), which contained 32% of the dry floc mass. Also it was observed that the resultant aggregates had significantly lower settling velocities than those of the earlier sample. Where the macroflocs for sample 21-1 had a mean settling rate of 3.6 mms^{-1}, for sample 21-4, this value had reduced to just 2.1 mms^{-1}. From a settling flux perspective, even after adjusting for the difference in concentration between the two samples, the increasing turbulent shear rate meant that sample 21-4 produced a 45% decrease in the total mass settling flux rate.

5.2.3 Flood Tide - Master Variables

During the spring tide flood run conducted during the afternoon of the 22nd September, the first sign of saline water (Figure 5.16.A) was not apparent at Station A until 16:40hr. As with the previous tide, the salt intrusion arrived at Calstock on the flood as a well mixed saline wall and reached a salinity of 3.2 by 18:20hr. The variations in current velocity can be seen in Figure 5.16.B, and it was evident that the surface current did not alter to the flood direction until 15:50hr, some 1 hour 30 minutes after predicted local low water. The flood dominance of the tidal flow in the Tamar estuary was very well displayed by the rapid acceleration in the surface current velocity. It only took 50 minutes to reach a peak velocity of 0.77 ms^{-1} at 16:40hr. This velocity was then sustained for a further 50 minutes, whereafter it steadily decreased to 0.12 ms^{-1} by 18:30hr. Figure 5.16.C showed that the SPM concentration increase did not start to significantly respond to the surface current until 25 minutes into the flood, when the velocity had accelerated to 0.43 ms^{-1}.

There was no distinct double peak in the surface velocity record, as observed during the neap flood conditions. However a minor peak was observed 25 cm above the bed, at 16:20hr, which coincided with a first peak in the TSS of 0.7 Nm^{-2} (Figure 5.16.D) at the same height. It was this period that saw high magnitudes or values of particulates entrained above the lower 0.5 m of the water column. There was no concentration record closer to the bed, as the lower OBS sensors were saturated. This would be consistent with the strong fast spring flood tide causing a significant amount of bed erosion. At 17:15hr the SPM concentration 58 cm above the bed had increased to 8 gl^{-1}, and extrapolation indicated the presence of fluid mud conditions closer to the bed (SPM > 10 gl^{-1}). A comparison between concentration measurements made at Stations A and B showed that the concentration rose simultaneously at both stations at 16:15hr, and then decreased at 17:35hr when the current velocity fell below 0.7 ms^{-1}. This implied that the spring flood tide was dominated by erosion, with only a minor advection

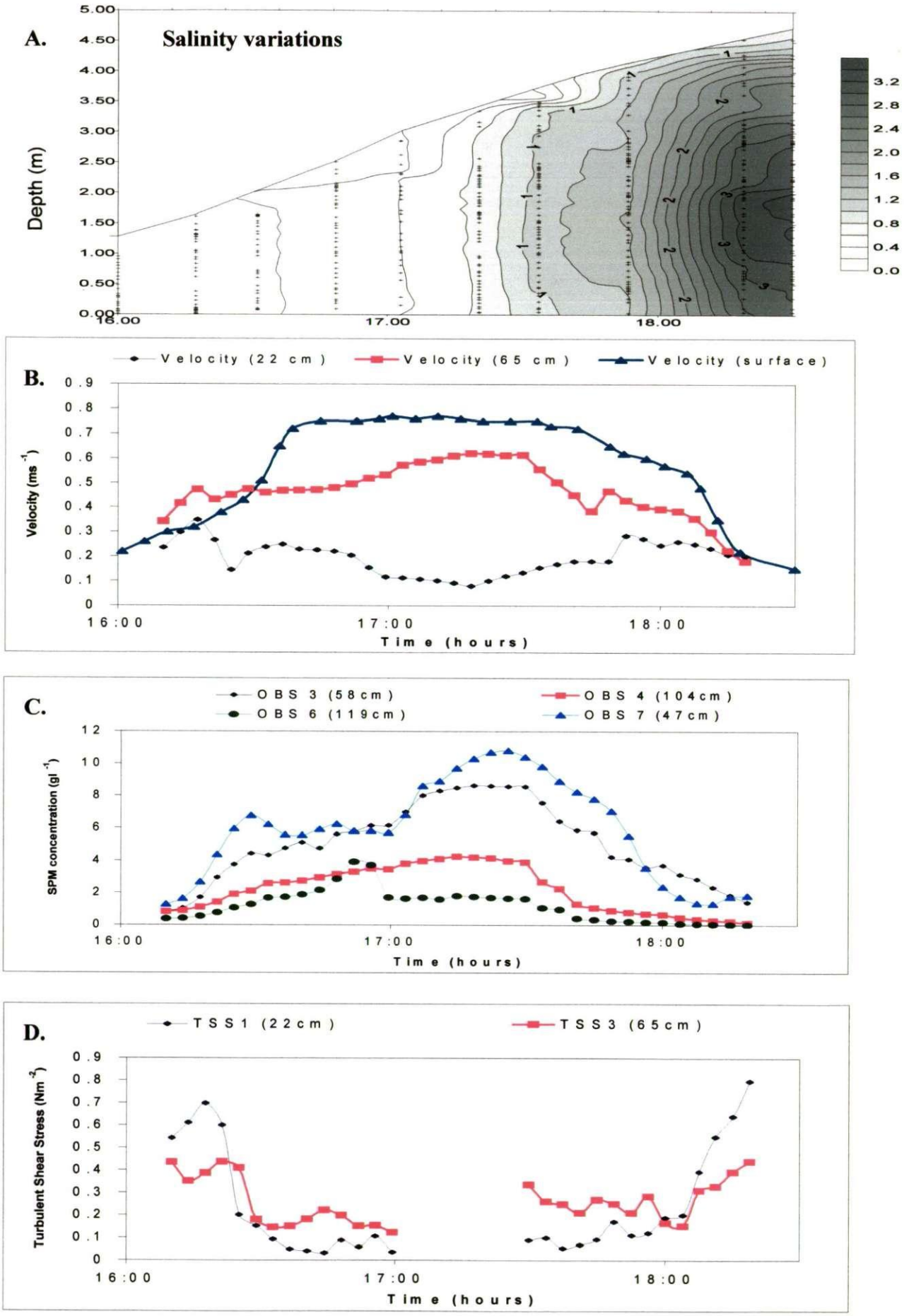

Figure 5.16. Time series of variations in: ***A.*** salinity, ***B.*** velocity, ***C.*** suspended particulate matter concentration, and ***D.*** turbulent shear stress for the spring tide on the 22nd September 1998.

$$\frac{U_j^{n+1} - U_j^{n-1}}{2\times\Delta t} + U_j^n \left(\frac{U_{j+1}^n - U_{j-1}^n}{2\Delta x}\right) = \left(\frac{\quad - \quad}{2\Delta x}\right)$$

$$\zeta_j^{n+1} = \zeta_j^n + \frac{dt}{\quad} U_j^n$$

component. Water level measurements (Figure 5.17) showed that the water slope changed from a negative gradient to a positive at around 17:00hr. Soon after, the slope altered and reduced up to 18:00hr. As with the neap tides, the gradient change appeared to separate the turbidity maximum from the advancing saline intrusion.

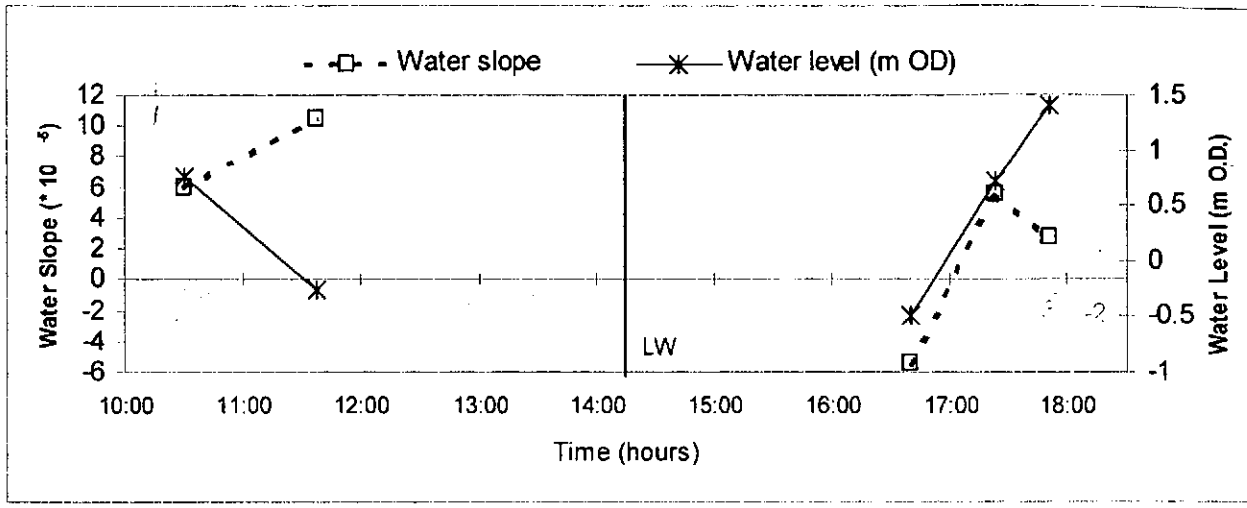

Figure 5.17 Water slopes between the lower and upper measuring positions on the neap tide of the 22nd September 1998, and the water level at the lower position. Water levels are shown relative to Ordnance Datum. Slopes are positive when water slopes downwards towards the sea (from Dyer et al., 2000a).

Within the wall region, under normal estuarine conditions it would be expected that if the constant stress layer was thinner than 65 cm (the height of the upper EMCM sensor group), the turbulent intensity would decrease with distance above the bed. However, the TSS record showed there was a sudden dip in the TSS of the EMCM sensor 22 cm above the bed, occurring at 16:15hr. This resulted in the TSS (at 22 cm) remaining under 0.1 Nm^{-2} until 17:45hr, where the SPM at the 58 cm height was seen to have reduced to 4 gl^{-1}. Further examination showed that for the period 16:20-17:40hr, the Ri_g (for the region 0.22-0.65 m above the bed) was approximately 0.04. This suggests some near bed turbulence damping (within the CBS layer) due to the density stratification. This caused a higher TSS to be observed at the upper EMCM sensor height. As the CBS layer concentration increased with time, so it thickened and the lutocline rose higher above the bed. As the lutocline moved closer to the upper flow sensors, the TSS at the upper level continued to increase beyond those closer to the bed. It was not until 18:00hr, when the lutocline had fallen below the 25 cm EMCM sensors, that the TSS at that height started to rapidly exceed the shear higher in the water column, with a TSS of 0.8 Nm^{-2} measured at 18:15hr.

This phenomenon of the shear at the boundary being reduced and the turbulent shear being temporarily concentrated to a higher level in the water column is known as drag reduction. Both Best and Leeder (1993) and Li and Gust (2000) have attributed this to the presence of

high concentrations. Dyer et al. (2000a) suggested that when the concentration gradient exceeds a value of 4 kgm^{-4}, drag reduction would occur. From this Dyer et al. (2000a) suggested that shear stress does not monotonically decrease from the bed to the surface, but has a maximum in the flow. This hence causes a feed-back mechanism that reduces the potential for erosion from the bed, as well as the sediment transport capacity of the flow.

5.2.4 Flood Tide - Flocs

Figure 5.18 shows the floc characteristics for sample 22-7, which was collected at 16:10hr on the 22nd September. This was just prior to the turbidity maximum reaching Station A, which accounted for a low ambient concentration of 858 mgl^{-1}. Although early into the flood, an already fast flowing surface current had created a TSS of 0.44 Nm^{-2} (G = 6.6 s^{-1}) at the INSSEV sampling height. The floc population size spanned from 36 up to 523 μm in diameter. Although the larger flocs displayed higher settling velocities, the smaller sized aggregates showed a more varied settling rate. The macrofloc / microfloc ratio of SPM was relatively even for the 120-400 μm size flocs (SB4-8), which cumulatively constituted 86% of the total dry floc mass. The majority of the flocs under 240 μm in diameter had effective density values in excess of 200 Kgm^{-3}. This translated into porosity and fractal dimension values of 80% and 2.45, respectively.

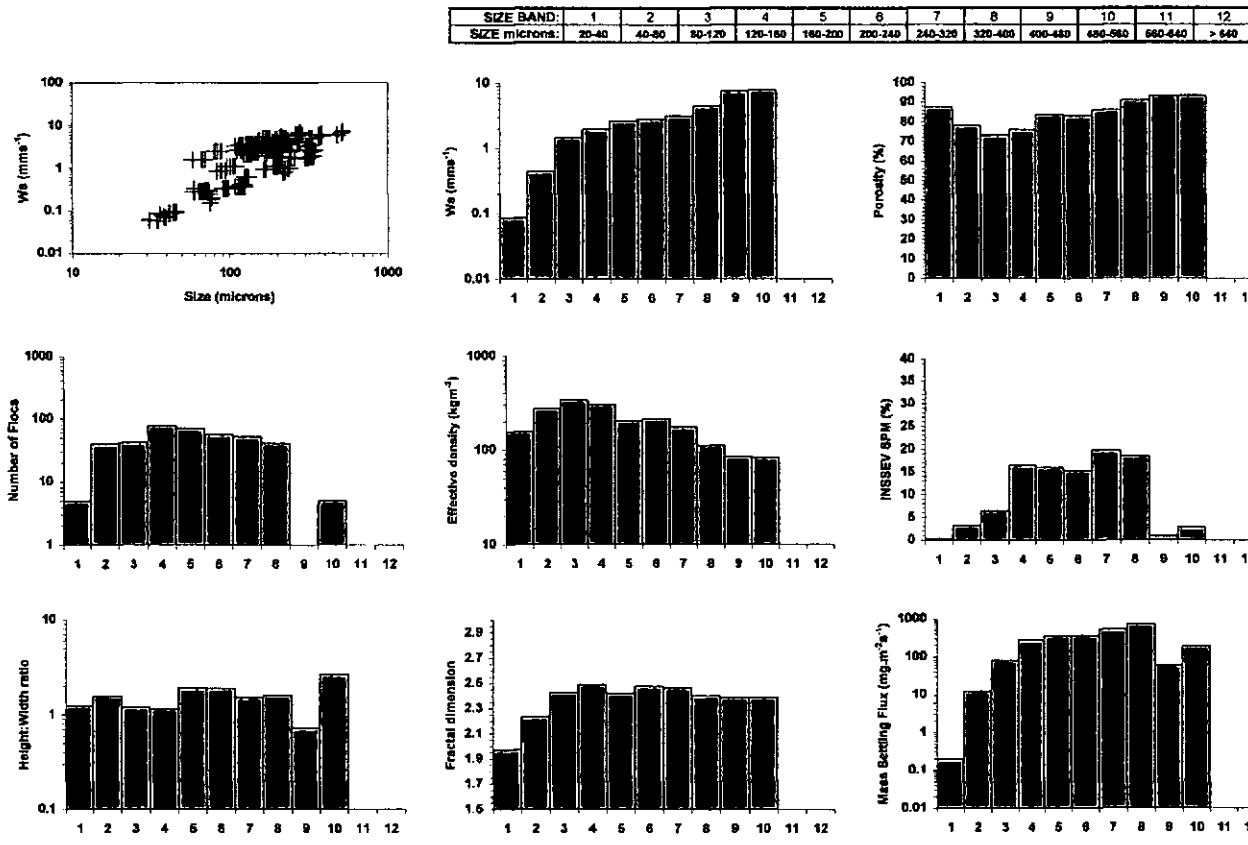

Figure 5.18 Floc characteristics for INSSEV sample 22-7 collected at 16:10hr.

Sample 22-9 (Figure 5.19) was obtained at 17:30hr from within the CBS layer which had formed during the advection of the main body of the TM. The ambient SPM was 8.5 gl^{-1} at 0.5 m above the bed, and the associated turbulent energy damping of this high concentration level suppressed the TSS to only 0.29 Nm^{-2} (G = 4.9 s^{-1}). A very distinctive change had occurred within the floc population. The earlier even floc distribution, had been replaced by a very bi-modal population, both modes demonstrating very different floc characteristics. The first mode was composed of both microflocs and macroflocs up to 232 in diameter. This was 1672 individual flocs which represented 80% of the total population. However in terms of dry floc mass, this only constituted 41% of the total content. The microflocs were generally dense slow settling aggregates, with typical effective density values of 200-320 kgm^{-3} and settling velocities ranging from 0.2-0.8 mms^{-1}. The remaining 20% of the floc population were large macro flocs ranging from 410-640 μm in diameter. The division of 59% of the mass into only 20% of the flocs resulted in this larger fraction having settling velocities between 5-7 mms^{-1}, and this translated into 91% of the total mass settling flux which equalled 31.7 $g.m^{-2}s^{-1}$. It may be hypothesised that orthokinetic bonding had promoted a greater degree of flocculation as the concentration level rose with a corresponding fall in the TSS.

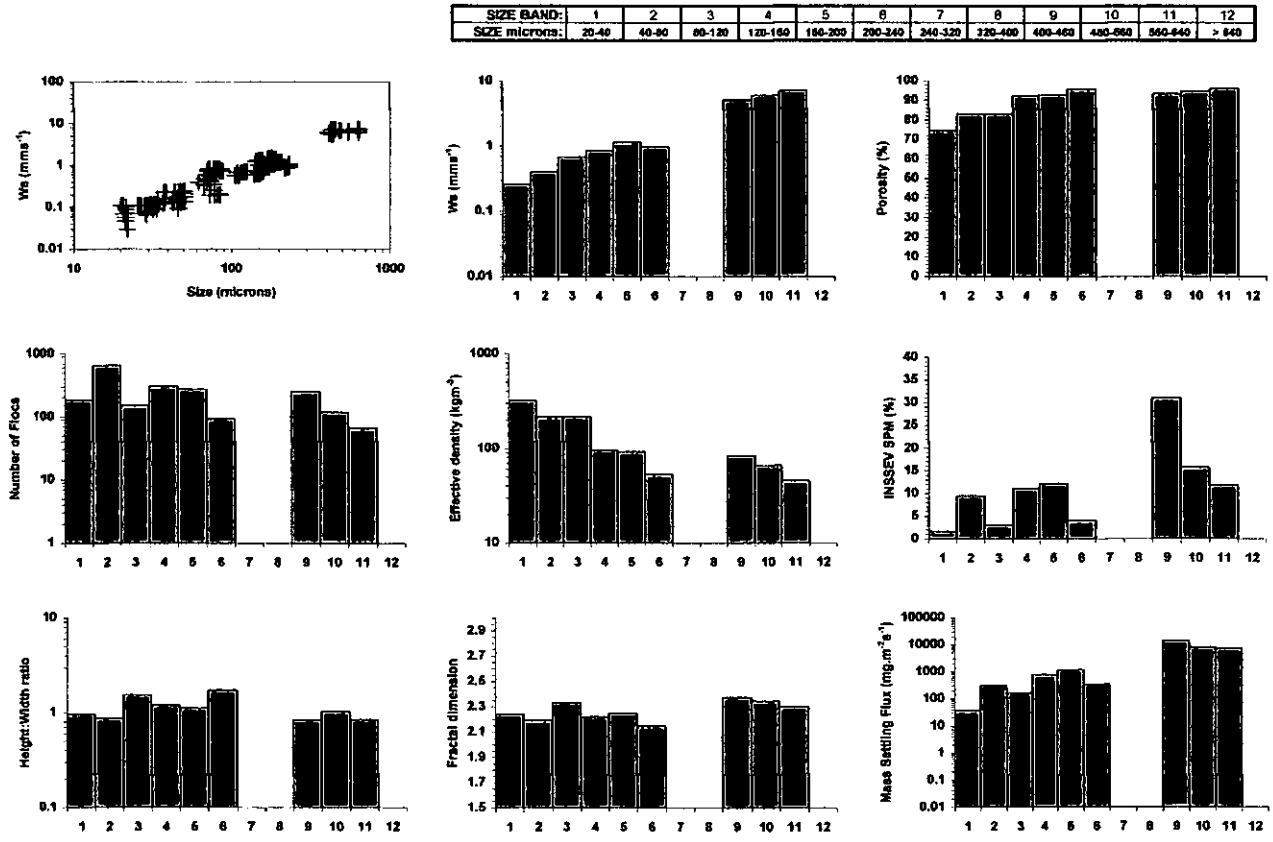

Figure 5.19 Floc characteristics for INSSEV sample 22-9 collected at 17:30hr.

By 17:49hr, the CBS layer had started to decrease in thickness and the concentration had fallen to 4.2 gl^{-1}. This 50% reduction in SPM, from that observed during sample 22-9, together with a further reduction in TSS to 0.24 Nm^{-2} (G = 4.2 s^{-1}), brought a return to a definite negative skewness to the floc population as shown by sample 22-11 (Figure 5.20). The 80-160 μm sized flocs constituted 54% of the total flocs, and 32% of the particulate mass. This cluster of small slow settling flocs represents a portion of the population which had not been incorporated into higher order flocs. The microflocs could be either: not yet aggregated, the result of break-up, or a fraction that would not aggregate. The remaining particulate matter was relatively evenly distributed through near-spherical macroflocs which reached up to 616 μm in diameter. This sub-group of macroflocs had size band mean settling velocities which increased progressively with increasing size band. The respective mean settling rates of SB5 and SB 11, were 0.9 mms^{-1} and 6.2 mms^{-1}. This gave the > 160 μm fraction a mean settling velocity of 4.2 mms^{-1}, and 92% of the MSF.

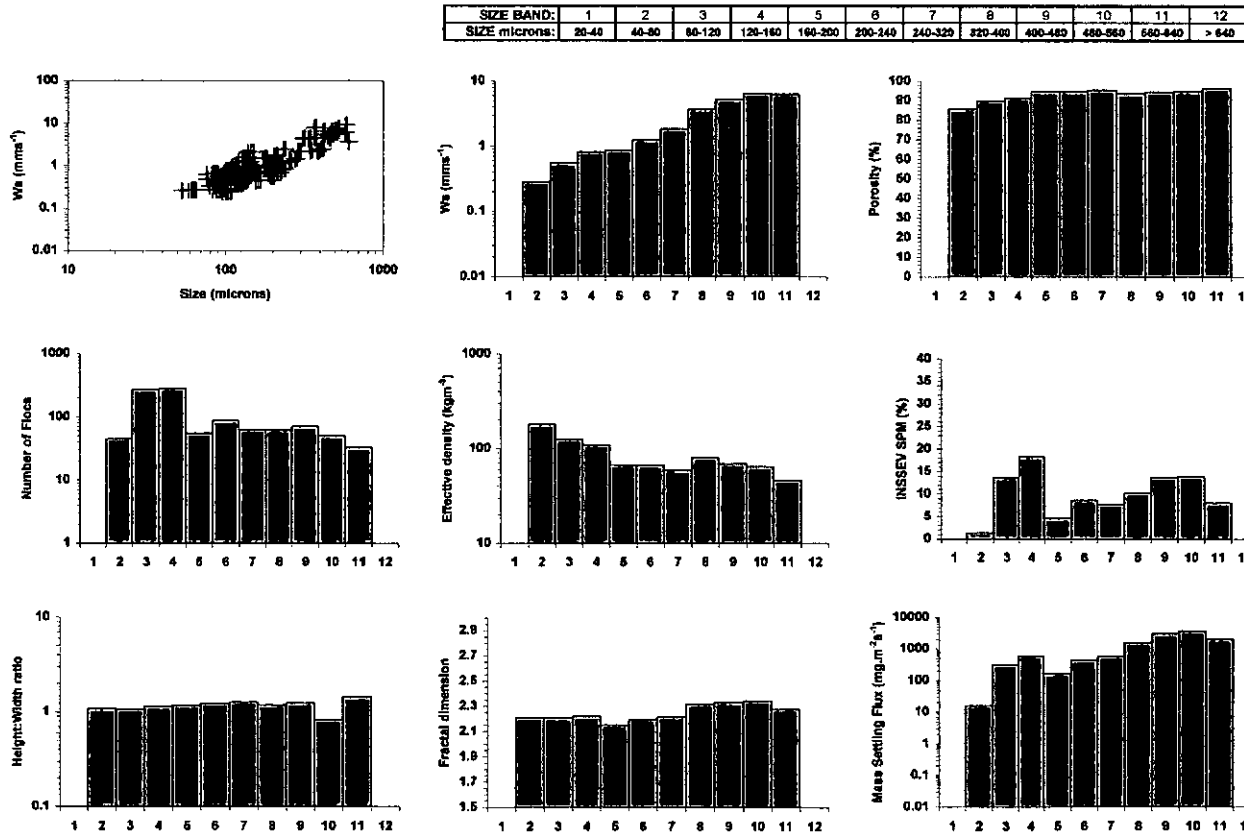

Figure 5.20 Floc characteristics for INSSEV sample 22-11 collected at 17:49hr.

5.2.5 Summary of Tamar estuary experiment 3

The river discharge was approximately the annual mean of 20 m^3s^{-1} throughout the experiment 3 duration. Neap tide measurements were made between the 15-17th September 1998 at Station A (Calstock) and the results were presented in section 5.1. A very distinct

salinity gradient developed early into the ebb on the 15th; at 14:30hr the nearbed salinity reached 10, whilst there was freshwater at the surface. Current velocities remained below 0.6 ms^{-1} for the neap tides, and consequently TSS 25 cm above the bed very rarely rose beyond 0.5 Nm^{-2}. A double peak in surface velocity occurred either side of the TM formation at Station A on the ebb and flood of the 16th September. This produced a negative water slope between the two peaks. Dyer et al. (2000a) described this as a "bow-wave" phenomenon whereby a bulge in the water surface precedes the saline intrusion moving upstream on the flood tide. The bulge causes a temporary reduction in the water slope, and consequently the reduction in flow velocity. It was suggested that the presence of this feature controlled the separation of the salt intrusion from the turbidity maximum, at this time.

Nearbed SPM concentrations were typically under 50 mgl^{-1}, and attained 1 gl^{-1} within the TM on the 17th. Bio-chemical analysis revealed that the total carbohydrate concentration peaked at 5.53 mgl^{-1} on the more turbid conditions of the 17th. Organic content (as particulate carbon) generally ranged between 10-28%, and chlorophyll-a levels indicated a maximum of ~ 1 μgl^{-1}.

Early into the ebb on the 15th most of the aggregates observed were compact in structure, some demonstrating effective densities ~ 9600 kgm^{-3}. Within the TM on the 15th, where the TSS was 0.27 Nm^{-2} (SPM = 271 mgl^{-1}), the maximum floc size reached 750 μm (Ws = 7.5 mms^{-1}). The flocs > 160 μm represented 77.4% of the ambient SPM, and of the total MSF which equalled 622 $mg.m^{-2}s^{-1}$, this fraction constituted 92.5%.

Spring tide sampling for experiment 3 was conducted from 21st-23rd September 1998. Advective transport was more apparent at spring tides where nearbed SPM rose to 8 gl^{-1}, and surface currents were nearly double those of neap tides. Background particulate concentrations were of the order of 400 mgl^{-1}. The water column remained fresh throughout most of the sampling, with a maximum of ~ 3 measured during the flood on the 22nd. CBS layers tended to develop 1-1.5 hours into the flood and ebb tides, and this created turbulence damping within the CBS and drag reduction above the lutocline interface. Organic content was much less than neap tides (~ 5-6%), but total carbohydrate concentrations were 2-3 times greater than those sampled during neap tide conditions.

As with neap tides, the largest flocs during spring tide conditions were observed whilst the main body of the TM advected through Station A. This was demonstrated by sample 22-9 (ambient SPM = 8.5 gl^{-1} and the TSS = 0.29 Nm^{-2}) where flocs up to 635 μm in spherical

equivalent diameter were viewed. The floc population was distinctly a bi-modal distribution; 41% of the dry mass (80% of the individual flocs) constituted flocs 20-240 μm in size, these were dense slow settling aggregates (ρ_e ~ 60-320 kgm^{-3} and Ws ~ 0.28-1.1 mms^{-1}). In contrast, the remaining 20% of flocs constituting SBs 9-11 displayed settling velocities of 5-7 mms^{-1} and this translated into 91% of the total MSF which equalled 31.7 $g.m^{-2}s^{-1}$.

At more turbulent, less turbid periods of the spring tide conditions, such as when sample 21-4 (ambient SPM = 2 gl^{-1} and the TSS = 0.68 Nm^{-2}) was collected, the maximum floc size was restricted to 485 μm. The population distribution was unimodal, with the primary mode SB7 (240-320 μm) containing 32% of the dry floc mass. The fraction > 160 μm had a mean Ws of 2.1 mms^{-1} producing a total MSF of 3.1 $g.m^{-2}s^{-1}$.

5.3 Tamar estuary June 1998 - SPRING TIDES

Experiment 1 was the first of the two preliminary Tamar experiments conducted during 24th June 1998, from Station A. A total of eleven INSSEV samples were acquired (Table 5.7). Due to high precipitation preceding this experiment, the river flow was nearly twice the annual mean - approximately 40 m^3s^{-1}, which meant that the water remained predominantly fresh throughout sampling. Table 5.8 shows the predicted tidal data, and it indicated that the tidal range (4.9 m at Devonport) was nearing the maximum for spring tides in the Tamar estuary. During this deployment, a number of problems were experienced with vegetation obscuring the OBS sensors, so a constant check had to be made on them throughout a deployment. Both near bed concentrations and velocities were comparable to those of the September 1998 spring tides.

Table 5.7 Deployment summary for the Tamar estuary June 1998 experiment 1 during spring tides

Date	Time - BST (hrs)		INSSEV sample	Total floc samples	Description of run
	run start	run end	reference numbers		
24/06/98	12:15	13:55	25-1 to 25-5	5	ebb tide - afternoon
24/06/98	15:05	16:55	25-6 to 25-11	6	flood tide - late morning

Table 5.8 Predicted tides at Devonport for the Tamar estuary June 1998 experiment 1 during spring tides

Date	Time (hrs BST)	Height (m)
24/06/98	06:35	5.3
	12:54	0.6
	18:57	5.5

5.3.1 Master Variables

The spring tidal data comprised two separate deployments conducted on the 24th June 1998. The period of the tidal cycle covered was the end of the ebb, through the low water period and on to the middle of the flood. The high meant that salinity values remained below 0.5 for the entire sampling period, with no significant stratification present (Figure 5.21.A). During the ebb, the salinity fell below 0.1 after 13:00hr. The first detection of the saline water reaching Station A on the flood was at 15:30hr when the near bed salinity was 0.1.

Figure 5.20.B shows the variations in current velocity. The surface current was ebbing at a velocity of 0.8 ms^{-1} at 12:15hr. The asymmetric distortion in the tidal curve, primarily due to the estuary topography, was seen to have prolonged the ebb beyond the predicted time of low water at 13:15hr. The surface flow was still ebbing at a speed of 0.45 ms^{-1} when the rig was lifted at 13:55hr. The rapid flood, which is a well documented characteristic of the Tamar

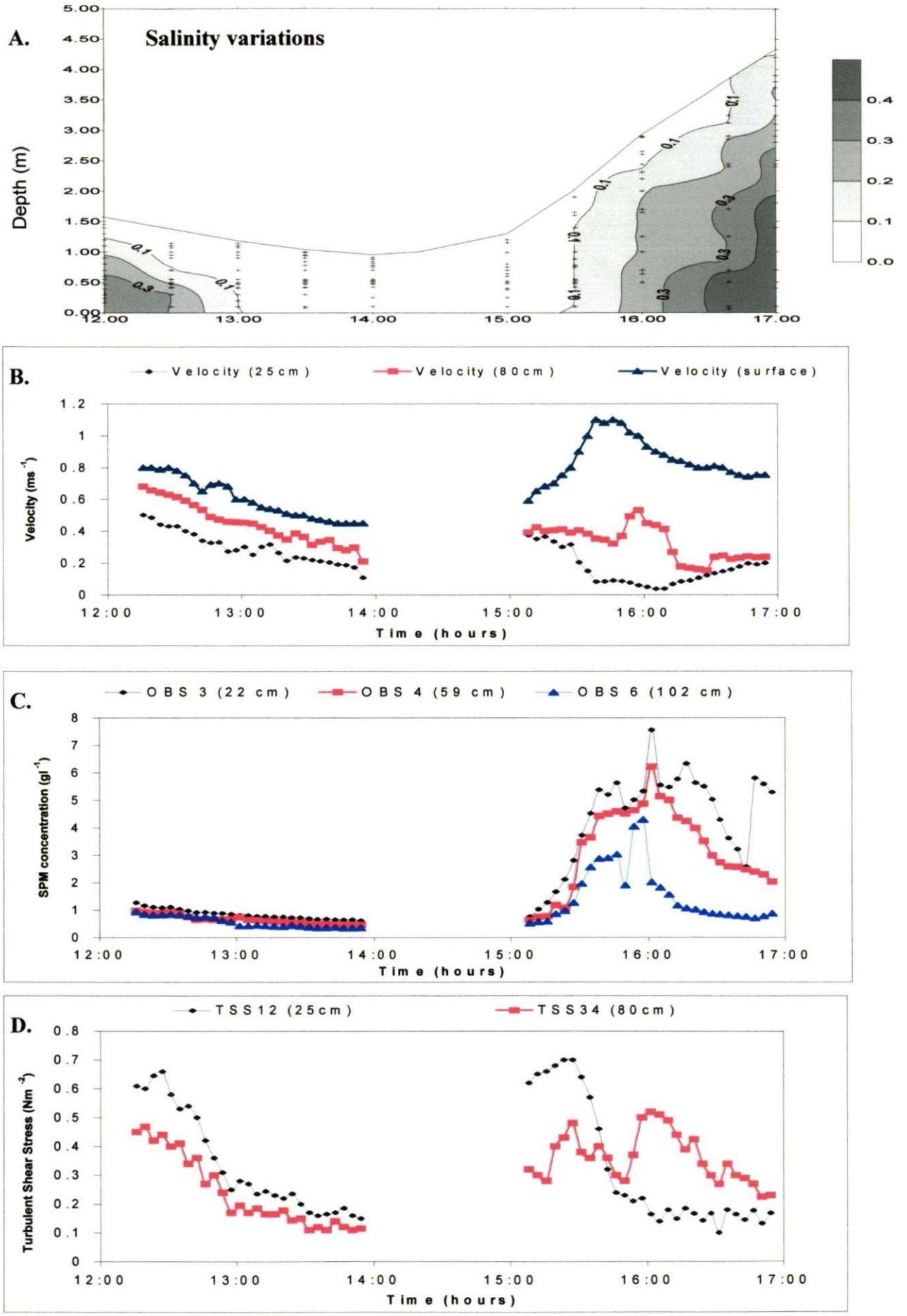

Figure 5.21. Time series of variations in: ***A.*** salinity, ***B.*** velocity, ***C.*** suspended particulate matter concentration, and ***D.*** turbulent shear stress for the spring tide on the 24th June 1998.

estuary, was demonstrated by a peak surface velocity (Figure 5.20.B) of 1.1 ms^{-1} being attained at 15:38hr; this was only 70 minutes after the initial transition to the flood. This peak was only sustained for 15 minutes after which a gradual deceleration in the surface flow occurred, resulting in a speed of 0.75 ms^{-1} at 16:55hr. Closer to the bed, a rapid decrease in the current speed was observed at 25 cm above the bed. Between 15:27hr to 15:38hr the flow speed at 25 cm slowed from 0.31 ms^{-1} down to 0.08 ms^{-1}.

The variations in SPM concentration are shown in Figure 5.21.C, and a maximum ebb concentration of 1.27 gl^{-1} was observed 22 cm above the bed at the start of the deployment (12:15hr), when the current velocities were at their strongest. The gradually decelerating flow velocity corresponded well to a reduction in suspended concentration throughout the water column. An SPM of 400 mgl^{-1} was measured just below the water surface close to LW at 13:55hr indicating the presence of a high background turbidity. On the flood tide, rapid growth in the near bed concentration started to occur at approximately 15:10hr. In response to the surface current, by 16:00hr the lutocline had risen to approximately the height of the INSSEV decelerator chamber roof above the bed (~ 0.6 m), with a flood peak CBS layer concentration of 6 gl^{-1}. In contrast, the near bed current had slowed even more to a minimum rate of 0.03 ms^{-1}. Thereafter, the surface flow velocity started to slow, and the concentration responded by flattening off.

The formation of the CBS layer had the net effect of reducing the TSS 25 cm above the bed (Figure 5.21.D) from 0.7 Nm^{-2}, at 15:27hr, to 0.14 Nm^{-2} by 16:00hr. The damping of the turbulent energy in the CBS layer was a product of the high concentration causing an increase in the effective water density. The increased stratification resulted in a Ri_g of 0.137 (measured at 16:12hr) in the region 0.25-0.8 m above the bed. The high particle abundance significantly contributing to the increased particle collision frequency. This reduction in shear at the boundary, and the consequent transfer of an increased turbulent shear intensity to a higher level in the water column, was also observed during the September 1998 spring tide experiments (see section 5.2.3). A comprehensive review of this aspect of the experimental results is given in Christie et al. (2000). It is interesting to observe that the concentration continued to increase 22 minutes after the maximum surface current velocity was achieved. This suggests that either a large portion of the particulate matter observed at Station A was a result of advection, or it could be a measure of the time taken to mix through the water column, or a combination of both aspects.

5.3.2 Ebb Tide - Flocs

The gradual reduction in TSS coupled with the decrease in ambient SPM, in the deployment period leading to low water, resulted in a general progressive reduction in maximum floc size. This was illustrated by the comparison of two INSSEV samples. The first floc sample, 24-2 (Figure 5.22), was obtained at 12:35hr where the ambient SPM and TSS were 885 mgl^{-1} and 0.47 Nm^{-2} (G = 6.9 s^{-1}), respectively. The scatter plot shows the presence of a single floc 650 μm in diameter with a settling velocity of 7 mms^{-1}. With decreasing size the flocs became more numerous and the spread in settling velocities increased. This suggests that the hydrodynamical stirring present was not permitting an optimum state of flocculation. As the flocs grew, the number of constructive collisions would be progressively reduced. This was well demonstrated by the 160-200 μm division (SB5) containing the largest portion (25 %) of particulate mass.

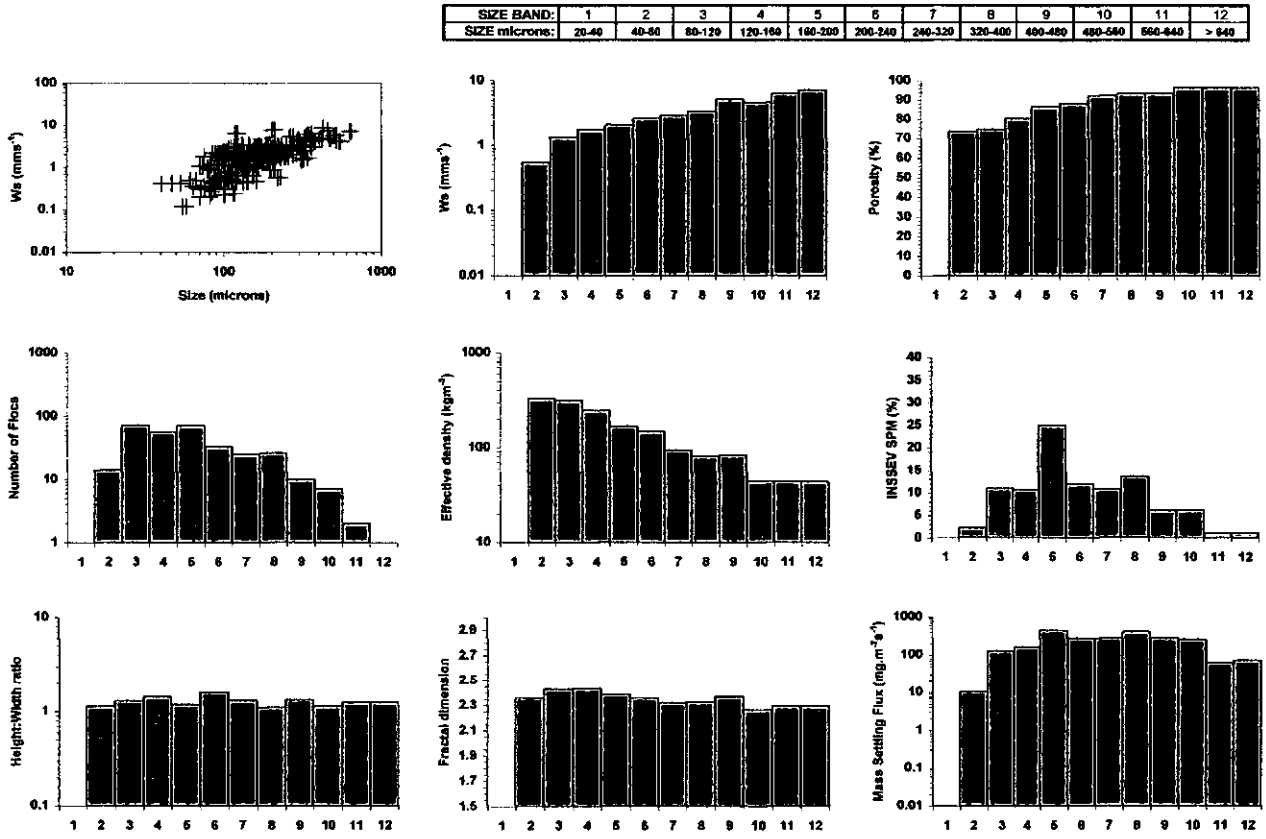

Figure 5.22 Floc characteristics for INSSEV sample 24-2 collected at 12:35hr.

Moving an hour closer to low tide, the decrease in concentration to 487 mgl^{-1} at 13:35hr saw a reduction in the maximum floc size of sample 24-5 (Figure 5.23) to 350 μm in diameter. This was a product of the much lower turbulent shear stress (0.14 Nm^{-2}; G = 2.8 s^{-1}), which was insufficient to create flocculation. There was a much greater number of very small flocs (68% of the total population), and these aggregates had settling velocities mainly between 0.1-0.9

mms^{-1}. Even so, SB5 (160-200 μm) contained the highest portion of dry floc mass (29%). The lower amount of flocculation occurring within sample 24-5 meant that the mean settling velocity for the flocs exceeding 160 μm in diameter was only 1.6 mms^{-1}; a fall rate decrease of 2 mms^{-1} from sample 24-2, which would significantly affect the mass settling flux (MSF).

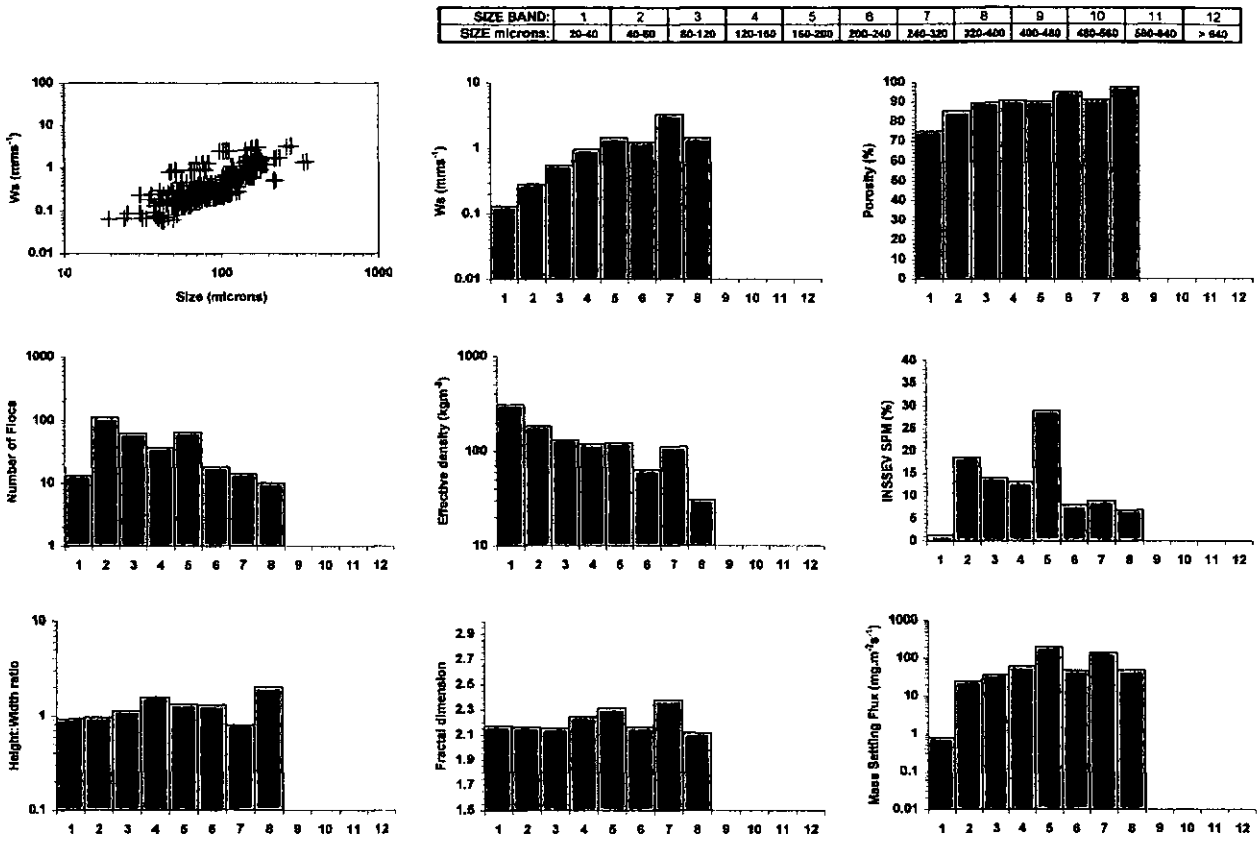

Figure 5.23 Floc characteristics for INSSEV sample 24-5 collected at 13:35hr.

5.3.3 Flood Tide - Flocs

The most evident changes in floc properties throughout the flood tide occurred during the advection of the turbidity maximum through Station A. The combination of large variations in concentration, together with the associated effects of drag reduction at particular times, had a significant effect on the aggregates formed. At 15:30hr the turbidity had risen to 2.6 gl^{-1} at 0.5 m, and signified the front tip of the TM. At this point in the tidal cycle, the corresponding TSS of 0.6 Nm^{-2} ($G = 8.2\ s^{-1}$) was entraining a large amount of solids into suspension, and floc sample 24-7 (Figure 5.24) was representative of the floc community at that time. The initial impression gained from examining the scatter plot showing the floc size against the settling velocity of the individual flocs (Figure 5.24), was that the floc numbers decreased rapidly with increasing size. Although flocs up to 650 μm in diameter were present, the very turbulent water column prevented the formation of numerous large aggregates. This was evident with nearly 47% of the 942 flocs being situated in the sub-160 μm size range. The primary mode of

the SPM distribution occurred at SB7 (240-320 μm), however the fraction > 240 μm in diameter, only constituted 54% of the particulate mass. This resulted in a mean settling velocity of the flocs over 160 μm in size of 2.9 mms^{-1}.

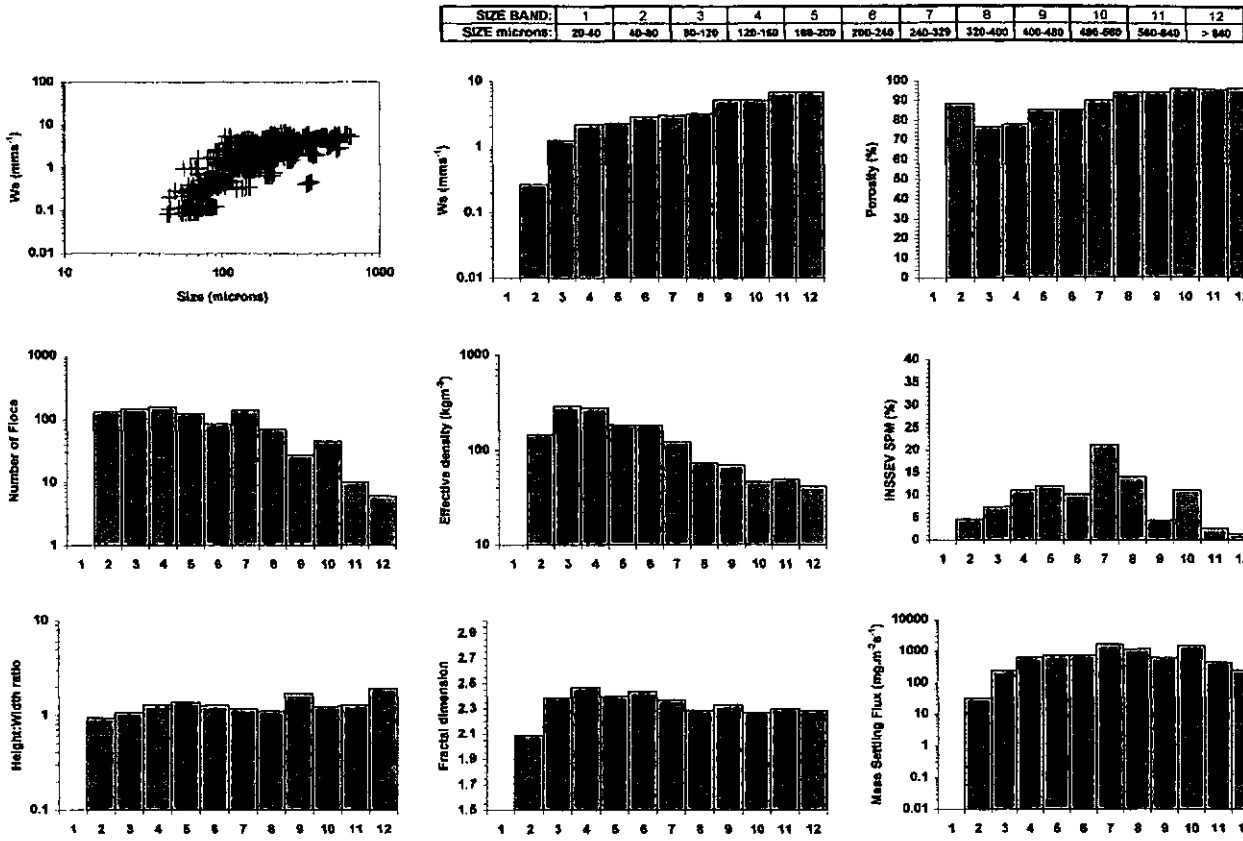

Figure 5.24 Floc characteristics for INSSEV sample 24-7 collected at 15:30hr.

In contrast, the main body of the TM produced an ambient concentration of 5.6 gl^{-1} at 16:00hr, and consequently restricted the turbulent energy and the TSS to 0.36 Nm^{-2} (G = 5.7 s^{-1}) at 0.5 m above the bed. This very quickly transformed the flocs into a weakly bi-modal population, as the record of sample 24-9 shows (Figure 5.25). Although the scatter plot showed a sub-group of slow settling (settling velocity < 0.3 mms^{-1}) flocs in the 30-70 μm size range, they only constituted 9.5% of the total population. The remainder of the flocs had fractal dimensions predominantly in the region of 2.4-2.5. The majority of the particulate mass, 49%, was contained within the larger sized aggregates of SB7-9 (240-480 μm). With a further 25% of the dry floc mass contained in the three largest size bands (SB10-12). This cluster of large flocs had settling velocities between 4-8 mms^{-1}. The resultant mean settling velocity for the fraction > 160 μm of 5 mms^{-1}, was an increase of over 2 mms^{-1} when compared to the earlier spring flood sample. This indicated a significant increase in flocculation efficiency during the maximum of the TM. The high percentage of floc mass contained by the macroflocs situated within the TM was also observed by Dyer et al. (2000b). As with the aggregates observed

from within the CBS layer during the September spring tide conditions, these larger flocs also exhibited a height:width ratio of 0.9-0.8. This may have been a product of partial compaction in the thick high concentration CBS layer.

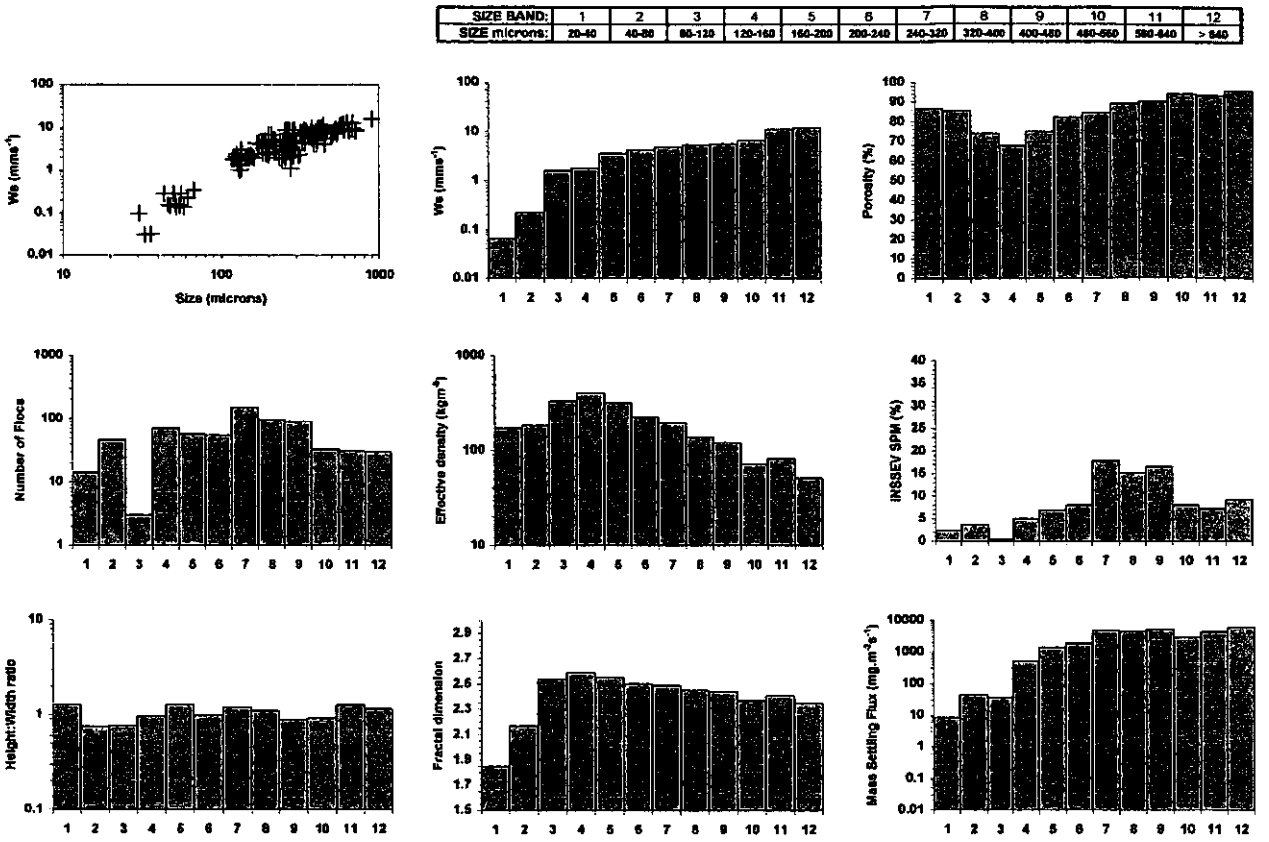

Figure 5.25 Floc characteristics for INSSEV sample 24-9 collected at 16:00hr.

5.4 Tamar estuary August 1998 - NEAP TIDES

The deployments at Station A between the 4-6th August 1998 (experiment 2), comprised the second preliminary Tamar estuary experiment (Table 5.9). The predicted tidal range of 3.8 m at Devonport for the 6th August 1998 (Table 5.10) indicates that the tide was in the latter stages of the neap cycle. The river flow was ~ 20 m^3s^{-1} which was the annual mean rate. The only problem that occurred during this set of measurements, was the neck section of POST EMCM 2$^{\#}$ broke during retrieval at the end of the deployment on the 6th August, and it had to be re-potted by Valeport Ltd prior to the COSINUS experiment (3). The salient results from the 5th August will be presented, as this was the most continuous deployment from this period.

Table 5.9 Deployment summary for the Tamar estuary August 1998 experiment 2 during neap tides

Date	Time - BST (hrs) run start	run end	INSSEV sample reference numbers	Total floc samples	Description of run
04/08/98	15:00	16:05	04-1 to 04-4	4	flood tide - afternoon
04/08/98	16:20	17:10	04-5 to 04-6	2	ebb tide - late afternoon
05/08/98	10:40	12:00	05-1 to 05-5	5	ebb tide - late morning
05/08/98	12:02	16:20	05-6 to 05-15	10	flood tide - early afternoon
06/08/98	10:30	12:50	06-1 to 06-9	9	ebb tide - late morning

Table 5.10 Predicted tides at Devonport for the Tamar estuary August 1998 experiment 2 during neap tides

Date	Time (hrs BST)	Height (m)
04/08/98	09:23	1.9
	15:51	4.6
05/08/98	10:23	1.6
	16:47	4.9
06/08/98	05:13	4.8
	11:17	1.3
	17:36	5.1

5.4.1 Master Variables

For the August neap tidal deployment, the last part of the ebb continuously through to the latter stages of the flood were covered. Figure 5.26.A shows the salinity variations during the neap tidal conditions of the 5th August 1998. The water column for the latter part of the ebb at Station A, was completely fresh. The first saline (salinity ~1) water started had arrived at Calstock by 14:30hr. The salt intrusion continued to move through Station A as a well mixed saline wall, and a near bed salinity of 8.45 was measured at 16:30hr.

The current velocity record (Figure 5.26.B) shows the surface ebb velocity was 0.5 ms^{-1} at 10:40hr. The near bed flow 81 cm above the bed tended to be approximately 0.1 ms^{-1} greater than the surface flow between 11:20hr-11:45hr. At 12:00hr the surface flow started to steadily

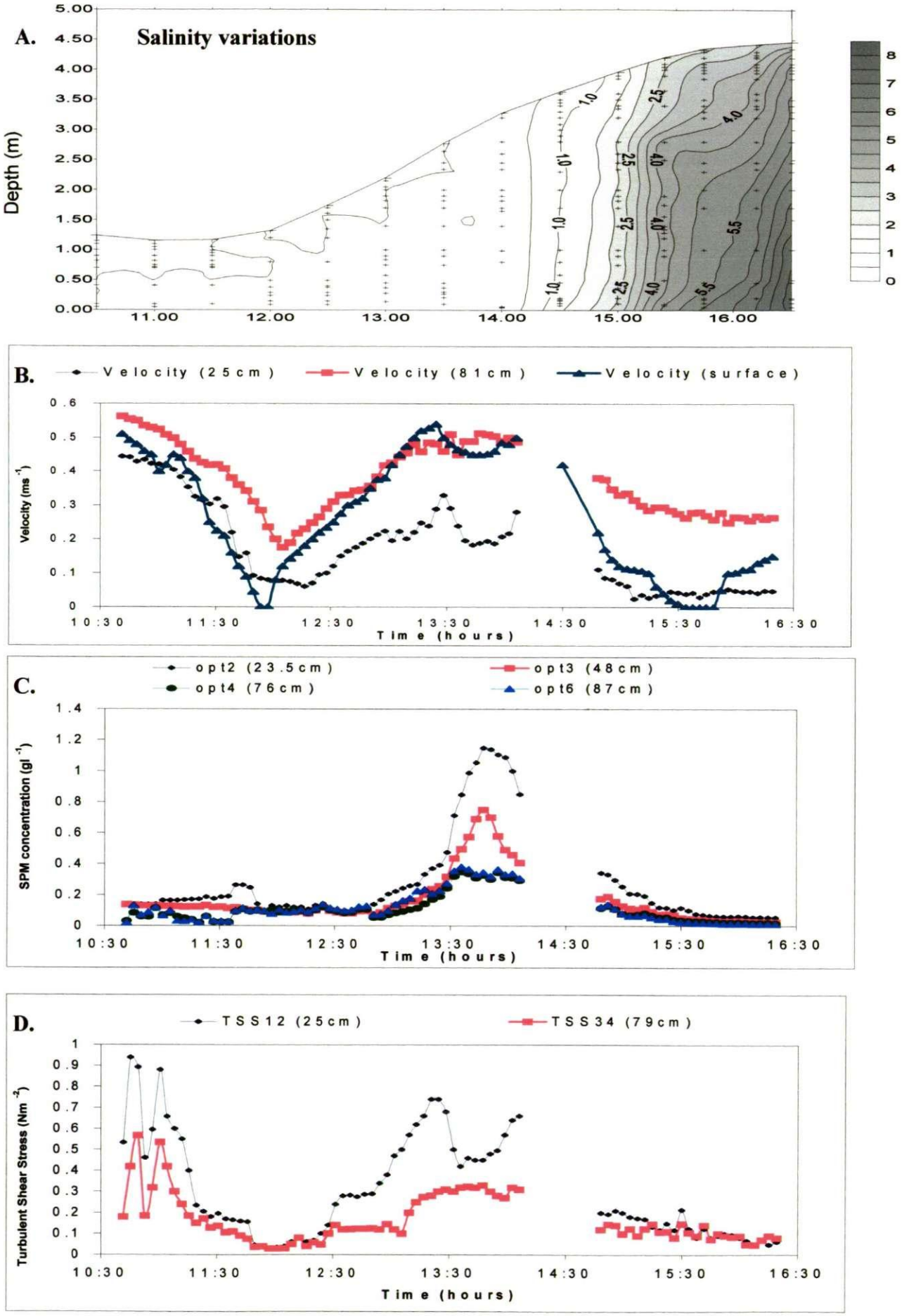

Figure 5.26. Time series of variations in: ***A.*** salinity, ***B.*** velocity, ***C.*** suspended particulate matter concentration, and ***D.*** turbulent shear stress for the neap tide on the 5th August 1998.

accelerate to a flood velocity peak of 0.54 ms^{-1} which was reached at 13:25hr. This was then followed by a dip in current speed down to 0.45 ms^{-1} at 13:47hr. A second peak of 0.51 ms^{-1} then occurred at 14:10hr, which was then followed by a progressive decrease in surface current speed to slack conditions by 15:45hr.

The SPM concentrations (Figure 5.26.C) throughout the ebb were typically under 190 mgl^{-1} at 23.5 cm above the bed. On the flood, the occurrence of the velocity peaks coincided with the entrainment of bed sediment into the water column. At 13:28hr the near bed concentration gradient was 0.32 kgm^{-4}, with an SPM of 475 mgl^{-1} measured 23.5 cm above the bed. The minimum velocity in both the surface and near bed current coincided with the peak turbidity maximum formation at Station A. At this point in the flood tide (13:47hr) the SPM at the 23.5 cm height had risen to 1.15 gl^{-1}, resulting in the concentration gradient increasing to 1.74 kgm^{-4}. As the concentration reduced, so the current velocity increased to the second peak at 14:10hr. This suggests that there was minimal particulate advection present at the Calstock site during the passing of the TM. The appearance of these two peaks in velocity are the "bow-wave" phenomena (Dyer et al., 2000a) also observed during the September experiments. The concentration at 23.5 cm had fallen to ~ 400 mgl^{-1} by 14:30hr, where the first saline water was detected. Once the salinity had risen to 5 at 15:40hr, the near bed concentration (at 23.5 cm) had further decreased to 77 mgl^{-1}.

The corresponding variations in turbulent shear stress are illustrated in Figure 5.26.D At 10:45hr, a high turbulent shear stress was present in the bottom layer of the water column (0.53 Nm^{-2} at 25 cm above the bed), predominantly generated by the relatively fast current velocities measured closer to the water surface. Although the velocity deceleration through the deployment was relatively linear, the TSS at the 25 cm height demonstrated two peaks during the early part of the record. The first peak was at 10:45hr with a TSS of 0.95 Nm^{-2}, and the second peak with a TSS rate of 0.9 Nm^{-2}, occurred 15 minutes later. After the second peak, the reduction in flow velocity causes a marked reduction in the TSS in the near bed region to 0.04 Nm^{-2}. During the flood the turbulent shear stress at the 25 cm height was no more than 0.1 Nm^{-2} for the initial 25 minutes. The TSS increased with the accelerating surface current to an initial peak rate of 0.74 Nm^{-2} by 13:24hr. The development of the high near bed concentration gradient had the effect of reducing the turbulent energy, and consequently by 13:35hr the TSS reduced to 0.42 Nm^{-2}. As the turbidity started to fall, the increasing current resulted in a second peak TSS of 0.66 Nm^{-2} at 14:06hr. After this point in the tidal cycle, the TSS continued to steadily decrease, in response to the slowing surface flood current.

5.4.2 Ebb Tide - Flocs

As with the spring ebb tide, the steady decrease in turbulent shear stress that occurred during the latter part of the ebb on the 5th August, had a direct influence on the resultant floc populations. Figure 5.27 shows the floc variations for sample 05-2 which was recorded at 10:53hr. The SPM concentration was 131 mgl^{-1} and the fast flowing current had produced an ambient TSS of 0.32 Nm^{-2} (G = 5.2 s^{-1}). The moderately high level of turbulent mixing was of a sufficient strength to encourage floc growth up to a maximum size of 300 μm. These flocs were of low effective density (~45 kgm^{-3}), predominantly "comet" shaped and exhibited settling velocities in the region of 3 mm s^{-1}. The flocs became more numerous with decreasing size, and demonstrated a negative skewing of the dry floc mass distribution, with 55% in the sub-160 μm fraction.

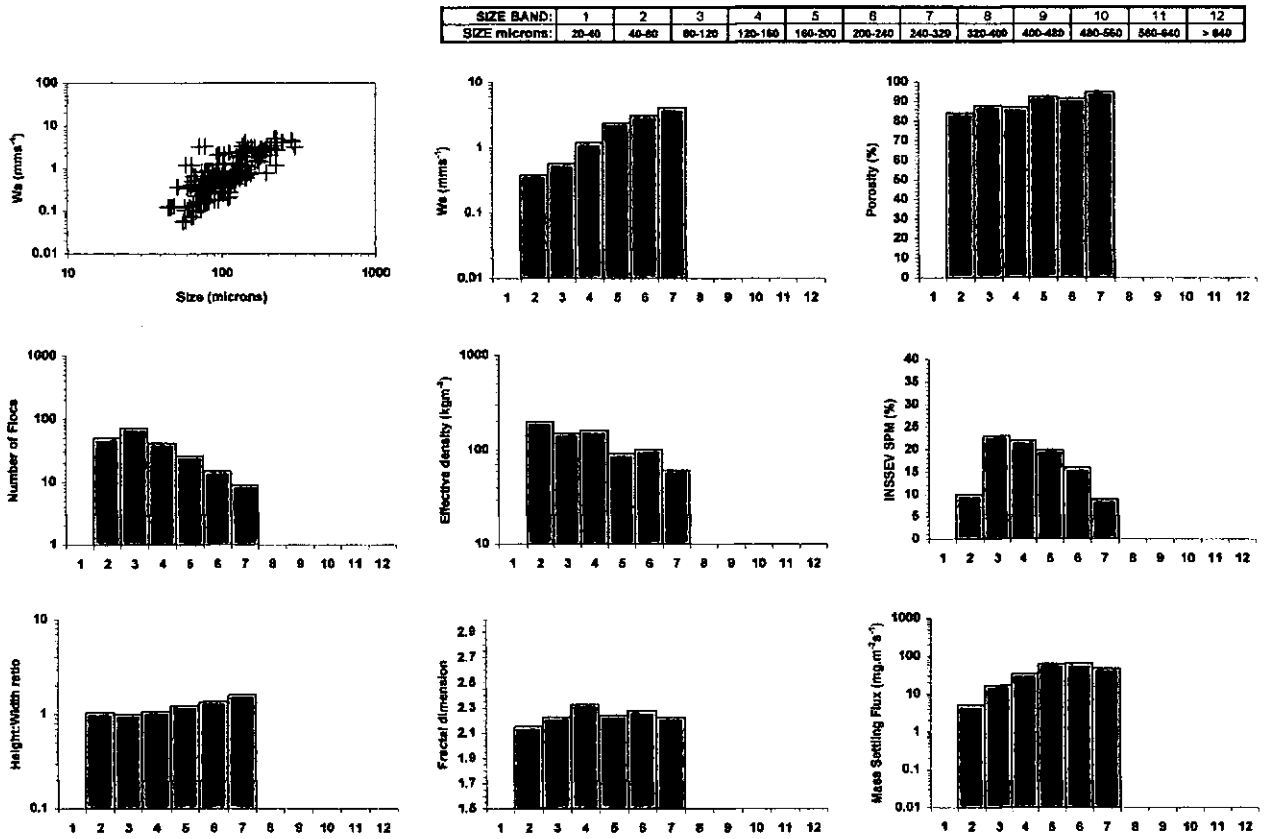

Figure 5.27 Floc characteristics for INSSEV sample 05-2 collected at 10:53hr.

As the ebb approached low water at 12:46hr, the reduction in turbulent energy gave a resultant TSS of 0.07 Nm^{-2} (G = 1.7 s^{-1}). The concentration was generally unaltered at ~100 mgl^{-1}. As the record for sample 05-7 (Figure 5.28) shows, this had the net effect of severely restricting floc growth. Three quarters of the flocs were less than 80 μm in size and had effective density values ranging between 200-1000 kgm^{-3}. This indicated that the vast majority of particulate matter did not progress beyond the zero or first order flocculation stage. Those which had

evolved into aggregates of up to a maximum size of 202 μm, were in the minority. Comparing the two samples, the mean Ws of the > 160 μm fraction for sample 05-2 was 2.8 mms^{-1}, whereas the later sample was only 0.8 mms^{-1}.

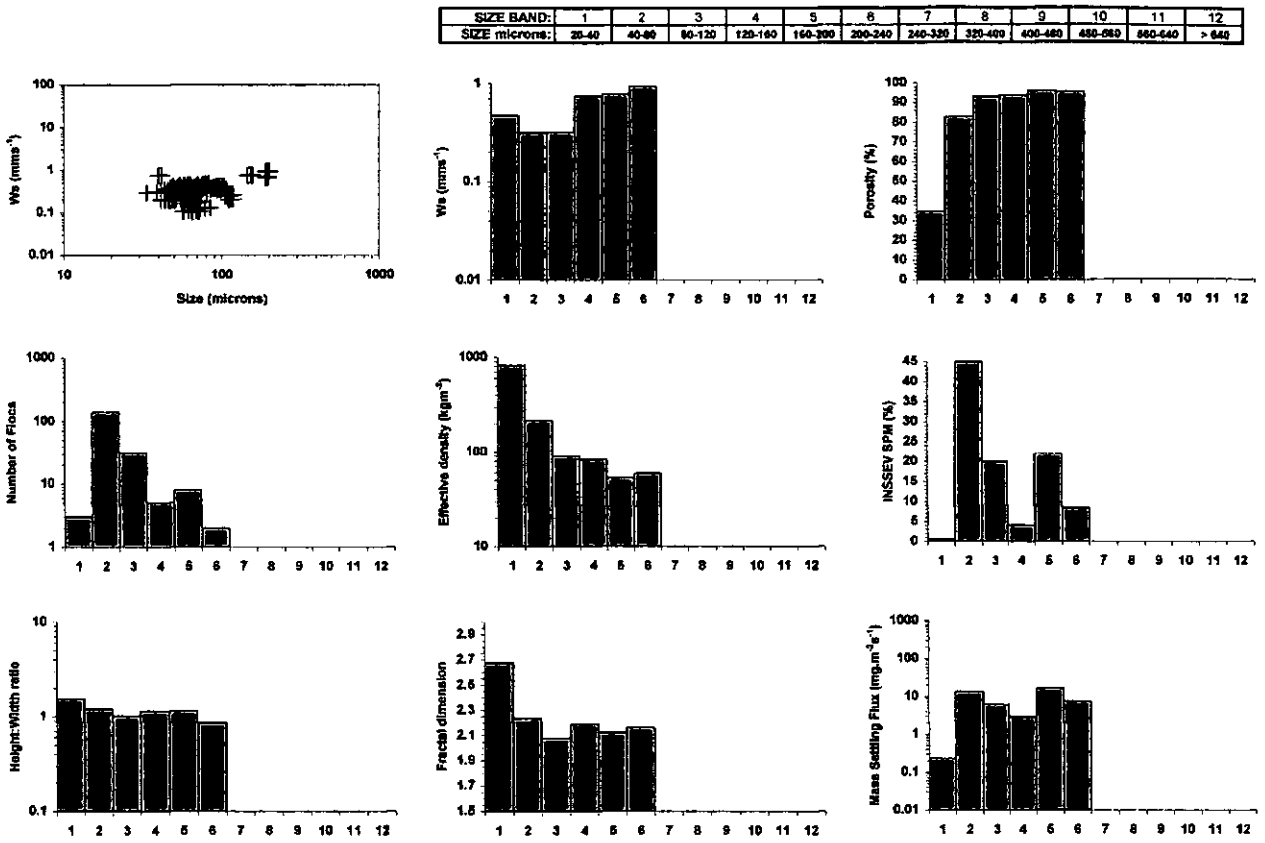

Figure 5.28 Floc characteristics for INSSEV sample 05-7 collected at 12:46hr.

5.4.3 Flood Tide - Flocs

The simultaneous concentration and TSS increases of the early part of the flood, brought about a progressive increase in the rate of orthokinetically induced floc growth. This was demonstrated by sample 05-9 (Figure 5.29) which was obtained at 13:25hr when the TSS had attained a peak of 0.55 Nm^{-2} ($G = 7.5\ s^{-1}$) at 0.5 m, and the SPM was 262 mgl^{-1}. The ambient conditions had encouraged a cluster of flocs to form in the 120-320 μm size range. These flocs accounted for 85% of the dry floc mass, with 40% of the total mass in SB7 (240-320 μm). As only 3.8% of the total population attained a floc size of up to 430 μm, it could be assumed that the high turbulence shear had imposed a limit on the maximum floc size.

A concurrent drop in the turbulent shear stress to 0.4 Nm^{-2} ($G = 6.1\ s^{-1}$) occurred as the main body of the TM advected through Station A at 13:46hr, raising the SPM to 750 mgl^{-1}. Figure 5.30 shows the floc variations of sample 05-10 which was collected at that time in the flood tide. The conditions had further stimulated flocculation. Now the main cluster of floc mass had

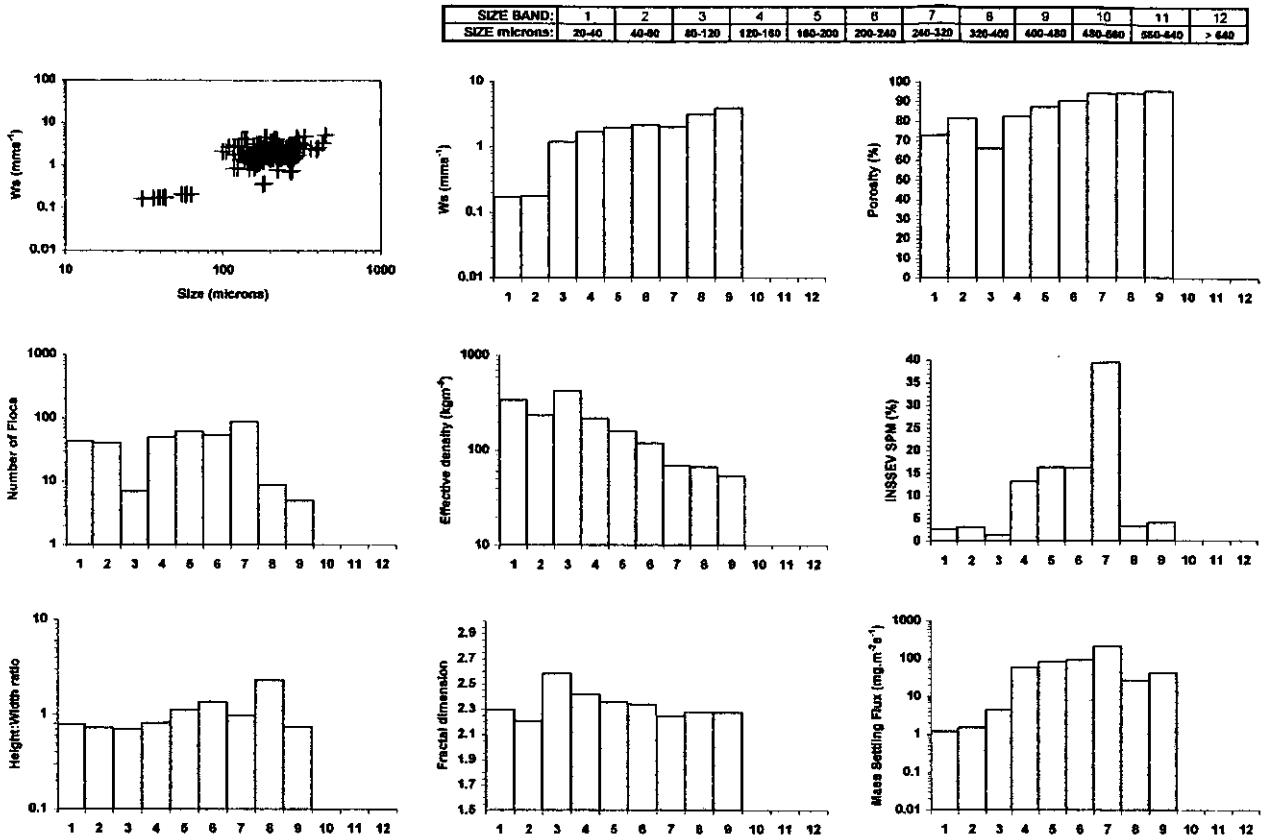

Figure 5.29 Floc characteristics for INSSEV sample 05-09 collected at 13:25hr.

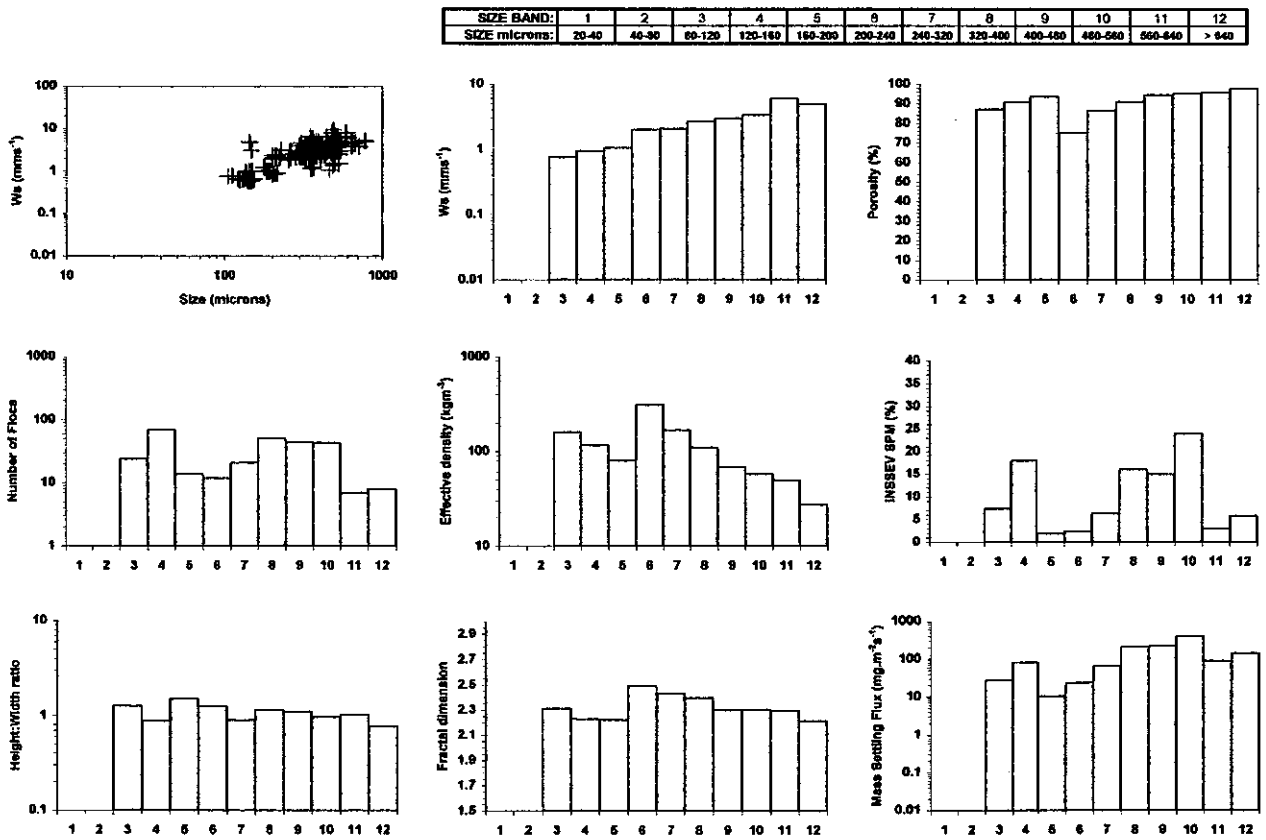

Figure 5.30 Floc characteristics for INSSEV sample 05-10 collected at 13:46hr.

moved to the 320-560 μm flocs, which represented 55% of the particulate matter. These flocs, together with aggregates which had grown to a maximum size of 778 μm, all exhibited settling velocities of ~3-5 mms^{-1}. This translated into a mean settling velocity of 3.1 mms^{-1} for the flocs > 160 μm in diameter, which was a fall rate increase of 0.8 mms^{-1} over the same fraction of the preceding sample. As the TM passed through, so the slowing current caused the SPM to back to ~200 mgl^{-1}, and the TSS to drop to 0.16 Nm^{-2} by 14:40hr. This had the net effect of producing less numerous constructive collisions. The maximum floc size was only 280 μm, and there was no real growth towards the higher size-banded flocs, but a generally even distribution throughout the size range. The settling velocity of the larger fraction was 1.8 mms^{-1}. The majority of the flocs observed throughout this neap tide flood period had fractal dimensions ranging between 2.25-2.35.

5.4.4 Summary of Tamar estuary experiments 1 and 2

Section 5.3 outlined the results from the spring tides on the 24th June 1998 (experiment 1) which experienced nearly twice the annual mean river flow (~ 40 m^3s^{-1}), and salinity did not exceed 0.5 at anytime during sampling. The latter part of the ebb saw the surface current fall from 0.8 ms^{-1} (at 12:15 hr) to an ebb of 0.45 ms^{-1} by 13:55hr. For this period, at 25 cm above the bed, TSS reduced from 0.65 to 0.2 Nm^{-2}; whilst SPM did not exceed 1.27 gl^{-1}. The afternoon flood saw surface currents approaching 1.1 ms^{-1} at 15:38hr, and a maximum TSS of 0.7 Nm^{-2} (at 25 cm) occurring 11 minutes earlier. This was followed by a sharp rise in the SPM concentration gradient and the formation of a CBS layer by 16:00hr. The CBS had a peak particle concentration of 6 gl^{-1} and a lutocline ~ 40-60 cm above the bed.

The moderately turbulent waters (TSS = 0.47 Nm^{-2}) of the mid-ebb period coupled with SPM concentrations of ~ 0.9 gl^{-1}, produced large low density flocs (D = 650 μm and ρ_e = 40 kgm^{-3}) with Ws = 7 mms^{-1}. However the ambient conditions prevented an optimum state of flocculation being attained; this was illustrated by the flocs becoming more numerous with decreasing size. This corresponded with a respective increase in floc effective density and reduction in settling velocity (with progressively decreasing floc size); e.g. ρ_e = 300 kgm^{-3} and Ws = 1.3 mms^{-1} for SB3 flocs. During the flood, turbulent damping occurred within the CBS layer reducing the TSS to 0.36 Nm^{-2}, and when combined with the abundance of particulates, this scenario produced the best conditions observed for flocculation. Nearly three quarters of the SPM constituted floc sizes between 240-900 μm with settling velocities predominantly ranging from 3-8 mms^{-1}; most of these large flocs had effective densities of less than 80 kgm^{-3}.

The experiment 2 results comprised neap tidal measurements made between 4-6th August 1998. The annual mean river flow allowed the nearbed salinity at Station A to reach 8 during the afternoon flood on the 5th August. Surface currents did not exceed 0.55 ms^{-1} and the SPM remained under 190 mgl^{-1}, with the exception of the TM formation at Station A 1.5 hours into the flood (13:30-14:30hr) where the nearbed SPM rose to 1.15 mgl^{-1}. The maximum flood TSS 25 cm above the bed was 0.74 Nm^{-2} and occurred prior to the TM formation (13:24hr).

The largest flocs were observed during the passage of the TM at 13:46hr (sample 05-10) on the flood. A combination of a SPM = 750 mgl^{-1} and TSS = 0.4 Nm^{-2} produced a population where 55% of the particle matter was to be found in the 320-560 μm (SBs 8-10) size cluster. These large flocs had ρ_e < 100 kgm^{-3} and settling velocities between 3-5 mms^{-1}. Maximum floc size was 778 μm.

5.4.5 Tamar estuary experiments INSSEV data quality summary

The Tamar estuary data for neap tidal conditions described in this chapter indicated INSSEV Q_c values ranging between 0.95-1.10. This meant that these floc samples were of a high quality and accurately represented the ambient floc populations present within the water column. For periods of very low SPM concentration (< 40 mgl^{-1}) there was a tendency for the INSSEV samples to over-estimate the dry floc mass as Q_c values of 1.3-1.4 indicated. This was primarily a result of the low number of flocs present in suspension at those times, and the measurement of a few additional flocs from the INSSEV camera video replays would significantly alter the INSSEV computed floc dry mass for those low SPM conditions.

The INSSEV samples collected throughout spring tides on the Tamar estuary showed the same high quality of floc data as those of the neap tides; Q_c values were generally of the order of 0.9-1.2. It was observed that occasionally when the ambient SPM concentration exceeded ~ 4 gl^{-1}, the Q_c fell below 0.8. This was mainly the result of these samples constituting a total population of 1000-1500 individual aggregates, many of them fast settling flocs. This had the potential to lead to under-estimation due to the manual interrogation of the video recordings from either: unintentionally not including floc images, or not being able to properly observe flocs which passed behind other flocs as they settle in the INSSEV instrument settling column within the visible focal depth of field (nominally 1 mm deep).

5.5 Gironde estuary June 1999 - NEAP TIDES

Table 5.11 summarises the periods of data acquisition during the SWAMGIR1 experiment conducted near Le Verdon, in the Gironde estuary. Sampling was conducted between the 21st-24th June. A total of thirty nine INSSEV samples were recorded, together with nearly twelve hours of concentration and current flow time series. This data was collected from a series of five individual deployments. Sheltered sampling locations away from the main channels, but with sampling depths of > 10 metres were chosen. Also the sea state remained calm throughout all sampling periods. This allowed any potential influence of wave action contributing to the generation of the near bed turbulent shear stress to be ignored. Predicted tidal variations are presented in Table 5.12. The low tidal coefficients indicates that these deployments were undertaken early in the neap tidal cycle. Near bed concentrations were typically under 300 mgl^{-1}, with surface current velocities approaching 1.4 ms^{-1}. The ambient air temperature reached 28°C on most days, and this meant that the electronic sensors (particularly the INSSEV video camera) had to be covered during on deck calibrations to avoid overheating. Only the data collected on the 23rd June 1999, from site *A* (see Figure 3.2) in the seaward limit region of the Gironde estuary will be presented in this thesis, as it was judged to be the best quality data set and most representative of the ambient conditions.

Table 5.11 Deployment summary for the Gironde estuary June 1999 *SWAMGIR1* experiment during neap tides

Date	Time - BST (hrs)		INSSEV sample reference numbers	Total floc samples	Description of run
	run start	run end			
21/06/99	17:40	18:00	21G-1	1	ebb tide - afternoon
22/06/99	14:40	16:40	22G-1 to 22G-8	8	ebb tide - afternoon
23/06/99	11:00	15:00	23G-3 to 23-18	15	flood tide - late morning
23/06/99	15:00	16:20	23G-19 to 23-21	3	ebb tide - afternoon
24/06/99	11:00	15:10	23G-1 to 24G-12	12	flood tide - afternoon

Table 5.12 Predicted tides at Le Verdon for the Gironde estuary June 1999 *SWAMGIR1* experiment during neap tides

Date	Time (hrs CET)	Height (m)	coefficient
21/06/99	05:41	1.8	
	12:26	4.4	50
	18:06	2	
22/06/99	06:47	1.9	
	13:32	4.3	46
	19:12	2	
23/06/99	07:53	1.9	
	14:32	4.4	48
	20:17	2	
24/06/99	08:52	1.8	
	15:21	4.5	52
	21:13	1.9	

5.5.1 Master Variables

The 4.5 hours leading to high water and the initial part of the ebb tide from the 23rd June 1999 were examined. Figure 5.31. A shows the variations in salinity throughout the six hour sampling duration. At 11:00hr the near bed salinity was 24, freshening very slightly to ~21 at the surface. By high water (15:00hr) the water column salinity had risen to a near homogeneous peak value of 25. The high salinities experienced were a consequence of the closeness of the sampling location to the Atlantic Ocean (approximately 5 km).

The time series of variations in the current velocity are shown in Figure 5.31.B. A peak surface flood velocity of 1.2 ms^{-1} was attained at 11:35hr, whereafter it steadily decreased to slack conditions by 15:15hr. Closer to the seabed, the velocity at the INNSEV sampling height of 0.6 m above the bed was significantly lower than at the surface, with a maximum flow velocity of only 0.3 ms^{-1} recorded at 11:00hr. However it was noticed that although the near bed velocity decreased as high water was approached, the flow did not become stationary. From closer examination of the corresponding directional data, this indicates the formation of a slow turning gyre in the lower layers of the water column, during the transition from flood to ebb tidal flow.

The SPM concentrations (Figure 5.31.C) were typically low for neap conditions. Up to 11:30hr the OBS 1# record showed that the ambient turbidity 32 cm above the bed did not exceed 55 mgl^{-1}. Peak turbidity levels occurred at 12:30hr (approximately 2.5 hours before local high water) where the particulate concentrations were measured at 46 mgl^{-1} and 180 mgl^{-1} at the upper (133 cm) and lower (32 cm) OBS heights, respectively. Within the mouth region of the Gironde estuary, bathymetric surveys show there are deposits of mud surrounded by areas of non-cohesive sediment. With the peak turbidity level occurring as the velocity was slowing (i.e. the maximum surface current speed was measured one hour earlier), indicates that a large portion of the particulate matter observed was most likely eroded from a nearby source, and then advected through the sampling location on the advancing flood tide. At 13:30hr the near bed concentration had fallen to ~10 mgl^{-1} suggesting a high degree of floc settlement occurring at that time, and by the deployment termination at 16:20hr, the amount of particulates observed in suspension was nearing zero.

Throughout this deployment the turbulent shear stresses (Figure 5.31.D) at 60 cm above the bed ranged between 0.055-0.52 Nm^{-2} (G = 1.4-7.6 s^{-1}). The peak TSS was measured at 12:03hr, which coincided with the initially increasing near bed concentration, which at that

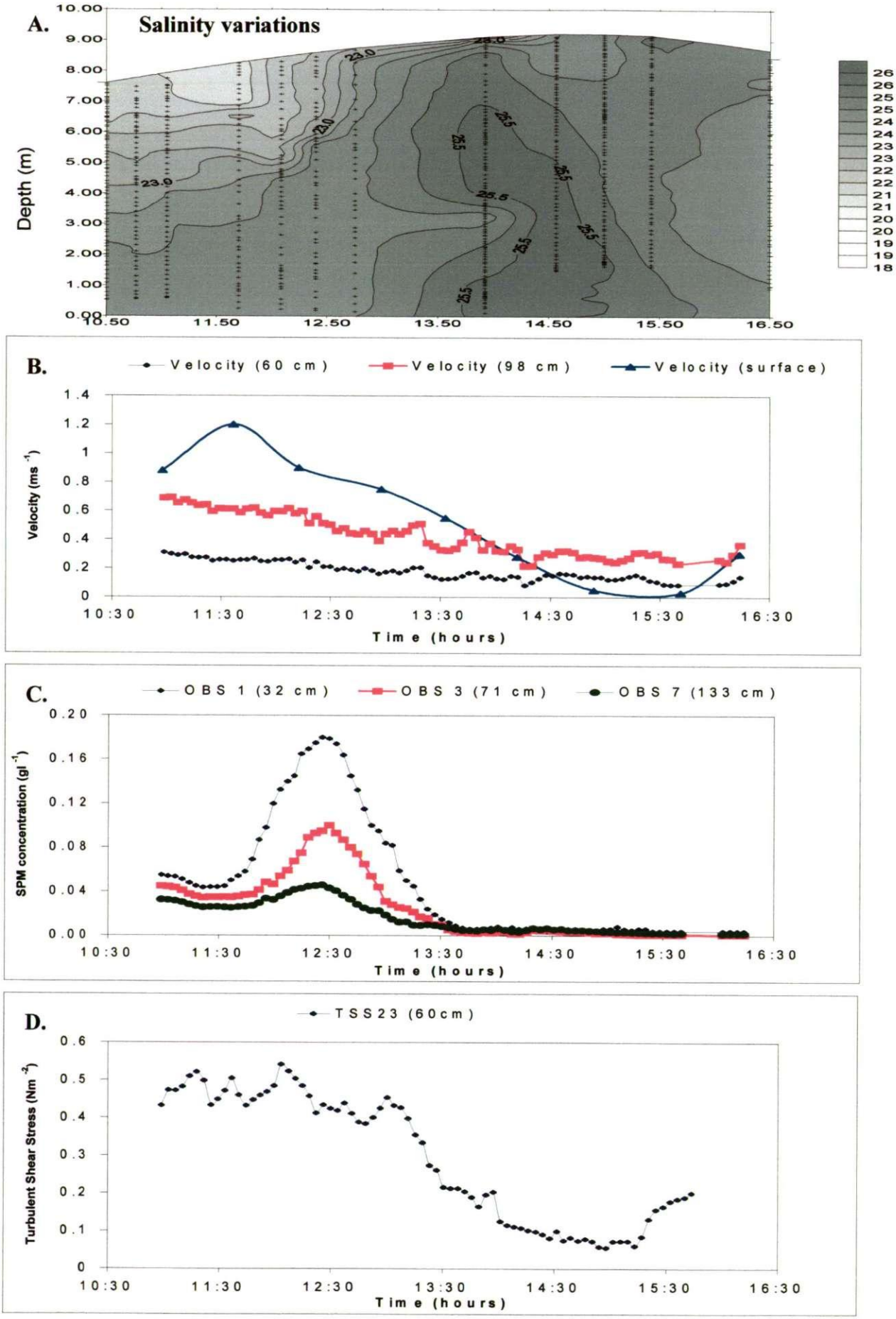

Figure 5.31. Time series of variations in: ***A.*** salinity, ***B.*** velocity, ***C.*** suspended particulate matter concentration, and ***D.*** turbulent shear stress for the neap tide on the 23rd June 1999.

point in the tide had risen to 133 mgl^{-1} (at 32 cm OBS). However as the particle concentration continued rising, the TSS fell; this also illustrated the advectional transport of the sediment to the sampling location from a nearby source. As the turbidity reduced (84 mgl^{-1} at 32 cm OBS), a second but albeit lower peak in TSS (0.45 Nm^{-2}) was observed at 13:00hr. The minimum values of turbulent shear were measured around high water.

5.5.2 Flood Tide - Flocs

The initial eight INSSEV samples (23G-3 to 23G-10) were obtained when the turbulent shear stress was at a consistently high level; fluctuating between 0.38-0.52 Nm^{-2}. During this flood period from 11:00hr (HW-3:30) through to 13:05hr (HW-1:25), the suspended particulate matter ranged from 68-139 mgl^{-1}. The first sample, 23G-3 (Figure 5.32), was collected at 11:00hr when the SPM concentration was 81 mgl^{-1} and the TSS was 0.43 Nm^{-2} ($G = 6.6\ s^{-1}$). Fifty percent of the 83 floc population were in the SB 3 (80-120 μm) category, and this was reflected in this band containing 46% of the sample dry floc mass. These generally spherical flocs, had a mean settling velocity of 0.4 mms^{-1}. The largest floc measured was 253 μm in diameter, and possessed a settling velocity of 2.7 mms^{-1}; nearly seven times greater than the smaller aggregates.

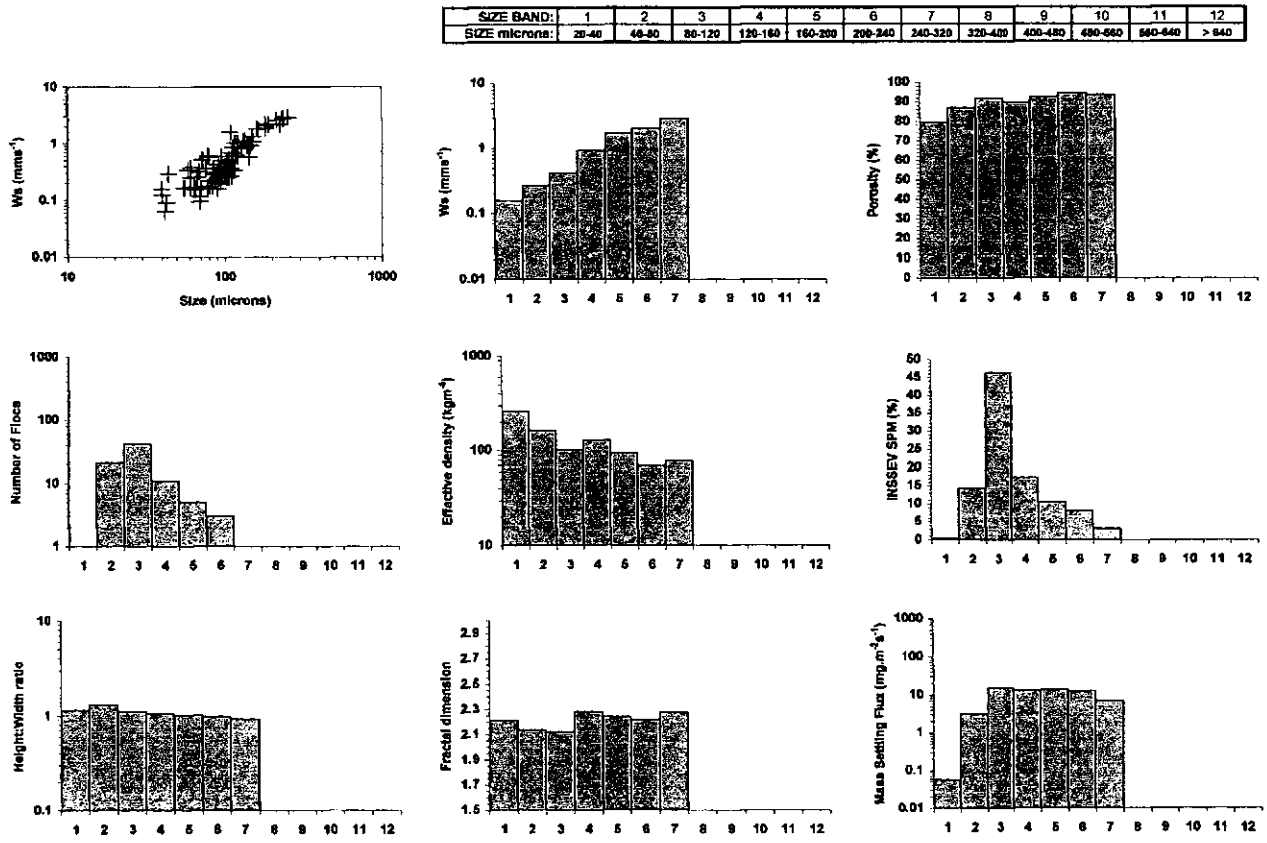

Figure 5.32 Floc characteristics for INSSEV sample 23G-3 collected at 11:00hr.

With the turbulent shear stress remaining the same (0.43 Nm^{-2}) and the concentration rising to 103 mgl^{-1} (at 11:30hr), sample 23G-5 (Figure 5.33) showed that the number of flocs in SB 3 (80-120 μm) had reduced by 30%, and this has been replaced by subtle floc growth in the higher size bands. A maximum aggregate diameter of 330 μm was observed, which had a corresponding settling velocity and effective density of 2.4 mms^{-1} and 58 kgm^{-3}, respectively. In comparison, now 63% of the particulate mass was held within SBs 3 and 4 (80-160 μm), but by virtually the same number of flocs contained in the SB 3 sub-division in sample 23G-3. Hence a 25 % increase in the ambient concentration was being held by 17% less individual flocs. The main difference now being that these slightly larger, denser (mean effective densities ~110 kgm^{-3}, as opposed to ~100 kgm^{-3} for sample 23G-3) flocs also had significantly faster settling velocities (up to 0.7 mms^{-1}, as opposed to 0.42 mms^{-1}), and four size divisions of sample 23-5 had MSF rates exceeding 15 $mg.m^{-2}s^{-1}$, compared to only one in sample 23G-3. This again emphasises how the flocculation process can dramatically change the dynamics of the particulates in suspension.

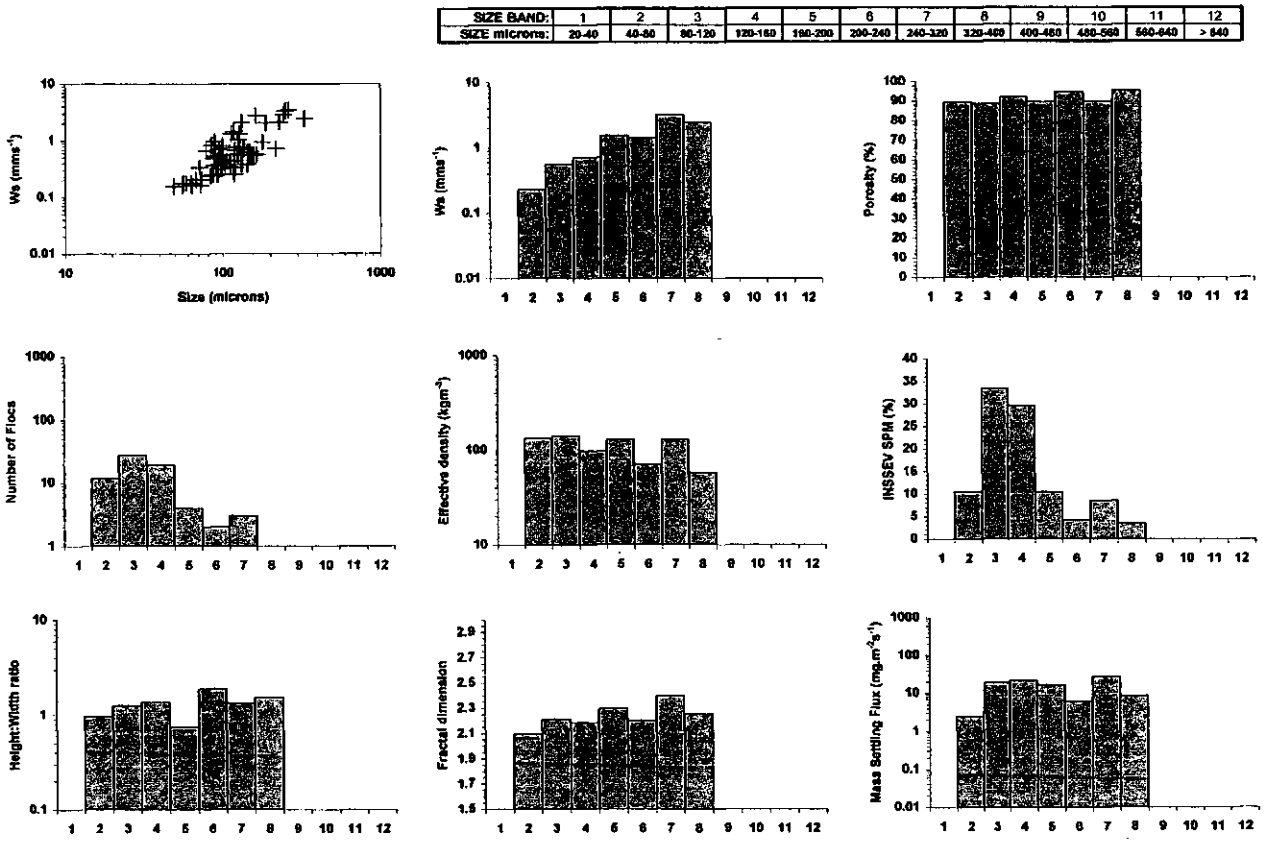

Figure 5.33 Floc characteristics for INSSEV sample 23G-5 collected at 11:30hr.

Increasing the turbulent shear stress by 0.03 Nm^{-2} to 0.46 Nm^{-2} (G = 6.9 s^{-1}), and maintaining a similar turbidity level as from sample 23G-5, further enhanced the construction of more macroflocs, as sample 23G-6 (collected at 11:40hr) demonstrated. The various floc

characteristics of this sample are shown in Figure 5.34. Although the maximum floc size had dropped to 307 μm, the cumulative mass settling flux contribution from the flocs exceeding 200 μm in diameter (SB6 and greater) was 104 $mg.m^{-2}s^{-1}$, compared to the 42.6 $mg.m^{-2}s^{-1}$ from sample 23-5 (with the SPM concentrations identical for both floc samples). This was a result of both samples having a mean settling velocity of ~2.1 mms^{-1} for the fraction exceeding 160 μm in size, but sample 23G-6 had twice the number of flocs (hence more dry mass) in that size grouping.

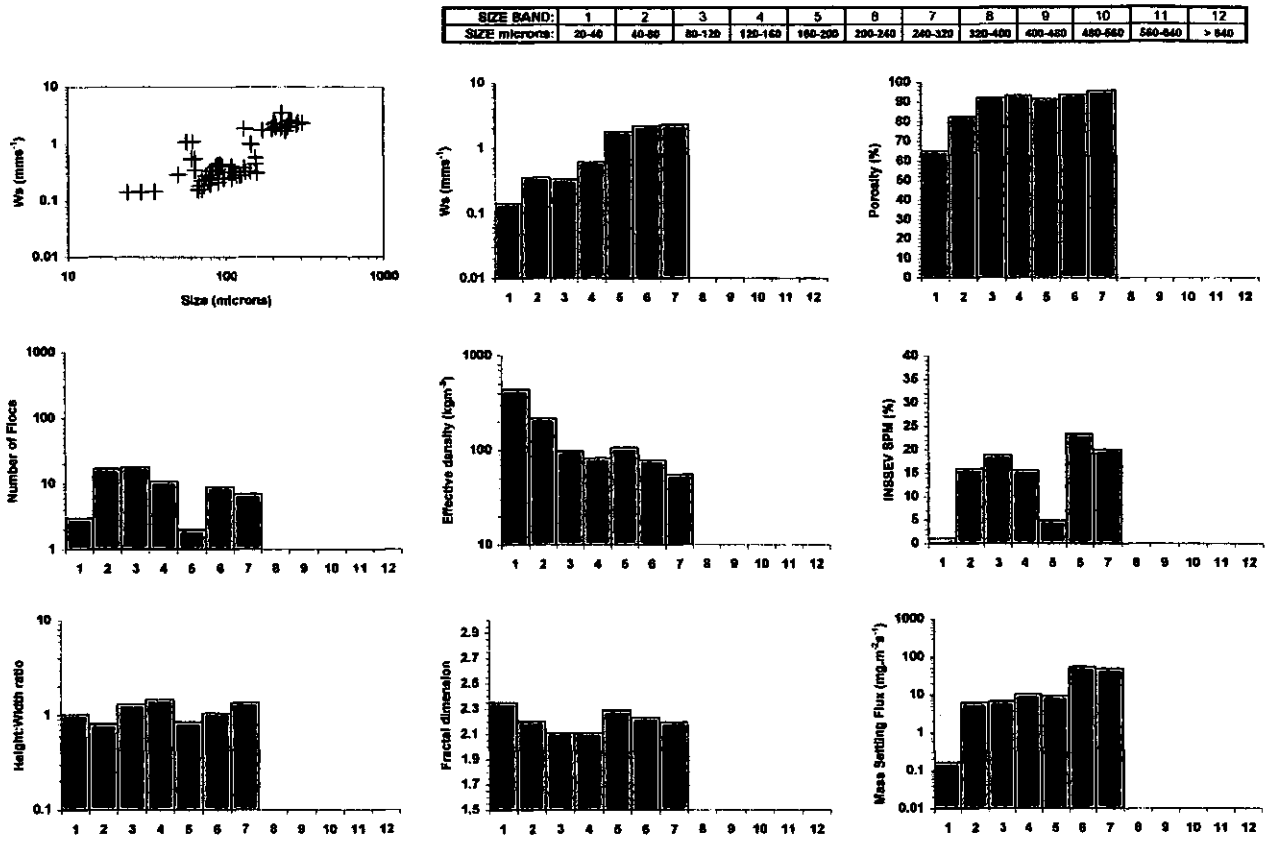

Figure 5.34 Floc characteristics for INSSEV sample 23G-6 collected at 11:40hr.

The maximum concentration of 139 mgl^{-1} occurred at 12:20hr (HW-2:10), when sample 23G-8 (Figure 5.35) was recorded. The TSS remained unchanged from the preceding sample. The settling velocities spanned three orders of magnitude from 0.075-2.3 mms^{-1}, and the effective densities ranged between 35-496 kgm^{-3}. It can be seen that a more bi-modal distribution had developed in both the population and mass distributions, with the peaks in both the variables being SBs 3 (80-120 μm) and 6 (200-240 μm). For the two groups, this gave 86 flocs encompassing 65% of the dry floc mass in the former group, compared to 20 flocs constituting the remaining 35% of the mass in the later group. This was a 5:1 population difference and a 2:1 SPM distribution ratio between the small floc group and the larger fraction. However,

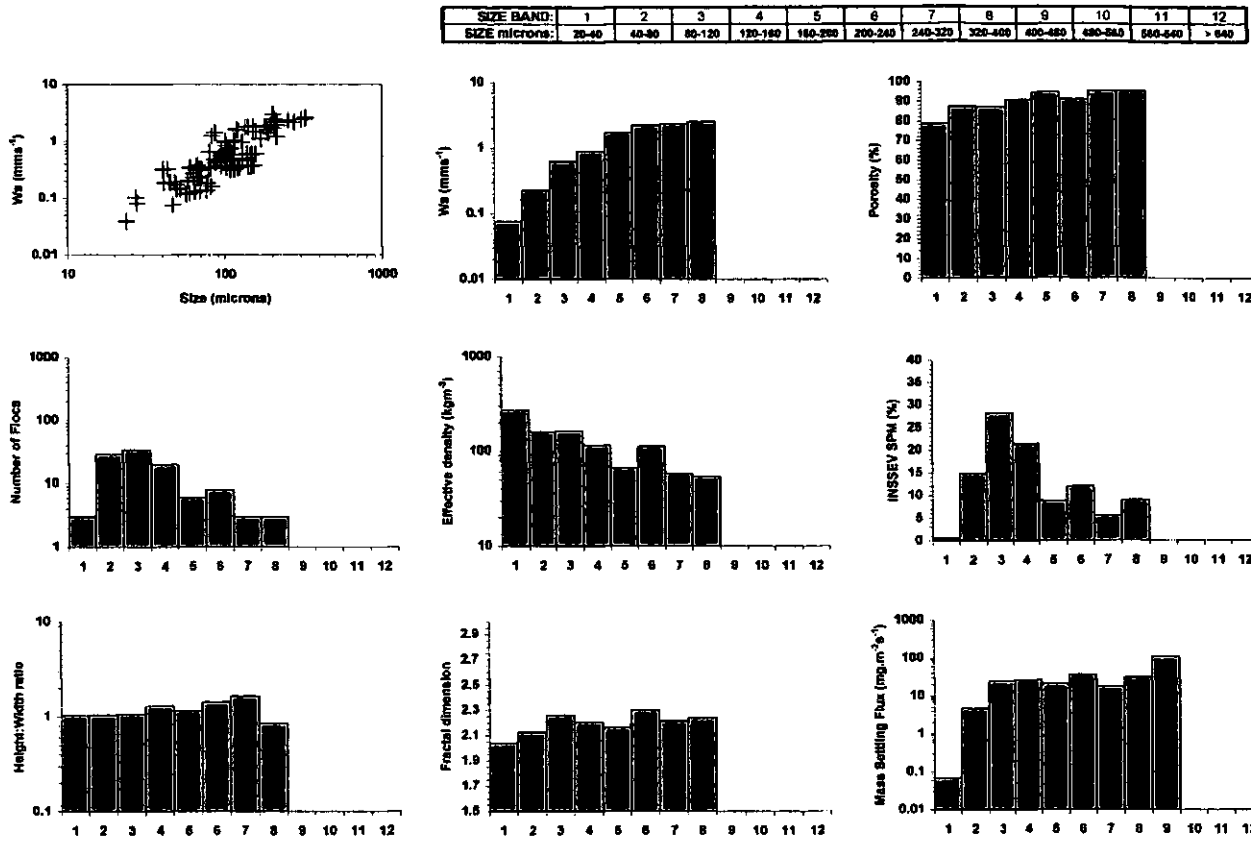

Figure 5.35 Floc characteristics for INSSEV sample 23G-8 collected at 12:20hr.

66% of the MSF was contained in the larger floc groupings of SB5-8 (160-400 μm), as a result of their significantly faster settling velocities.

By 13:48hr (HW-0:42), a reduction in the current speed, had brought about a decrease in the turbulent shear stress and thus ambient SPM fell, due to a cessation in bed erosion, to ~40 mgl^{-1}. This lower abundance of particulates in suspension coupled with a reduced turbulent energy level (which was required to bring the particles together), created a much lower effective collision frequency. At this point in the tidal cycle, sample 23G-13 (Figure 5.36) was collected, and the associated turbulent shear stress was 0.16 Nm^{-2} (G = 3.2 s^{-1}). Closer examination of the porosity histogram suggests that most of the flocs in this sample were constituents of more loosely constructed larger aggregates created earlier in the tidal cycle. The majority of the flocs displayed porosity values from 70% up to 88%. As these flocs settled in to a higher shear field, they were broken-up until the individual aggregate structure that remained was in equilibrium with the ambient shear stress, and then re-suspended. The low turbulent shear stress conditions of this sample indicate that the main structure of the flocs sampled were not formed directly at this point in the tide. Even so, the ambient conditions may have added some small amount of growth to a number of the aggregates present, especially

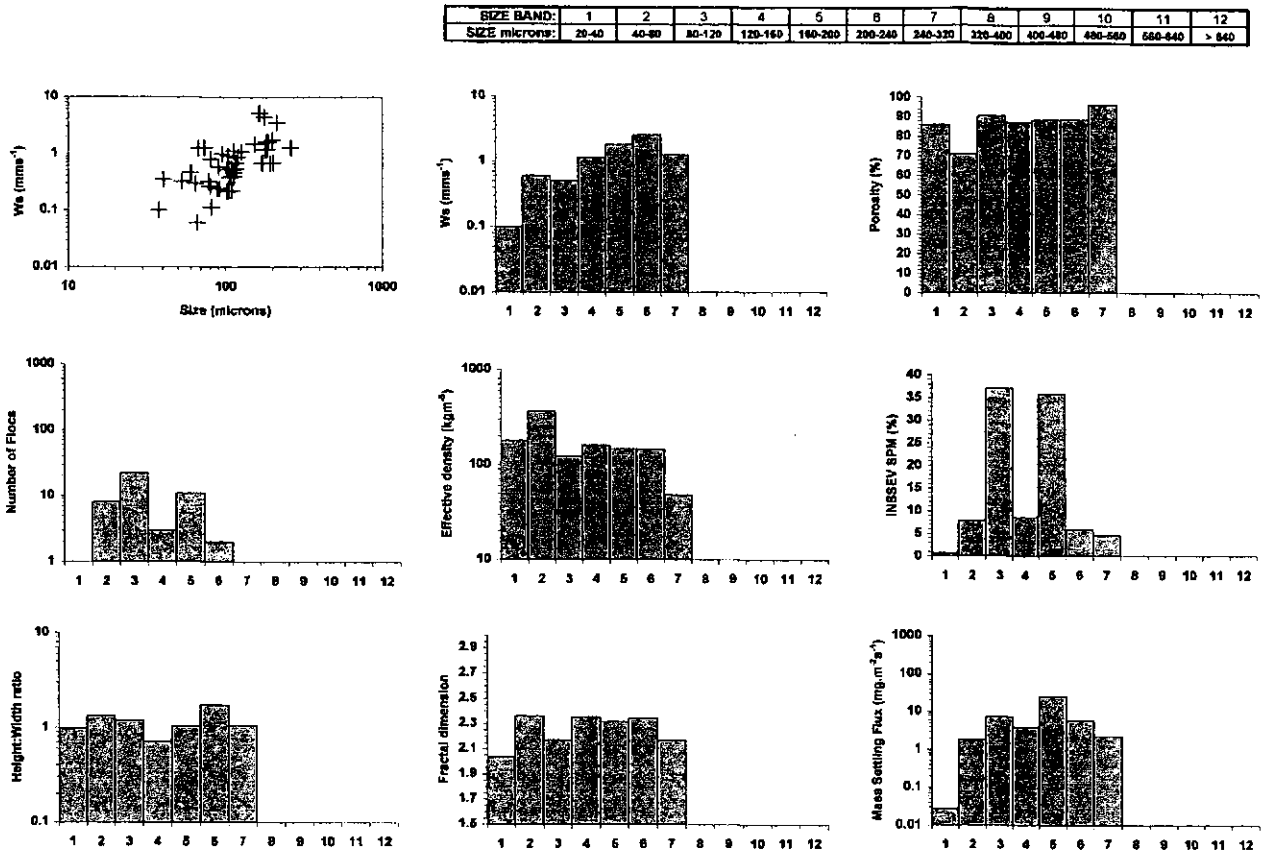

Figure 5.36 Floc characteristics for INSSEV sample 23G-13 collected at 13:48hr.

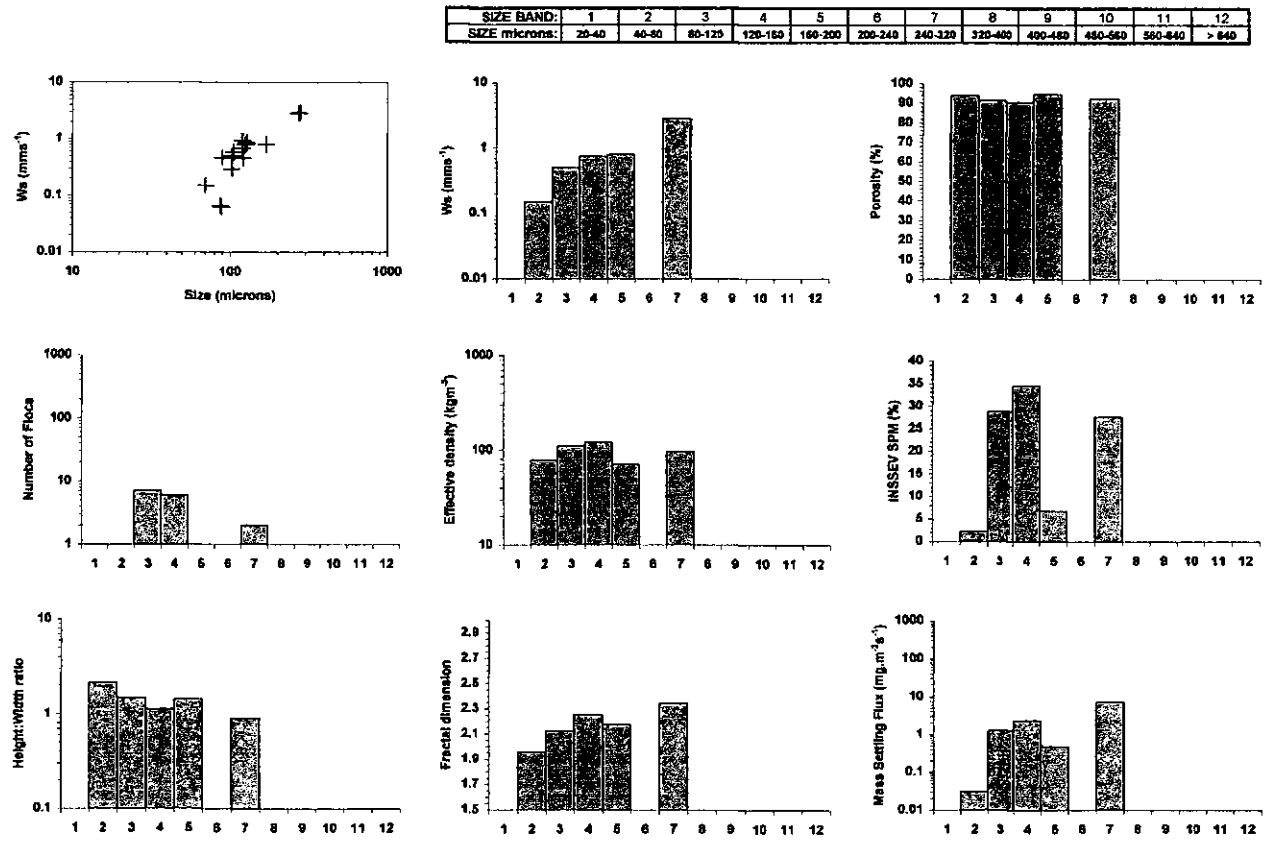

Figure 5.37 Floc characteristics for INSSEV sample 23G-19 collected at 15:13hr.

through differential settling in the more quiescent conditions. For this sample, SBs 3 (80-120 μm) and 5 (160-200 μm) contained 73% of the particulate matter.

5.5.3 Ebb Tide - Flocs

At local high water slack (15:13hr), the SPM had fallen below 10 mgl^{-1} and the turbulent shear stress was only 0.06 Nm^{-2} (G = 1.5 s^{-1}). At this time in the tide, the INSSEV instrument only captured 17 individual flocs to form sample 23G-19 (Figure 5.37). Only one floc had a settling speed greater than 1 mm s^{-1}. This means that most flocs were probably constructed higher in the water column, and their lower rates of fall, meant that it had taken longer for them to reach the sampling height. The two large flocs in SB 7 (240-320 μm), may have been the product of particle scavenging through differential settling. Having a settling velocity of 2.85 mms^{-1}, the members of this sub-group were falling at a rate significantly faster than the rest of the captured population.

5.5.4 Summary of Gironde estuary experiment

Five hours of continuous measurements made on the 23rd June 1999 during neap tides in the lower reaches of the Gironde estuary were reported in section 5.5. Surface currents peaked at 1.2 ms^{-1} at 11:35hr, which corresponded with a maximum TSS of ~ 0.55 Nm^{-2} (0.6 m above the bed). Both turbulence and current velocity progressively decayed as local high water was approached (15:13hr); whereby the salinity at the surface had risen by 4 to a homogeneous 25 (an increase of only 1 at the bed). Although the particulate concentrations were generally low, the initial nearbed SPM rose sharply from 55 mgl^{-1} (11:30hr) to a peak of 180 mgl^{-1} at 12:30hr, whereafter it decreased to ~10 mgl^{-1} one hour later.

A total of 18 INSSEV samples were collected on the 23rd, 15 of which were on the flood tide. At 11:30hr the highly turbulent water column restricted the maximum floc size to 253 μm. The floc size grew in response to the rise in SPM and moderately high TSS of the mid-flood period (12:30hr). At this stage a bi-modal population was evident, and although only 35% of the SPM constituted the sub-group of flocs 160-320 μm, their significantly faster settling velocities (1-3 mms^{-1}) meant they represented 66% of the MSF. Closer to HW, the lower abundance of particulates in suspension, and reduced turbulence, created a much lower effective collision frequency. This curbed maximal floc growth, and restricted 73% of the SPM to the slower settling (Ws between 0.5-1.5 mms^{-1}) flocs of SBs 3 and 5.

5.6 University of Plymouth Laboratory Experiments

See Appendix I.

5.7 LEGI Laboratory Experiments

To review, the experimental programme utilised natural mud from both the Tamar (experiment 1) and Gironde estuary (experiment 2), plus mud from the Gironde estuary which had the organic matter removed by chemical pre-treatment (experiment 3). Each mud was pre-sieved at 100 μm, and mixed into separate base concentrations of 200 mgl^{-1}, 600 mgl^{-1}, 1 gl^{-1} (1.8 gl^{-1} for Gironde estuary natural mud), and 5 gl^{-1} (Tamar mud only). A slurry was then decanted into the LEGI grid tank and allowed to attain equilibrium with the induced turbulent shear stress of the oscillating grid which was located just above the base of the tank. After a 40 minute duration, flocs were withdrawn from three different depths: A, B and C, which translated into respective heights of: 10 cm, 15 cm and 20 cm, above the grid when it was at mid-stroke (i.e. 5 cm above the tank base). The flocs were then quickly transferred to a settling column. A detailed outline of the protocols and apparatus used is given in section 3.4.

Both the water and air temperature were kept as constant as possible throughout each experiment by the laboratory climate control system. These measures helped minimise both molecular viscosity fluctuations and prevented the formation of thermals in the water column. Monitoring of these aspects was achieved by means of a digital thermometer. Throughout the three experiments, ambient air temperature ranged between 23.3-24 °C. The water used in both the grid tank and settling column was within $\pm$0.2 °C of the surrounding laboratory air temperature.

The grid tank salinity was maintained at 16.4 ($\pm$0.1) for all measurements, as this was typical of the saline intrusion passing through Calstock on the Tamar estuary, and of the salinity encountered at Le Verdon on the Gironde estuary. With salinity not a major factor in the formation of estuarine flocs, variations of other constituents such as SPM concentration were regarded as more important. The settling column was filled with a clear solution of equal salinity to that used in the LEGI grid tank. A WTW conductivity meter was used to measure the water salinity.

The floc extraction process did not affect the flocs removed from the grid tank. The transfer time from extraction from the water tank to settling commencing in the column, did not exceed five seconds. This time duration would have restricted any flocculation activity occurring in the pipette to a minimum. The INSSEV quality factor, Q_c values, ranged between 0.94-1.05 for most

samples. Only the samples with high SPM levels, had Q_c values of the order of 0.8-0.9, due to the number of flocs required to constitute the population. For example, a sample with an SPM of 5 gl^{-1} may be composed of several thousand flocs, and some may be missed by the manual processing, plus some flocs may be over-lapping each other as they settle in the column. However, due to the number of flocs measured, these samples are still regarded as valid records. A backtracking analysis was conducted on a number of randomly selected samples and suggested that no excess turbulence had affected the settling velocities measured in the settling column. These factors indicated that the flocs of each sample were all representative of their respective populations and environmental conditions.

5.7.1 Shear stress data

Figures 5.38.A and 5.38.B show the profiles of turbulent shear stress throughout the water column (induced by oscillating the grid at a frequency of 4 Hz) made during experiments 1 and 3. The turbulent shear stress was computed in the format of G-values, which are the root mean square of the gradient in turbulent velocity fluctuations. These G-values were computed from acoustic velocity profile measurements made by the LEGI velocimeter. These are compared to the theoretical model for clear water conditions. Both records showed a general mid-depth reduction from the theoretical curve in the turbulent energy dissipation rate, resulting in lower measured G-values. At the sampling depths A and C, the G-values for a 200 mgl^{-1} concentration were typically 16.6 s^{-1} and 7.7 s^{-1}, respectively. In both experiments the G-values further reduced as the ambient SPM concentration exceeded ~1 gl^{-1}; especially within a CBS layer. Because the turbulence was generated at the bottom of the tank, the drag reduction phenomena which occurred at the lutocline interface during in-situ CBS layer formation, was not observed within the grid tank experiments. Also, due to a malfunction with the LEGI velocimeter, velocity measurements were not made during experiment 2. However, it was deemed reasonable to apply the G-value profiles obtained for experiment 1, also for experiment 2.

5.7.2 SPM concentration data

Gravimetric concentration data was collected simultaneously with each floc sample, by means of a peristaltic pump withdrawal system. The sub-samples were filtered for suspended solids content. The main feature of the LEGI grid tank was that the oscillating grid positioned in the lower part of the tank would produce a gradually decaying level of turbulent mixing with increasing distance above the grid. The only drawback with this type of system would be that it may not create enough shear to keep the SPM in suspension. However the shear stress range produced by the LEGI grid at 4 Hz was sufficient to keep homogeneous base concentrations of up

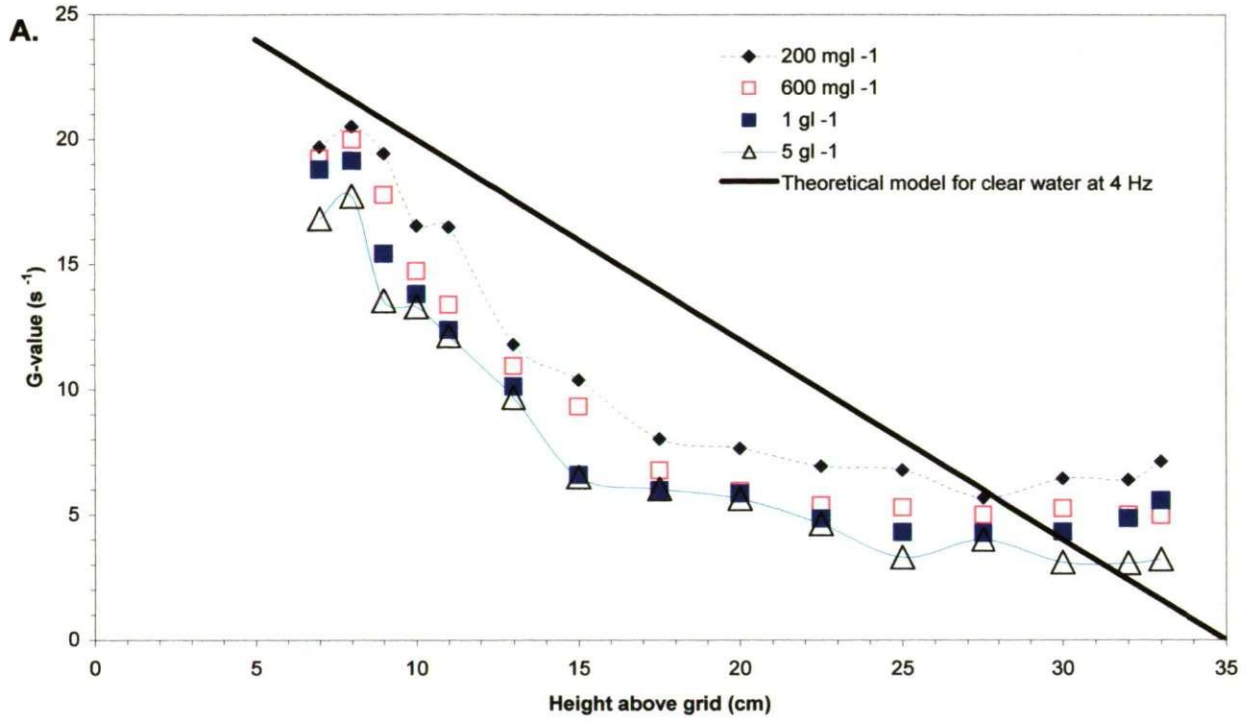

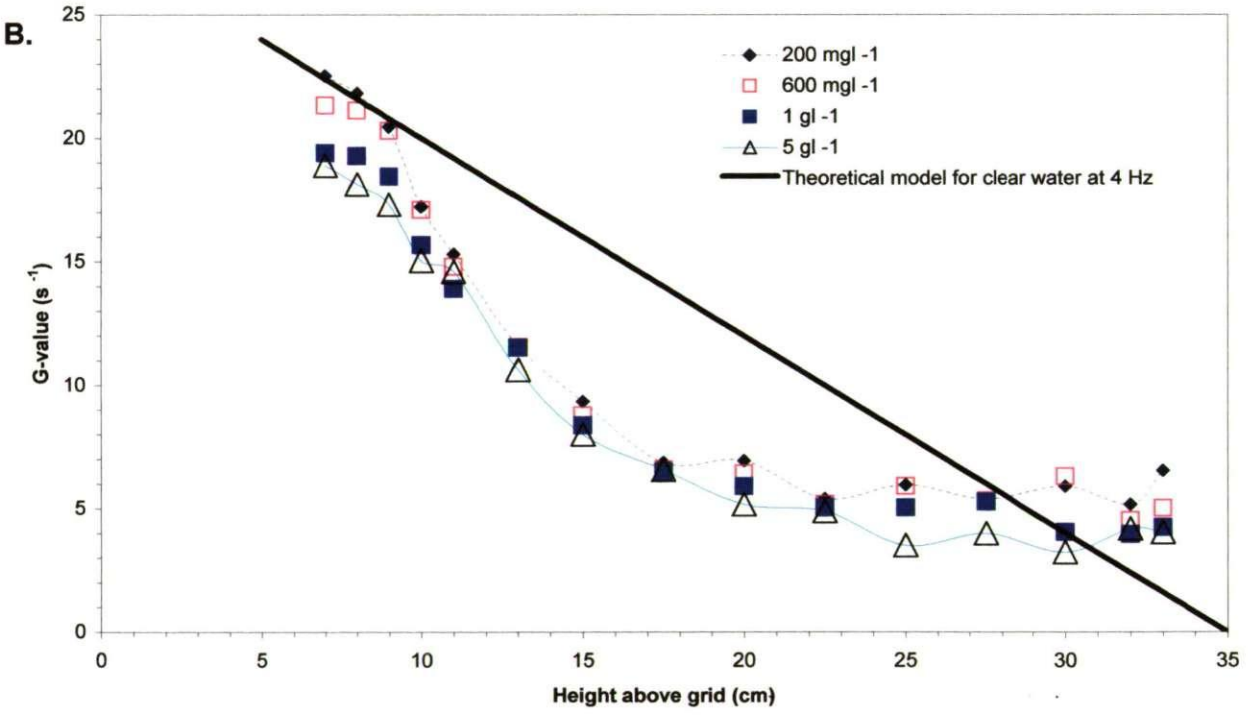

Figure 5.38 Profiles of G measured in LEGI grid tank with: ***A.*** Natural Tamar estuary mud, ***B.*** Gironde estuary mud with organic content removed

to 2 gl^{-1} in suspension, within the floc extraction region of the water column, without a significant amount of settlement occurring. This held true for all three mud types used, as a maximum observed deviation of only 5% from a base concentration of 1.8 gl^{-1}, indicated.

The situation changed once the base concentration was raised to 5 gl^{-1}, as the concentration in the grid tank was too high to maintain a suspension in the lower turbulence region of the upper part of the water column. An equilibrium concentration profile was established 25 minutes into the initial shearing period. A CBS layer formed in the lower part of the tank and exhibited an SPM concentration of ~8.3-8.5 gl^{-1}. At the time of extracting the floc samples, the sharply defined lutocline was 22 cm above the base of the tank i.e. in-between sampling heights B and C. Above the lutocline at point C, the ambient concentration had fallen to ~3 gl^{-1}. This scenario produced a concentration gradient of 55.5 kgm^{-4} between sampling heights A and C.

5.7.3 Floc characteristics

To assist in the identification of floc samples with the various combinations of turbulent shear stress and concentration, the following abbreviations were used:

- tam200-A would indicate a sample taken at height A (highest TSS), with a base concentration of 200 mgl^{-1} using Tamar estuary mud.
- gir/no600-B relates to the purely inorganic Gironde sediment at a nominal SPM of 600 mgl^{-1} extracted from point B (mid-range shear stress level)
- whilst gir1800-C refers to the natural Gironde mud (at a nominal concentration of 1800 mgl^{-1}) withdrawn from the lowest turbulent region of the water column.

A summary of floc samples obtained together with the ambient conditions is given in Table 5.13.

5.7.3.a 200 mgl^{-1} base SPM

The 200 mgl^{-1} base concentration was very representative of the near bed SPM conditions observed during the advection of the main body of the TM through the upper Tamar estuary during neap tidal conditions. Figure 5.39 shows the floc records for the Tamar estuary mud samples (experiment 1) collected from the three different turbulence levels. The most noticeable feature displayed by the individual floc populations, was the progressive increase in SPM concentration towards the larger flocs with decreasing turbulent shear. The sample collected at the lower sampling height (Figure 5.39.A) was within a shear field of 16.6 s^{-1}, which was much greater than would be encountered in most estuaries. For this sample the scatter plot of floc size against settling velocity indicates the presence of two distinct population clusters, with a division occurring at 100 μm. From the 175 floc total, 61 flocs constituted the smaller size cluster and 15% of the dry floc mass. These were flocs that had a dense compact structure (effective density ~250-300 kgm^{-3}) and settling rates generally less than 0.7 mms^{-1}. In contrast, the larger floc cluster was composed of very porous, low density (ρ_e ~ 25-75 kgm^{-3}) aggregates. However, their settling velocities were very similar to the smaller floc cluster. This suggests that the very high

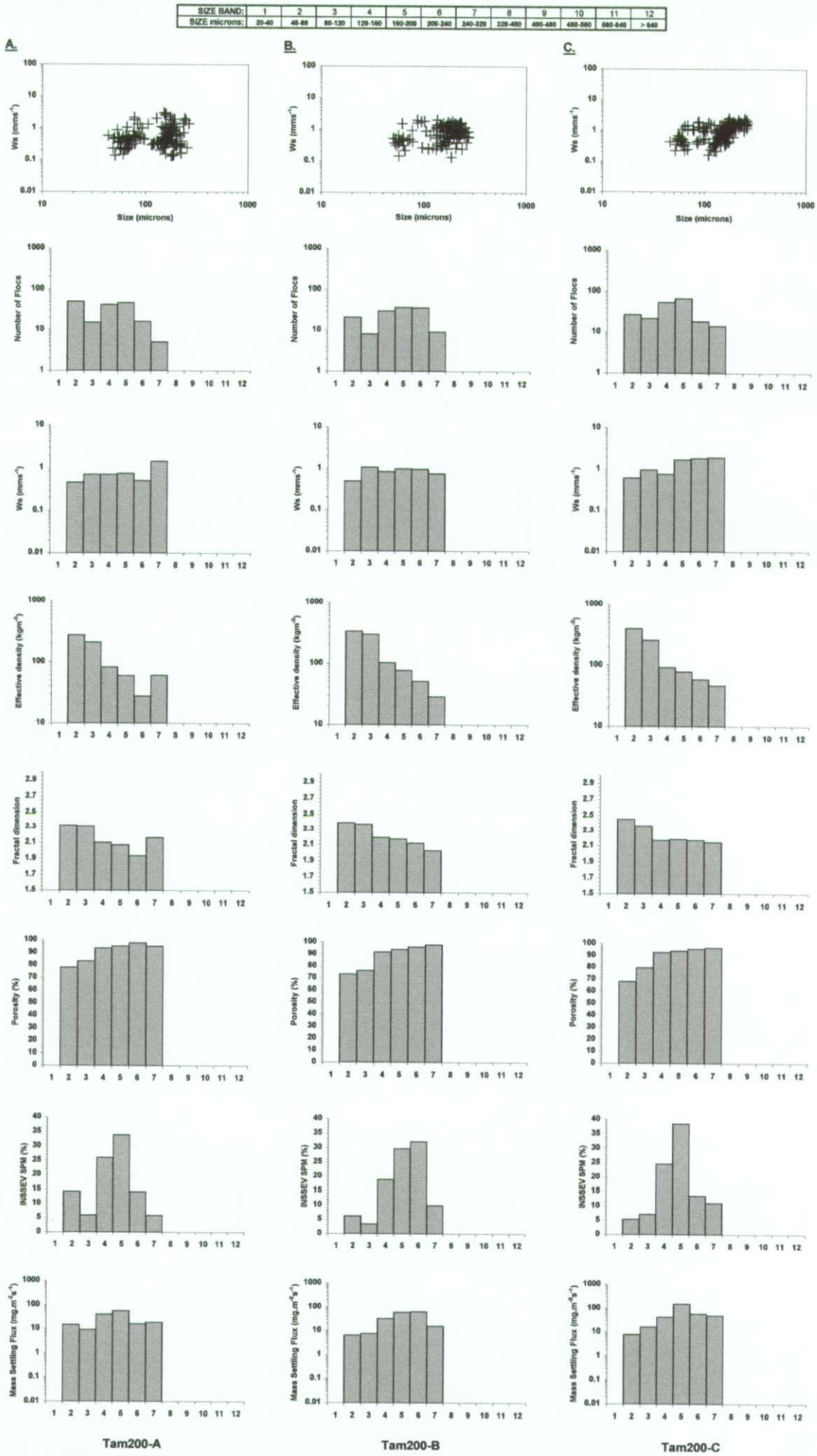

Figure 5.39 Floc characteristics for samples tam200 - A, B & C

Table 5.13 Summary of G-values (s^{-1}) and SPM concentrations (gl^{-1}) with corresponding floc sample references.

Experiment number	Floc sample	Sampling position	SPM (gl^{-1})	TSS (Nm^{-2})	G (s^{-1})	Kolmogorov eddy size (μm)
1	tam200-A	A	0.209	1.49	16.55	251
1	tam200-B	B	0.206	0.75	9.90	324
1	tam200-C	C	0.210	0.53	7.67	368
1	tam600-A	A	0.630	1.27	14.75	266
1	tam600-B	B	0.620	0.69	9.33	334
1	tam600-C	C	0.585	0.38	5.96	418
1	tam1000-A	A	1.048	1.17	13.83	274
1	tam1000-B	B	1.039	0.47	7.00	385
1	tam1000-C	C	1.045	0.37	5.86	421
1	tam5000-A	A	8.650	0.88	11.20	305
1	tam5000-B	B	8.242	0.43	6.52	399
1	tam5000-C	C	3.096	0.35	5.65	429
2	gir200-A	A	0.208	1.49	16.55	251
2	gir200-B	B	0.210	0.75	9.90	324
2	gir200-C	C	0.206	0.53	7.67	368
2	gir600-A	A	0.630	1.27	14.75	266
2	gir600-B	B	0.609	0.69	9.33	334
2	gir600-C	C	0.625	0.38	5.96	418
2	gir1800-A	A	1.811	1.17	13.83	274
2	gir1800-B	B	1.754	0.47	7.00	385
2	gir1800-C	C	1.766	0.37	5.86	421
3	gir/no200-A	A	0.203	1.57	17.23	246
3	gir/no200-B	B	0.207	0.69	9.35	334
3	gir/no200-C	C	0.192	0.47	6.95	387
3	gir/no600-A	A	0.621	1.55	17.10	247
3	gir/no600-B	B	0.629	0.64	8.79	344
3	gir/no600-C	C	0.571	0.42	6.43	402
3	gir/no1000-A	A	0.976	1.38	15.68	258
3	gir/no1000-B	B	0.959	0.60	8.38	352
3	gir/no1000-C	C	0.953	0.38	5.92	419

turbulent shear stress produced very ragged large flocs, and the smaller floc cluster were particles stripped from the larger aggregates.

Moving to a less turbulent zone (tam200-B), the bi-modal floc distribution was still evident (Figure 5.39.B), but now the population division was more biased towards the larger flocs. This larger fraction was composed of floc SB4-7 (120-320 μm), all with effective densities under 100 kgm^{-3}. These flocs represented 80% of the population and contained 90.6% of the SPM; this was an increase over the previous sample of 15% and 5.6%, respectively. The further decrease in TSS from 9.9 s^{-1} to 7.7 s^{-1} (Figure 5.39.C) proved to be significantly more stimulating to the production of fast settling flocs. The maximum floc size had increased by 15 μm (from the sample at B) to 260 μm. However where the previous two samples displayed a wide range in

settling velocities in the larger flocs, sample tam200-C showed a much tighter grouping in the settling velocities of the flocs over 160 μm in size. This resulted in that fraction of flocs having a mean settling rate of 1.8 mm^{-1}, which was nearly double the fall rate of the over 160 μm fraction of sample tam200-B. This demonstrates the significant impact a subtle variation in TSS can have on a floc community.

There was a great deal of similarity between the Gironde flocs (experiment 2) and those formed with the natural Tamar mud at the nominal concentration of 200 mgl^{-1}. However, the larger flocs formed with Gironde sediment at all three increments of turbulent shear stress, were faster in settling when compared to the corresponding Tamar mud samples. This indicates that the composition of the Gironde mud with organic content had better aggregational potential at low concentrations. The 200 mgl^{-1} base concentration was typical of the peak near bed concentrations observed during neap tides at Le Verdon region of the Gironde Estuary (see section 5.5.1). Like the Tamar flocs sampled at position A (Figure 5.40.A), the natural Gironde mud (sample gir200-A) also produced a bi-modal distribution, with the division at 120 μm. The larger fraction represented 70% of the flocs, which had a mean settling velocity of 1.26 mms^{-1}; an increase of 110% when compared to the similar Tamar mud sample (tam200-A). Examining the SPM distribution showed that SB4 (120-160 μm) contained over half (52%) of the particulate matter, with a rapid decrease in SPM% as the size band increases. This indicates that the very turbulent conditions curbed floc growth in the larger fractions, and SB4 appears to be the pivot around which the floc production revolved.

The decrease in TSS to 9.9 s^{-1} created a large scattering in the floc population (Figure 5.40.B). The sub-120 μm flocs had settling velocities which ranged between 0.03-6.6 mms^{-1}. This would suggest that this combination of ambient SPM and turbulent stirring was causing a great deal of instability within the resultant floc population. Three or four clusters of flocs can be identified, which indicates the level of flocculation occurring within this sample. Figure 5.40.C shows the Gironde mud floc sample collected from the lower shear field of 7.7 s^{-1}. The very low settling velocity cluster observed from sample gir200-B, have been scavenged by a less aggressive level of orthokinetic bonding. This has produced a significantly faster settling larger fraction, with the flocs greater than 160 μm possessing a mean settling rate of 2.25 mms^{-1}. This compared to a mean settling velocity (of the >160 μm sub-group) for the preceding sample, of only 1.33 mms^{-1}; a product of the large scattering in aggregate settling rate. In terms of mass settling, sample gir200-C had a MSF of 375 $mg.m^{-2}s^{-1}$, which was a 5% rise over gir200-B.

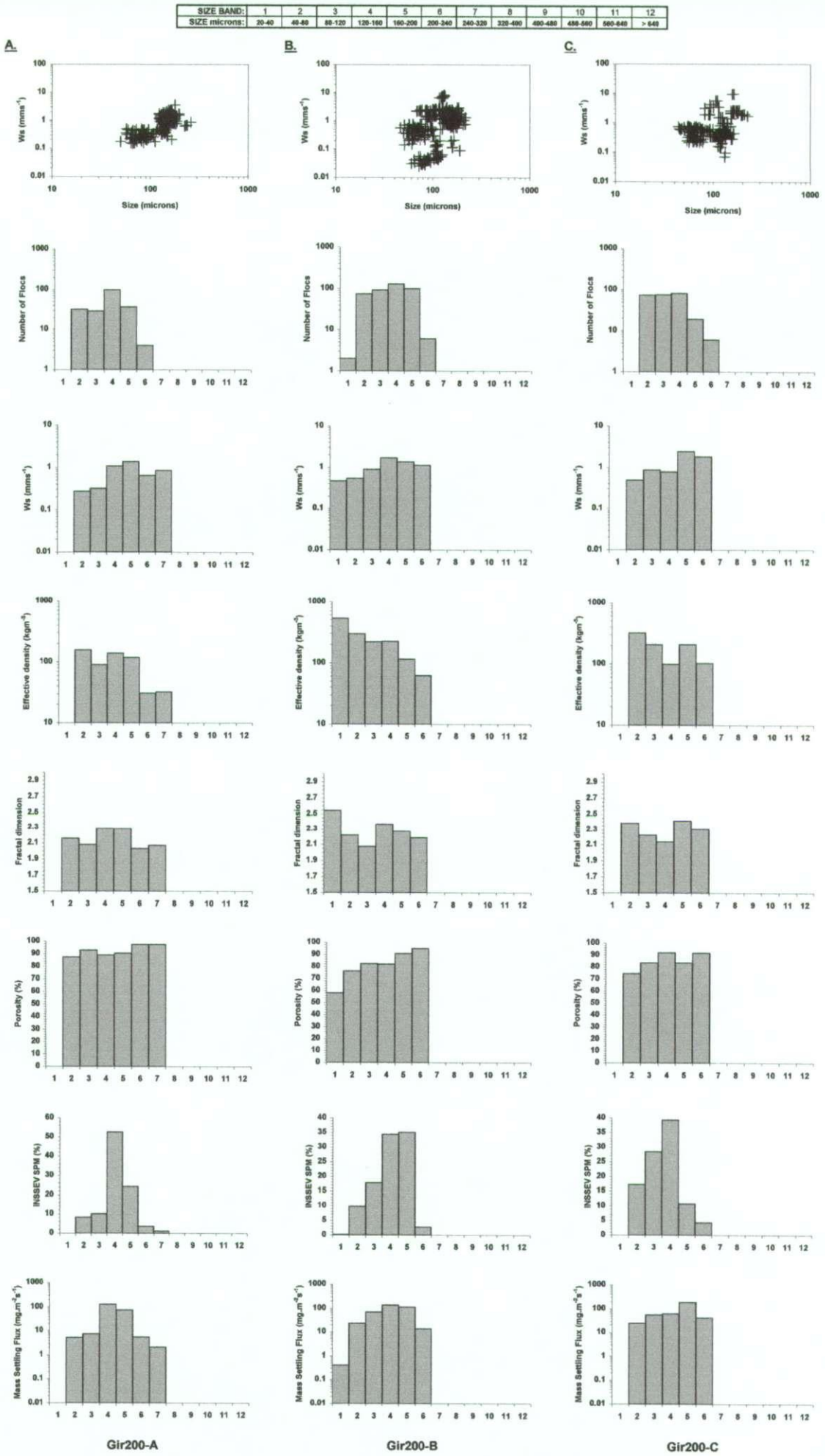

Figure 5.40 Floc characteristics for samples gir200 - A, B & C

The removal of the organic fraction from the Gironde mud slurry (experiment 3) dramatically affected the flocculation potential of the particulates throughout the low SPM concentration level. Figure 5.41 shows the floc characteristics for experiment 3 at all three TSS levels. At the highest shear stress (gir/no200-A), the scatter plot (Figure 5.41.A) shows a tight clustering of the aggregates, as opposed to the very bi-modal distributions demonstrated by the natural muds at the same turbulent intensity. The difference between the two samples was that for the natural muds, the sub-groups demonstrated significant increases in floc size range with increasing settling; a consequence of decreasing ρ_e with increasing floc size. Whereas for the purely mineral sediment, the progression between the clusters showed only significant increases in settling velocity (which spanned three orders of magnitude), whilst the size ranges remained relatively constant. The general absence of flocculation by the purely inorganic mud-type, signifies that aggregate density increased with increasing settling velocity, i.e. the reverse of what occurs for natural muds. The smallness of the aggregates was a consistent observation for the inorganically composed flocs, with the maximum floc size not exceeding 100 μm.

Figure 5.41.C shows the floc population for sample gir/no200-C ($G = 7\ s^{-1}$). It was composed of 368 flocs, ranging from 23-84 μm in diameter. The sample had a mean settling velocity of ~1 mms^{-1}. The primary mode for the SPM concentration occurred at SB2 (40-80 μm) with a values of 93.7%. This consisted of 91.6% of the floc population. These flocs demonstrated very low porosities (~36%), high fractal dimensions of 2.8, and effective densities typically greater than 1000 kgm^{-3}. In summary, the removal of the organic matter from the Gironde mud severely reduced the ability for the low concentration of particles to coagulation beyond that of zero or first order flocs (see section 2.3.1). This was evident at all three of the turbulent mixing levels, so variations in collision frequency made no difference. Similarly the high ambient salinity (16.4) had no major influence on the cohesion. Thus, this experiment indicates that the addition of organic matter, primarily the sticky extra-cellular polymetric substances (EPS), are a very important property of the cohesive sediment in promoting floc growth. It was also observed that the combination of the oscillatory nature of the generated turbulence and the effect of sieving at 100 μm, tended to make all of the aggregates near-spherical in shape, compared to the different manner in which turbulent shear is generated in an estuarine water column. This led to an absence of "stringer" or "comet" shaped flocs from the grid tank samples, which are commonly observed in-situ.

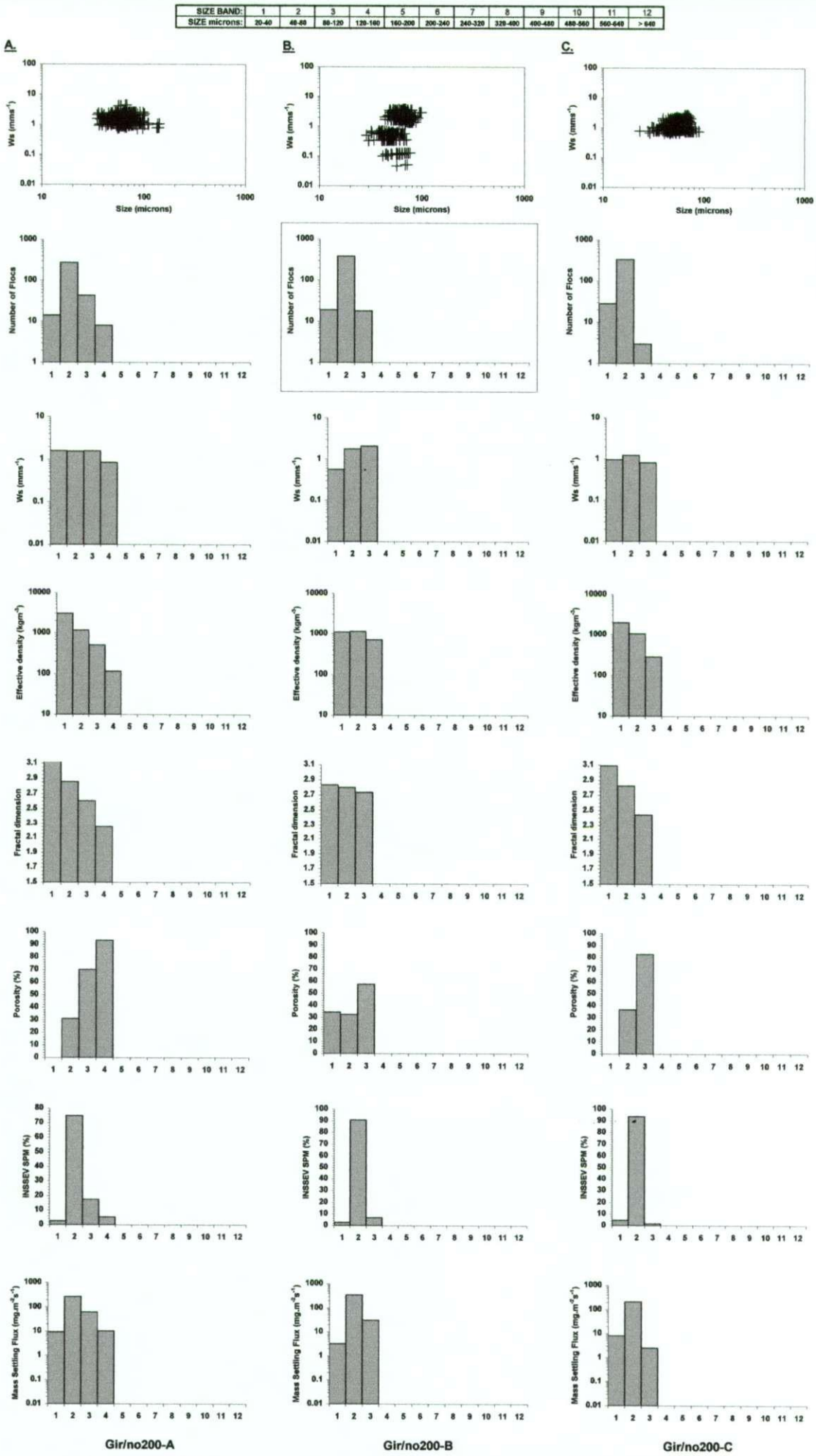

Figure 5.41 Floc characteristics for samples gir/no200 - A, B & C

5.7.3.b 600 mgl^{-1} base SPM

Increasing the base concentration by 400 mgl^{-1}, acted as a catalyst for the two natural mud samples, stimulating the growth of a greater number of larger flocs within the lower shear stress environment. Figure 5.42.C shows the floc properties of the Tamar mud aggregates formed in a shear field of 6 s^{-1}. The scatter plot shows that the percentage of flocs in SB 5 (160-200 μm) and over had risen to 71%, compared to only 49% for the corresponding 200 mgl^{-1} sample (tam200-C). This translated into a respective SPM% increase of 21.8% for the same size fraction to a total of 84.8% for the higher concentration sample. Although the number of large flocs had become more abundant for the Tamar mud sample, the maximum floc size had not increased from that observed at the lower concentration.

In contrast, the greater abundance of particulates of the natural Gironde sediment (Figure 5.43.C) combined with a shear stress of 6 s^{-1}, created a floc size increase of 33% with a maximum aggregate size of 300 μm. The proportion of particulates in the >160 μm fraction rose from 15 % (for the 200 mgl^{-1} base concentration) to 65%. Examination of the settling velocity histogram shows the flocs from SB6-8 (200-400 μm) had mean settling rates ranging from 1.8-2.8 mms^{-1}. This was a result of a small cluster of flocs 193-245 μm in size, which had settling velocities up to 20 mms^{-1}. At the higher turbulent shear stress levels, the primary mode of SPM for the Gironde mud samples was SB5 (160-200 μm). Whereas for the Tamar mud, the mode shifted from SB5 to SB6 (200-240 μm), with shear stress decreasing from 9.3 s^{-1} to 6 s^{-1}, respectively.

With regards to the purely inorganic Gironde mud (Figure 5.44), the floc spectra distributions at all three shear stress levels looked very similar. The scatter plots show a cluster of flocs ranging from 35 to 129 μm, with settling velocities spanning between 0.9-3 mms^{-1} at each floc size. As with the lower concentration samples, the modal SPM size band was still SB2 (40-80 μm); varying between 65-84% dependent on the TSS. These small aggregates were predominantly high density particles (effective density ~2000 kgm^{-3}), which had fractal dimensions nearing 3, and virtually no porosity. This suggests that as the majority of aggregates did not exceed the sieving mesh diameter of 100 μm, and most of the aggregates sampled from the inorganic Gironde mud were unflocculated particulates behaving as inert particles.

5.7.3.c 1000 mgl^{-1} / 1800 mgl^{-1} base SPM

Raising the base concentration of the Tamar mud slurry to 1 gl^{-1} resulted in the production of three very different floc populations. At the low shear stress level (5.9 s^{-1}), the scatter plot (Figure 5.45.C) of the measured flocs indicated a weakly bi-modal distribution, inter-connected by a

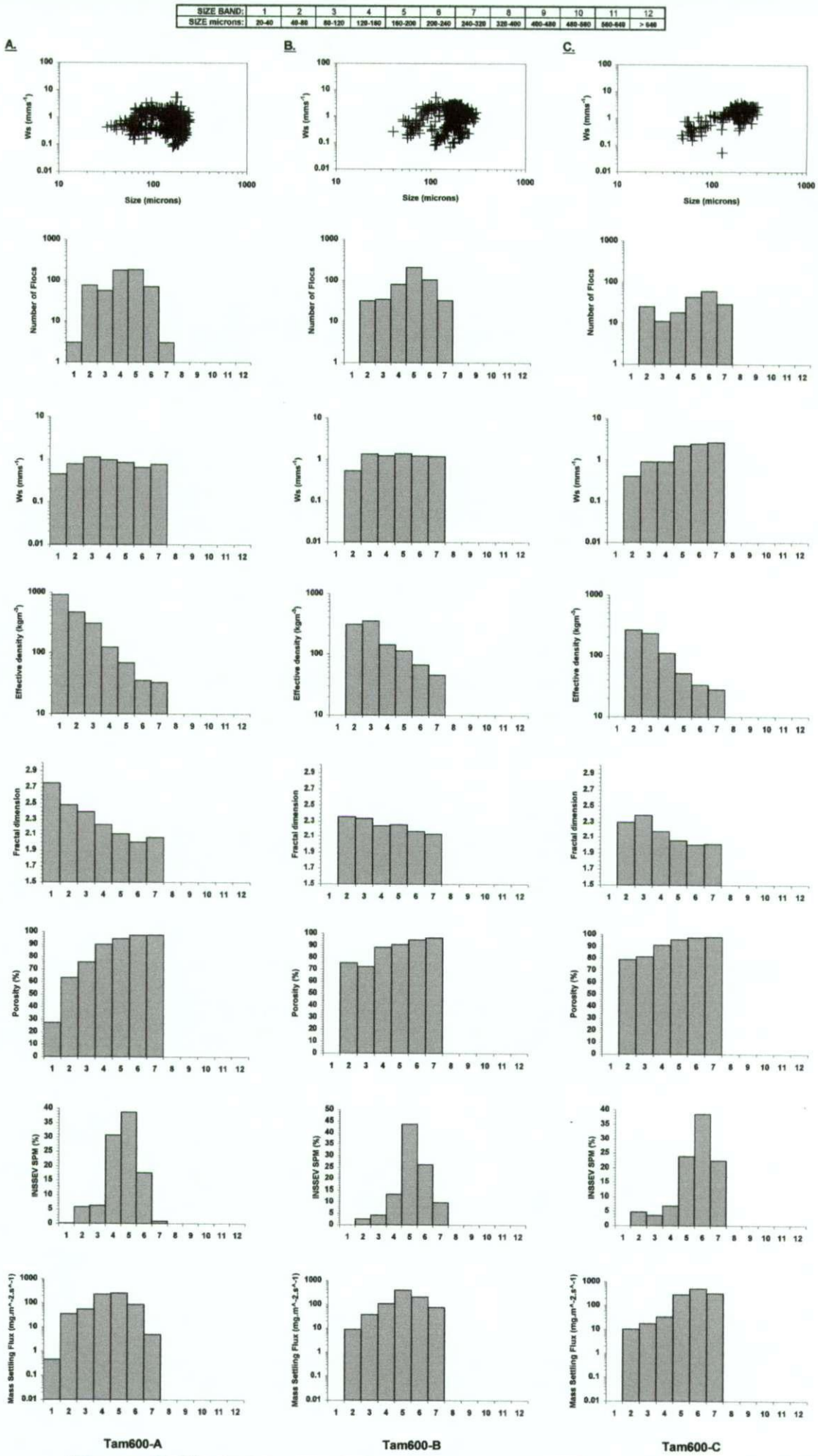

Figure 5.42 Floc characteristics for samples tam600 - A, B & C

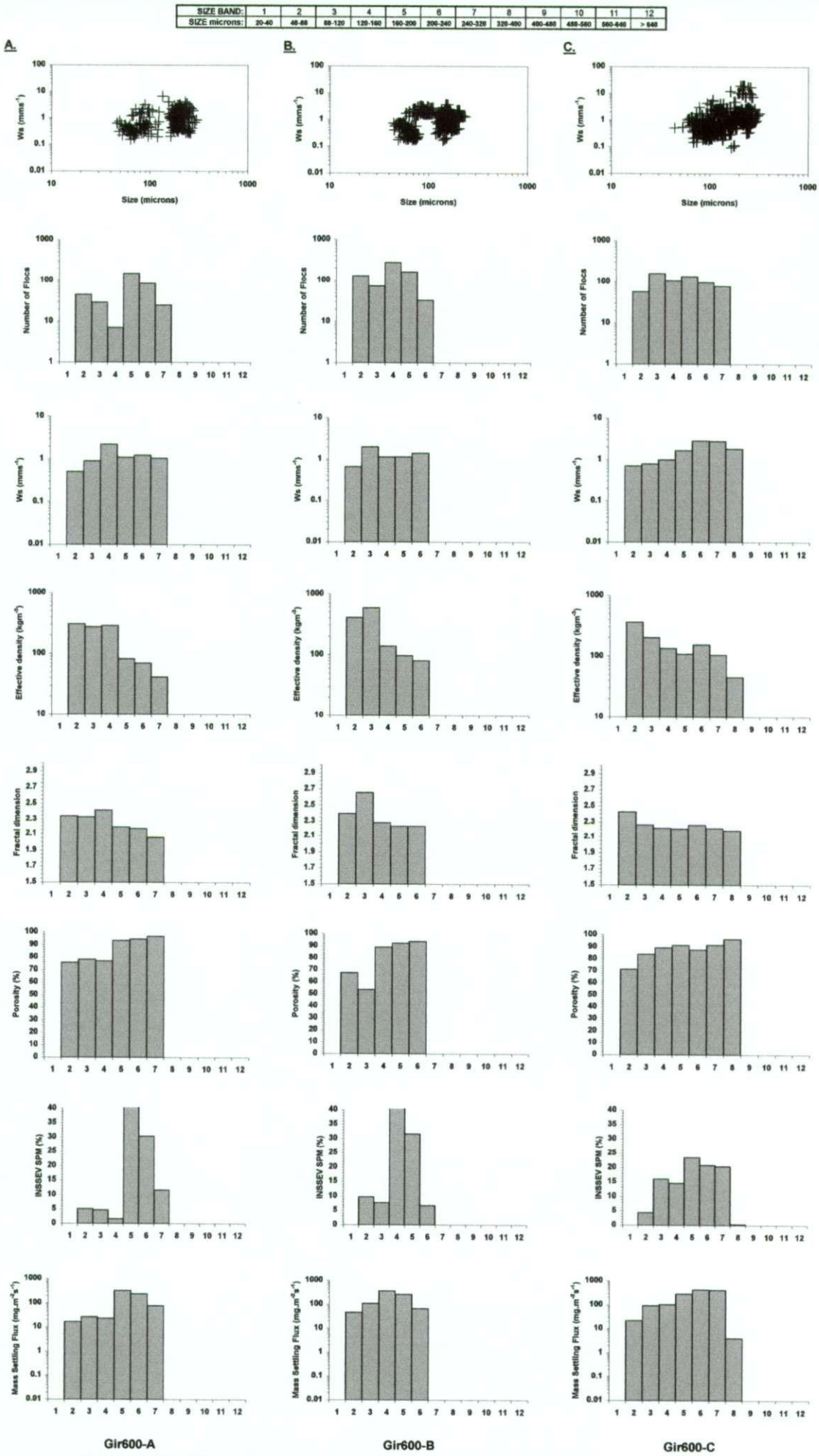

Figure 5.43 Floc characteristics for samples gir600 - A, B & C

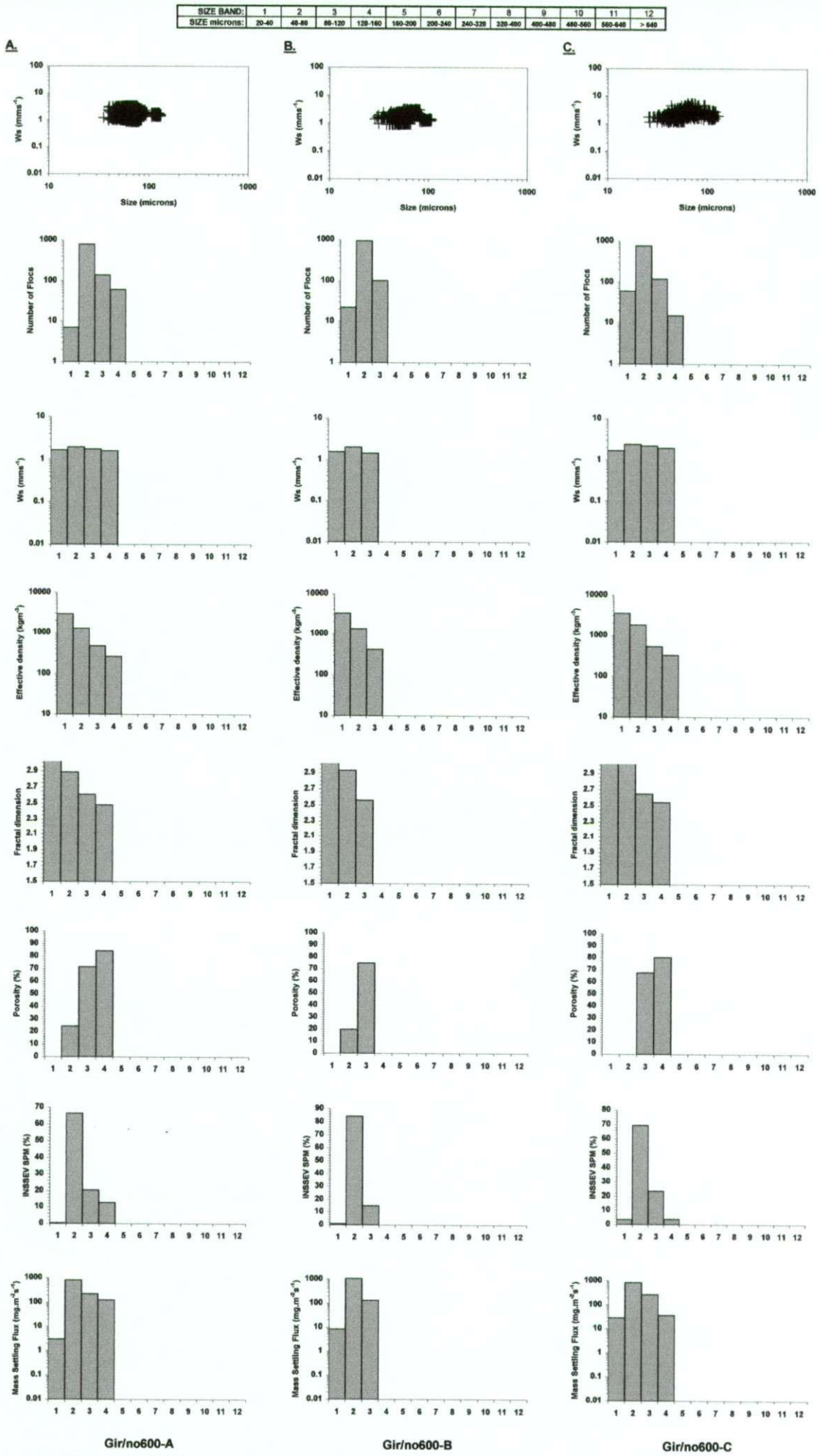

Figure 5.44 Floc characteristics for samples gir/no600 - A, B & C

number of transitional flocs (i.e. between the two main sub-groups). The smaller of the clusters accounted for 15% of the total population. It was composed of flocs ranging from 43-72 μm in diameter, with high effective density values of 360-490 kgm^{-3}, and possessing a relatively compact structure (fractal dimensions up to 2.6). These flocs had settling velocities under 1 mms^{-1} and only accounted for 4.5% of the dry mass. The remaining flocs were low density aggregates ranging from 160 μm, up to 478 μm in diameter. This fraction was composed of 92% of the particulate matter, with 59% of the total SPM contained in SB7-10 (240-560 μm). The latter sub-group had settling velocities spanning from 1-18 mms^{-1}. This translates into a mean settling rate of 3.3 mms^{-1} for the flocs greater than 160 μm.

Increasing the turbulent shear stress by an increment of 1.1 s^{-1} to 7 s^{-1} (Figure 6.45.B) was sufficient to control the production of the larger flocs. The maximum floc size was only 366 μm, and there was a high proportion of slow settling (Ws < 0.6 mms^{-1}) flocs in the 170-230 μm size range. This gave the sub-group >160 μm a mean settling velocity of 2.3 mms^{-1}; a 30.3% reduction from the corresponding settling rate of sample tam1000-C. Like the previous sample, 59% of the dry mass was contained by the flocs > SB7 (240-320 μm). However 51.5% of this was in SB7 which only had a mean settling velocity of 2.3 mms^{-1}. From a mass settling flux perspective, this sample had a total MSF of 2.5 $g.m^{-2}s^{-1}$, which was a decrease of 28.7% from the lower shear stress sample.

Figure 5.46 shows the floc characteristics for the natural Gironde mud at a nominal concentration of 1.8 gl^{-1}. Both the high (13.8 s^{-1}) and mid-range (7 s^{-1}) shear stress environments produced floc spectra comparable to the lower concentration levels. The high shear stress created a very bi-modal distribution with the division occurring at 160 μm. Both sub-populations had settling velocities ranging between 0.1-4.5 mms^{-1}. However, the smaller flocs had effective densities of 200-400 kgm^{-3} and a mean fractal dimension of 2.4. Whereas the flocs >160 μm had fractal dimensions around 2, and effective densities generally less than 50 kgm^{-3}, but a mean settling velocity of only 1.04 mms^{-1}. Flocs less than 160 μm in size accounted for 42% of the population; a result of the turbulent environment coupled with an abundance of particles in suspension causing a high frequency of non-constructive collisions. All of this resulted in a MSF of 1.4 $g.m^{-2}s^{-1}$. In contrast the less turbulent environment of 5.9 s^{-1} (Figure 5.46.C), also produced a strongly bi-modal population, but each cluster was separated by SB5 (160-200 μm) which contained only one floc. The division of flocs was 62:38 in favour of the larger size fraction. These flocs had only grown up to 324 μm in diameter, which was 154 μm smaller than the flocs produced by Tamar mud at 1 gl^{-1} for the same shear stress. However, the large Gironde mud flocs

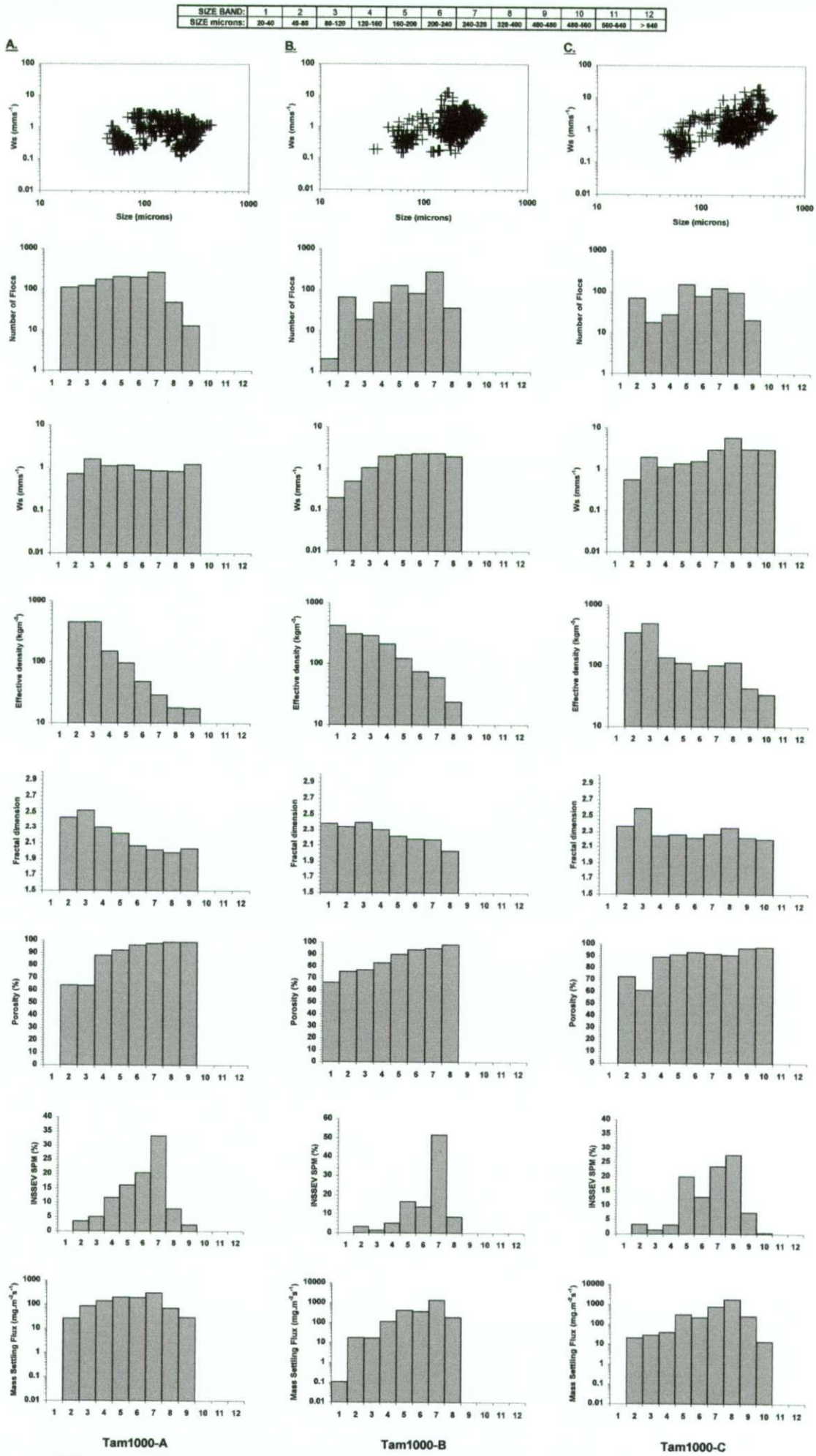

Figure 5.45 Floc characteristics for samples tam1000 - A, B & C

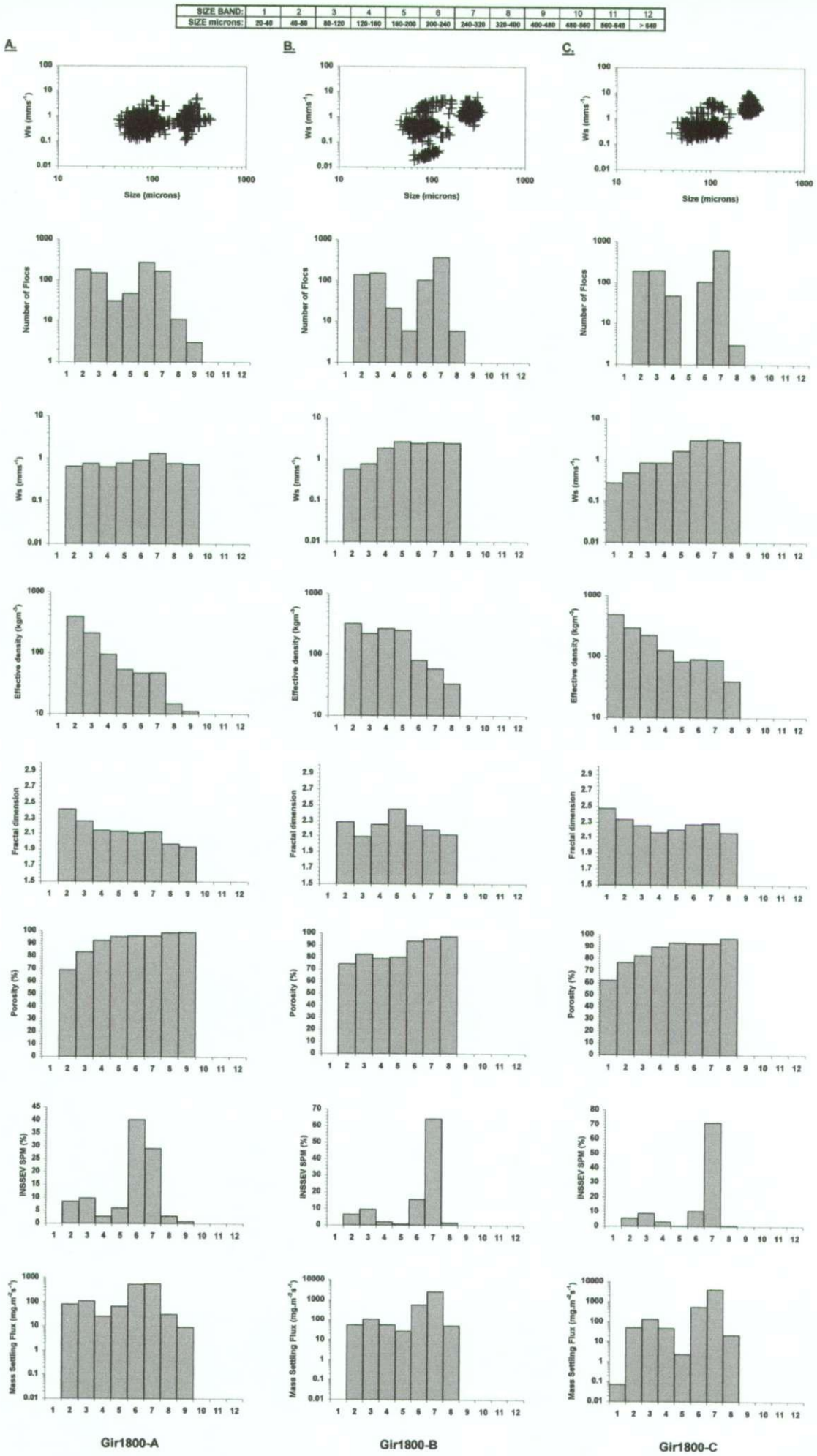

Figure 5.46 Floc characteristics for samples gir1800 - A, B & C

showed settling velocities ranging from 1.6-9 mms^{-1}, and this cluster contained 82.4% of the particulate matter. This gave a resultant total MSF of 5 $g.m^{-2}s^{-1}$; an increase of 253% over sample gir1800-A. Furthermore, after adjusting for the difference in base concentration, sample tam1000-C would have produced a MSF 14.5% greater than that of sample gir1800-C.

For the purely inorganic Gironde mud, raising the nominal particulate concentration to 1 gl^{-1} (Figure 5.47), showed no significant size spectral differences from those observed at the lower ambient concentrations of 200 gl^{-1} and 600 gl^{-1}. This further reinforces the important role of the organic matter which coats natural particulates, towards the growth of large macroflocs at higher concentrations.

5.7.3.d 5000 mgl^{-1} base SPM

The formation of a CBS layer with an SPM concentration of ~ 8-8.5 gl^{-1} during the initial stirring period, had a profound influence on the Tamar estuary mud floc characteristics. The lutocline stabilised at 22 cm above the bottom of the tank, 3 cm below sample height C, which meant that the ambient concentration at C was only 3.1 gl^{-1}. All three samples (Figure 5.48) demonstrated bi-modal floc distributions, with the smaller cluster generally containing flocs less than 100 μm in size, and settling velocities under 1 mms^{-1}. The most significant spectral variations occurred within the larger fraction, which typically commenced at 160 μm.

The lower concentration and more gentle stirring of the sample extracted from above the lutocline (Figure 5.48.C) showed that flocs had been encouraged to grow up to 920 μm in diameter, although beyond SB8 (320-400 μm) the numbers of flocs rapidly decreased with increasing size. As would be expected, the range in settling velocities became larger as the spectra approached SB5, however the maximum settling rate did not exceed 5 mms^{-1} at any point. This resulted in a mean settling velocity of 3.5 mms^{-1} for the floc >160 μm. This was an increase of only 0.18 (for the same size fraction) when compared to the corresponding sample (tam1000-C) at a base concentration of 1 gl^{-1}.

Of the two samples observed within the CBS layer, the quiescent conditions of sample tam5000-B (G = 6.5 s^{-1}) produced the optimum conditions for flocculation. There were very few flocs in SB5 (160-200 μm) which separated the two sub-populations. The maximum floc size was restricted to 720 μm, a high proportion of the floc cluster SB6 (200-240 μm) and over, possessed settling velocities of 4-30 mms^{-1}. This cluster (>200 μm) contained 97% of the SPM, with the primary mode occurring at SB8 (320-400 μm), and a mean settling velocity of 5.75 mms^{-1}. This

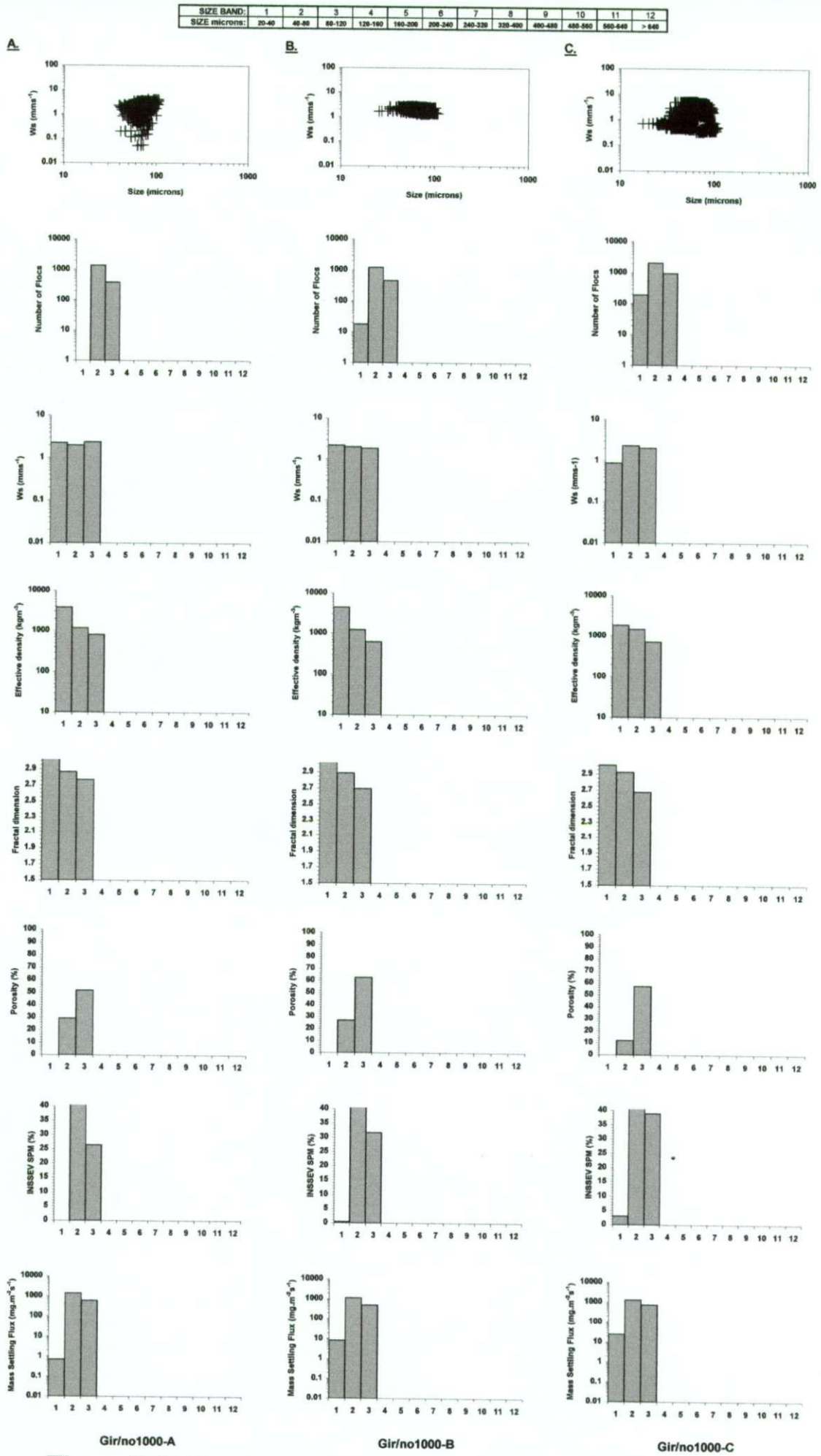

Figure 5.47 Floc characteristics for samples gir/no1000 - A, B & C

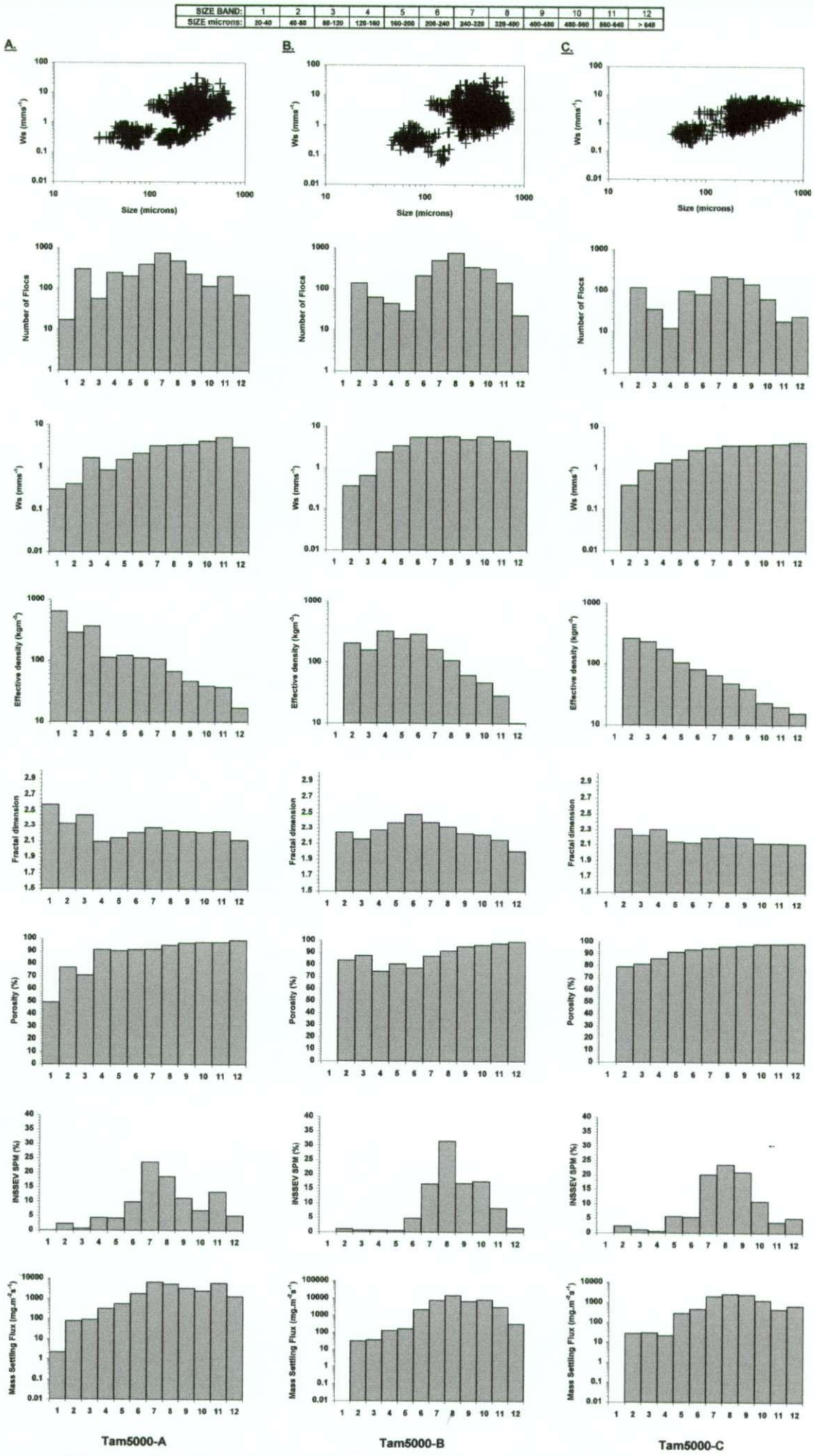

Figure 5.48 Floc characteristics for samples tam5000 - A, B & C

very high mean settling velocity, agrees with the observations made of floc populations formed within natural estuarine CBS layers (see section 5.2.4 and 5.3.3).

In comparison, the more turbulent region coupled with the very high CBS concentration of sample tam5000-A created a combination of both flocculation and break-up. This was shown by a decrease of 16.2% in the floc population constituting >200 μm, compared to 89.2% for sample tam5000-B. This translated into a reduction of 8.6% in the SPM content of the fraction >200 μm, from 97% for sample tam5000-B. For sample tam5000-A, the SPM was redistributed towards the smaller slower settling flocs. Consequently the sample tam5000-B had a total MSF of 43.5 $g.m^{-2}s^{-1}$, which was 57% larger than the high shear stress sample collected from position A. This suggests that the within a CBS layer, the high abundance of particulates significantly increases the flocculation potential, but the turbulent shear stress has the ultimate control on the resultant floc populations. Preliminary results explaining some aspects of the CBS layer formations, observed during the LEGI experiments, can be found in Mory et al., (2000).

5.7.4 Summary of LEGI experiments

Section 5.7 reported the results from a series of laboratory experiments conducted at LEGI during July 1999. During calibration, an ambient SPM concentration of 200 mgl^{-1} indicated that the oscillating grid (set at a frequency of 4 Hz) produced turbulent shear levels of 16.5 s^{-1} and 7.7 s^{-1} at the floc extraction heights 10 cm (A) and 20 cm (C) above the grid mid-stroke position, respectively. After a 40 minute agitation, a base concentrations of 5 gl^{-1} produced a CBS layer in the lower part of the tank with an SPM of 8 gl^{-1}, and a consequent reduction in shear to 11.2 s^{-1} at position A.

At a base SPM concentration of 200 mgl^{-1}, the natural Tamar estuary mud (tam200) demonstrated a progressive increase in SPM content towards the larger flocs with decreasing turbulent shear. Within a shear of 16.6 s^{-1} (tam200-A), 100 μm divided two clusters of flocs; small dense flocs, and a number of larger low density (ρ_e ~ 22-75 kgm^{-3}) "ragged" flocs (a product of the high turbulence). The natural Gironde mud (gir200) produced flocs similar to the Tamar mud. The low concentration of Gironde mud however created larger flocs at all three increments of turbulent shear stress, which were faster in settling when compared to the corresponding Tamar mud samples. This indicates that the composition of the Gironde mud with organic content had better aggregational potential at low concentrations.

For a base Tamar estuary mud SPM concentration of 5 gl^{-1}, all three samples demonstrated bi-modal floc distributions, with the smaller cluster generally containing flocs less than 100 μm in size, with settling velocities under 1 mms^{-1}. Within the CBS layer, a $G = 6.5\ s^{-1}$ produced the optimum conditions for flocculation (see sample tam5000-B). This was illustrated by a maximum floc size of 720 μm. Furthermore, the sub-population >200 μm contained 97% of the SPM; those flocs exhibited settling velocities of 4-30 mms^{-1}, and a mean settling velocity of 5.75 mms^{-1}. Thus resulting in a comparative MSF rate 57% higher than the sample obtained from the more turbulent region of the CBS layer (see sample tam5000-A). The purely inorganic Gironde mud (gir/no) displayed a distinct inability to flocculate beyond its pre-sieving size at all SPM concentrations and turbulent shear levels employed.

Chapter Six:

Discussion and Interpretation

This chapter draws on the results presented in Chapter 5, and uses them to identify the most prominent processes which contribute to either floc formation or break-up. The first section, 6.1, explains the principle floc parameterisations used to describe the empirical data. The next two sections (6.2 and 6.3) qualitatively examine the in-situ data, whilst sections 6.4 and 6.5 look at the correlations given from the various laboratory results. The empirical work is statistically assessed for interrelated trends in section 6.6, and these stochastic findings are generalised as a quantitative conceptual model for estuarine flocculation. The performance of this new model is compared to existing mathematical aggregation parameterisations based on theory and laboratory work, in the last section (6.7).

6.1 Floc sample parameterisation

The floc data has so far been presented as either scatter plots of the individual floc populations, or as size spectra which divided floc samples into twelve sub-groups according to floc size. To further assist in the interpretation of the results, the floc parameters of sample mean, MAX6, and changes in macrofloc and microfloc proportions, were also calculated for each INSSEV sample. The determination of each will be explained.

6.1.1 Arithmetic Sample Mean

The mean is the most commonly referred-to floc parameter within the current literature. Although from a quantitative point of view, the large variations in density, size and settling velocity which are apparent in any one sample tend to negate the validity of single mean value. However, the mean can be a useful basic marker to detect when major changes are occurring within the floc community. Also the arithmetic mean (calculated on a dry mass weighted basis) allows a comparison to be made with the mean floc size determined by the PML Lasentec P100 particle sizer (see section 3.4.1.a) which operated during the Tamar estuary field experiments.

6.1.2 MAX6

The second set of descriptive parameters are determined from the mean of the six largest flocs from each sample, and are referred to as MAX6 values. This allows the changes in the largest part of the floc spectra to be inspected in more detail, as the largest aggregates tend to

contain the most mass and a major proportion of the settling flux. MAX6 mean values were also dry mass weighted.

6.1.3 Macrofloc and microfloc

For a quantitative study, a delicate balance between sufficiently describing the floc spectra, whilst limiting the detail to the key components, must be achieved. As described in section 2.3.1, the classic way of meeting these goals has been to segregate the populations into two generalised communities: macroflocs and microflocs. Previously this segregation has been done in a very arbitrary way, due to a lack of good quality empirical data.

A qualitative appraisal of both the in-situ and laboratory floc data was employed to determine which size band division most commonly separated the two distinctly different sub-populations. Using the size band floc data presented in Chapter 5, various size divisions were chosen and sub-population mean floc values were determined (e.g. macrofloc and microfloc settling velocity). The data set combinations were then statistically assessed using multiple regression to produce inter-correlations between the various floc and turbulence data; this analysis is described in more detail in section 6.6. The floc data sets which produced the best overall R^2 fit values were used to identify the size division.

The study revealed that for the various ranges of turbulent shear and SPM concentration, 160 μm provided the optimum segregation point (i.e. settling velocities generally reduced significantly under most combinations of shear and SPM concentration once the flocs fell below 160 μm in diameter). Macrofloc characteristics for a sample were determined by calculating the dry mass weighted arithmetic mean, for each parameter, from the flocs which were > 160 μm in diameter. Microflocs values were calculated similarly for the sub-group < 160 μm in size.

6.2 Tamar estuary experiment

To reiterate from Chapter 5, the Tamar estuary field experiments provided the most comprehensive data set of all the empirical programmes which contribute towards this thesis. For this reason, the Tamar results are regarded as the main focus of the qualitative and quantitative analysis. The remainder will be used to explore the generality of the results. For discussion purposes, all parameters mentioned are interpolated at the INSSEV sampling height, unless otherwise stated.

This section looks at the neap then spring conditions from the September 1998 COSINUS experiments from Station A at Calstock. The characteristics demonstrated by the floc populations both within the turbidity maximum and at times of lower SPM concentration are discussed. This is then followed by a time series comparison between spring and neap conditions. Where appropriate, results from the other participating COSINUS partners will be drawn on, together with findings from the current literature.

6.2.1 Floc observations - September 1998 NEAP TIDES

Either side of the passage of the turbidity maximum (TM) the floc populations consisted of small, slow settling flocs (Ws_{mean} ~ 0.6-1.4 mms^{-1}). The mean floc size was typically 150-200 μm, with the MAX6 size never exceeding 250 μm. This size restriction was imposed by the combined low ambient SPM concentrations, which were less than 50 mgl^{-1}, and slow stirring rates. Even though biochemical analysis indicated that these particles were high in total carbohydrate mass, their high spatial separation severely reduced their potential to coagulate, and this was enhanced even more by the low level of turbulent shear present - it rarely exceeded 0.15 Nm^{-2} (G ~3 s^{-1}). So it would be logical to assume that with these low floc populations, most break-up would occur as a result of surface stripping due to turbulent drag, as opposed to destructive collisions between aggregates. The small nature of the flocs, meant that only 30-50% of the particulate mass was contained in macroflocs. However, with most of the microflocs possessing settling velocities < 0.4 mms^{-1}, this translated into the larger fraction having around 60-70% of the mass settling flux (MSF).

The results of the early part of the ebb (see Figure 5.2), showed the presence of needle-like aggregates which had height:width (H:W) ratios of the order of 3.6-7 and very high effective densities (ρ_e up to 10000 kgm^{-3}). These have been interpreted as fragments of tourmaline and hornblende, which have an origin predominantly from the Dartmoor granite which the River Tamar drains. From examining the surface current record of the 15th September (see Figure 5.1.B), it is suggested that a zone of high turbulent velocity shear exists higher in the water column (above the INSSEV rig) as a result of the ebbing surface water moving over the lower salt wedge which still advanced up to 1 hour 30 minutes after high water. Hence this only allowed these very strong dense aggregates to settle, whilst the more fragile flocs which were not stronger than the shear field were broken-up and kept in suspension in the upper layer. This observation agrees with previous studies made by Fennessy et al. (1994b). Alternatively, these high density aggregates may the product of floc break-up by shear occurring at the salt wedge - freshwater interface.

Within the TM, peak concentrations rose up to ~600 mgl^{-1} (on the flood tide of the 17th September) and this brought about an increase in the number of macroflocs (see Figure 5.11). Subsequently, the centroid of the dry floc mass distribution moved more towards the larger macroflocs, with this sub-group constituting two thirds of the SPM. In this concentration range, floc growth, as opposed to aggregate break-up, was mainly attributed to the turbulent shear stress (TSS) generally falling to a rate of 0.2-0.3 Nm^{-2} (from ~0.5-0.6 Nm^{-2}). Still, although the MAX6 sizes reached 750 μm, the overall number of macroflocs had not increase substantially, as the comparative mean floc size of only 280 μm indicates. The macroflocs in the TM typically demonstrated settling velocities of ~2 mms^{-1}, which accounted for their 85-90% contribution to the MSF; an increase of 20% over the floc populations observed outside of the TM. These changes in size and settling velocity suggest that the effective density of the floc population within the TM must decrease.

In contrast, throughout the more turbulent stages of the tide, when the bed was being eroded to form the TM (advection was minimal during neap tides), the TSS at times reached 0.6 Nm^{-2}. This high rate of stirring coupled with SPM concentrations of 250-400 mgl^{-1} caused a great deal of disruption to floc growth. It seems the continually rising collision frequency was resulting in disaggregation, as opposed to stimulating flocculation. This was demonstrated by INSSEV sample 17-1 (see Figure 5.10), where the particulate matter was evenly divided between the macroflocs and microflocs, together with a third of the floc mass being contained within the 80-120 μm (SB3) fraction. Even though the MAX6 floc size was 335 μm, the size control imposed by the high shear stress significantly restricted the number of macroflocs, as a sample mean size of only 170 μm demonstrates.

6.2.2 Floc observations - September 1998 SPRING TIDES

The increased tidal energy experienced during spring tides, meant that throughout the formation of the TM at Station A, concentrations tended to increase from 500 mgl^{-1} to peak levels of 6-8 gl^{-1} in the space of 90 minutes. The background concentrations of spring tides were generally higher than those encountered within the main body of the TM throughout neap tides, and a larger portion of the particulate mass was the result of advective transport.

In the initial stages of the TM formation (see Figure 5.18), the combination of TSS of 0.4-0.5 Nm^{-2} ($G = 6.2\text{-}7.2\ s^{-1}$) and low spring tide concentrations (~1 gl^{-1}) produced MAX6 flocs up to 500 μm, with settling velocities of 4-5 mms^{-1}. The continued rise in concentration tended to form a CBS layer, and at peak concentration the lutocline was observed 60-70 cm

above the bed. This created drag reduction at the interface, but also a damping effect on the turbulent shear within the CBS layer, and consequently this stimulated floc growth. Although MAX6 floc sizes rose to 950 μm, the most significant changes again occurred within the floc effective densities. This was demonstrated by the macrofloc population in the TM having settling velocities of 4-6 mms^{-1}, in contrast to the macroflocs from the more turbulent zone where settling rates were predominantly 2-3 mms^{-1}. These variations in macrofloc settling velocity were due to the continual re-distribution of the dry floc mass through the spectrum, which was driven by the turbulent activity. The following three generalised scenarios will illustrate this point:

1. Under moderate to high turbulence (TSS ~ 0.4-0.55 Nm^{-2}), between 60-75% of the SPM was in the macrofloc sub-group. These were predominantly high density aggregates, which resulted in sample mean effective densities of 230-245 kgm^{-3}. The well compacted nature of these flocs was a by-product of the ambient shear stress being of a rate, sufficient to bring the particles together with a strong orthokinetic force - hence minimising the number of voids, but enough to promote a high level of break-up.

2. In contrast, within a CBS layer (see Figure 5.19), the macrofloc effective density fell to around 60-70 kgm^{-3}, and these flocs constituted up to 90% of the dry mass. The improved flocculation conditions permitted MAX6 floc size growth up to ~650-800 μm. This also resulted in the production of numerous fast settling macroflocs, and this translated in to ~97% of the MSF for this fraction. This was an increase of 8% over the more turbulent environment experienced earlier in the tide prior to the CBS formation (0.5 m above the bed). It was noticeable that most of these macroflocs in the CBS had H:W ratios of ~0.8. This was probably a result of partial compaction due to low impact collisions from the high abundance of flocs directly above (i.e. also within the dense CBS layer), causing the flocs to be slightly squashed. The absence of stringer flocs in the CBS layer indicates that these impacts did not result in additional differential settling type flocculation. The reduced turbulent energy dissipation that was present in the water column, combined with the very high SPM content, meant that this larger fraction of flocs totally dominated the characteristics of the CBS layer. Thus, it is apparent that as the concentration rose, and the turbulent shear stress decreased to a level of 0.3-0.38 Nm^{-2} (G = 5-5.9 s^{-1}), orthokinetic bonding promoted a much greater degree of flocculation. It is this subtle inter-balance between SPM and TSS that can significantly

alter the absolute MSF rate, and perfectly illustrates why an understanding of these interactions is necessary for accurate predictive sediment transport modelling.

3. Increasing the TSS to a level of 0.6-0.7 Nm^{-2} (G = 8.4-9.4 s^{-1}) was seen to instigate severe disruption to the flocs held in suspension. This was demonstrated by sample 21-4 (see Figure 5.14) collected on the ebb tide where the ambient concentration was ~2 gl^{-1}. The number of inter-particle contacts had curbed the floc size to a MAX6 diameter of 340 μm. Assuming longitudinal uniformity, this suggests that the fast settling large macroflocs, that were numerous 45 minutes earlier in the tide when the turbulence was lower, did not have the structural integrity to withstand the shear field created during sample 21-4 (see Figure 5.15). These large macroflocs had now been disrupted to form smaller aggregates, resulting in a macrofloc settling velocity of only 2.1 mms^{-1}. This de-flocculation would initially have been achieved by detachment along the weakest adhesional bond (where two high order flocs had joined) to reduce the floc back to their respective lower order. As the aggregates in suspension became more numerous, further aggregate break-up would occur as the result of destructive collisions (induced by the high turbulent shear) between neighbouring flocs. This feature would account for the presence of the greater number of very slow settling (settling velocities as low as 0.04 mms^{-1}) microflocs ranging down to the 20 μm resolution limit. Although some of these floc changes could potentially be attributed to advection, a TSS this high would bring the ambient floc population into equilibrium very rapidly. This point is discussed later in more detail.

Throughout times of lower concentrations at spring tides, a number of the macroflocs were classified as "stringer" type flocs. These estuarine stringers differ from those observed by divers or submersibles in the open sea (Nishizawa et al., 1954; Shanks and Trent, 1979; Alldredge, 1979), in that the latter are largely organic material to which inorganic material becomes attached. While the estuarine stringers are thought to be composed from a number of the more dense flocs inter-connected by sticky organic fibres. The largest stringers had an actual length of 1.4 mm and a H:W ratios of 7:1. They had settling velocities of 8.5 mms^{-1} and spherically equivalent effective densities of ~80 Kgm^{-3}. It was the added contribution of these flocs that accounted for macrofloc settling rates of ~3 mms^{-1}. The influence of stringers is further examined in section 6.2.3.

6.2.3 SPRING / NEAP tide comparison of floc properties

To compare the typical floc variations exhibited during spring and neap tide conditions, respective time series data from the 24th June and 5th August will be examined. For the analysis, only samples 05-1 to 12 were utilised from the 5th August record, so as to make both time series of equal length (4 hrs 25 mins). Primarily, the characteristics of the largest flocs from each sample will be focused upon, as they have the potential to contain a high proportion of the particulate mass. For the spring tide conditions the MAX6 floc size ranged between 304-1598 μm. The largest of these aggregates were formed at the time the main body of the TM advected through the Calstock sampling location, and despite being of very low density (effective densities < 50 kgm^{-3}) had settling velocities of up to 16.6 mms^{-1}. In comparison, the MAX6 neap flocs were both 50% smaller in size and in settling velocity, at the occurrence of peak concentration. It was also noticeable that the MAX6 fractal dimensions were generally 0.1-0.2 lower during neap conditions, giving values of ~2.15.

Averaging through both time series showed that 76.4% of the particulate mass was held in the macrofloc portion during the spring tide (samples 24-1 to 24-11). This translated into mean macrofloc:microfloc ratios of floc numbers and SPM concentration of 1.7 and 6.8 respectively. Comparably, the same ratios computed for the neap conditions (calculated from samples 05-1 to 12) were 1.6 and 1.6 meaning that only 54.6% of the ambient SPM was contain within the macrofloc sub-population throughout the neap tidal condition. The result of this indicated that the fast settling macroflocs from the spring tide, accounted for a time series average of 88.5% of the MSF. Whereas during neap tides, the macroflocs contributed 16.1% less to the MSF rate. This was partly due to a time series averaged macrofloc settling velocity of 3.5 mms^{-1} from the spring tides, being 1.8 mms^{-1} faster than that computed for neap tides. The contrasting cumulative totals of MSF for the macrofloc sub-population, at the time the main body of the TM advected through the sampling location, were 83 $g.m^{-2}s^{-1}$ and 1.74 $g.m^{-2}s^{-1}$ for spring tides (samples 24-7 to 11) and neap tides (samples 05-9 to 11), respectively. The high contribution of the macroflocs towards the MSF, agrees with the conclusions of the results for the Gironde estuary, in France (Manning et al., 2000).

During neap tidal conditions of experiment 3 (see Table 5.3), near-bed SPM ranged between 50-500 mgl^{-1}, with an organic content of between 14.5-28%. These relatively low SPM conditions coincided with higher levels of mean chlorophyll-a (up to 0.98 μgl^{-1}), when compared to the spring tidal conditions (chlorophyll-a up to 0.24 μgl^{-1}) which produced concentration levels up to an order of magnitude greater than those of the neap tides, with

significantly lower average organic levels (10-14%). This is explained by the erosion of lower organic and chlorophyll-a content sediment from the bed at the spring tidal conditions, diluting the previously suspended material. Similarly the mean carbohydrate content per mass of sediment was higher on the neap tides (up to 34 mg/g SPM) than the spring tides (up to 5.9 mg/g SPM). However, with significantly higher SPM experienced on the spring tides, overall carbohydrate concentrations were seen to be up to seven times greater during the spring tidal conditions of experiment 3 (see Table 5.6).

The basic mechanism controlling the rate of flocculation is the number of positive inter-particle collisions that occur during hydrodynamically induced stirring within the water column. The theoretical representation of particle collision frequencies was shown in section 2.2.1. However the combination of a low particulate abundance and a quiescent water column, resulted in an extremely low collision frequency. A good example of this effect was demonstrated by the slack lower water period during the neap tides (sample 05-07, Figure 5.28), when the SPM was ~100 mgl^{-1}, but the TSS was only 0.07 Nm^{-2}. Three quarters of the flocs were less than 80 μm in size and had effective density values ranging between 200-1000 kgm^{-3}. In early work on estuarine flocculation, both Krone (1963, 1986) and Partheniades (1965) suggested that flocs were constructed in a progressive order. Primary particles glued together form zero order flocs, these in turn combine to form 1st order flocs etc; this was known as the order of aggregation theory. This indicated that the vast majority of particulate mater did not progress beyond the zero or first order flocculation stage (as classified by Krone). Those which had evolved into aggregates of up to a maximum size of 202 μm, were in the minority. Comparing this sample (05-07) to 05-02 (see Figure 5.27) where the SPM was 131 mgl^{-1}, but the TSS was 0.32 Nm^{-2}, the mean Ws of the > 160 μm fraction for sample 05-2 was 2.8 mms^{-1}, whereas the latter sample was only 0.8 mms^{-1}.

The added presence of a high total carbohydrate concentration, was seen to optimise the production of a high percentage of fast settling macroflocs during the high turbulent mixing activity and SPM levels of the spring tidal conditions, by hence causing greater inter-particle adhesion. This was particularly evident with the observation of a large number of stringer type flocs during the spring conditions. These are smaller aggregates connected together by a network of fine organic strands. The comparison of floc samples 21-4 and 17-1 will demonstrate the importance of stringer flocs.

- Floc sample 21-4 (see Figure 5.15), from the Tamar spring tide ebb deployment, illustrates the above phenomena. Although the TSS was 0.68 Nm^{-2} and the particulate carbon content was only 5.3%, a high total carbohydrate concentration of 10.3 mgl^{-1} most probably aided in the coagulation of the particulates (ambient SPM concentration ~ 2 gl^{-1}), resulting in 40% of the SPM constituting fast settling (Ws ranging from 1.8-3.7 mms^{-1}) macrofloes with spherically equivalent diameters of 240-480 μm. Demonstrating H:W ratios ranging between 1.8-6, these long stringers had a very loose structure as effective densities of 18-70 kgm^{-3} and porosities up to 98.6%, showed.

- In contrast, the high turbulent conditions (TSS = 0.6 Nm^{-2}) of the Tamar neap tide flood of the 17th September (sample 17-1, see Figure 5.10) coupled with a total carbohydrate concentration 50% lower than that of sample 21-4, limited the floc growth potential to a maximum size of 400 μm. Comparably, much less mass was held in the larger floc fraction (26% in the 200-400 μm region), and although the neap tide organic content was significantly high (particulate carbon = 22.2%), the low amount of carbohydrate present meant that this matter could not adhere and thus produce a stringer-type floc composition as seen during spring tide conditions. This had a definite effect on the resultant MSF, in that the neap tide flocs > 200 μm had settling velocities of 1.8-2 mms^{-1}, whereas the more abundant stringer population (> 240 μm) observed during the spring tide demonstrated settling rates of 1.8-3.8 mms^{-1}. Ultimately, this suggests that the total amount of sugars present seems to be a more important factor with regards flocculation than that of the mean organic content.

Van Leussen (1994) suggests that the Kolmogorov microscale of turbulence is a good measure of the maximum floc size. At quiescent periods during neap tides the Kolmogorov microscales were ~1 mm, with the corresponding MAX6 flocs less than 200 μm in diameter. As the TM formed at Station A, the Kolmogorov lengths reduced by 50% to coincide with maximum floc sizes of ~500 μm. Conversely, at times of low turbulent activity during spring tides, maximum floc sizes were half of the Kolmogorov microscale eddies which were typically 600 μm. As the turbulence increased, the eddies reduced to 400-480 μm. These smaller eddy sizes stimulated floc growth up to MAX6 sizes ranging from 640-1100 μm. A further decrease in the eddy size down to 310-350 μm, created a significant level of de-flocculation, and restricted the MAX6 floc size to ~280-300 μm.

In summary, this suggests that during spring tides macroflocs continue to grow in response to the decreasing eddy size and the rising concentration, to the point where the largest aggregates are two to three times larger than the Kolmogorov microscale. These are very porous loosely structured aggregates, which display very low effective densities (typically < 50 kgm^{-3}), but settling velocities between 5-20 mms^{-1}. Then as a critical turbulent intensity is attained, growth is severely retarded, and the fragile macroflocs are rapidly broken-up into their stronger constituent microflocs. The microflocs tend to have a much greater spread in effective density (80-1000 kgm^{-3}), but their average settling rates (< 1 mms^{-1}) are significantly lower than those of the macroflocs. Throughout neap tidal conditions, the macroflocs in the near bed region very rarely grew beyond the ambient microscale eddy size.

6.2.3.a Comparison of floc measuring techniques

An important factor to consider when comparing floc data from different sources is to examine both the reliability and repeatability of the techniques employed to measure the floc characteristics. This point was highlighted by a comparison of the mean floc size determined by INSSEV and the PML Lasentec P100 during the September COSINUS experiment. Figure 6.1.A shows the mean floc time series for the neap ebb deployment on the 15th September, whilst 6.1.B shows the comparative mean floc sizes for the same time period, as determined by profiles with the Lasentec. Before the appearance of the TM on the 15th September, when the neap concentrations fell below 25 mgl^{-1}, the Lasentec mean sizes were up to 80% smaller. This was probably a consequence of the 20 μm lower size limit of INSSEV detection biasing the mean towards larger sizes, whereas the Lasentec mean floc size was determined from the volume-weighted count of floc numbers with a lower limit of 2 μm.

For the higher concentrations of the flood deployment from the spring conditions of the 22nd September, INSSEV (Figure 6.2.A) showed that the mean floc size within the TM did not exceed 350 μm. However the Lasentec data (Figure 6.2.B) suggested that a mean floc size approaching 600 μm was present. This was an over-estimation of 71%. The mean INSSEV floc sizes were of a similar order to those obtained by the HR video camera at Station B, after adjusting for advective transport (Feates et al., 1999). The higher mean floc size reported by the Lasentec data was most likey a characteristic of its measurement technique. Previous laboratory studies have shown that the Lasentec views high concentrations of very small flocs in close viscinity (such as those present in suspension during Tamar spring tides), as a single very large aggregate, hence increasing the mean floc size.

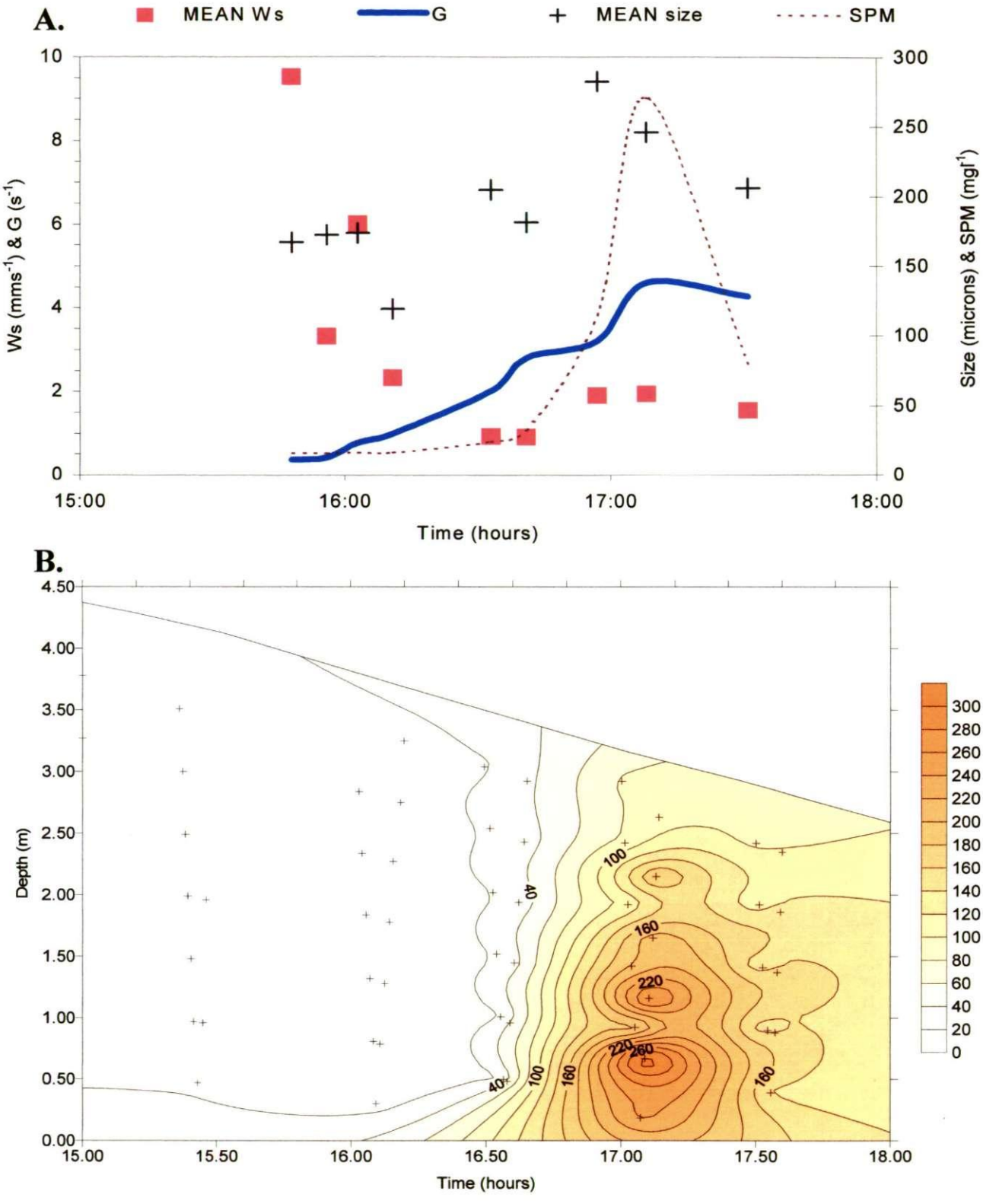

Figure 6.1 *A*) The variation of settling velocity, mean floc size, the turbulence parameter G, and suspended particulate matter concentration in the turbidity maximum during the ebb on a neap tide on the 15th September 1998 at Station A. ***B***) Contour plot of mean floc size obtained with the Lasentec system over the same period as Figure 6.1.A. The crosses show the time and height of the measurements.

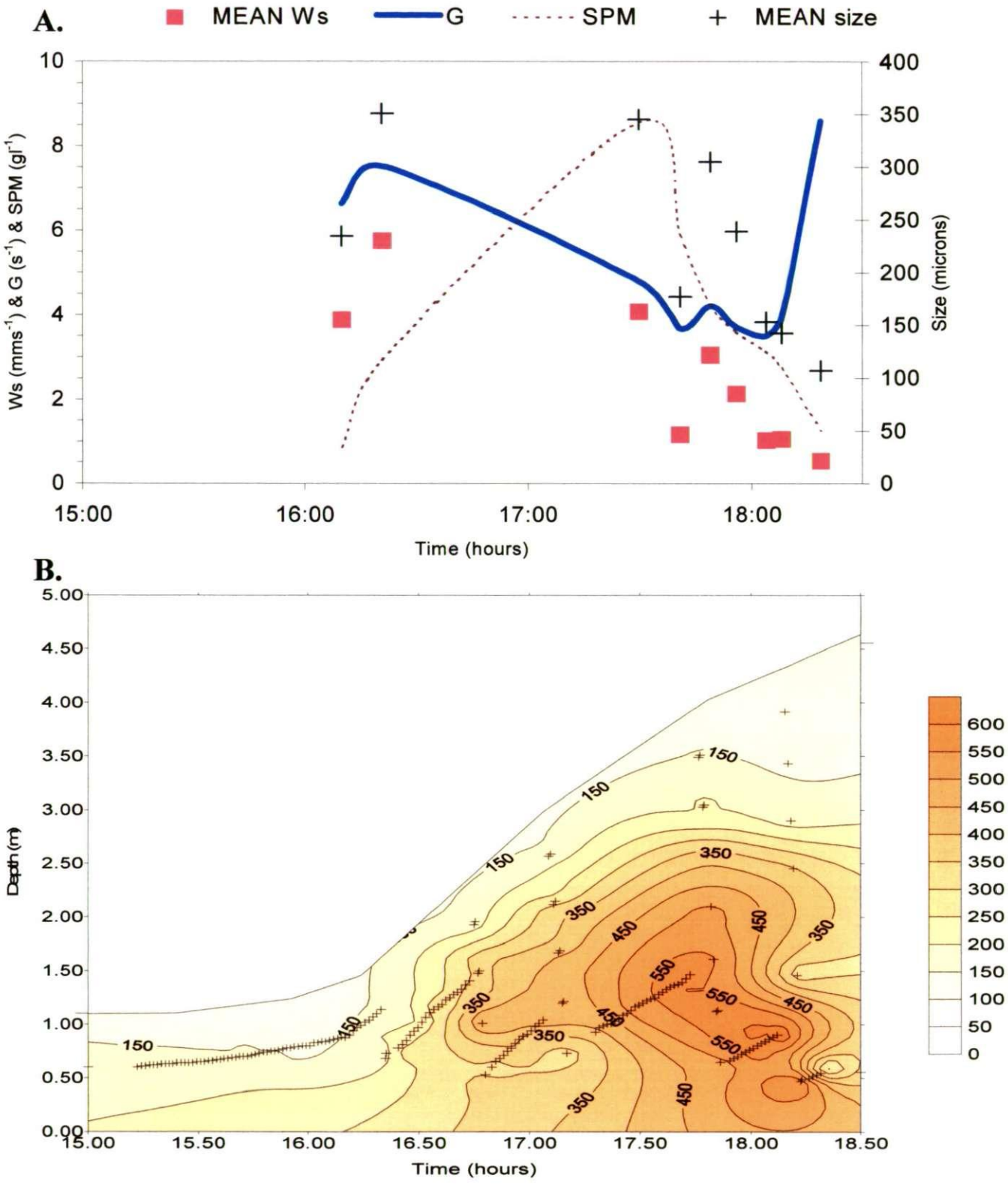

Figure 6.2 *A*) The variation of settling velocity, mean floc size, the turbulence parameter G, and suspended particulate matter concentration in the turbidity maximum during the flood on a spring tide on the 22nd September 1998 at Station A. ***B***) Contour plot of mean floc size obtained with the Lasentec system over the same period as Figure 6.2.A. The crosses show the time and height of the measurements.

Although laser particle sizers are non-intrusive instruments, these examples show how size measurement errors can easily occur. Couple this with a poor estimation of the floc density, and this could easily lead to a complete misinterpretation of floc responses to varying turbulence and concentration. Additionally, Partec type instruments have no way of checking the quality of the data, as only one floc component (i.e. size) is measured. The ability to physically visualise the flocs settling is a key advantage of the INSSEV system. It allows the effective density of each aggregate to be computed, and hence permits the floc spectra to be accurately referenced to the ambient SPM concentration. The Qc values (refer to section 4.1.2 for the determination of these values) provide an insight into how representative a floc sample is of the ambient population, although it must be noted that it assumes that the filtered SPM concentration (collected simultaneously with the INSSEV floc sample) is the correct SPM value and hence has the same total of particulate mass. Consequently, descriptive floc models based on INSSEV data are considered more reliable, because of the high quality and consistency of the floc data collected.

It must be stated that even though INSSEV provides a number of self-checks (e.g. floc backtracking analysis and the Qc values) on the floc data, errors from inter-comparisons can occur. Primarily, it is assumed that the volume of water captured within the INSSEV decelerator chamber contains an identical floc spectral composition to that observed by the other instrument, such as the Lasentec. Other potential sources of error regarding the INSSEV instrument data are: it is assumed that no further flocculation occurs within the sampling apparatus; misalignment of the instrument can create vortex shedding at the decelerator chamber entrance and subsequently break-up large fragile flocs by artificial means; also the failure to maintain a correct level of positive saline balance within the settling chamber will produce unwanted turbulent mixing in the stilling column. It must also be stated that the manual interrogation of the floc video images can effect the accuracy of the INSSEV results if observed by an inexperienced operator.

6.3 Gironde estuary experiment - Floc observations

The floc populations observed during neap conditions in the Gironde estuary displayed a number of different patterns from those sampled at neap tides in the Tamar estuary. The most significant difference was in the distribution of the particulate matter throughout the size spectra. At peak concentration the macroflocs only represented 38-52% of the ambient SPM with SPM ratios of 0.6-1.1, compared to 65-75% and ratios of 1.8-2 for the Tamar flocs. This difference could be attributed to a differences in the mineralogical composition

and types of organic coatings, but also the G-values in the Le Verdon region of the Gironde estuary were generally 2 s^{-1} greater (than those at Station A on the Tamar) during times of maximum entrainment. This more turbulent environment appears to be less conducive for macrofloc production. This was reflected in the mean floc size which only ranged between 83-114 μm throughout the entire sampling duration.

The utilisation of sample mean floc characteristics is quite common in estuarine oceanographic surveys. If these techniques were employed to analyse the Gironde data collected during SWAMGIR1, it would have concluded that the floc communities demonstrated floc characteristics of effective densities up to 180 kgm^{-3}, and mean settling velocities of 0.4-0.6 mms^{-1}. However the few macroflocs that were present within each sample had settling velocities of 1.8-2.6 mms^{-1}, which gave this larger size fraction between 60-80% of the MSF at peak concentrations; this was very similar to the Tamar flocs. This translated into MSF ratios between 1.5-4. So it can be concluded that there is a high margin of error when characterising floc populations solely by their sample mean values, when compared to the use of a macrofloc:microfloc representation. It also suggests that the MSF distribution across the macrofloc:microfloc sub-groups of a floc time series is a more reliable descriptive and inter-comparative parameter than apportioning either the settling velocity or the dry floc mass per sub-group.

At periods of high entrainment, the MAX6 flocs were approximately 50-60 μm less than the Kolmogorov eddy sizes which were ~ 400 μm. These flocs were quite fragile and prone to disaggregation with increased shear stress, as the effective density of 41 kgm^{-3} indicates. Around slack high water the eddy sizes rose to 860 μm , which encouraged the macroflocs to settle to the bed, leaving only small slow settling flocs in suspension, and hence this accounted for the MAX6 size reduction to approximately 170 μm. Most estuarine flocs tend to exist in a state of quasi-equilibrium, continually passing through zones of high and low turbulent shear. These aggregates would have retained their history from such events, and their higher effective density of ~140 kgm^{-3} (3.5 times denser than the larger MAX6 flocs sampled earlier in the flood tide) suggests that they may have been advected through a zone of high turbulence prior to reaching the near bed region at more quiescent conditions; i.e. as the result of a settling lag occurring during deposition in the deeper Gironde waters.

6.4 LEGI laboratory studies

The principle range of turbulent shear used for the grid tank experiments was 5.7 to 16.6 s^{-1}. Van Leussen (1994) stated that an rms of the gradient in turbulent velocity fluctuations (G) of 0.1 to 1.0 s^{-1} was representative of slack water, whilst the region between 1.0 and 10 s^{-1} tended to contribute more to the aggregation growth. Beyond 10 s^{-1} was indicative of highly turbulent conditions which could be expected to occur in the bottom boundary layer during periods of high current velocities.

There was a great deal of similarity in the patterns displayed by the LEGI macroflocs and those observed in-situ. For the Tamar mud, the 200 mgl^{-1} base concentration was representative of the advection of the main body of the TM through the upper Tamar estuary during neap conditions. At the highest shear (16.6 s^{-1}) the MAX6 floc size was 210 μm, which was slightly less than the Kolmogorov eddy size of 251 μm. An SPM ratio of 1.2 signified a fairly even division of floc dry mass between the macroflocs and microflocs. The high velocity particle collisions resulted in both floc groups having significantly low settling velocities of 0.6 mms^{-1}. Those experiments with G ~7.7 s^{-1} was a closer reflection of in-situ turbulent shear stress in the upper Tamar, at times of maximum entrainment from the bed. For this situation improved coagulation due to the less aggressive inter-particulate impacts raised the macrofloc settling velocity to 1.8 mms^{-1}, and the SPM ratio had risen to 1.8 as a result of floc growth from the same base concentration. This translated into the macroflocs constituting 64% of floc mass, and 80% of the MSF. This is a very similar distribution displayed by Tamar estuary neap tide flocs.

In contrast, the same base concentration of 200 mgl^{-1}, the natural Gironde mud displayed significantly faster settling macroflocs at each shear stress increment, but a MAX6 floc size of the same order as the Tamar mud flocs. Also, the SPM distribution showed the macroflocs only constituting 20-30% of the particulate mass. However, the fast settling rate transformed the low macrofloc mass into 62% of the MSF. These were features demonstrated by the in-situ Gironde estuary flocs from the SWAMGIR1 experiment, and is probably a characteristic of the Gironde sediment composition.

At the higher ambient concentrations equivalent to the Tamar mud CBS layer (see Figure 5.47), the maximum floc diameter was approximately double the corresponding eddy size (400-430 μm). The shear of 6.5 s^{-1} combined with an SPM of 8.2 gl^{-1} effectively stimulated aggregate formation to such a high degree, that only 3% of the floc mass was in the

microfloc range. Further more, the macroflocs had a settling velocity of 5.75 mms^{-1}, which meant that the ratio of MSF between the macroflocs and microflocs was 221:1. When comparing this to the in-situ Tamar estuary CBS flocs, apart from a 2-3% decrease in the dry floc mass division (with respect to the in-situ macroflocs), the macrofloc settling rates and contribution to the MSF are virtually identical. This demonstrates that the grid tank and settling column experimental set-up simulated in-situ conditions under laboratory conditions with a high level of accuracy and repeatability.

The Gironde mud with all the organic components removed, showed a consistent lack of floc growth, at all concentration and shear stress levels. Very few aggregates were observed exceeding the pre-sieving mesh diameter of 100 μm. This must have been the result of removing the polysaccharide-type substances, which are an important feature of natural muds. The salinity of 16.4 is unlikely to have contributed to flocculation. This illustrates how flocculation is as much reliant on biological processes, as it is from hydrodynamical forces.

The distinct advantage of a laboratory study over the field experiments is that it allows certain physical aspects to be controlled so that it is possible to isolate various pertinent components or processes. An important component with regards to this study was the residence time of the flocs in-situ. In order to quantify flocculation within a required level of accuracy, it must be determined whether the flocs are in dynamic equilibrium with their surrounding environment. Turbulent shear initiates floc growth by bringing the constituent particles together. Conversely, as the TSS continues to rise, it can break apart the fragile macroflocs formed under the lower imposed shear stresses. There is theoretically a finite point at which the break-up and growth potentials equate.

Winterwerp (1999) claims that the floc size is inversely proportional to the turbulent shear when the residence time of the flocs in the turbulent shear field is unlimited. This hypothesis is shown as a dotted line on Figure 6.3 which illustrates the theoretical conceptual flocculation model of Winterwerp (1999), where flocs are treated as self-similar fractal entities. The solid lines on Figure 6.3 indicates how flocs would respond to increasing turbulent shear stresses within an estuarine water column where the tidal cycle time scales do not create an unlimited residence time for the flocs.

The LEGI oscillating grid was employed to shear the flocs in suspension for a duration 10-20 times longer than that of the predicted F_T. This would allow the assessment of whether

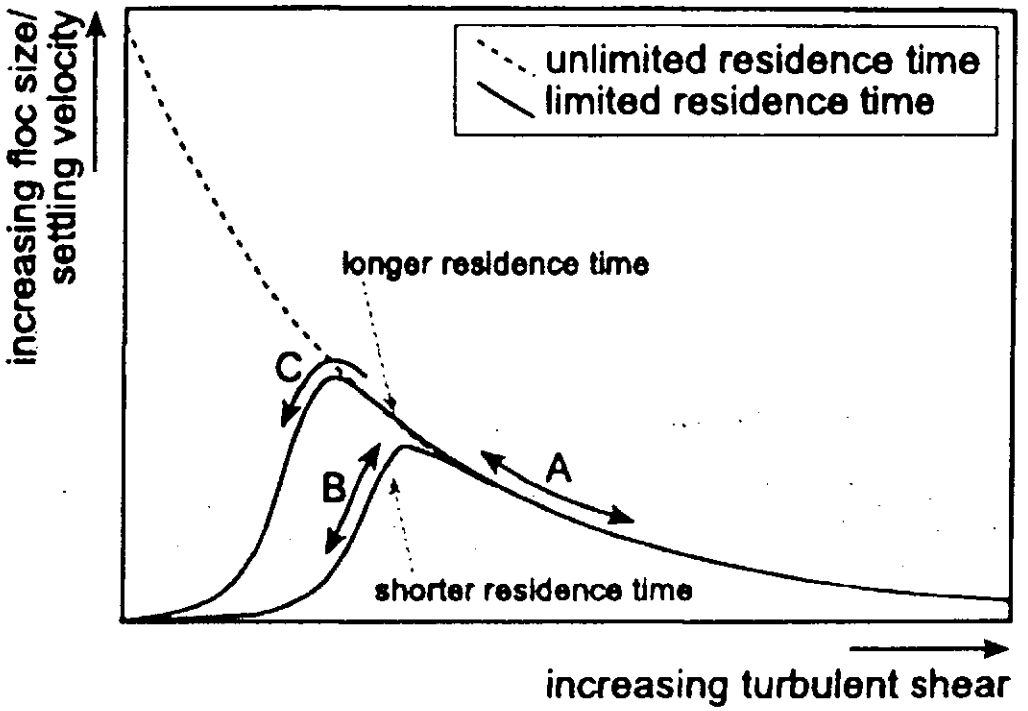

Figure 6.3 Floc size and settling velocity as a function of turbulent shear (After Winterwerp, 1999). The ***B*** arrow indicates a rise in D or Ws with a corresponding rise in TSS. A progressive decrease in D or Ws due to a continuing increase in TSS is illustrated by arrow ***A***. The attainment of a higher D or Ws due the longer resistance time of the suspended particulates in a slowly decreasing TSS field is shown by arrow ***C***.

additional floc growth or break-up had occurred when comparing the LEGI floc spectra with those obtained from similar ambient conditions in-situ. The LEGI results showed a close correlation between the in-situ macrofloc settling velocities produced in shear ranging from 5.7-9.3 s^{-1}. This indicates that for those conditions an equilibrium between floc growth and break-up had been established both in-situ and in the laboratory.

However the findings are partially inconclusive, as the lower region of TSS used for the LEGI experiments, was found to correspond with the most flocculation-productive shear range encountered in-situ. It may be inferred that at the lower shear rates experienced in-situ, the flocs may not have reached the potential of their floc growth. However, the fact that the flocs were sampled close to the bed (where the majority of the TSS is generated due to flow drag) means that the highest shear stresses would always be encountered in that region of the water column at most points in a tidal cycle. Therefore, even though the flocs settling through the water column would retain their structural history, on reaching the near bed region they would either respond to the shear stress imposed at that depth, or deposit to the bed. However the latter generally only occurs at times of very low near bed turbulence, i.e. slack water. This agrees with the findings of Mehta and Partheniades (1975) who stated that

the turbulent shear close to the bed was the primary control on the flocs. The flocculation time aspect is further examined in section 6.6.1.

6.5 UOP laboratory studies

The laboratory experiments conducted at the UOP, examined low ambient concentrations (< 200 mgl^{-1}), over a turbulent shear stress range of 0.1-0.6 Nm^{-2}. The experimental set-up of the shallow water column within the annular flume channel (see Plate 3.13), together with the induced shear range used, had a net result of producing flocculation solely by turbulent shear, with a negligible influence of differential settling; this probably accounted for the relatively small sizes of the macroflocs sampled. It is for these reasons, that the maximum floc sizes are probably less than the corresponding Kolmogorov microscale eddy size. Nevertheless, the turbulent shear stress values used for the experimental work showed a good correspondence with floc size according to the relationship of Hunt (1986) i.e. $D_x \propto G^{-m}$, where the exponent m varied between 0.47 and 1.29 for the 80 and 200 mg l^{-1} concentrations, respectively. The flocs measured at the zero shear level are only indicative of those conditions, as a different experimental method had to be used to produce them. The consistently lower size of the aggregates (than those measured at the corresponding 0.1 Nm^{-2} rate) can be attributed to a limitation on eddy size by the flume depth. This significantly lowered the collision frequency rate, and the probability that equilibrium floc sizes may not have been achieved.

Figures 6.4 and 6.5 show log-linear plots which illustrate the respective variations in MAX4Ws (the arithmetic mean parameters calculated from the four fastest settling flocs in each sample) floc size and settling velocity, plotted against shear stress. Power regression lines of the form floc parameter (D_X, W_S or ρ_e) = f $(TSS)^h$, have been plotted through the data points. However, the zero shear points were not included in the regression analysis as they were taken under different experimental conditions, and are only presented as an indication of those conditions. A summary of each regression equation coefficients (h and f), together with their R^2 values, is given in Appendix I (the reprint of Manning and Dyer, 1999). The graphs show that at the lowest shear stress (0.1 Nm^{-2}) there was a distinctive near-linear increase in floc size with increasing SPM concentration. Correspondingly, the settling velocities also rose with the presence of higher ambient particle concentrations. The mean effective density of the 200 mgl^{-1} sample at 0.1 Nm^{-2} was 37 kgm^{-3}, which indicates these flocs are fragile in nature, and subject to potential disaggregation as they pass through higher shear fields. The formation of aggregates of this type, are primarily as a result of the

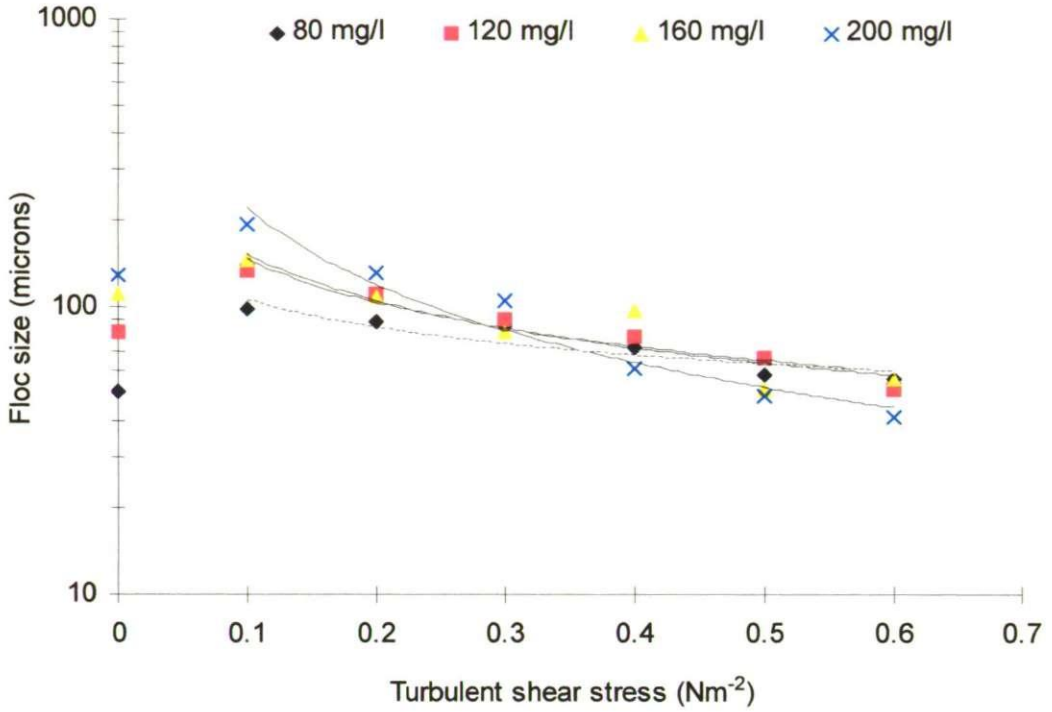

Figure 6.4 Variations in MAX4Ws floc size over the UOP annular flume generated experimental turbulent shear stress range, with SPM concentration as a parameter. Power regression lines have been added (from Manning and Dyer, 1999).

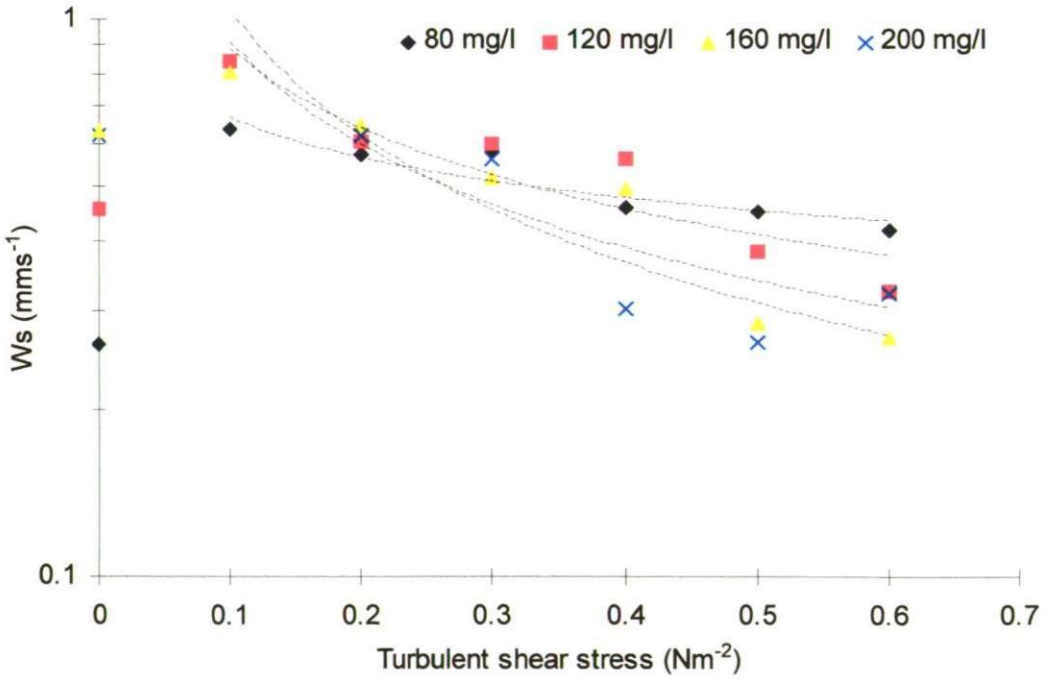

Figure 6.5 Variations in MAX4Ws floc settling velocity over the UOP annular flume generated experimental turbulent shear stress range, with SPM concentration as a parameter. Power regression lines have been added (from Manning and Dyer, 1999).

abundance of particulates present within the water column tending to dominate the flocculation process, with the turbulence generally producing constructive particle collisions. The effect diminishes with the increase in shear stress when the turbulence disruption reduces the floc size and increases the density. This process could be seen on the monitor screen during data processing; at high shear rates a population dominated by microflocs could be recognised. As the turbulent shear decreased, the percentage of small microflocs was seen to drop as they were involved in flocculation.

An important feature highlighted from the data was the cross-over points on the regression lines between shear stresses of about 0.25-0.4 Nm^{-2}. These are conjectured to mark the shear magnitudes where the effect of the increasing turbulent shear on the floc size and settling velocity, together with the higher concentrations, causes disruption rather than enhancing the flocculation process. Thus the higher concentrations result in larger flocs for low shear stresses and the lowest SPM concentration produced the larger mean floc size for the higher shear stress. A similar pattern was observed for the settling velocities. These cross-over points were not directly observed for the field data, primarily because in a natural environment the SPM concentration was constantly varying in response to the flow generated turbulent shear stress. However, both the in-situ and the LEGI results indicate that the region between 0.3-0.45 Nm^{-2} signifies a point whereby if the shear was increased, disruption to the macroflocs would occur and hence their settling velocities would progressively reduce.

Extrapolation from the regression lines of Figure 6.4 indicates that for a 200 mgl^{-1} concentration a 2.3 Nm^{-2} shear stress would be required to restrict the maximum floc size to 40 μm. However shear stresses of this magnitude would not be expected to exist within a typical estuarine water column, so therefore both an increase in particulate concentration together with shear would be required to produce the smaller maximum floc sizes.

6.6 Development of a conceptual flocculation model

There have been many approaches to mathematically describing the flocculation process and a selection of these was reviewed in section 2.5. However, from the perspective of this study, it was more practicable to generate statistical relationships from the experimental data, as opposed to trying to develop an entirely theoretical model. A theoretical approach would allow the development of depositional algorithms which could easily be incorporated into numerical simulation models without the addition of a high volume of complex coding (i.e.

which would increase both the computer model run times and cost). As stated earlier, the 160 μm division has been identified as a key separation point between the two different floc types. Consequently, to identify the significance of various floc enhancement and retardation factors, a statistical regression analysis of the macrofloc and microfloc parameters was undertaken for each of the data sets.

6.6.1 Multiple regression analysis

Previous studies have shown that flocculation seems to be reliant on the physical processes of inter-particle collision and the level of adhesion demonstrated by the constituent particles. Results presented earlier in this thesis have shown that these aggregational processes are primarily controlled by the turbulent shear stress, and the abundance of natural particles in suspension. The combination of these processes either stimulate floc growth, or lead to disaggregation. It was for this reason that the main statistical analysis employed was of a multiple parametric regression type. The statistical package *Minitab for Windows - version 10.1* was used for all the regression analysis, with a default statistical confidence level of 95%.

The regression was conducted only for the macrofloc and microflocs parameters, determined from the in-situ INSSEV and LEGI laboratory video floc data; summary tables of the multiple regression data points can be found in Appendices II and III, respectively. Different combinations of independent and dependant variable were assessed, so as to reveal where the strongest inter-correlations existed. Many previous examinations of flocculation have produced interrelative equations, but which were of no practical application. So the decision as to which characteristics to choose for the statistical analysis was based on their practical applicability to be integrated into mathematical sediment transport simulations.

With this objective in mind, both the results and logic suggested that the following floc characteristics were considered both the most important and relevant: Ws_{macro}, Ws_{micro}, $SPM\%_{macro}$, $SPM\%_{micro}$, total SPM and TSS, or G. The division of particulate matter within a floc population, and the relative rates at which they settle, are the key variables which govern the deposition of the matter in suspension; i.e. the mass settling flux, and these are represented by the first five terms. Also the physical descriptors of SPM concentration, and a turbulence parameter represented the basic factors which govern the collision rate and subsequent degree of flocculation of particles in estuarine waters. Numerous existing aggregational algorithms focus on the floc size as an important variable included as a single

mean value, whereas the use of a two size band approach includes the effect of aggregate size variations. Salinity was not regarded as a prime instigator or controller of flocculation as significant floc variations occurred where the water was predominantly fresh. Also, the organic matter descriptors were omitted from the quantitative analysis, as there were only a limited number of bio-chemical samples analysed. A more detailed study of extra-cellular polymetric substance (EPS) levels, together with the respective flocculation characteristics, would provide a useful insight into the quantification of these natural biological "glues" and their degrees of influence would form a valuable area of future work.

Floc samples which consisted predominantly of high density, single, non-cohesive particles, such as the hornblende and tourmaline crystals, were excluded from the analysis. These values would unfairly bias the regressions. The omission of these samples was further justified as these high density particles were only encountered at times of very low concentration, such as the period just after high water, when the MSF was not significantly high.

A key assumption used in the analysis of the various matrices of experimental data was that there was no inclusion of a flocculation time (F_T) component. This aspect has been discussed for the controlled laboratory studies in section 3.4.2, where it was possible to allow the flocs to obtain equilibrium with the turbulent flow, and some inferences regarding the in-situ floc data were made for turbulent shear values greater than 5.7 s^{-1}. In order to assess the various combinations of SPM and TSS for the field results, the F_T was considered in terms of the mean TSS values which were generated from a 3 minute 47 second duration file (i.e. 4096 data rows at 18 Hz). Referring again to Figure 3.6 and using equation 3.5, this time period would be a valid F_T for a combined G value of 1 s^{-1} and SPM concentration of approximately 65 mgl^{-1} (i.e. the lowest collision rate attainable) to achieve flocculation equilibrium. For G and SPM concentrations above these values, floc equilibrium would theoretically occur within the duration of a file.

From examination of the combinations of G and SPM from the entire data matrix, only 9% of the data points had F_T exceeding the TSS file duration. This 9% represented flocs which were measured at quiescent periods during neap tides when most of the larger macroflocs had probably settled to the bed. This implies that the majority of the neap flocs and all of those observed during spring tides had attained equilibrium with the ambient conditions. Thus, even though a number of the macroflocs present in the TM during spring tides may

have been brought in by advection, this shows that these low density aggregates sampled by INSSEV would have responded very quickly to the shear stresses imposed in the near bed region as the F_T was very short. If any of the 9% cluster was seen to register as an "unusual observation" from the regression summary given by the statistical software, it was rejected. Therefore, the F_T assumption employed was justified for all the in- situ data used for the regression analysis. Many combinations of independent variables were considered, but only the simplest inter-relationships, with correspondingly high R^2 fit values, will be presented as algorithms. The UOP flume experiment data was omitted from this stage of the analysis as only the largest flocs were examined.

For consistency, the following units were used for each parameter included in the multiple regression analysis: TSS = Nm^{-2}, G = s^{-1}, SPM = gl^{-1}, Ws = mms^{-1}, and D (floc size) = μm.

6.6.1.a Macrofloc settling velocity

Macroflocs (> 160 μm) are recognised as the most important sub-group of flocs, as their fast settling velocities tend to have the most influence on the mass settling flux. However, their fragile, low density structure makes them very sensitive to physical disruption during sampling. This lack of high quality floc measurements has meant that very few of the earlier analytical studies have been conducted on the settling rates of macroflocs over a wide range of ambient conditions; most tended to emphasise the smaller microflocs. This illustrates the importance of the findings from this sub-section.

The data was divided into five independent data sets. Figure 6.6.A shows the results from the first multiple regression which examined the Tamar estuary neap tides ($_{TN}$) at Station A. This comprised of 55 observations obtained from both the August and September 1998 experiments. The range of near bed turbulent shear stress (0.04-0.6 Nm^{-2}) entrained sediment concentrations ranging from 10-588 mgl^{-1} into the water column, predominantly by bed erosion. The macrofloc settling velocity showed a stronger dependence on turbulent shear than that of concentration by a ratio of 1.4:1. The form of the regression equation (6.1) which best represented the data was plotted for a concentration of 200 mgl^{-1} on Figure 6.6.A.

$$Ws_{macroTN} = 0.614 + 1.73\ SPM + 8.2\ TSS - 12.7\ TSS^2 \qquad R^2 = 0.733 \qquad \textbf{(6.1)}$$

This representation indicates a settling velocity of ~ 1 mms^{-1} under quiescent conditions (SPM < 0.1 gl^{-1}), which rises to a peak settling rate of 2.27 mms^{-1} at a turbulent shear stress of 0.3 Nm^{-2}. The further increase in turbulent stirring beyond 0.3 Nm^{-2} inhibited the formation of fast settling macroflocs, by both increasing the frequency of aggregate fracture

and surface stripping of constituent particles. The settling velocity reduced to 1.3 mms^{-1} at a TSS of 0.7 Nm^{-2}. The R^2 value of 0.733 suggests that this is a fair reflection of the natural data. Figure 6.6.B shows the data re-plotted to identify the data points pertinent to the neap tides of experiment 2 (August 1998) and experiment 3 (September 1998) and shows that the macroflocs observed during the two neap tide experiments demonstrated consistently similar Ws_{macro} rates throughout the ambient turbulent shear stress range.

Error bars showed that the experimentally calculated $Ws_{macroTN}$ values, from which the multiple regression equation 6.1 was based, had potential errors ranging between $\pm$0.04-0.011 mms^{-1} (see Appendix II for a complete listing of individual error bar values).

The second regression analysis was conducted on June and September 1998 Tamar spring tides ($_{TS}$) which provided 36 observations. The expression (6.2) relating the Ws_{macro} dependent variable was valid for SPM concentrations of 487-8560 mgl^{-1} and TSS between 0.14-0.7 Nm^{-2}.

$$Ws_{macroTS} = 0.142 + 0.457\ SPM + 12.3\ TSS - 16\ TSS^2 \qquad R^2 = 0.914 \qquad \textbf{(6.2)}$$

The high mass of particulate matter which advected through Station A during spring tides had a very significant influence on the macrofloc formation and consequently their settling velocities. Regression analysis showed that simply relating Ws_{macro} to the ambient SPM, as is commonly postulated in the literature, resulted in an R^2 of 0.58. This lower fit value would translate into a much larger predictive error for Ws_{macro}. However, the inclusion of turbulence parameters raised the R^2 to 0.914; an increase of 0.334. Although this translates into a dependence ratio of approximately 1.7:1 in favour of the ambient SPM, the regression indicates that variations in turbulent mixing still have a significant effect on the settling velocity of a macrofloc population during the high concentrations of spring tides.

The 36 spring tide Ws_{macro} data points have been plotted against turbulent shear stress in Figure 6.7.A, together with trend lines calculated from equation 6.2. The regression curve shows a similar shape to that of the neap tides. For a concentration of 4 gl^{-1}, the settling velocity gradually increased to a peak of 4.3 mms^{-1} at 0.38 Nm^{-2}. At this point the collision frequency was at its greatest, and flocculation stimulated the growth of a fast settling cluster of flocs over 160 μm in size. Thereafter, the macrofloc settling velocity fell as the turbulence continued to rise, and on attaining a TSS of 0.7 Nm^{-2}, it indicated a 63% decrease in Ws_{macro}. This is the effect of the continued increase in shear within this high concentration creating more destructive collisions between the abundant macroflocs, as opposed to causing

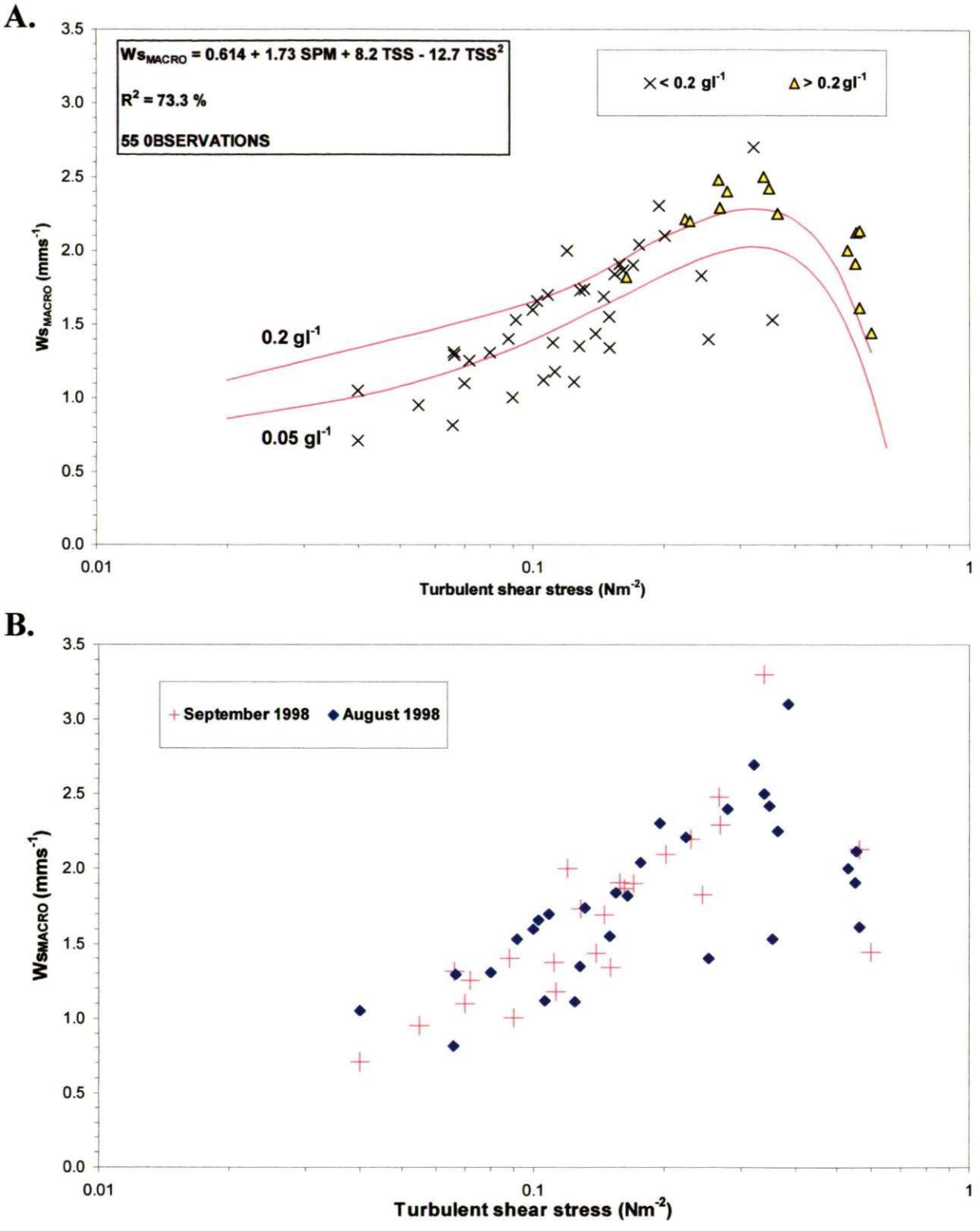

Figure 6.6 *A*) Macrofloc settling velocity plotted against turbulent shear stress for Tamar estuary observations during neap tide conditions (experiments 2 and 3). Lines illustrating constant SPM concentrations, using equation 6.1, are added. ***B***) Shows the data from Figure 6.6.A re-plotted to identify the data points pertinent to the neap tides of experiment 2 (August 1998) and experiment 3 (September 1998).

coagulation which promotes the floc to a higher order of aggregation. The decrease in settling velocity would therefore be attributed to a general reduction in the floc size range which comprise the macrofloc sub-grouping.

Now if the regression equation for neap tides (6.1) was used to predict spring tide conditions, it would imply a maximum Ws_{macro} of 8.85 mms^{-1} at an SPM of 4 gl^{-1}. This is a settling velocity over-estimate of 106% from equation 6.2, and stresses the danger of extrapolating beyond the physical limits of an empirical algorithm. This also illustrates that it is not a purely linear relationship between increasing concentration and the rising macrofloc settling velocity.

Statistical analysis highlighted that the $Ws_{macroTS}$ values employed to produce equation 6.2 produced errors of $\pm$0.13-0.18 mms^{-1} for SPM concentrations of 2-4 gl^{-1}; the error bars were seen to increase to $\pm$0.2-0.25 mms^{-1} for particulate levels above 4 gl^{-1} (see Appendix II for a complete listing of individual error bar values).

Again, as for the Tamar neap tides, the Tamar spring tides data was re-plotted to distinguish between those data points obtained during June 1998 (experiment 1) and those from September 1998 (experiment 3). As with the neap tides, both spring tidal experiments were seen to generate SPM and TSS values of similar magnitudes, and hence both replicated consistently similar patterns in macrofloc settling velocity. This suggests that the macrofloc:microfloc analysis approach was identifying very significant floc inter-relationships. A conventional sample mean floc property approach would not have indicated these trends.

The 19 observed Ws_{macro} values from the neap tides SWAMGIR1 Gironde estuary experiment ($_{GN}$) were plotted against turbulent shear stress in Figure 6.8. The multi-regression analysis expression 6.3 had a highly significant R^2 of 0.833, but was only valid for concentrations less than 140 mgl^{-1}, and for TSS not exceeding 0.52 Nm^{-2}.

$$Ws_{macroGN} = 0.812 + 8.21\ SPM + 7.68\ TSS - 14.7\ TSS^2 \qquad R^2 = 0.833 \qquad \textbf{(6.3)}$$

The main difference between this equation and that of the Tamar neap tides (equation 6.1), was the high SPM coefficient. It was 4.7 times larger for the Gironde neap macroflocs. The results showed that most of the Gironde macroflocs were of a low effective density, so the higher coefficient value represented a greater particulate cohesion with the potential to

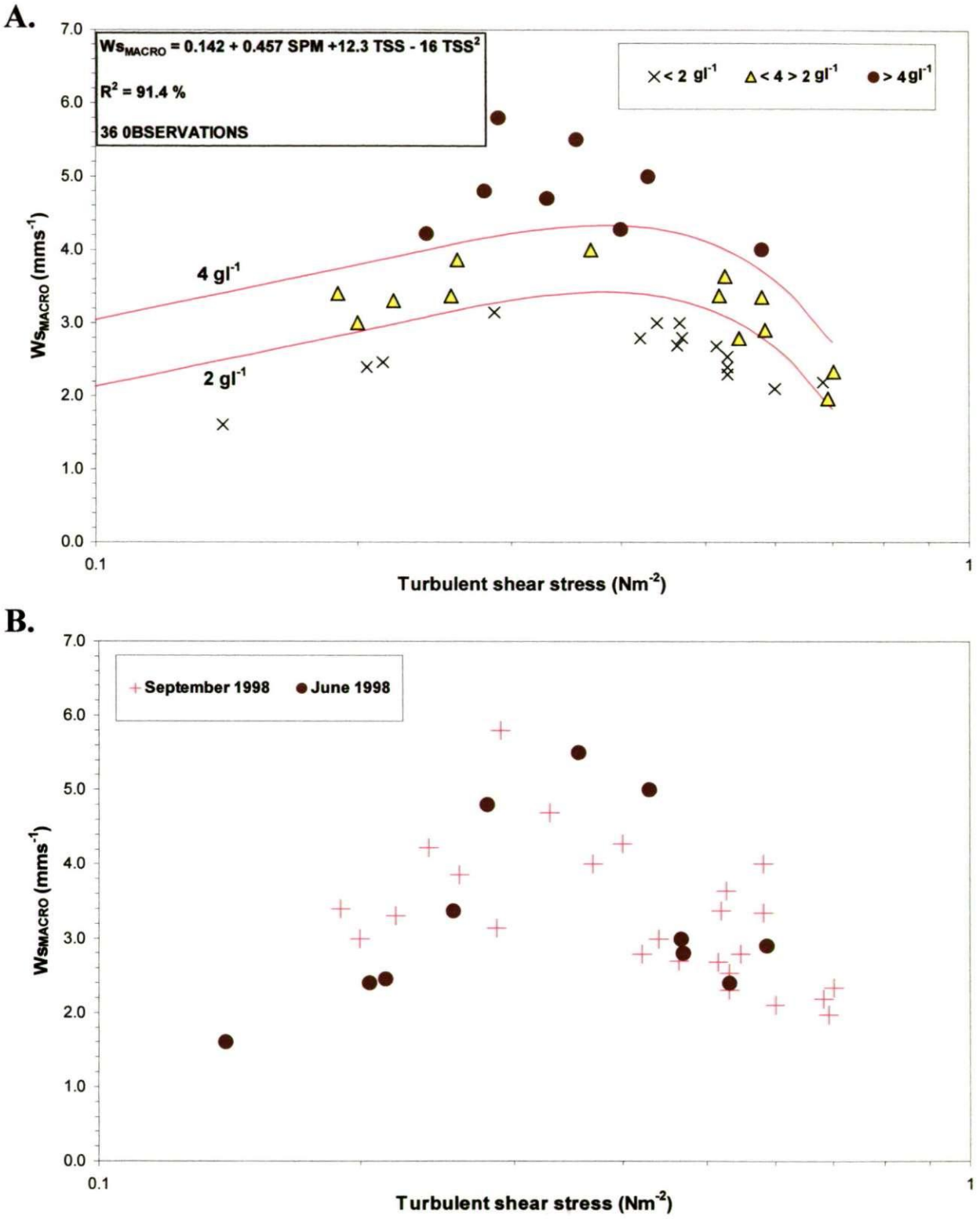

Figure 6.7 *A*) Macrofloc settling velocity plotted against turbulent shear stress for Tamar estuary observations during spring tide conditions (experiments 1 and 3). Lines illustrating constant SPM concentrations, using equation 6.2, are added. ***B***) Shows the data from Figure 6.7.A re-plotted to identify the data points pertinent to the spring tides of experiment 1 (June 1998) and experiment 3 (September 1998).

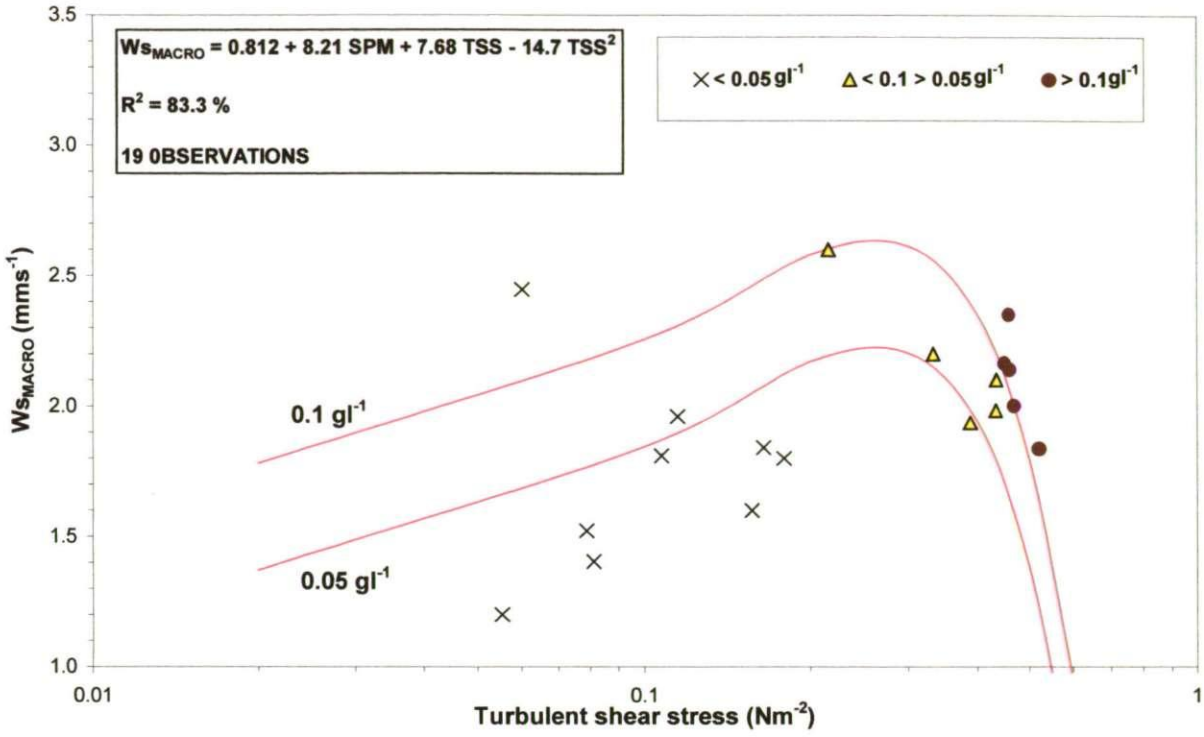

Figure 6.8 Macrofloc settling velocity plotted against turbulent shear stress for Gironde estuary (*SWAMGIR1*) observations during neap conditions on 23rd June 1999. Lines of constant SPM concentration are plotted.

flocculate into faster settling macroflocs at low concentrations. Consequently, a peak settling velocity was achieved at a TSS of only 0.25 Nm^{-2}; this was 0.05 Nm^{-2} lower than for the Tamar neap tides algorithm.

By comparison, a SPM concentration of 100 mgl^{-1} would produce a maximum Ws_{macro} of 2.1 mms^{-1} for the Tamar neap tides algorithm (6.1). Whereas the Gironde multi-regression (6.3) calculated a peak Ws_{macro} of 2.65 mms^{-1} for the same ambient concentration, which was an increase of 26%. However, the underlying Gironde bed substrate suggests a much higher critical erosion shear stress than the bed surface, and so particulate levels beyond 100 mgl^{-1} were only seen to occur when the near bed shear stress levels exceeded 0.4 Nm^{-2}. Thus, the macroflocs that were formed in this more turbulent environment became significantly smaller in size with increasing shear stress, as the break-up rate continued to out-weigh the floc growth and this accounted for the lower settling rates of the >100 mgl^{-1} macroflocs.

Figures 6.9 and 6.10 represent the Ws_{macro} values obtained from the LEGI experiments with natural Tamar estuary ($_{LT}$) and natural Gironde estuary ($_{LG}$) mud, respectively. The multiple regression of these data sets produced expressions 6.4 and 6.5, where the turbulence parameter G was used.

$$Ws_{macroLT} = 7.07 + 0.383\ SPM - 1.01\ G + 0.0376\ G^2 \qquad R^2 = 0.947 \qquad \textbf{(6.4)}$$

$$Ws_{macroLG} = 6.95 + 0.201\ SPM - 0.929\ G + 0.0351\ G^2 \qquad R^2 = 0.916 \qquad \textbf{(6.5)}$$

Both regression curves showed similar patterns with a reduction in macrofloc settling velocity up to 9 s^{-1}, after which the settling rates remained relatively constant to the shear stress experimental limit of 16.2 s^{-1}. In this higher shear region Tamar concentrations of < 1 gl^{-1} had macrofloc settling velocities restricted to under 1 mms^{-1}, whilst the slightly more cohesive Gironde mud caused the Ws_{macro} to level out at 1.4 mms^{-1}. Progressively raising the SPM concentrations up to 8 gl^{-1} in the more turbulent region, resulted in a restriction in the macrofloc size, as opposed to the complete disaggregation which occurs at the lower concentrations. The more particulates in suspension, the closer proximity of particles to each other. These macroflocs may display the characteristics of an unstable population where large flocs are formed, but quickly broken-up and then re-aggregated. However, the macroflocs would show a net higher settling velocity than that demonstrated by a lower concentration sample within a shear field of the same intensity. In summary, it seems that the smallest macroflocs the turbulence was capable of breaking down to, corresponded to Ws_{macro} ~1 mms^{-1}.

6.6.1.b Microflocs settling velocity

The smaller microflocs (<160 μm) are generally attributed to being the building blocks from which the macroflocs are composed. This was the basis of Krone's order of aggregation (Krone, 1963) and fractal theory. The results presented in Chapter 5, showed that the microfloc class of aggregates tended to display a much wider range in effective density and settling velocity than the larger flocs. It was, therefore, necessary to reveal the settling trends of the microflocs.

A multiple regression analysis of the Tamar neap and spring tide data with the Ws_{micro} as the dependent variable was undertaken. The best representations of the respective data sets were given by equations 6.6 and 6.7.

$$Ws_{microTN} = 0.237 + 3.4\ TSS - 3.67\ TSS^2 \qquad R^2 = 0.785 \qquad \textbf{(6.6)}$$

$$Ws_{microTS} = 0.052 + 5.72\ TSS - 7\ TSS^2 \qquad R^2 = 0.683 \qquad \textbf{(6.7)}$$

The most prominent difference between Ws_{macro} and Ws_{micro} to be revealed from these regressions was the negligible influence of SPM concentration variations on the latter. The high correlation with turbulent shear stress was indicated by an R^2 of 0.785 for equation 6.6, and is shown in Figure 6.11. The Ws_{micro} variations for Tamar spring tides are illustrated against turbulent shear stress in Figure 6.12. Both regression lines show Ws_{micro} of ~0.4

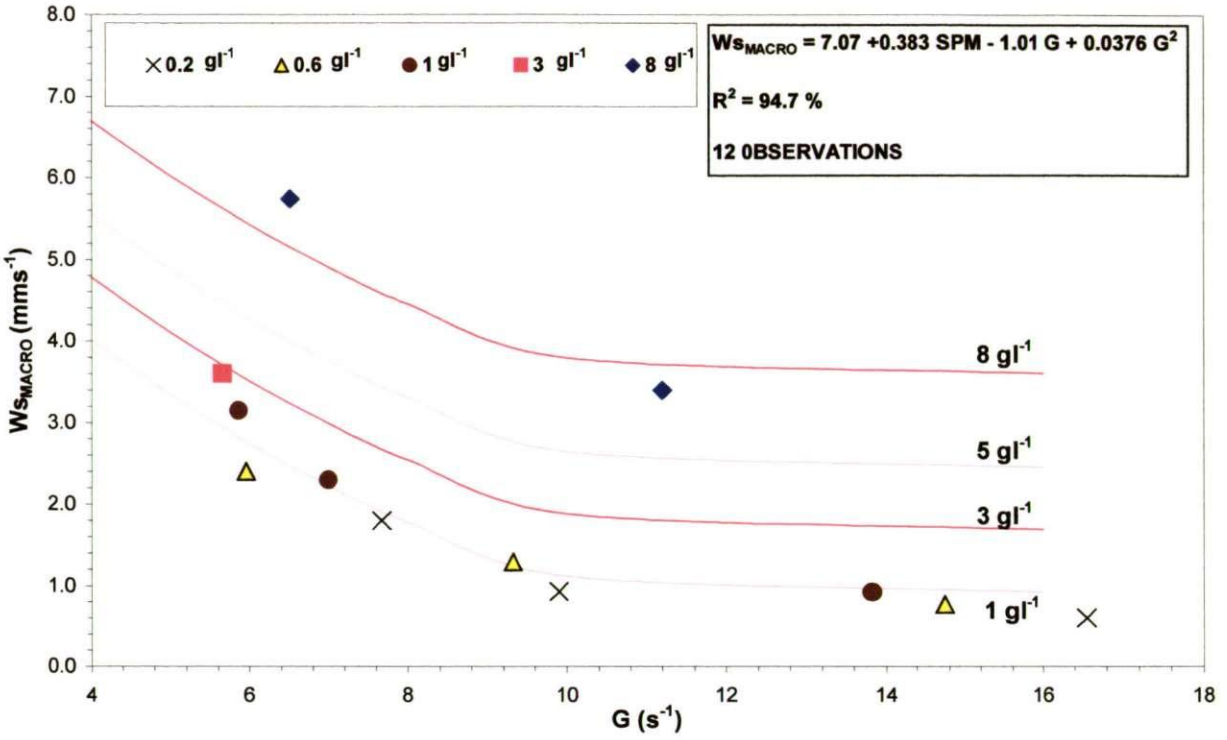

Figure 6.9 Macrofloc settling velocity plotted against turbulent shear stress for LEGI experiment 1 (natural Tamar estuary mud). Lines illustrating constant SPM concentrations, using regression equation 6.4, are added.

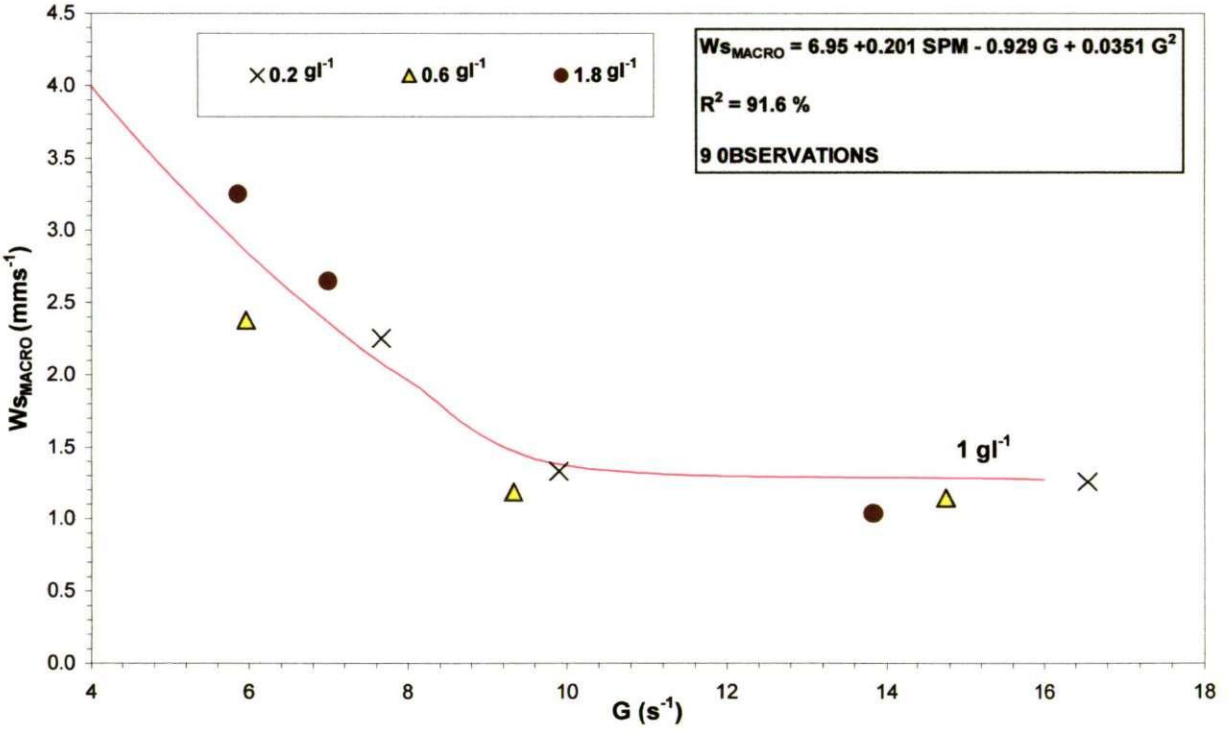

Figure 6.10 Macrofloc settling velocity plotted against turbulent shear stress for LEGI experiment 2 (natural Gironde estuary mud). A line illustrating a constant SPM concentration, using regression equation 6.5, is added.

mms^{-1} at a TSS of 0.1 Nm^{-2}. Like the macroflocs, the settling velocity continued to increase with turbulent shear, whereby a maximum of ~ 1 mms^{-1} was attained at 0.3-0.4 Nm^{-2}. This represents the growth of the larger fraction of microflocs from SB4 (120-160 μm), during the conditions which were most conducive for flocculation. The spring tides data showed a more rapid decrease in Ws_{micro} as the turbulent shear rose to 0.7 Nm^{-2}, whereby the settling rate returned to 0.4 mms^{-1}. This is a product of larger aggregates progressively rupturing into smaller slower settling low-order flocs, with the increasing turbulence.

The lower R^2 for spring tides was a result of the larger amount of scatter in the data points. The reason for the scatter is that during the low turbidity, neap tides, microflocs constitute 40-60% of the floc population, which very rarely exceed 100 flocs in total. Whereas, during spring tides, although the microflocs tend to only comprise between 5-20% of the dry floc mass, there could be as many as several hundred microflocs for an ambient concentration of 3 gl^{-1}. This would have an effect on the Ws_{micro} value computed, however the R^2 of 0.683 for equation 6.7 suggests that the scatter is relatively small and the equation is still deemed very representative of the data.

The Ws_{micro} values used in the multiple regressions to determine both the neap and spring tide equations (6.6 and 6.7), both produced error bars ranging from $\pm$0.02-0.0.6 mms^{-1} (see Appendix II for a complete listing of individual error bar values). These microfloc errors were much less than those for the macrofloc settling velocities presented earlier in this section.

6.6.1.c SPM ratio

To categorise the distribution of particulate matter throughout the macrofloc and microfloc sub-populations, the dimensionless SPM ratio is the best parameter. This was calculated by dividing the percentage of SPM_{macro} by the percentage of SPM_{micro}. Some qualitative results for the SPM ratio were discussed earlier in this chapter. It must be stressed that this type of computation is unique to instruments such as INSSEV, which measure the floc effective density (by simultaneous size and settling velocity observations) of each individual floc from a respective population. Without this type of measurement, it is not possible to apportion the SPM concentration accurately between the microfloc and macrofloc groups. Although this may seem restrictive from an instrumentational perspective, the remainder of this chapter will demonstrate how important a knowledge of the size spectral distribution of particulate matter is to accurate depositional modelling.

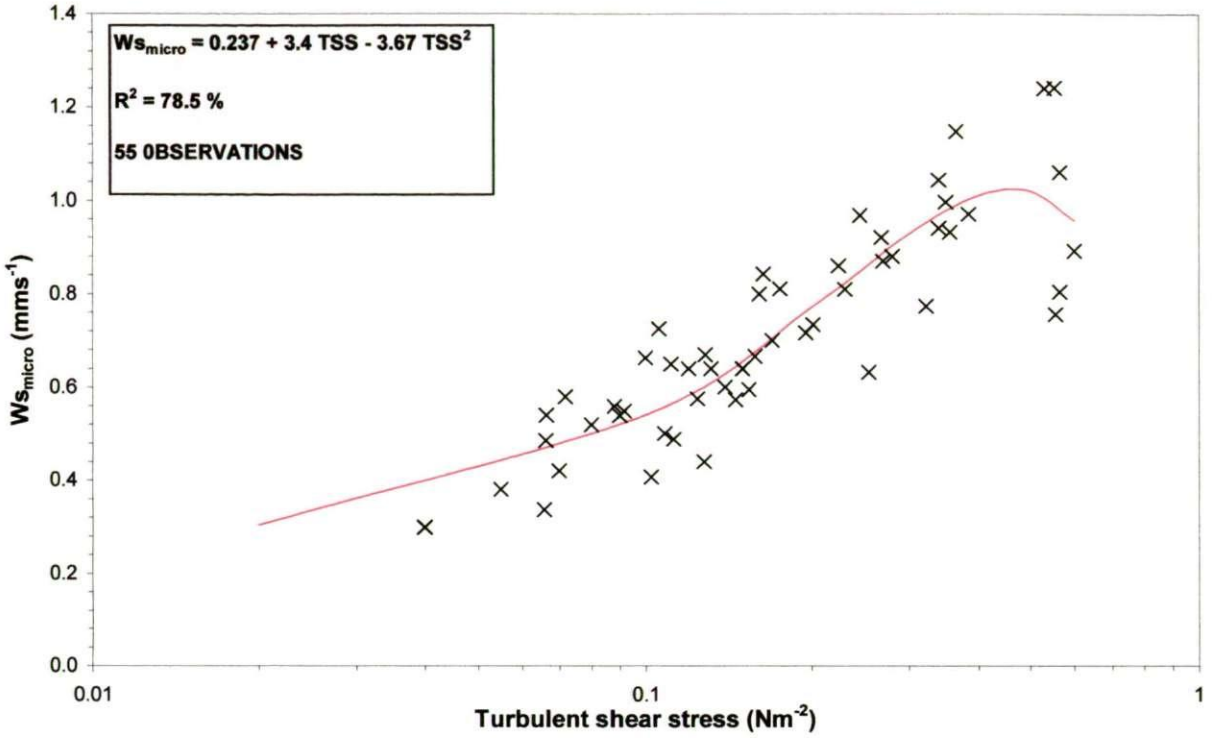

Figure 6.11 Microfloc settling velocities plotted against turbulent shear stress for Tamar estuary neap tidal conditions (experiments 2 and 3). A regression line representing equation 6.6 is plotted.

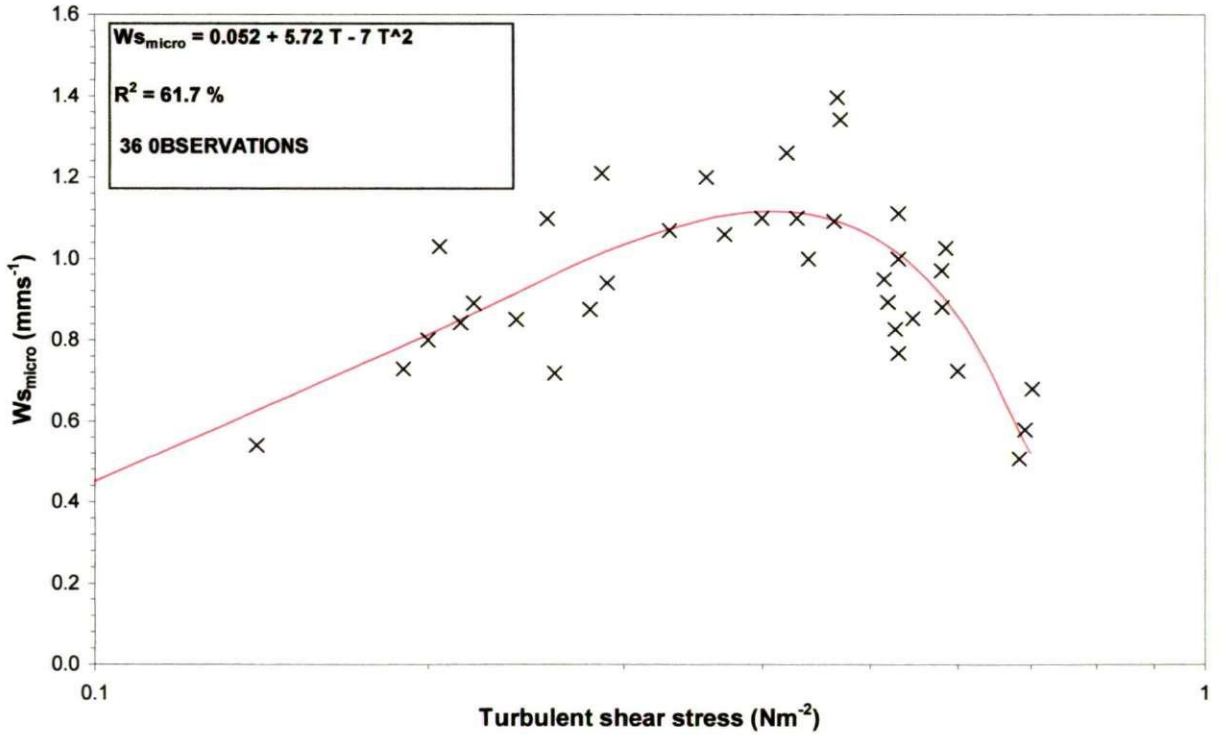

Figure 6.12 Microfloc settling velocities plotted against turbulent shear stress for Tamar estuary spring tidal conditions (experiments 1 and 3). A regression line representing equation 6.7 is plotted.

Figure 6.13 shows the SPM ratio variations for Tamar neap tides plotted against suspended matter concentration. The regression for the empirical data gave equation 6.8 and is also included in Figure 6.13.

$$SPM_{ratioTN} = 1.362 + 1.806\ SPM \qquad R^2 = 0.255 \qquad \textbf{(6.8)}$$

The low R^2 fit of 0.255 was a consequence of the low range in SPM ratio experienced during neap tides. Although large, fast-settling macroflocs were observed at neap tides, the low ambient concentration restricted the number of large flocs produced. Typically, the macroflocs at neap tides constituted between 20-75% of the dry floc mass, which corresponded to SPM ratios of 0.25-3 respectively. However, the greatest scatter occurred at concentrations under 140 mgl^{-1}, so this would have very little effect on the MSF values calculated for a complete tidal cycle numerical deposition simulation (see section 6.7).

In comparison, the generally high ambient concentrations measured at spring conditions in the upper Tamar estuary, resulted in much higher values of SPM ratio, as is illustrated in Figure 6.14. The data was best summarised by equation 6.9, and the R^2 of 0.848 was highly significant.

$$SPM_{ratioTS} = 2.3357\ SPM^{\,1.0958} \qquad R^2 = 0.848 \qquad \textbf{(6.9)}$$

Concentrations above 3.6 gl^{-1} indicated macroflocs contained over 90% of the particulate matter, which corresponded to SPM ratios > 10. If it was not possible to measure the floc mass distribution, and it was assumed that the division of SPM was equal between the microflocs and macroflocs, this could result in a significant error in the MSF. The following example will illustrate this point. Assuming an SPM = 4 gl^{-1} and TSS = 0.4 Nm^{-2}, and using equations 6.2, 6.7, 6.9, apportioning the SPM between the floc size-fractions resulted in a MSF of 16.34 $g.m^{-2}s^{-1}$. Whereas, assuming the SPM distribution to be evenly divided gave a MSF of 8.66 $g.m^{-2}s^{-1}$, which was an under-estimate of 47%. Summarising, the quantitative analysis showed that the SPM ratio generally had a strong correlation with SPM (over a wide range of concentrations), but held very little dependence on turbulent shear stress.

6.6.2 General conceptual model

To meet the requirements for both this thesis and the COSINUS project, a generalised conceptual model ($_{CM}$) for estuarine flocculation was required using all of the data. It should describe the salient interactive physical components attributed to flocculation, without the inclusion of superfluous fine detail, so it could easily be implement into numerical simulation models of sediment transport. With this goal in mind, the findings of the multiple regression results presented in section 6.6.1 were used to determine the model structure.

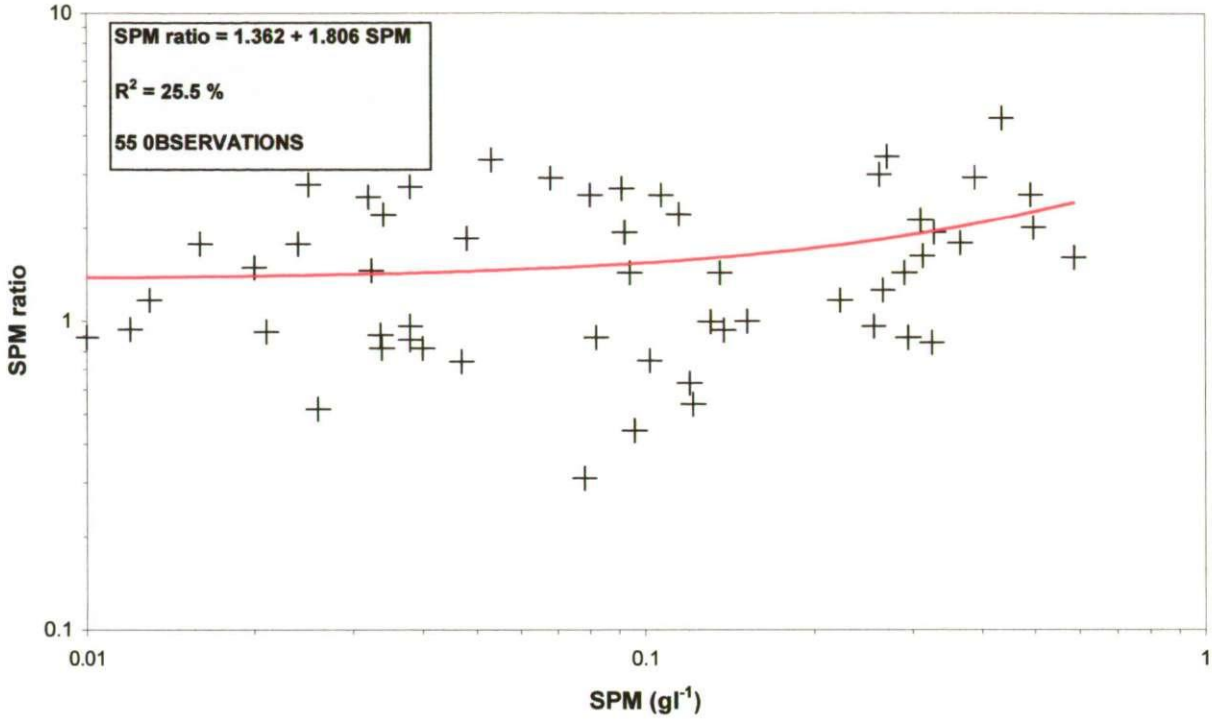

Figure 6.13 SPM ratios plotted against SPM concentration for Tamar estuary neap tidal conditions (experiments 2 and 3). A regression line representing equation 6.8 is plotted.

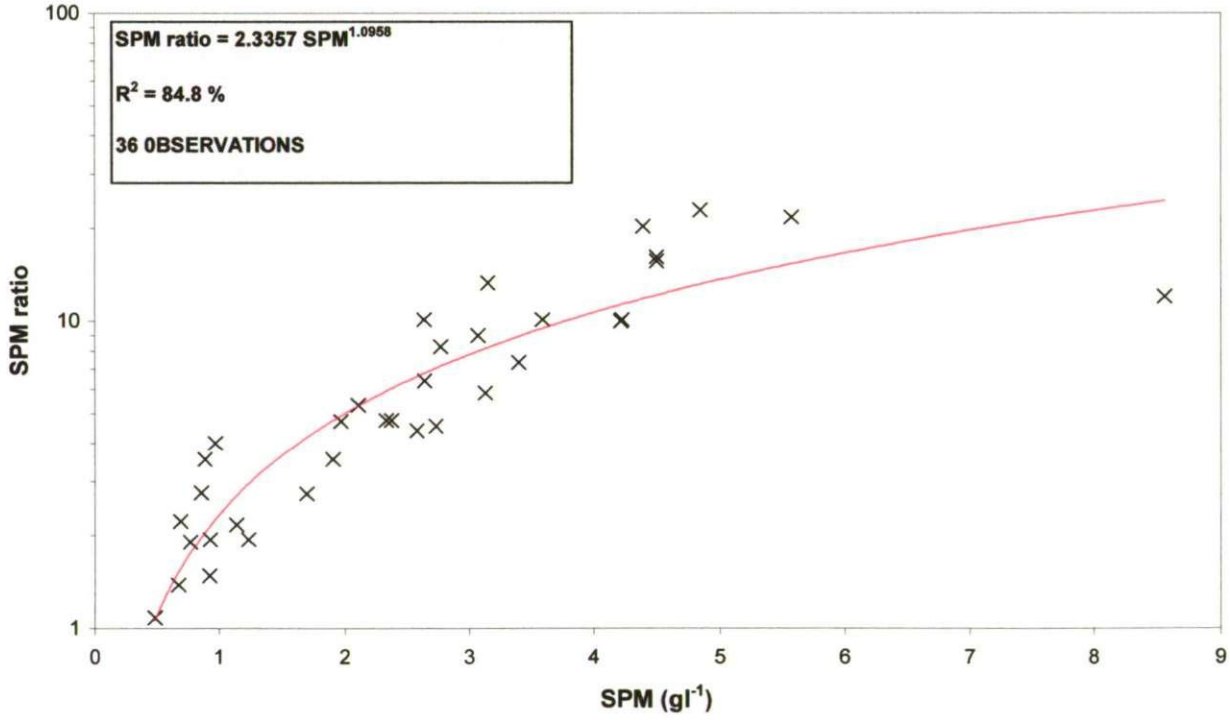

Figure 6.14 SPM ratios plotted against SPM concentration for Tamar estuary spring tidal conditions (experiments 1 and 3). A regression line representing equation 6.9 is plotted.

Only the in-situ data analysis results were used, as it is natural estuarine systems that were to be modelled.

The INSSEV data sets for the Tamar neap tides, Tamar spring tides, and Gironde neap tides were combined to form a single matrix of 110 observations; this is listed in Appendix II. Multiple regression produced expression 6.10 to describe the Ws_{macro}, with a highly significant R^2 of 0.906.

$$Ws_{macroCM} = 0.599 + 0.492\ SPM + 9.33\ TSS - 12.8\ TSS^2 \qquad R^2 = 0.906 \qquad \textbf{(6.10)}$$

Similarly the same data matrix was used to obtain the general relationships for both Ws_{micro} and SPM_{ratio}, and these are shown as equations 6.11 and 6.12, respectively.

$$Ws_{microCM} = 0.17 + 4.15\ TSS - 4.95\ TSS^2 \qquad R^2 = 0.723 \qquad \textbf{(6.11)}$$

$$SPM_{ratioCM} = 0.671 + 3.4\ SPM - 0.175\ SPM^2 \qquad R^2 = 0.761 \qquad \textbf{(6.12)}$$

A comparison of the three R^2 fit values indicates that macrofloc settling velocity is the more consistently predictable parameter, with an R^2 of 0.906, but the R^2 of 0.723 and 0.761 for the remaining two parameters still means that these stochastic representations are highly significant at a confidence level of 95%.

To justify the representations described by equations 6.10-6.12, there must be no direct correlation between TSS and SPM. A linear regression of all 110 TSS and SPM observations resulted in an R^2 fit of 0.12, which indicates no correlation and hence the multiple regressions presented in this chapter are valid.

The regression equations 6.10-6.12 are illustrated graphically as Figures 6.15A-6.15C (respectively). Generally, $Ws_{macroCM}$ displays a similar relationship to that proposed by Dyer (1989, see Figure 2.4), with an increase in settling velocity at low shear stresses due to flocculation enhanced by shear, and a decrease in settling velocity due to floc disruption at higher stresses for the same concentration; the limit being a turbulent shear stress of about 0.36 Nm^{-2} (equivalent G = 5.67 s^{-1} and Kolmogorov microscale eddy size = 428 μm). This shear stress threshold corresponds very closely to the value observed during the UOP laboratory annular flume experiments (see section 6.5). A number of authors have attributed very large floc formation to differential settling, but if this mechanism was to be significant it would only be able to operate within a very calm water column. From examination of Figure 6.15A, the data points identify the SPM concentrations which occur in a natural estuarine near bed location, and this shows that concentrations > 500 mgl^{-1} were only present

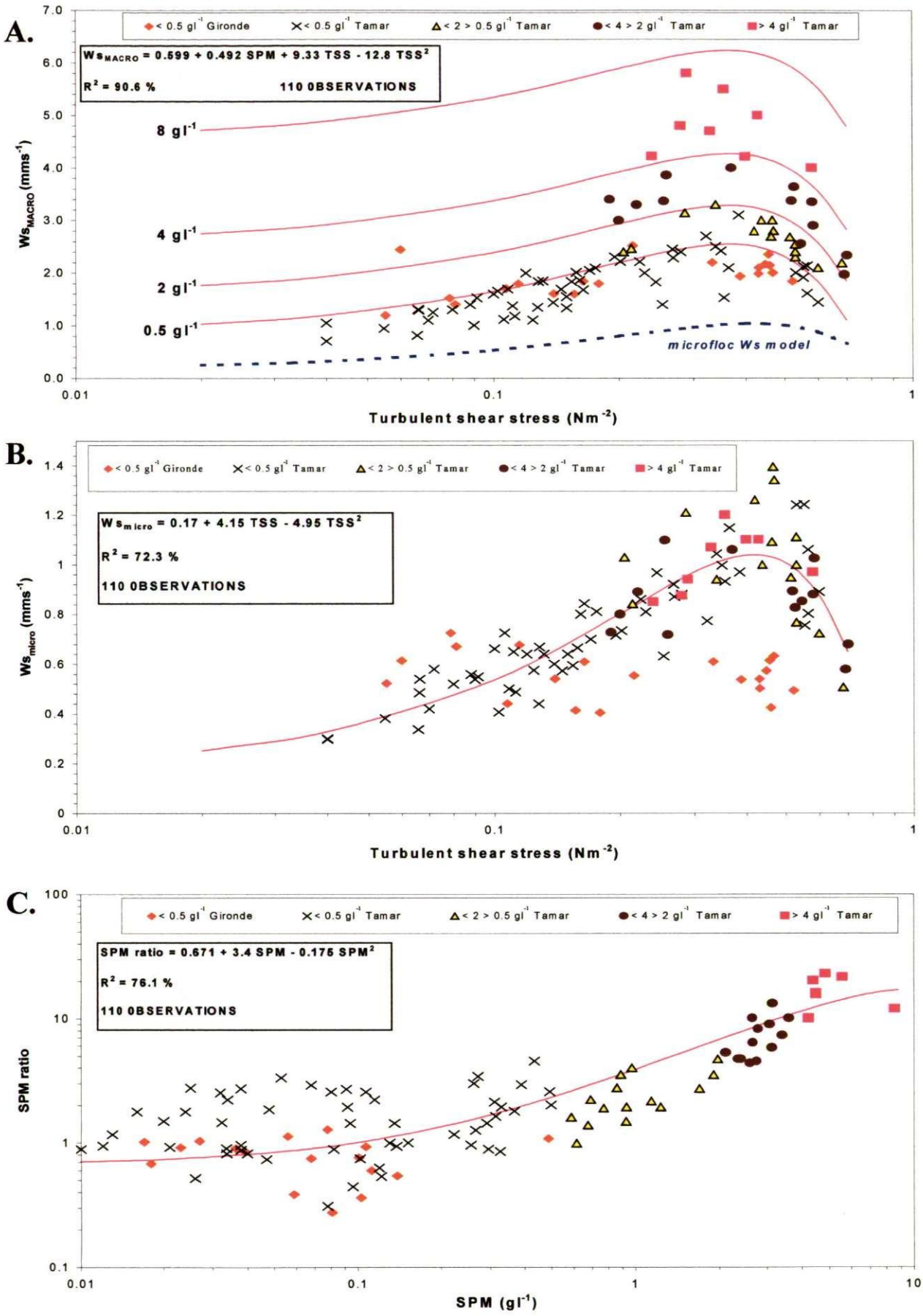

Figure 6.15 Representative plots of the conceptual model illustrating the three contributing equations: ***A***) equation 6.10 with equation 6.11 inset, ***B***) equation 6.11, and ***C***) equation 6.12.

when the TSS exceeded 0.2 Nm^{-2} which would negate the effects of differential settling over turbulent shear.

The peak macrofloc settling velocities (~4-5 mms^{-1}) were representative of flocs which formed within the CBS layer which typically developed during mid-tide conditions during spring tides, when a certain amount of shear thinning reduced the magnitude of the turbulent stirring. Beyond 0.4 Nm^{-2}, the regression shows the $Ws_{macroCM}$ values to decrease rapidly in response to disaggregation as the TSS increased. The maximum TSS encountered during the estuarine field studies was 0.7 Nm^{-2} (equivalent G = 9.44 s^{-1} and Kolmogorov microscale eddy size = 332 μm). However, if the LEGI multiple regression results (equations 6.4 and 6.5) were to be used to extrapolate up to a TSS of 1.4 Nm^{-2}, it would produce a more gentle "flattening-out" to the upper shear stress region of the macrofloc settling velocity model. One could hypothesise that beyond 1 Nm^{-2} only a limited number of very resilient macroflocs would exist, and further growth would be eradicated with rising shear stress. This small number of very strong macroflocs would have been created during a very highly turbulent event, and retained that "history" as it became trapped in the estuary's residual circulation and moved towards the head.

Only the $Ws_{macroCM}$ showed an inter-dependency towards both TSS and SPM concentration variations. $Ws_{microCM}$ (Figure 6.15B) was very closely correlated with just the TSS. As with the macroflocs, the microfloc settling velocity rose with increasing shear stress until a limiting TSS of ~ 0.42 Nm^{-2} (equivalent G = 6.43 s^{-1} and Kolmogorov microscale eddy size = 402 μm) was reached, whereby the regression model predicted a peak $Ws_{microCM}$ of ~1 mms^{-1}. This was significantly slower than the comparative macroflocs. The higher limiting shear stress for the microflocs can be attributed to their stronger inter-connective bondings, together with their residence time history. The influence of turbulent shear stress on the formation of natural mud microflocs agrees with the findings of Eisma (1986). Their lack of correlation with SPM concentration comes from them being the building blocks from which the large macroflocs are formed. The converse could be said for the $SPM_{ratioCM}$ (Figure 6.15C), which posed a strong interdependency with SPM concentration. Low ambient concentrations (10-100 mgl^{-1}) such as ebb conditions during neap tides, tended to create an equally balanced floc population with an $SPM_{ratioCM}$ of approximately unity. The advent of spring tides entraining higher amounts of particulates into suspension, causes the $SPM_{ratioCM}$ to rise to between 10-20 for SPM concentration > 4 gl^{-1}. This corresponds to 91-95.3% of the

particulate matter being contained by macroflocs. This would have a significant effect on the mass settling flux.

Equations 6.10-6.12 are then combined to form equation 6.13 from which the mass settling flux rate (MSF_{CM}) with the units of $g.m^{-2}s^{-1}$ can be calculated.

$$MSF_{CM} = \left[1 - \frac{1}{1+SPM_{ratioCM}} \cdot (SPM \cdot Ws_{macroCM})\right] + \left[\frac{1}{1+SPM_{ratioCM}} \cdot (SPM \cdot Ws_{microCM})\right] \quad \textbf{(6.13)}$$

This is a very practical way of expressing the inter-relationship between the three equations and can easily be implemented in mathematical simulation models. This type of expression describes the fundamental aspects of estuarine flocs (i.e. their impact on deposition) throughout the continually changing levels of turbulent mixing and SPM concentration. As opposed to a formulation which just has floc settling velocity as the dependent variable.

6.7 Evaluation of conceptual model

In order to quantify the accuracy of the conceptual floc model presented in the previous section, it will be tested and compared with a number of existing approaches to floc modelling. Numerical models are used to simulate deposition rates, not settling velocities, so this inter-comparison will be in the form of a prediction of mass settling flux. This requires a MSF value to be calculated for the entire floc spectra as opposed to just a single group of flocs, so approaches that do not use variable settling velocities, will implement sample mean values to represent the floc population. To make the comparison as realistic as possible the comparisons were made with the actual field data results from both the Tamar and Gironde estuary experiments which constituted 110 observations (see Appendix II). This permits the absolute MSF rates for each sample to be determined (i.e. the cumulative MSF from the individual flocs). Then the ambient TSS and SPM levels which existed at the specific time of an INSSEV sample can be input into each formulation to estimate the MSF.

6.7.1 Comparison methods used

A total of eight methods were employed for the comparison (a summary is provided in Table 6.1), and each parameterisation technique will be outlined in turn.

- The first approach (*1*) utilises the conceptual flocculation model described in section 6.6.2 in the form of equation 6.13. This formulation only required the inputs of TSS and SPM concentration to calculate the MSF.

Table 6.1 Summary of floc parameterisation approaches used during the testing of the conceptual model presented in this thesis.

Method number	Description
1	Conceptual model from this thesis in the form of equation 6.13
2	constant settling velocity, Ws = 0.5 mms^{-1}
3	constant settling velocity, Ws = 1 mms^{-1}
4	constant settling velocity, Ws = 2.5 mms^{-1}
5	constant settling velocity, Ws = 5 mms^{-1}
6	SPM power regression (equation 6.14)
7	Lick et al. (1993) approach - equations 6.15 and 6.16
8	van Leussen (1994) approach - equation 6.17

- The next four methods (*2-5*) employed single constant values of floc settling velocity. This is a very common approach used in numerical modelling, as it requires the least amount of code, and a model can run faster. This single value says very little about the floc characteristics or how they change throughout the tidal cycle. The settling velocity values used could either be calculated from direct in-situ measurements and averaged over a tidal cycle, or determined on a more arbitrary basis (i.e. used to fine tune the model). The values used for this inter-comparison are: *2.* 0.5 mms^{-1}, *3.* 1 mms^{-1}, *4.* 2.5 mms^{-1}, *5.* 5 mms^{-1}. The slowest of these settling velocities was representative of mean settling rates determined by Owen tube style instruments which were very disruptive and hence were biased towards the smaller slower settling microflocs. Whereas the highest settling rate is a value which has been employed in a recent simulation model of the Tamar estuary by Peterson et al. (2000).

- Early work on cohesive sediments found that the median floc settling velocity was exponentially related to the SPM concentration level. Examples of these relationships are illustrated in Figure 2.9, and it shows considerable differences in the exponential relationship between estuaries (Dyer, 1989). Dyer (1989) suggests that these variations are probably a result of floc density variations, and differences in ambient hydrodynamic conditions. This basis forms comparative method *6*. After using a single settling value, this method is deemed the least complex settling velocity relationship. As stated earlier in this section, it was a requirement that the MSF computations should represent the entire floc size spectra from a single INSSEV sample, so the mean settling velocity, Ws_{mean}, was used. Figure 6.16 shows the 110

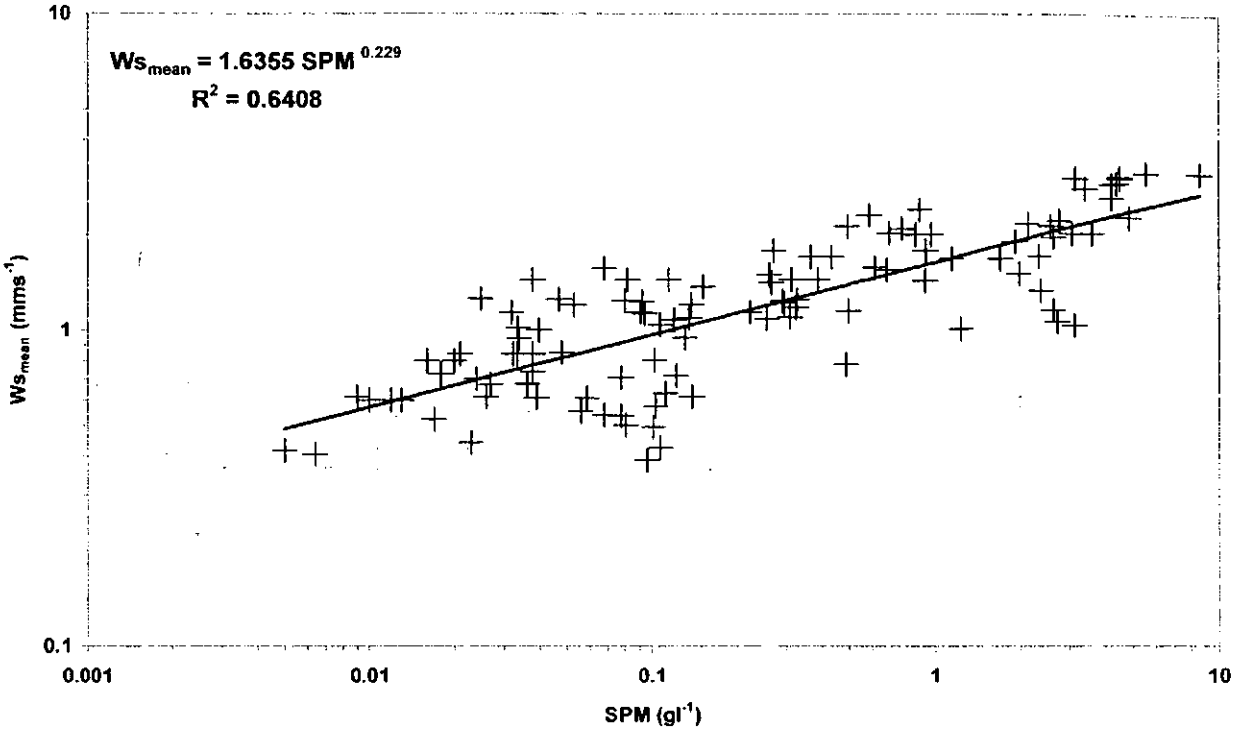

Figure 6.16 A plot of mean floc settling velocity against suspended particulate matter concentration. The regression line illustrates the relationship defined by equation 6.14.

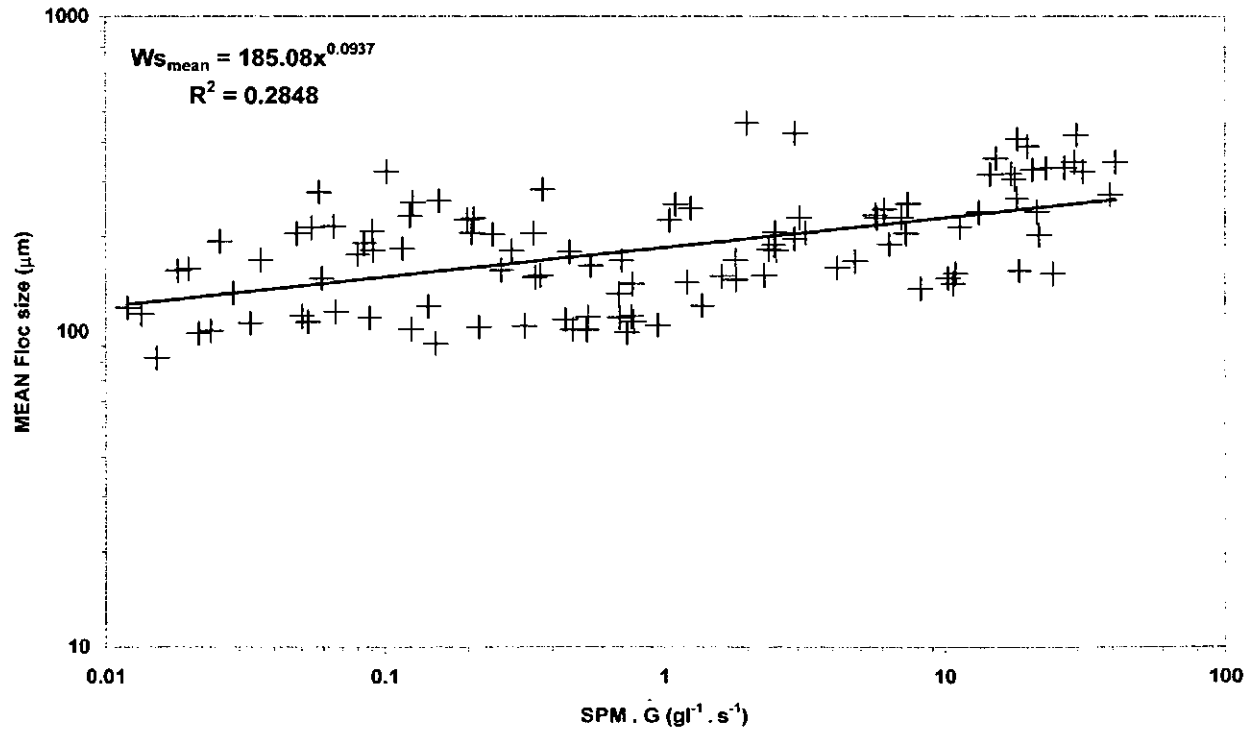

Figure 6.17 A plot of mean floc size against the product of the suspended particulate matter concentration and the turbulence parameter G. The regression line illustrates the Lick et al. (1993) relationship as defined by equation 6.15.

Ws_{mean} observations from the Appendix IV data matrix plotted against SPM concentration. This produced regression equation 6.14.

$$Ws_{mean} = 1.6355\ SPM^{0.229} \qquad R^2 = 0.641 \qquad \textbf{(6.14)}$$

It was noted that the value used for the exponent in the concentration power law is 0.229, i.e. much less than the values determined by previous authors, who showed values closer to unity. This is important for limiting the influence of concentration on the calculated settling velocity.

- The penultimate method used (*7*) was the empirical relationship derived from a laboratory study by Lick et al. (1993) where floc size was seen to vary as a function of the product of SPM and the turbulence parameter, G (see equation 2.18). This relationship for the 110 data points is shown in Figure 6.17, and is summarised by equation 6.15.

$$D_{mean} = 185.08\ (SPM.G)^{0.0937} \qquad R^2 = 0.285 \qquad \textbf{(6.15)}$$

The Lick et al. (1993) approach has been included in this comparison as it has been a flocculation parameterisation technique which has been applied by modellers to previous mathematical sediment transport engineering models. However, it must be noted that Lick et al. (1993) derived their algorithm structure empirically using significantly higher shear rates (G values of 100-400 s^{-1}) and SPM concentrations not exceeding 800 mgl^{-1}, all within a laboratory environment.

It can be seen from Figure 6.17 that this in-situ data indicates an increase in floc size with increasing SPM.G. This is the complete opposite to the findings of Lick et al. (1993) and could either be a result of their experimental procedure, or due to the algorithm structure (see the previous paragraph). This also highlights the potential dangers of directly applying a laboratory technique to an in-situ environment. The settling velocity was then approximated as a function of the calculated mean floc diameter (Gibbs, 1985; Ten Brinke, 1993) as shown in Figure 6.18, and gave:

$$Ws_{mean} = 6E^{-5}\ D_{mean}^{1.9049} \qquad R^2 = 0.588 \qquad \textbf{(6.16)}$$

- Method *8* utilised the formula (see equation 2.15) advocated by van Leussen (1994) which heuristically attempted to describe Dyer's (1989) conceptual flocculation diagram (see Figure 2.4). This relationship has the effect of increasing settling velocity at moderate values of G, where increased turbulence increases the

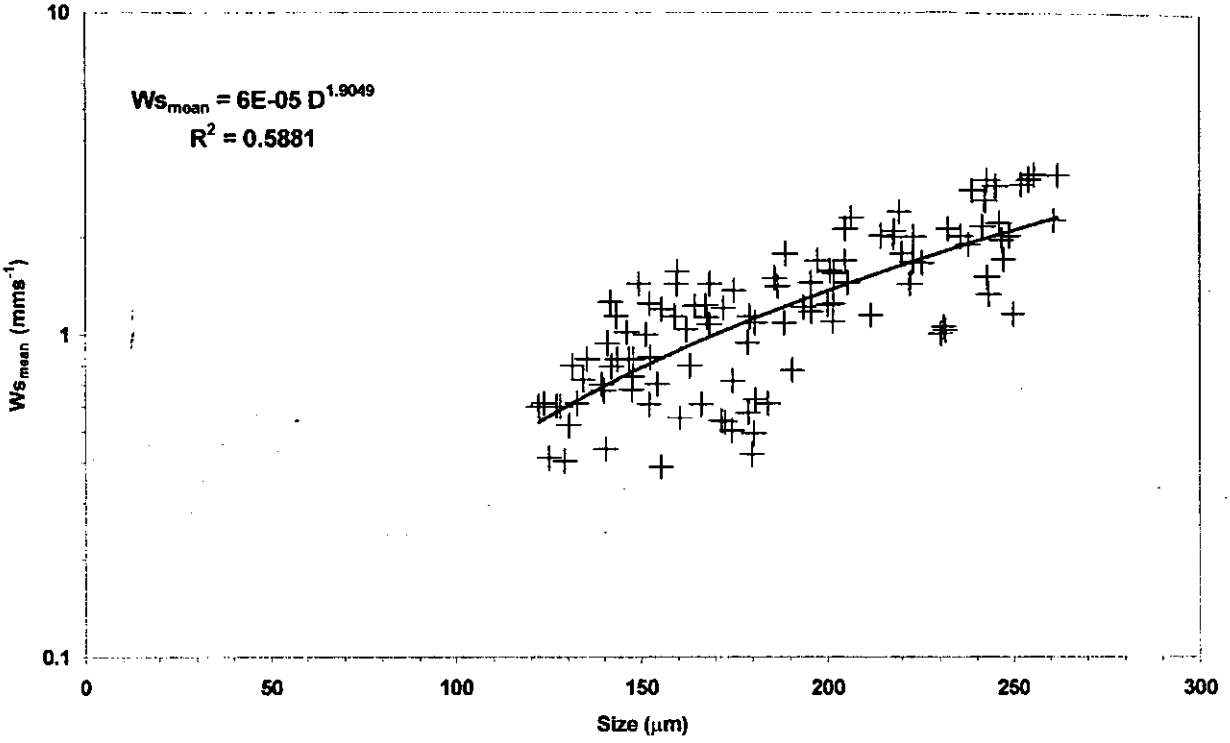

Figure 6.18 A plot of mean settling velocity against mean floc size values calculated from equation 6.15. The regression line illustrates the relationship defined by equation 6.16 which was used to calculate the Ws_{mean} values.

probability of collisions, and decreasing settling velocity at high values of G, when floc break-up processes dominate. Using the power law of concentration of equation 6.14, the best fit (albeit quite poor) to the 110 data point matrix was achieved with the constants: $a = 0.3$, and $b = 0.05$. The complete expression is:

$$Ws_{mean} = (1.6355\,SPM^{0.229})\,\frac{1+0.3G}{1+0.05G^2} \qquad (6.17)$$

These coefficients were similar to constants obtain by Roberts (pers. Comm, 1999) also for the Tamar estuary, whilst the b coefficient was nearly double that found by van Leussen (1994) for the Ems estuary.

Equation 6.17 was used to calculate mean settling velocity fluctuations at progressively increasing increments of G, for constant levels of concentration. These velocities were plotted as Figure 6.19, with actual empirical Ws_{mean} values overlaid. From examination, the Van Leussen (1994) model predicted that at a shear rate of only ~2 s^{-1} a peak settling velocity would be attained at any concentration up to 8 gl^{-1}, and thereafter the fall rate would decrease with growing shear. Whereas in reality, the empirical results showed that the highest Ws_{mean} tended to occur at shear

rates of 4-6.5 s^{-1}. The effect of this distortion given by the model will be examined in the following sub-section where the various methods are compared.

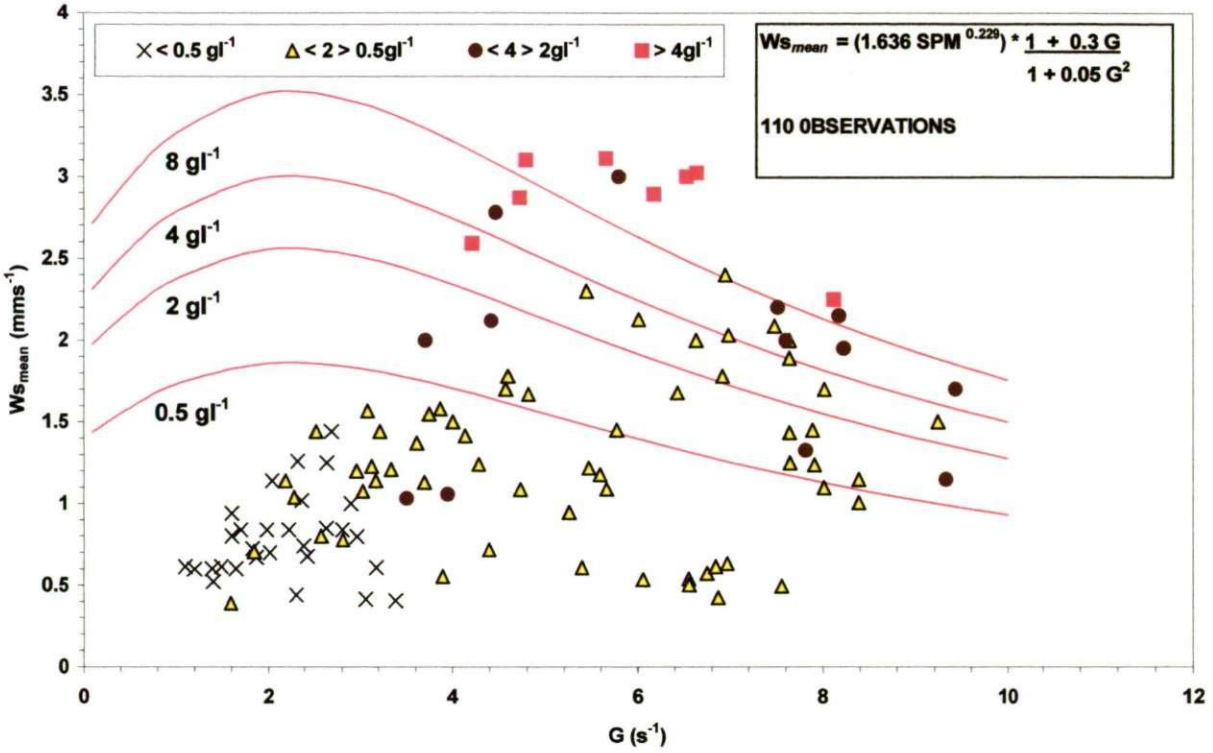

Figure 6.19 A plot of mean settling velocity, as determined by equation 6.17 (van Leussen, 1994), against the turbulence G. Lines of constant SPM concentration are added.

6.7.2 Discussion

The MSF rates predicted by each of the eight modelling approaches were individually compared with the 110 in-situ empirical results (listed in Appendix II) with varying turbulent shear stress and these are shown in Figure 6.20. For the conceptual model (Figure 6.20-1) the MSF values calculated by equation 6.13 showed a very close fit throughout the entire shear stress range. Whereas the constant settling velocity approaches indicated a considerable amount of both over- and under-prediction, with a fall rate of 2.5 mms^{-1} (method ***4***, Figure 6.20-4) seeming to provide the closest fit with the in-situ results. Both the SPM power regression (***6***, Figure 6.20-6) and Lick et al. (*7*, Figure 6.20-7) approaches produced very similar patterns of calculated MSF throughout the range of turbulent shear stress. Greater under-estimation of MSF was seen to occur for methods ***6***, *7*, and ***8*** (Van Leussen, see Figure 6.20-8) at times of moderate turbulent shear stress and high concentration, such as the ambient nearbed conditions created within a turbidity maximum.

To gain a greater insight into how these models performed during different tidal conditions, the cumulative MSF rate totals determined for each tidal scenario were compared to the

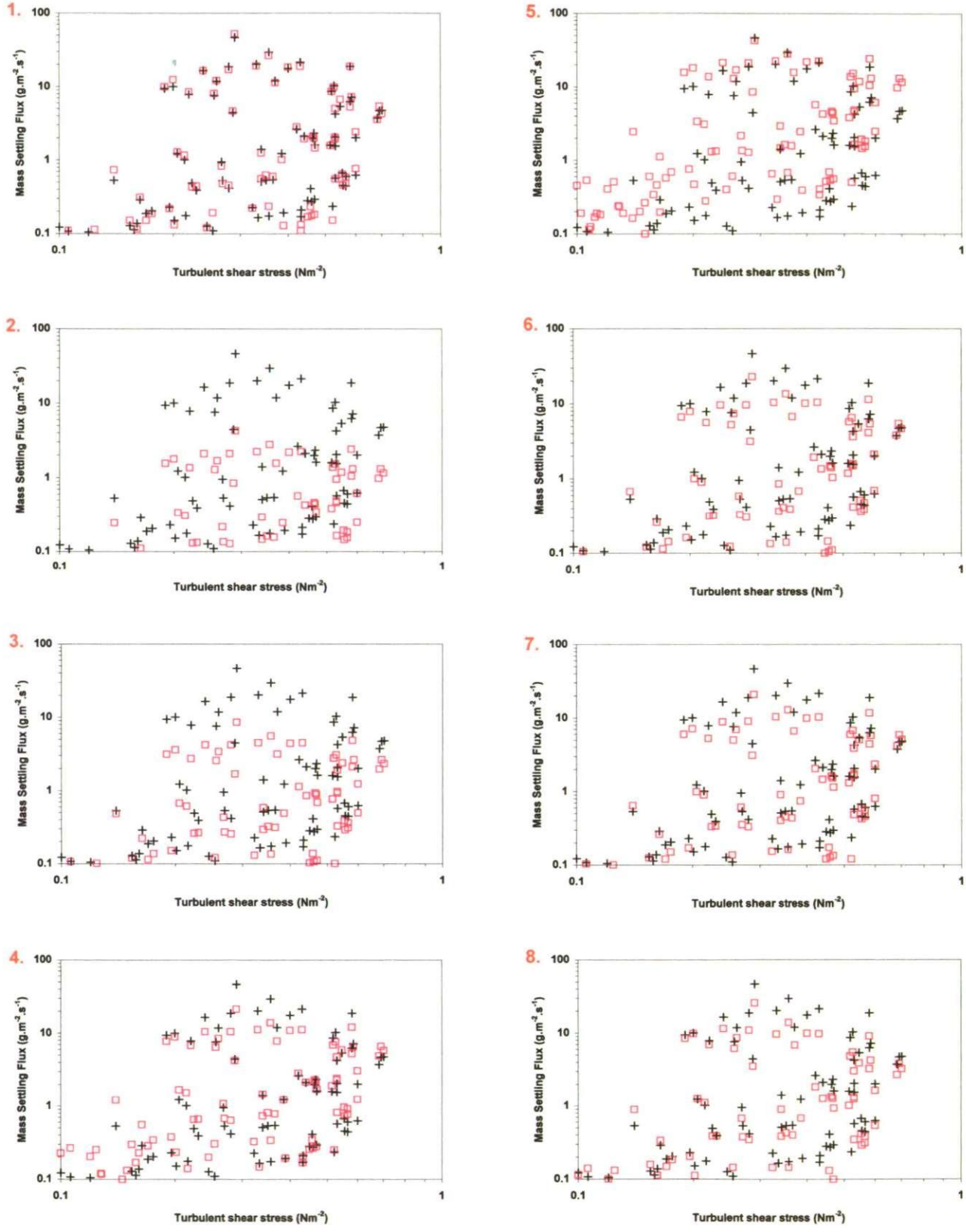

Figure 6.20 A comparison of absolute values of mass settling flux (+) determined from the in-situ measurement, and mass settling flux values computed from the corresponding ambient conditions of the absolute values, for each of the eight modelling approaches represented by □ . Plots 1-8 correspond to the respective modelling approaches listed in Table 6.1.

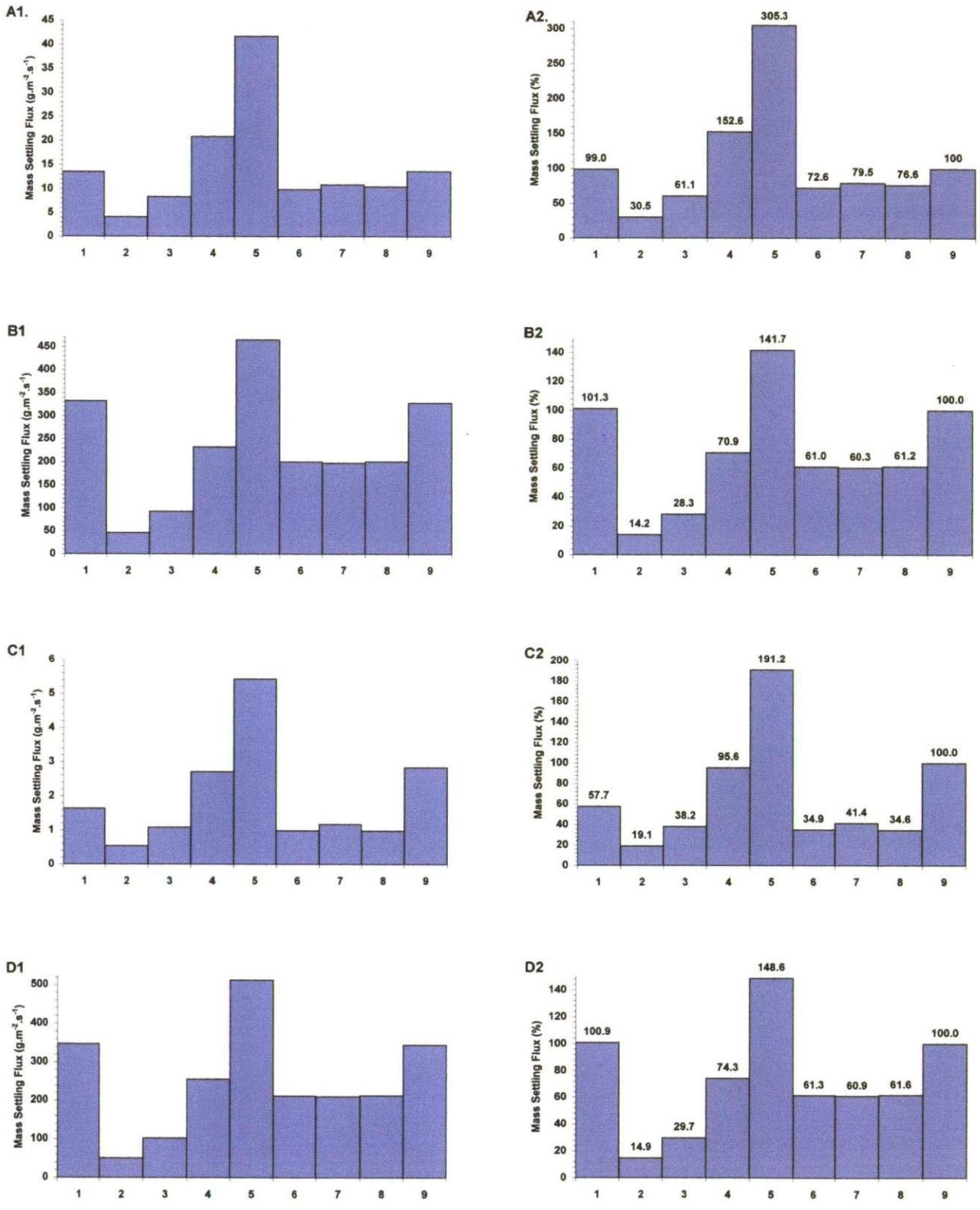

Figure 6.21 Histograms comparing the mass settling flux cumulative totals computed by the eight modelling approaches (1-8), and 9 which was the absolute cumulative total from the in-situ measurements. ***A***: Tamar neaps (experiment 2 and 3), ***B***: Tamar springs (experiment 1 and 3), ***C***: Gironde neaps (SWAMGIR1), and ***D***: all 110 data points used for the multiple regression analysis (see Appendix II). Plots with ***1*** refer to MSF with the units of $g.m^{-2}.s^{-1}$, and ***2*** refer to MSF as a relative percentage. For each scenario, mass settling flux is depicted as a cumulative total, and as a percentage compared to the absolute total which equalled 100%.

absolute MSF rates obtained from the respective in-situ results (Figure 6.21-1). The findings are also illustrated as a comparison of relative MSF in Figure 6.21-2, where the absolute MSF total determined from the in-situ results (i.e. column 9 on the histograms) for each scenario equalled 100%. The 55 Tamar neap tides observations (Figure 6.21-A1 and A2) produced a total MSF of 13.7 $g.m^{-2}s^{-1}$, and the model *1* (equation 6.13) estimate was within 1% of this total. The low level of suspended concentration resulted in a 27.4% and 20.5% under-estimate by the SPM power regression (*6*) and Lick et al. (*7*) approaches, respectively. The inclusion of the turbulence parameter as implemented by the Van Leussen method (*8*) did not fare much better, with a predicted MSF total of 10.5 $g.m^{-2}s^{-1}$. The very simplified constant settling velocities provided a wide range of error depending upon the value chosen. The 0.5 mms^{-1} and 1 mms^{-1} rates were more reflective of what sub-section 6.6.1.b classified as typical microfloc settling velocities, and so under-predicted by 70% and 39%, respectively. However, the 205% over estimate by method *5* (5 mms^{-1}) shows that just assigning a faster settling velocity, to operate in a static sense, would produce an even greater misrepresentation of the settling flux from a simulation model output.

The significant increase in SPM during spring tides did not affect the MSF prediction of method *1* (equation 6.13) which calculated a MSF of 333 $g.m^{-2}s^{-1}$, which was only 1.3% greater than the absolute rate. This demonstrates the flexibility of the macrofloc and microfloc approach advocated in this thesis. Apart from method *5* which still over predicted by nearly 42%, the remaining methods all under-estimated by 39-86%. At spring tides this translated into comparative errors in MSF totals of 128-282 $g.m^{-2}s^{-1}$. In numerical sediment transport modelling terms, this would minimise or even negate the significant influence of events where flocculation is a major contributor, principally within the TM formation. In the longer term, such as a year ahead, one could imagine how the poor estimation of deposition rates could significantly alter predictions of future sedimentation patterns to such a high degree, in that the final output from a simulation model would be regarded as very unreliable.

Chapter Seven:

Conclusions

In-situ observations of floc characteristics, coupled with hydrodynamical measurements, were made with the primary objective of describing the response of estuarine floc settling velocities and the associated compositional characteristics to variations of turbulent shear stress and suspended particulate matter concentration. A series of laboratory experiments were also employed to examine floc populations generated within a more controlled environment to isolate factors controlling the flocculation process. A summary of the main findings and conclusions drawn from each aspect of this study are presented here, together with an insight into avenues which require further development and research.

7.1 Field experimental programmes

i. The INSSEV instrument and the POST system were mounted together on a specially designed bed frame. This combined instrumentation rig was successfully deployed within both the Tamar estuary in south west England (1998) and the Gironde estuary in south west France (1999). This provided high frequency time series of three-dimensional flow velocity (from which turbulent fluctuations and shear stress could be calculated), and suspended particulate matter concentration (both on a sub-tidal time scale), together with floc size and settling velocity spectra measurements at 10-25 minute intervals. All measurement were made in the near-bed region.

ii. Deployments within the turbidity maximum region of the upper Tamar estuary during June, August and September 1998 yielded a total of 67 floc samples during neap tides, and 40 floc samples from spring tide conditions.

iii. A further 39 floc samples (of which 18 are presented in this thesis) were collected using INSSEV from the lower reaches of the Gironde estuary during June 1999.

iv. The University of Plymouth research pontoon "*R.P. AMAP-1*", was designed and co-fabricated by the author between January and April 1998 as part of the EC MAST III COSINUS project. It was successfully employed for instrumentation rig deployments at the Calstock Station A location during the 1998 Tamar estuary experimental series. *R.P.*

AMAP-1 is currently on loan to Calstock Boat Yard, where it is in use as a mooring sinker re-location platform.

7.2 Tamar estuary field experiments

i. The turbidity maximum at Calstock during neap tides was primarily generated by bed erosion, whereby ambient, near-bed SPM concentrations reached up to 500 mgl^{-1}, and the current flow attained velocities of ~ 0.6 ms^{-1}. Advective transport was more apparent at spring tides where near-bed SPM rose to 8 gl^{-1}, and surface currents were nearly double those at neap tides.

ii. The macroflocs generally demonstrated settling velocities ranging from 2-20 mms^{-1}. This is a significantly faster rate than generally attributed in previous sediment transport modelling. Settling rates of 0.5-1 mms^{-1} have been commonly used in mathematical depositional flux simulations, and these were seen to be more representative of the smaller, denser microflocs sampled in the Tamar.

iii. Across the various tidal conditions, aggregate effective densities ranged from: very high (ρ_e ~ 10000 kgm^{-3}) for needle-like fragments of tourmaline and hornblende observed early in the ebb during neap tides; whilst at the other extremity, very porous low density (ρ_e ~ 20-50 kgm^{-3}) flocs were abundant during spring tides, particularly within a CBS layer where SPM concentrations were high causing the turbulence to be damped to a level of 0.3-0.4 Nm^{-2}.

iv. At spring tides the largest (MAX6) floc sizes of 1598 μm, were observed at the time the main body of the TM passed through the Calstock sampling location. These flocs had effective densities < 50 kgm^{-3} and settling velocities of up to 16.6 mms^{-1}. In comparison, the MAX6 neap flocs were 50% smaller in size and settling velocity at peak SPM concentrations.

v. Approximately three quarters of the particulate mass was held in the macrofloc portion during an average spring tide cycle, whereas the division with microflocs was relatively even throughout neap tidal conditions. SPM_{ratio} was approximately unity for SPM concentrations <100 mgl^{-1}, suggesting an equally balanced population of macroflocs and microflocs during neap tides.

vi. At neap tides, macrofloc settling velocity showed a stronger dependence on turbulent shear than that on concentration by a ratio of 1.4:1 (i.e. ratio of coefficients). The higher particulate concentrations of spring tides resulted in a dependence ratio of approximately

1.7:1 in favour of the ambient SPM (as opposed to TSS), however variations in turbulent mixing still had a significant effect on the settling velocity of a macrofloc sub-population.

vii. The advent of spring tides entraining higher amounts of particulates into suspension, caused the SPM_{ratio} to rise to between 10-20 for SPM concentrations > 4 gl^{-1}. This corresponds to 91-95.3% of the particulate matter being contained by macroflocs.

viii. The presence of total carbohydrate concentrations > 10 mgl^{-1}, which occurred during high SPM concentrations found during spring tidal conditions, was seen to greatly assist in the formation of a high percentage of fast settling (Ws ranging from 1.8-3.7 mms^{-1}) stringer-type macroflocs. This was particularly evident during periods of high turbulent mixing (TSS > 0.5 Nm^{-2}). These stringers demonstrated H:W ratios ranging between 1.8-6, and a very loose structure as effective densities of 18-70 kgm^{-3} and porosities up to 98.6%, showed. Ultimately, the total amount of sugars present seems to be a more important factor with regards flocculation than that of the mean organic content.

7.3 Gironde estuary field experiments

i. During times of maximum entrainment in the Le Verdon region of the Gironde estuary, the G-values were generally 2 s^{-1} greater than those at Station A on the Tamar. Conversely, the SPM concentrations during neap tides at the Le Verdon sampling location did not exceed 150 mgl^{-1}.

ii. The more turbulent environment appears to be less conducive for macrofloc production. This was reflected in mean floc sizes which ranged between 83-114 μm throughout the entire sampling period on the 23rd June 1999.

iii. At peak concentration the macroflocs only represented 38-52% of the ambient SPM with SPM ratios of 0.6-1.1, compared to 65-75% and ratios of 1.8-2 for the Tamar flocs. This difference could be attributed to differences in the mineralogical composition, organic coatings, and / or the higher ambient turbulence.

iv. The limited number of macroflocs present within each sample had settling velocities of 1.8-2.6 mms^{-1}, which gave this larger size fraction 60-80% of the MSF at peak concentrations; this was very similar to the Tamar flocs.

v. At periods of high entrainment, the MAX6 flocs were approximately 50-60 μm less than the Kolmogorov eddy sizes which were ~ 400 μm. These flocs exhibited effective densities of < 40 kgm^{-3}, which indicate they were quite fragile and prone to disaggregtion with increased shear stress. Around slack, high water, eddy sizes rose to 860 μm, which

encouraged macroflocs to settle to the bed, leaving only small, slow-settling flocs in suspension.

7.4 LEGI laboratory experiments

i. The LEGI grid tank could repeatably produce turbulent shear levels (G) between 5.7 s^{-1} and 16.6 s^{-1} for nominal particle concentrations ranging from 200 mgl^{-1} to 5 gl^{-1}.

ii. The turbulent motion produced flocs with comparable characteristics to those observed in-situ. The combination of the pipette extraction process and the video camera floc interrogation technique did not appear to significantly affect the flocs.

iii. Very few floc aggregates were observed exceeding the pre-sieving mesh diameter of 100 μm, at all concentration and shear stress levels, for the Gironde mud with the organic components removed. This lack of aggregation is attributed to the absence of polysaccharide-type coatings which are present in natural muds.

iv. For low concentrations of natural Tamar estuary mud (tam200) at the highest shear, the MAX6 floc size was 210 μm, which was slightly less than the Kolmogorov eddy size of 251 μm. The high velocity particle collisions resulted in both macroflocs and microflocs having settling velocities of only 0.6 mms^{-1}.

v. Lowering the shear to ~7.7 s^{-1} (for tam200 mud) produced improved flocculation, due to less aggressive inter-particulate impacts and raised the macrofloc settling velocity to 1.8 mms^{-1}. The SPM ratio rose to 1.8, which translated into the macroflocs constituting 64% of floc mass, and 80% of the MSF.

vi. Low concentrations of natural Gironde mud (gir200) displayed significantly faster settling macroflocs at each shear stress increment, but a MAX6 floc size of the same order as the tam200 mud flocs. The SPM distribution showed the macroflocs only constituting 20-30% of the particulate mass. However, the fast settling rate transformed the low macrofloc mass into 62% of the MSF.

vii. For tam5000, the maximum floc diameter was approximately double the corresponding eddy size (400-430 μm).

viii. Within a suspension representing a CBS layer, a shear of 6.5 s^{-1} combined with an SPM of 8.2 gl^{-1} effectively stimulated aggregate formation to such a high degree that only 3% of the floc mass fell in the microfloc range. The macroflocs had a settling velocity of 5.75

mms^{-1}, which meant that the ratio of MSF between the macroflocs and microflocs was 221:1.

7.5 UOP laboratory experiments

i. Suspensions of natural Tamar estuary sediment with concentrations up to 200 mgl^{-1} were successfully sheared within a laboratory annular flume, at increments rising up to turbulent shear stresses of 0.6 Nm^{-2}. The size and settling velocity of the twenty largest flocs were measured by a miniature underwater video camera mounted in a viewing port on the flume channel wall.

ii. The turbulent shear stress values used for the experimental work showed a good correspondence with floc size according to the relationship of Hunt (1986) i.e. $D_x \propto G^{-m}$, where the exponent m varied between 0.47 and 1.29 for the 80 mgl^{-1} and 200 mgl^{-1} concentrations, respectively.

iii. At the lowest shear stress (0.1 Nm^{-2}) there was a distinctive near-linear increase in floc size with increasing SPM concentration. Correspondingly, the settling velocities also rose with the presence of higher ambient particle concentrations.

iv. The mean effective density of the 200 mgl^{-1} sample sheared at 0.1 Nm^{-2} was 37 kgm^{-3}, which indicated these flocs were very fragile. In an estuarine water column, these flocs would be highly susceptible to disaggregation as they pass through zones of higher shear stress.

v. Log-linear plots of variations in MAX4Ws floc size plotted against turbulent shear stress, indicated a critical shear region of about 0.25-0.4 Nm^{-2}. Once this was exceeded, together with a simultaneous increase in suspended concentration, disruption causing aggregate break-up was created, as opposed to enhancement of the flocculation process. A similar pattern was observed for the settling velocities.

7.6 Conceptual model for estuarine flocculation

i. An initial qualitative appraisal of both the in-situ and laboratory floc data compiled for this thesis, primarily with respect to settling velocity (as it is regarded as the most important floc characteristic), revealed that for the various ranges of turbulent shear and SPM concentration, 160 μm provided the optimum segregation point between the sub-populations of macroflocs (> 160 μm) and microflocs (< 160 μm).

ii. A parametric multiple regression statistical technique was used to establish correlation patterns for in-situ hydrodynamic and macrofloc / microfloc data using 110 data sets listed in Appendix II. Three primary equations were generated which could calculate: $Ws_{macroCM}$ (equation 6.10), $Ws_{microCM}$ (equation 6.11), and $SPM_{ratioCM}$ (equation 6.12). The three equations could be combined so as to be able to calculate estimates of mass settling flux (equation 6.13).

iii. The inclusion of both turbulent shear stress and SPM concentration as independent variables produced a highly significant R^2 of 0.906 for equation 6.10 and illustrated the importance of both these factors in controlling macrofloc settling velocity.

iv. $Ws_{macroCM}$ displays a similar relationship to that proposed by Dyer (1989, see Figure 2.4), with an increase in settling velocity at low shear stresses due to flocculation enhanced by shear, and floc disruption at higher stresses for the same concentration; the transition being a turbulent shear stress of about 0.36 Nm^{-2}.

v. $Ws_{microCM}$ was very closely correlated with just the TSS. As with the macroflocs, the microfloc settling velocity rose with increasing shear stress until a limiting TSS of ~0.42 Nm^{-2} was reached, at this point the regression model predicted a peak $Ws_{microCM}$ of ~1 mms^{-1}; this was significantly slower than the comparative macroflocs.

vi. The higher limiting shear stress for the microflocs can be attributed to their stronger inter-connective bondings, together with their residence time history. The influence of turbulent shear stress on the formation of natural mud microflocs agreed with the findings of Eisma (1986).

vii. Conversely, the $SPM_{ratioCM}$ showed a strong interdependency principally with SPM concentration.

viii. Equation 6.13 predicted the MSF of the 110 floc samples from neap and spring tides (see Appendix II), with a cumulative error of only +0.9%. In comparison, the use of single settling velocity values of 0.5 mms^{-1} and 5 mms^{-1} were both in error by -85.1% and +48.6%, respectively. Representing mean floc settling velocity by: *i)* a simple SPM concentration power-regression relationship, *ii)* the Lick et al. (1993), and *iii)* the van Leussen (1994) approaches, all under predicted MSF by ~29%.

7.7 Future work

Further research would initially take the form of implementing equations 6.10-6.13 (the conceptual model for estuarine flocculation) into existing sediment transport models, and

evaluating the response of the model. This needs to be done for the situation where real situations are simulated.

Next, because of the scarcity of good quality floc and hydrodynamical data (such as that presented in this thesis), it would be envisaged that a series of follow-up experiments to those reported in Chapters 3-6 of this thesis would be conducted, and possibly in a number of different estuaries where mathematical sediment dynamical models exist.

Studies would be conducted both within turbidity maximum regions, and lower concentration locations in closer proximity to the estuary mouth, to increase the range of environmental conditions represented by the data. Seasonal variations in the flocculation study would also be desirable. A more detailed analysis of the biological aspects of floc aggregation would be added to future experiments. Particular emphasis would be placed on obtaining measurements of extra-cellular polymetric substances (EPS), which have been shown to be important biological binding agents with respect to estuarine mud coagulation. Generic EPS values could be obtained from water bottle samples, whilst EPS levels present in the different sub-groups of a specific floc population could be acquired using water samples gathered with a Braystoke tube. Studies which include the effects of waves may also be interesting because of the period nature of the shear with respect to creep in floc strength.

The use of two or three sampling sites in close proximity, each using identical instrumentation, may provide a more conclusive quantitative examination of the advection aspects of SPM over a tidal cycle. This would require the manufacture of two duplicate INSSEV instruments. Section 6.2.3.a of the discussion illustrated how different particle sizers (i.e. INSSEV and the Lasentec P100) can suggest that the same floc population possessed different floc characteristics. Thus the ability of the INSSEV instrument to provide estimates of individual floc effective density, has been shown to be a distinct advantage.

New data would be used to examine the 160 micron size division between micro and macroflocs and the conceptual flocculation model hypothesises presented in this thesis. This would either corroborate the findings of this thesis (i.e. equations 6.10-6.13), and show whether those relationships are generic or site specific. Otherwise the data might identify whether additional components (e.g. biological factors) are required to provide a ***significant*** difference when

attempting to parameterise the mass settling flux throughout the various tidal states within an estuarine system.

The follow-up field experiments would utilise the same general data acquisitional protocols explained in this thesis, but with the following recommended modifications to the INSSEV and POST systems:

- Replace the monochrome INSSEV video camera with a white LED back-lit colour camera, linked to a digital storage facility. The colour floc images may provide more insight into the various organic and mineral components which constitute natural estuarine mud flocs.
- INSSEV would also be controlled by a PC base unit, which would provide greater control of the instrument whilst situated on the sea bed, plus the digital floc images could be processed much faster by currently available image tracking software (a tentative demonstration of a possible unit was given by National Instruments in April 2000).
- The addition of either four more 2 cm discoidal EMCMs or four 3-channel acoustic Doppler velocimeters (ADV) would provide greater resolution to the near bed turbulence structure.

References

Al Ani, S., Dyer, K.R. and Huntley, D.A., (1991). *Measurement of the influence of salinity on floc density and strength.* Geo-Marine Letters, 11: 154-158.

Alldredge, L.L., (1979). *The chemical compostion of macroscopic aggregates in two nertic seas.* Limnol. Oceanogr., 24: 855-866.

Alldredge, A.L. and Gotschalk, C., (1988). *In-situ settling behaviour of marine snow.* Limnol. Oceanography, 33: 339-351.

Alldredge, A.L. and Silver, M.W., (1988). *Characteristics, dynamics and significance of marine snow.* Prog. Oceanograhy 20:41-82.

Allen, G.P., (1971). *Relationship between grain size parameter distribution and current patterns in the Gironde estuary (France).* J. Sed. Petrol., Tulsa, 41 (1): 74-88.

Allen, G.P., (1972). *Etude des processus sedimentaires dans l'estuaire de la Gironde.* These Doct, es Sci. Univ. Bordeaux, No. 369, 310 pp.

Allen, G.P., Castaing, P., Jouanneau, J.M. and Klingebiel, A., (1974). *Les processus de charriage a l'embouchure de la Gironde.* Mem. Inst. Geol. Bassin d'Aquitaine, Bordeaux, 7: 191-206.

Allen, G.P., Salomon, J.C., Bassoulet, P., Du Penhoat, Y. and De Grandpre, C., (1980). *Effects of tides on mixing and suspended sediment transport in macrotidal estuaries.* Sedimentary Geol., 26: 69-90.

Allen, T., (1975). *Particle size measurement.* Chapman and Hall, London, 454pp.

Anderson, G.F., (1986). *Silica, diatoms and a freshwater productivity maximum in Atlantic coastal plain estuaries, Chesapeake Bay.* Estuarine, Coastal and Shelf Science, 22: 183-197.

Argaman, Y. and Kaufman, W.J., (1970). *Turbulence and flocculation.* J. Sanitary Eng., ASCE, 96: 223-241.

Ayesa, E., Margeli, M.T., Florez, J. and Garcia-Heras, J.L., (1992). *Estimation of break-up and aggregation coefficients in flocculation by a new algorithm.* Chemical Eng. Sci., 46 (1): 39-48.

Bale, A.J., (1987). *The characteristics, behaviour and heterogeneous chemical reactivity of estuarine suspended particles.* Ph.D. Thesis, Plymouth, U.K., 216 pp.

Bale, A.J., Morris, A.W. and Howland, R.J.M., (1985). *Seasonal sediment movement in the Tamar estuary.* Oceanologica Acta, Vol. 8, No. 1, 1-6.

Bale, A.J. and Morris, A.W., (1987). *In-situ measurement of particle size in estuarine waters.* Estuarine, Coastal and Shelf Science, 24: 253-263.

Berlamont, J. and Toorman, E.A., (2000). *EC MAST III COSINUS project – project summary flyer (2nd edition).*

Best, J.L. and Leeder, M.R., (1993). *Drag reduction in turbulent muddy seawater flows and some sedimentary consequences.* Sedimentology, 40: 1129-1137.

Bishop, O., (1991). *Practical electronic filters.* Bernard Babini Publishing Ltd., ISBN 0859342441.

Blewett, J.C., (1998). *Measurement of suspended sediment transport processes off the Holderness coast – southern North Sea, England.* Ph.D. Thesis, University of Plymouth, pp.

Bonnefille, R., (1971). *Remarques sur les ecoulements moyens a l'aval de la Gironde.* Bull. Inst. Geol. Bassin d'Aquitaine, Bordeaux, 11: 361-364.

Bowen, K.F., (1964). *Turbulence – part I.* Oceanogr. Mar. Biol. Ann. Rev., 2: 11-30.

Burban, P.Y., (1987). *The flocculation of fine-grained sediments in estuarine waters.* MSc. thesis, Dep. of Mech. Eng. Univ. of Calif., Santa Barbara, USA.

Burban, P-Y., Lick, W. and Lick, J., (1989). *The flocculation of fine-grained sediments in estuarine waters.* J. Geophys. Res., 94 (C6): 8323-8330.

Burban, P-Y., Xu, Y-J., McNeil, J. and Lick, W., (1990). *Settling speeds of flocs in fresh water and seawater.* J. Geophys. Res., 95 (C10): 18,213-18,220.

Cadee, G.C., (1985). *Macroaggregates of Emiliana huxleyi in sediment traps.* Mar. Ecology. Prog. Ser., 24: 193-196.

Cameron, W.M and Pritchard, D.W., (1963). *Estuaries.* In *The Sea* (Ed. Hill, M.N.), Vol. 2, Wiley, New York, 306-324.

Christie, M.C., (1997). *The in-situ erosion of intertidal muds.* Ph.D. Thesis, University of Plymouth, 220 pp.

Christie, M.C., Dyer, K.R., Turner, P. and Manning, A.J., (2001). *The effects of density gradients upon water column turbulence within a turbidity maximum* (In preparation).

Christie, M.C., Quartley, C.P. and Dyer, K.R., (1997). *The development of the POST system for in-situ intertidal measurements.* The 7th Int. Conf. On Elec. Eng. In Oceanography, 23-25 June 1997, p.39-45 of Conference Publication No. 439, by Inst. Elec. Eng., London.

Clifton, R.J. and Hamilton, E.I., (1979). *Lead-210 chronology in relation to levels of elements in dated sediment core profiles.* Estuarine, Coastal and Shelf Science, 8: 259-269.

Dalrymple, R.W., Zaitlin, B.A. and Boyd, R., (1992). *A conceptual model of estuarine sedimentation.* J. Sedim. Petrol, 62: 1130-1146.

Davies, J.H., (1964). *A morphogenetic approach to world shorelines.* Z. Geomorphol., 8: 127-142.

Dearnaley, M.P., (1996). *Direct measurements of settling velocities in the Owen Tube: a comparison with gravimetric analysis.* Journal of Sea Research, Vol. 36, Nos. 1-2, 41-47.

Delo, E.A., (1988). *Estuarine muds manual.* Hydraulics Research, Wallingford, Report No. SR164, 23-26.

Dionne, J.C., (1963). *Towards a more adequate definition of the St. Lawrence estuary.* Z. Geomorphology, 7, 36-44.

Downing, J.P. and Beach, R.A., (1989). *Laboratory apparatus for calibrating optical suspended solids.* Mar. Geol., 86: 243-249.

Duncan, W.J., Thom, A.S. and Young, A.D., (1970). *Mechanics of Fluids.* 2nd Edition, London, Arnold, 725 pp.

Dyer, K.R., (1986). *Coastal and Estuarine Sediment Dynamics.* Wiley & Sons, Chichester, 342pp.

Dyer, K.R., (1989). *Sediment processes in estuaries: future research requirements.* J. Geophys. Res., 94 (C10): 14,327-14,339.

Dyer, K.R., (1994). *Estuarine sediment transport and deposition.* In *Sediment transport and depositional processes* (Ed. Pye, K.), Pub. Blackwell Scientific Publications, 193-215.

Dyer, K.R., (1995). *Sediment transport processes in estuaries.* In: Geomorphology and Sedimentology of Estuaries (Ed. Perillo, G.M.E.), Elsevier Science, Oxford, 423-449.

Dyer, K.R., (1997). *Estuaries: A physical introduction.* 2nd Edition, Wiley & Sons Ltd., Chichester, 195 pp.

Dyer, K.R., Bale, A.J., Christie, M.C., Feates, N., Jones, S. and Manning, A.J., (2001a). *The turbidity maximum in a mesotidal estuary, the Tamar estuary, UK. Part I: Dynamics of suspended sediment.* INTERCOH 2000. Delft (in press).

Dyer, K.R., Bale, A.J., Christie, M.C., Feates, N., Jones, S. and Manning, A.J., (2001b). *The turbidity maximum in a mesotidal estuary, the Tamar estuary, UK. Part II: The floc properties.* INTERCOH 2000. Delft (in press).

Dyer, K.R., Cornelisse, J., Dearnaley, M.P., Fennessy, M.J., Jones, S.E., Kappenberg, J., McCave, I.N., Pejrup, M., Puls, W., Van Leussen, W., and Wolfstein, K., (1996). *A comparison of in-situ techniques for estuarine floc settling velocity measurements.* Journal of Sea Research, 36 (1-2): 15-29.

Dyer, K.R. and Manning, A.J., (1998). *Observation of the size, settling velocity and effective density of flocs, and their fractal dimensions.* Journal of Sea Research, 41: 87-95.

Edzwald, J.K. and O'Melia, C.R., (1975). *Clay distributions in recent estuarine sediments.* Clays and Clay Minerals, 23:39-44.

Eisma, D., (1993). *Suspended matter in the aquatic environment.* Pub. Springer-Verlag, Berlin, Heidelberg, Germany, 315 pp.

Eisma, D., (1986). *Flocculation and de-flocculation of suspended matter in estuaries.* Neth. Journal of Sea Res., 20 (2/3): 183-199.

Eisma, D., Schuhmacher, T., Boekel, H., Van Heerwaarden, J., Franken, H., Lann, M., Vaars, A., Eijgenraam, F. and Kalf, J., (1990). *A camera and image analysis system for in situ observation of flocs in natural waters.* Neth. J. Sea Res., 27: 43-56.

Eisma, D., Bernard, P., Cadee, G.C., Ittekkot, V., Kalf, J., Laane, R., Martin, J.M., Mook, W.G., Van Put, A. and Schuhmacher, T., (1991). *Suspended matter particle size in some west European estuaries.* Neth. J. Sea Res., 28 (3): 193-220.

Eisma, D., Boon, J., Groenewegen, R., Ittekkot, V., Kalf, J. and Mook, W.G., (1983). *Observations on macro-aggregates, particle size and organic composition of suspended matter in the Ems estuary.* Mitt. Geol.-Palaontol. Inst. niv. Hamburg, SCOPE/UNEP Sonderbereich, 55: 295-314.

Etcheber, H., (1978). *Etude de la repartition et du comportement de quelques oligo-elements metalliques (Zn, Pb, Cu, Ni) dans le complexe fluvio-estuarien de la Gironde.* These 3eme cycle Univ. Bordeaux 1, No. 1455, 2t., 169 pp.

Faas, R.W., (1984). *Time and density-dependent properties of fluid mud suspensions in NE Brazilian Continental Shelf.* Geo-Marine Letters, 4:147-152.

Feates, N.G., Hall, J.R., Mitchener, H.J. and Roberts, W., (1999). *COSINUS field experiment, Tamar estuary: measurement of properties of suspended sediment flocs and bed properties.* Hydraulics Research, Wallingford, Report No. TR 82, 8 pp.

Fennessy, M.J., (1994). *Development and testing of an instrument to measure estuarine floc size and settling velocity in-situ.* Ph.D. Thesis, University of Plymouth, 128 pp.

Fennessy, M.J. and Dyer, K.R., (1996). *Floc population characteristics measured with INSSEV during the Elbe estuary intercalibration experiment.* Journal of Sea Research, 36 (1-2): 55-62.

Fennessy, M.J., Dyer, K.R. and Huntley, D.A., (1994a). *INSSEV: an instrument to measure the size and settling velocity of flocs in-situ.* Marine Geology, 117: 107-117.

Fennessy, M.J., Dyer, K.R. and Huntley, D.A., (1994b). *Size and settling velocity distributions of flocs in the Tamar Estuary during a tidal cycle.* Netherlands Journal of Aquatic Ecology, 28: 275-282.

Fennessy, M.J., Dyer, K.R., Huntley, D.A. and Bale, A.J., (1997). *Estimation of settling flux spectra in estuaries using INSSEV.* Proc. INTERCOH'94, Wallingford, England. John Wiley & Son, Chichester, 87-104.

Fitzpatrick, F., (1991). *Studies of sediments in a tidal environment.* Ph.D. Thesis, Department of Geological Sciences, University of Plymouth, 221 pp.

Friedlander, S.K., (1977). *Smoke, dust and haze.* In Fundamentals of Aerosol Behaviour, Wiley, New York, 317 pp.

George, K.J., (1975). *The tides and tidal streams of the Tamar Estuary.* Ph.D. Thesis, University of London, 555 pp.

Gibbs, R.J., (1977). *Suspended sediment transport and the turbidity maximum.* In: Estuaries, Geophysics and the Environment, National Academy of Sciences, Washington, DC, 104-109.

Gibbs, R.J., (1983). *Coagulation rates of clay minerals and natural sediments.* J. Sed. Petrol. 53 (4), 1193-1203.

Gibbs, R.J., (1985). *Estuarine flocs: their size settling velocity and density.* J. Geophys. Res., 90 (C2): 3249-3251.

Gibbs, R.J. and Konwar, L.N., (1983). *Sampling of mineral flocs using Niskin bottles.* Environ. Sci. Technol., 17 (6): 374-375.

Glangeaud, L., (1939). *Le role de la suspension tourbillonnaire et de la traction sur le fond dans la formation des sediments de la Gironde.* C. r. Acad. Sci. Paris, 208: 1595.

Glasgow, L.A. and Kim, Y.H., (1989). *A review of the role of the physico-chemical environment in the production of certain floc properties.* Water, Air and Sea Pollution, 47:153-174.

Glasgow, L.A. and Lucke, R.H., (1980). *Mechanisms of deaggregation for clay-polymer flocs in turbulent systems.* Ind. Eng. Chem. Fundam., 19: 148-156.

Gratiot, N., (2000). *Etude experimentale de la formation des couches de crème de vase turbulentes.* Ph.D. Thesis, L'Universite Joseph-Fourier, Grenoble 1, France.

Gratiot, N., Mory, M. and Auchere, D., (2000). *An acoustic Doppler velocimeter (ADV) for the characterisation of turbulence in concentrated fluid mud.* Continental Shelf Research, (in press).

Gregory, J., (1978). *Effects of polymers on colloid stability.* In: *The Scientific Basis of Flocculation* (Ed. Ives, K.J.), Pub. Sijthoff & Noordhoff, Alphen aan den Rijn, The Netherlands: 89-99.

Gust, G. and Walger, E., (1976). *The influence of suspended cohesive sediments on boundary layer structure and erosive activity of turbulent seawater flows.* Marine Geology, 22: 189-206.

Hayter, E.J. and Mehta, A.J., (1982). *Modelling of estuarial fine sediment transport for tracking pollutant movement.* Final Report No. UFL/COEL-8L/009, University of Florida.

Heathershaw, A.D., (1979). *The turbulent structure of the bottom boundary layer in a tidal current.* Geophys. J. R. astr. Soc., 58: 395-430.

Hicks, G.F., (1988). *Sediment rafting: a novel mechanism for the small scale dispersal of intertidal estuarine meiofauna.* Marine Ecology – Progress series, 48: 69-80.

Hill, P.S., (1996). *Sectional and discrete representations of floc breakage in agitated suspensions.* Deep-Sea Res., 43: 679-702.

Hinze, J.O., (1975). *Turbulence.* 2nd edition, McGraw-Hill, New York.

Hopfinger, E.J. and Toly, J.A., (1976). *Spatially decaying turbulence and its relation to mixing across density interfaces.* J. Fluid Mech., 78: 155-175.

Houghton, J.T, Jenkins, G.J. and Ephraums, J.J., (1990). *Climate change: The intergovernmental panel on climate change* (Scientific Assessment). Pub. Cambridge University Press.

Hunt, J.R., (1986). *Particle aggregate break-up by fluid shear.* In: Mehta, A.J. (Ed.), Estuarine Cohesive Sediment Dynamics. Springer, Berlin, 85-109.

Jackson, G.A., (1990). *A model of the formation of marine algal flocs by physical coagulation processes.* Deep Sea Research, 37: 1197-1211.

Joint, I.R., (1983). *Measurement of microbial processes.* In: A.W. Morris (Ed.), Practical Procedures for Estuarine Studies. The Natural Environment Research Council, Chapter 4: 101-138.

Jones, S.E. and Jago, C.F., (1996). *Determination of settling velocity in the Elbe estuary using QUISSET tubes.* J. Sea Res., 36: 63-67.

Jouanneau, J.M., (1979). *Evaluation du volume et de la masse de matieres en en suspension dans le systeme bouchon vaseux crème de vase de la Gironde.* Bull. Inst. Geol. Bassin d'Aquitaine, Bordeaux, 25: 111-120.

Jouanneau, J.M. and Latouche, C., (1981). *The Gironde estuary.* In: Contributions to Sedimentology (Eds. Fuchtbauer, H., Lisitzyn, A.P., Milliman, J.D. and Seibold, E.), 10, 115 pp. Pub.: E. Schweizerbart'sche Verlagsbuchhandlung (Nagele u. Obermiller), Stuttgart, Germany. ISBN: 3510570103.

Kirby, R., (1986). *Suspended fine cohesive sediment in the Severn estuary and Inner Bristol channel.* Rept. ESTU-STP-4042, Department of Atomic Energy, Harwell, U.K.

Kitchener, J.A., (1972). *Principles of action of polymeric flocculants.* Br. Polymer, 4: 217-229.

Kolmogorov, A.N., (1941). *The local structure of turbulence in incompressible viscous fluid for very large Reynolds numbers.* C. R. Acad. Sci. URSS, 30: 301; Dissipation of energy in locally iscotropic turbulence. C. R. Acad. Sci. URSS, 32: 16.

Kramer, K. J. M., Warwick, R. M. and Brockmann, U.H., (1992). *Manual of sampling and analytical procedures for tidal estuaries.* Joint European Estuaries Project – JEEP 92.

Kranck, K., (1984). *The role of flocculation in the filtering of particulate matter in estuaries.* In: The Estuary as a Filter (Ed. Kennedy, V.), Academic Press, Orlando Inc, 159-175.

Kranck, K. and Milligan, T.G., (1988). *Macroflocs from diatoms: in-situ photography of particles in Bedford Basin, Nova Scotia.* Mar. Ecology. Prog. Ser., 4: 183-189.

Kranenburg, C., (1994). *The fractal structure of cohesive sediment aggregates.* Estuarine, Coastal and Shelf Science, 39: 451-460.

Krone, R.B., (1963). *A study of rheological properties of estuarial sediments.* Hyd. Eng. Lab. and Sanitary Eng. Lab., University of California, Berkeley, Report No. 63-68.

Krone, R.B., (1986). *The significance of aggregate properties to transport processes.* In Estuarine Cohesive Sediment Dynamics (Mehta, A. J., ed.), Springer-Verlag, Berlin, pp. 66-84.

La Mer, V.K. and Healy, T.W. (1963). *Adsorption-flocculation reactions of macro molecules at the solid-liquid interface.* Review of Pure Applied Chemistry 13: 112-132.

Latouche, C., (1971). *Les argiles des basisins alluvionnaires aquitains et des dependances oceaniques. Contribution a l'etude d'un environment.* These Doct, es Sci. Univ. Bordeaux 1, 415 pp.

Law, D.J., Bale, A.J. and Jones, S.E., (1997). *Adaptation of focused beam reflectance measurement to in-situ particle sizing in estuaries and coastal waters.* Marine Geology, 140: 47-59.

Leob, G.I. and Neihof, R.A., (1975). *Marine conditioning films.* Adv. Chem. Ser. 145: 319-335.

Li, M.Z. and Gust, G., (2000). *Boundary layer dynamics and drag reduction in flows of high cohesive sediment suspensions.* Sedimentology, 47: 71-86.

Lick, W., (1994). *Modelling the transport of sediment and hydrophobic contaminants in surface waters.* In: U. S. / Israel Workshop on monitoring and modelling water quality, May 8-13, 1994, Haifa, Israel.

Lick, W., Huang, H. and Jepsen, R., (1993). *Flocculation of fine-grained sediments due to differential settling.* J. Geophs. Res., 98 (C6): 10,279-10,288.

Lick, W. and Lick, J., (1988). *On aggregation and disaggregation of fine grained lake sediments.* Journal of Great Lakes Research, 14 (4): 514-523.

MacKinney G., (1941). *Absorption of light by chlorophyll solutions.* J. biol. C17ein. 140, 315-22.

Manning, A.J., (1996). *A laboratory study to examine the response of fine cohesive sediment suspensions to turbulent shearing.* M.Sc. Thesis. Institute of Marine Studies, University of Plymouth, 86 pp.

Manning, A.J., (2001). *The design and fabrication of the University of Plymouth research pontoon "R.P. AMAP-1".* Internal Report for Institute of Marine Studies, University of Plymouth (in prep).

Manning, A.J. and Dyer, K.R., (1999). *A laboratory examination of floc characteristics with regard to turbulent shearing.* Marine Geology, 160: 147-170.

Manning, A.J. and Dyer, K.R., (2001). *A comparison of floc properties observed during neap and spring tidal conditions.* INTERCOH 2000. Delft (in press).

Manning, A.J. and Fennessy, M.J., (1997). *INSSEV (In Situ Settling Velocity instrument) - 1.3: Operator Manual.* Internal Report for Institute of Marine Studies, University of Plymouth, 25 pp.

Manning, A.J., Dyer, K.R. and Christie, M.C., (2001). *Properties of macroflocs in the lower reaches of the Gironde estuary.* Proc. VII Colloque International D'Oceanographie Du Golfe De Gascogne, Biarritz, France, 4-6 April 2000 (in press).

Maude, A.D. and Whitmore, R.L., (1958). *A generalized theory of sedimentation.* Brit. J. Appl. Phys., 9: 477-482.

McCabe, J.C., (1991). *Observations of estuarine turbulence and floc size variations.* Ph.D. Thesis, Polytechnic South West, Plymouth, 118 pp.

McCave, I.N., (1975). *Vertical flux of particles in the ocean.* Deep-Sea Res., 22: 491-502.

McCave, I.N., (1979). *Suspended sediment.* In: Estuarine Hydrography and Sedimentation, Cambridge: Cambridge University Press.

McCave, I.N., (1984). *Size spectra and aggregation of suspended particles in the deep ocean.* Deep-Sea Res., 31: 329-352.

McDowell, D.N. and O'Connor, B.A., (1977). *Hydraulic behaviour of estuaries.* MacMillan, London, 292 pp.

Mehta, A.J. and Dyer, K.R., (1990). *Cohesive sediment transport in estuarine and coastal waters.* In *The Sea* (Ed. Le Mehaute, B. and Hanes, D.M.), Vol. 9, part B (*Ocean Engineering Science*), Wiley & Sons Ltd., 815-839.

Mehta, A.J. and Lott, J.W., (1987). *Sorting of fine sediment during deposition.* Proc. Specialty Conf. Advances in Understanding Coastal Sediment Processes. Am. Soc. Civ. Eng., New York, pp. 348-362.

Mehta, A.J. and Partheniades, E., (1975). *An investigation of the depositional properties of flocculated fine sediment.* J. Hydrol. Res., 92 (C13): 361-381.

Migniot, C., (1969). *Estuarie de la Gironde: synthese des phenomenes naturels. Etude de l'evolution des fonds.* Rapp. General Lab. Cent. Hydraul. Fr., Paris, 3.

Migniot, C., (1971). *L'evolution de la Gironde au cours des temps.* Bull. Inst. Geol. Bassin d'Aquitaine, Bordeaux, 11: 221-281.

Millero, F.J. and Poisson, A., (1981). *International one-atmosphere equation of state seawater.* Deep-sea Research, 28 (A): 625-629.

Mitchener, H.J., Whitehouse, R.J.S., Soulsby, R.L. and Lawford, V.A., (1996). *Estuarine morphodynamics – instrument development for mud erosion measurements. Development and testing of SedErode – Sediment Erosion Device.* HR Report No. TR 16, Hydraulics Research, Wallingford, October 1996.

Mory, M., Gratiot, N., Manning, A.J. and Michallet, H., (2001). *CBS layers in a diffusive turbulence grid oscillation experiment.* INTERCOH 2000, Delft (in press).

Nakagawa, H. and Nezu, I., (1975). *Turbulence in open channel flow over smooth and rough beds.* Proc. Japan Soc. Civ. Eng., 241: 155-168.

Neihof, R.A. and Leob, G.I., (1972). *The surface charge of particulate matter in seawater.* Limnol. Oceanography, 17: 7-16.

Neihof, R.A. and Leob, G.I., (1974). *Dissolved organic matter in seawater and the electrical charge of immersed surfaces.* J. Mar. Res. 32: 5-12.

Nishizawa, S., Fukuda, M. and Inque, H., (1954). *Photographic study of suspended matter and plankton in the sea.* Bull. Fac. Fish., Hokkaido Univ., 5: 36-40.

Nychas, S.G., Hershey, H.C. and Brodkey, R.S., (1973). A visual study of turbulent shear flow. J. Fluid Mech., 61: 513-540.

Offen, G.R. and Kline, S.J., (1975). *A proposed model of the bursting process in turbulent boundary layers.* J. Fluid Mech., 70: 209-228.

Officer, C.B., (1981). *Physical dynamics of estuarine suspended sediment.* Mar. Geol., 40: 1-14.

Owen, M.W., (1971). *The effects of turbulence on the settling velocity of silt flocs.* Proc. 14th Cong. Int. Assoc. Hydraul. Res. (Paris), pp. D4-1 - D4-6.

Owen, M.W., (1976). *Determination of the settling velocities of cohesive muds.* Hydraulics Research, Wallingford, Report No. IT 161, 8 pp.

Oseen, C.W., (1927). *Neuere methoden und ergebnisse.* Hydrodynamik, Akad Verlagsges, leipzig.

Pandya, J.D. and Spielman, L.A., (1982). *Floc break-up in agitated suspensions: theory and data processing strategy.* J. Colloid Interface Science, 90: 517-531.

Parker, D.S., Kaufman, W.J. and Jenkins, D., (1972). *Floc break-up in turbulent flocculation processes.* J. Sanitary Eng. Div., Proc. Am. Soc. Civil Eng., 98 (SA1): 79-97.

Parker, W. and Kirby, R., (1982). *Time dependent properties of cohesive sediment relevant to sedimentation management – a European experience.* In Estuarine Comparisons (Ed. Kennedy, V.S.), Academic Press, New york, 573-589.

Partheniades, E., (1965). *Erosion and deposition of cohesive soils.* J. Hydr. Div., Proc. Am. Soc. Civ. Engrs., 98: 79-99.

Paterson, D.M., (1989). *Short term changes in the erodibility of intertidal cohesive sediment related to the migratory behaviour of epipelic diatoms.* Limnology and Oceanography, 34 (1): 223-234.

Perrillo, G.M.E., (Ed., 1995). *Geomorphology and sedimentology of estuaries.* Elsevier, Amsterdam, 471 pp.

Peterson, O., Vested, H.J., Manning, A.J., Christie, M.C. and Dyer, K.R., (2001). *Numerical modelling of mud transport in the Tamar Estuary.* INTERCOH 2000, Delft (in press).

Postma, H., (1980). *Sediment transport and sedimentation.* In: *Chemistry and Biogeochemistry of Estuaries* (Ed. Olausson, E. and Cato, I.), John Wiley & Sons, 154-186.

Prandtl, L., (1938). *On fully developed turbulence.* Translated in: Modern Developments in Fluid Dynamics (Ed. Goldstein, S.), Vol. 1, Oxford, Oxford University Press.

Reynolds, O., (1895). *On the dynamical theory of incompressible viscous fluids and the determination of the criterion.* Philosophical Transactions of the Royal Society, 186A: 123-164.

Rodi, W., (1980). Turbulence models and their application in hydraulics. Int. Assoc. Hydr. Res., Delft, The Netherlands.

Ross, M.A., (1988). *Vertical structure of estuarine fine sediment suspensions.* Ph.D. thesis, University of Florida, Gainesville.

Ruehrwein, R.A. and Ward, D.W., (1952). *Mechanism of clay aggregation by polyelectrolytes.* Soil Science, 73: 485-492.

Shanks, A.L. and Trent, J.D., (1979). *Marine snow: microscale nutrient patches.* Limnol. Oceanogr., 24: 850-854.

Shannon, C.E., (1949). *Communication in the presence of noise.* Proc. Inst. Radio Eng., 37 (1): 10-21.

Soulsby, R.L., (1983). *The bottom boundary layer of shelf seas.* In: Physical Oceanography of Coastal and Shelf Seas (Ed. Johns, B), Elsevier, New York, 189-266.

Soulsby, R.L. and Humphery, J.D., (1989). *Field observations of wave-current interaction at the sea bed.* In: Proc. NATO Advanced Research Workshop on Water Wave Kinematics (Eds. Torum, A. and Gudmestad, O.T.), Kluwer Academic Publ. B. V., Dordrecht, 423-428.

Stapleton, K.R. and Huntley, D.A., (1995). *Sea bed stress determinations using the inetial dissipation method and the turbulent kinetic energy method.* Earth Surface Processes and Landforms, 20: 807-815.

Stephens, J.A., Uncles, R.J., Barton, M.L. and Fitzpatrick, F., (1992). *Bulk properties of intertidal sediments in a muddy, macrotidal estuary.* Marine Geology, 103: 445-460.

Stolzenbach, K.D. and Elimelich, M., (1994). *The effect of density on collisions between sinking particles: implications for particle aggregation in the ocean.* Journal of Deep Sea Research I, 41 (3):469-483.

Strickland, J. D. H. and T. R. Parsons., (1972). *A Practical Handbook of Seawater Analysis.* Fisheries Research Board of Canada, 167 pp.

Ten Brinke, W.B.M., (1993). *The impact of biological factors on the deposition of fine grained sediment in the Oosterschelde (The Netherlands).* Ph.D. Thesis, University of Utrecht, The Netherlands, 252pp.

Tennekes, H. and Lumley, J.L., (1972). *A first course of turbulence.* MIT Press, Cambridge.

Tambo, N. and Hozumi, H., (1979). Water Research, 13:409-419. *Physical characteristics of flocs – II. Strength of flocs.*

Toorman, E.A., (1997). *Sedimentation and self-weight consolidation: constitutive equations and numerical modelling.* Geotechnique 49 (6): 709-726.

Toorman, E.A. and Berlamont, J., (1999). *EC MAST III COSINUS project – home page, executive summary* (*URL* http://sun-hydr-01.bwk.kuleuven.ac.be/COSINUS/cosinus.html).

Tsai, C.H., Iacobellis, S. and Lick, W., (1987). *Flocculation of fine-grained sediments due to a uniform shear stress.* J. Great Lakes Res., 13: 135-146.

Tsai, C.H. and Lick, W., (1988). *Resuspension of sediments from Long Island Sound.* Water Science and Technology, 20 (6/7): 155-164.

Uncles, R.J., Bale, A.J., Howland, R.J.M., Morris, A.W. and Elliott, R.C.A., (1983). *Salinity of surface water in a partially-mixed estuary, and its dispersion at low run-off.* Oceanologica Acta, 6: 289-296.

Uncles, R.J., Barton, M.L. and Stephens, J.A., (1994). *Seasonal variability of fine-sediment concentrations in the turbidity maximum region of the Tamar estuary.* Estuarine, Coastal and Shelf Science, 38: 19-39.

Uncles, R.J., Elliott, R.C.A. and Weston, S.A., (1985). *Observed fluxes of water, salt and suspended sediment in a partly mixed estuary.* Estuarine, Coastal and Shelf Science, 20: 147-167.

Uncles, R.J. and Jordan, M.B., (1980). *A one-dimensional representation of residual currents in the Severn Estuary.* Estuarine, Coastal and Shelf Science, 10: 36-60.

Uncles, R.J. and Stephens, J.A., (1993). *Nature of the tubidity maximum in the Tamar estuary, U.K.* Estuarine, Coastal and Shelf Science, 36: 413-431.

Underwood, G. J. C., Paterson, D. M. and Parkes, R. J., (1995). *The measurement of microbial carbohydrate exopolymers from intertidal sediments.* Limnology Oceanography. 40 (7), 1243-1253.

Van de Ven, T.G. and Hunter, R.J., (1977). *The energy dissipation in sheared coaggulated soils.* Rheologica Acta, 16, 534-543.

Van Leussen, W., (1988). *Aggregation of particles, settling velocity of mud flocs : A review.* In Physical Processes in Estuaries (Dronkers, J. and W. van Leussen, ed.), Springer-Verlag, Berlin. pp. 347-403.

Van Leussen, W., (1991). *Fine sediment transport under tidal action.* Geo-Marine Letters, 11:119-126.

Van Leussen, W., (1994). *Estuarine macroflocs and their role in fine-grained sediment transport.* Ph.D. Thesis, University of Utrecht, The Netherlands, 488pp.

Van Leussen, W. and Cornelisse, J.M., (1994). *The determination of the sizes and settling velocities of estuarine flocs by an underwater video system.* Neth. J. Sea Res., 31 (3): 231-241.

Van Olphen, H., (1977). *An introduction to clay colloid chemistry. For clay technologists, geologists, and soil scientists.* 2nd edition, John Wiley and Sons, New York, London, 318 pp.

Von Helmholtz, H., (1858). *Uber Intergrale der hydrodynamischen Gleichungen, welche den Wisbelbewegungen extsprechen.* Wiss. Abn. 1: 101.

Wacholder, E. and Sather, N.F., (1974). *The hydrodynamic interaction of two unequal spheres moving under gravity through quiescent viscous fluid.* Journal of Fluid Mechanics, Vol. 5, 417-437.

Wells, J.T., (1989). *In-situ measurements of large aggregates over a fluid mud bed.* J. Coastal Res., Spec. Issue, 5: 75-86.

Wentworth, C.K., (1922). *A scale of grade and class terms for clastic sediments.* J. Geol., 30: 377-392.

Whitehouse, R.J.S., Soulsby, R.L., Roberts, W. and Mitchener, H.J., (1999). *Dynamics of estuarine muds: a manual for practical applications.* Hydraulics Research, Wallingford, Report No. SR 527, 77 pp.

Winterwerp, J.C., (1997). *A simple model for turbulence induced flocculation of cohesive sediment.* IAHR., J. Hydraulic Eng., Vol. 36, No. 3, 309-326.

Winterwerp, J.C., (1999). *On the dynamics of high-concentrated mud suspensions.* Ph.D. Thesis, Delft University of Technology, Faculty of Civil Engineering and Geosciences, The Netherlands, 172 pp.

INSSEV macrofloc and microfloc multiple regression data set for Tamar estuary experiments 1 and 2.

DATE	INSSEV sample	Time BST (hrs)	Estuary	Tide	SPM (mgl^{-1})	TSS (Nm^{-2})	G (s^{-1})	Kolmogorov eddy size (μm)	Ws_{macro} (mms^{-1})	Ws_{macro} error bar (±)	ρe_{macro} (kgm^{-3})	nf_{macro}	$Porosity_{macro}$ (%)	Ws_{micro} (mms^{-1})	Ws_{micro} error bar (±)	ρe_{micro} (kgm^{-3})	nf_{micro}	$Porosity_{micro}$ (%)	SPM_{macro} (%)	SPM_{micro} (%)	SPM ratio	MSF_{macro} (%)	MSF_{micro} (%)	MSF ratio	MSF ($mg.m^{-3}e^{-1}$)	Q_c value
240698	1	12:13	Tamar	spring	971	0.53	7.64	369	2.40	0.12	214	2.47	83.0	1.00	0.05	519	2.62	58.6	80.0	20.0	4.0	90.6	9.4	9.6	2059	1.082
240698	2	12:35	Tamar	spring	885	0.47	6.95	387	3.00	0.16	112	2.35	91.0	1.40	0.07	286	2.43	77.2	78.0	22.0	3.5	88.4	11.6	7.6	2343	1.088
240698	3	13:00	Tamar	spring	675	0.21	3.75	527	2.40	0.12	119	2.31	90.6	1.03	0.05	214	2.32	83.0	58.0	42.0	1.4	76.3	23.7	3.2	1231	1.145
240698	4	13:12	Tamar	spring	815	0.21	3.87	518	2.46	0.12	97	2.30	92.3	0.84	0.04	235	2.28	81.3	49.8	50.2	1.0	74.4	25.6	2.9	1014	1.242
240698	5	13:34	Tamar	spring	487	0.14	2.82	608	1.61	0.08	104	2.28	91.7	0.54	0.03	152	2.16	87.6	52.0	48.0	1.1	76.3	23.7	3.2	533	1.193
240698	6	15:10	Tamar	spring	690	0.47	6.98	386	2.80	0.14	141	2.38	88.8	1.34	0.07	302	2.38	76.0	69.0	31.0	2.2	82.3	17.7	4.6	1620	1.269
240698	7	15:30	Tamar	spring	2637	0.59	8.23	355	2.90	0.15	112	2.35	91.1	1.03	0.05	255	2.36	79.7	91.0	9.0	10.1	96.6	3.4	28.6	7203	1.177
240698	8	15:41	Tamar	spring	4501	0.43	6.53	399	5.00	0.25	162	2.45	87.1	1.10	0.06	396	2.49	68.5	94.0	6.0	15.7	98.6	1.4	71.2	21452	0.965
240698	9	15:59	Tamar	spring	5571	0.36	5.67	428	5.50	0.28	140	2.44	88.8	1.20	0.06	351	2.48	72.0	95.6	4.4	21.7	99.0	1.0	99.6	29586	0.802
240698	10	16:17	Tamar	spring	4227	0.28	4.74	469	4.80	0.24	176	2.34	93.9	0.88	0.04	238	2.29	81.0	91.0	9.0	10.1	98.2	1.8	55.5	18798	0.792
240698	11	16:37	Tamar	spring	2579	0.25	4.43	485	3.37	0.17	121	2.34	90.3	1.10	0.05	228	2.27	81.8	81.5	18.5	4.4	93.1	6.9	13.5	7604	0.861
40898	1	15:19	Tamar	neap	53	0.15	2.97	592	1.55	0.08	61	2.19	95.1	0.64	0.03	64	2.12	94.9	77.0	23.0	3.3	89.0	11.0	8.1	71	0.964
40898	2	15:28	Tamar	neap	48	0.13	2.83	629	1.35	0.07	38	2.10	97.0	0.44	0.02	92	2.05	92.7	65.0	35.0	1.9	85.1	14.9	5.7	50	0.989
40898	3	15:39	Tamar	neap	38	0.10	2.23	683	1.86	0.08	58	2.19	95.4	0.41	0.02	108	2.11	91.4	46.6	53.4	0.9	78.0	22.0	3.6	38	0.859
40898	4	16:00	Tamar	neap	34	0.07	1.81	804	1.29	0.06	54	2.15	95.7	0.54	0.03	165	2.31	86.9	68.9	31.1	2.2	84.2	15.8	5.3	36	0.796
40898	5	16:20	Tamar	neap	26	0.04	1.10	972	1.05	0.05	69	2.21	94.5	0.30	0.01	102	2.00	91.9	34.1	65.9	0.5	64.6	35.4	1.8	14	0.685
40898	6	16:37	Tamar	neap	25	0.11	2.33	669	1.70	0.09	54	2.20	95.7	0.50	0.03	83	2.11	93.4	73.5	26.5	2.8	90.4	9.6	9.4	35	0.895
50898	1	10:42	Tamar	neap	136	0.36	5.67	428	1.53	0.08	86	2.24	93.1	0.93	0.05	219	2.34	82.5	59.0	41.0	1.4	70.3	29.7	2.4	175	0.938
50898	2	10:53	Tamar	neap	131	0.32	5.26	445	2.70	0.14	88	2.25	93.0	0.77	0.04	164	2.25	86.9	49.9	50.1	1.0	77.7	22.3	3.5	227	0.765
50898	3	11:11	Tamar	neap	122	0.25	4.40	486	1.40	0.07	96	2.26	92.2	0.63	0.03	154	2.22	87.7	35.0	65.0	0.5	54.4	45.6	1.2	110	0.866
50898	4	11:28	Tamar	neap	120	0.15	3.03	586	1.84	0.09	90	2.26	92.8	0.59	0.03	187	2.23	86.7	38.6	61.4	0.6	66.1	33.9	1.9	129	1.054
50898	5	11:44	Tamar	neap	102	0.12	2.58	635	1.11	0.06	67	2.17	94.7	0.58	0.03	118	2.19	90.6	42.7	57.3	0.7	59.0	41.0	1.4	82	0.876
50898	6	12:14	Tamar	neap	78	0.08	1.85	750	1.31	0.07	92	2.24	92.7	0.52	0.03	154	2.18	87.8	23.7	76.3	0.3	43.8	56.2	0.8	55	1.186
50898	7	12:46	Tamar	neap	96	0.07	1.60	807	0.81	0.04	54	2.13	95.7	0.34	0.02	174	2.18	86.2	30.7	69.3	0.4	51.7	48.3	1.1	46	0.934
50898	8	13:04	Tamar	neap	138	0.18	3.34	558	2.20	0.11	95	2.28	92.5	0.81	0.04	211	2.31	83.2	48.4	51.6	0.9	71.8	28.2	2.5	205	0.850
50898	9	13:25	Tamar	neap	262	0.22	4.01	510	2.21	0.11	97	2.29	92.3	0.86	0.04	250	2.36	80.1	75.0	25.0	3.0	88.5	11.5	7.7	491	1.005
50898	10	13:46	Tamar	neap	492	0.39	6.01	416	3.10	0.16	89	2.33	93.0	0.97	0.05	121	2.23	90.4	72.0	28.0	2.6	89.2	10.8	8.2	1232	0.787
50898	11	14:41	Tamar	neap	223	0.16	3.17	573	1.58	0.08	103	2.28	91.8	0.84	0.04	194	2.33	84.5	53.9	46.1	1.2	69.9	30.1	2.3	288	0.857
50898	12	15:06	Tamar	neap	107	0.11	2.29	675	1.12	0.06	58	2.16	95.4	0.73	0.04	130	2.22	89.7	72.0	28.0	2.6	79.9	20.1	4.0	108	0.808
50898	13	15:25	Tamar	neap	91	0.10	2.19	689	1.60	0.08	52	2.15	95.8	0.66	0.03	96	2.14	92.4	73.0	27.0	2.7	86.7	13.3	6.5	123	0.859
50898	14	15:43	Tamar	neap	38	0.13	2.69	622	1.90	0.10	57	2.18	95.5	0.64	0.03	84	2.09	93.3	73.2	26.8	2.7	89.0	11.0	8.1	59	1.307
50898	15	15:56	Tamar	neap	32	0.09	2.05	713	1.53	0.08	58	2.17	95.4	0.55	0.03	132	2.11	89.5	71.7	28.3	2.5	87.6	12.4	7.1	40	0.675
60898	1	10:32	Tamar	neap	385	0.55	7.89	363	1.91	0.10	158	2.40	87.4	1.24	0.06	377	2.54	69.9	74.6	25.4	2.9	81.9	18.1	4.5	675	0.915
60898	2	11:02	Tamar	neap	328	0.53	7.65	369	2.00	0.10	110	2.34	91.2	1.24	0.06	193	2.37	84.6	66.0	34.0	1.9	75.8	24.2	3.1	571	1.139
60898	3	11:15	Tamar	neap	310	0.57	8.02	360	1.61	0.08	73	2.20	94.2	1.06	0.05	160	2.30	87.3	68.0	32.0	2.1	76.3	23.7	3.2	445	1.197
60898	4	11:30	Tamar	neap	291	0.56	7.91	363	2.12	0.11	104	2.29	91.7	0.76	0.04	162	2.24	87.1	59.0	41.0	1.4	80.2	19.8	4.0	454	1.037
60898	5	11:53	Tamar	neap	313	0.37	5.78	424	2.10	0.11	118	2.32	90.6	1.15	0.06	196	2.33	84.4	62.0	38.0	1.6	74.9	25.1	3.0	544	1.144
60898	6	12:06	Tamar	neap	325	0.35	5.60	431	2.42	0.12	96	2.26	92.4	1.00	0.05	186	2.32	85.2	46.0	54.0	0.9	67.4	32.6	2.1	537	1.089
60898	7	12:19	Tamar	neap	295	0.34	5.48	436	2.50	0.13	86	2.24	93.1	1.04	0.05	220	2.36	82.5	47.0	53.0	0.9	68.0	32.0	2.1	510	0.893
60898	8	12:30	Tamar	neap	256	0.28	4.74	469	2.40	0.12	101	2.22	91.9	0.88	0.04	172	2.20	86.3	49.0	51.0	1.0	72.4	27.6	2.6	416	0.938
60898	9	12:50	Tamar	neap	152	0.20	3.62	536	2.30	0.12	111	2.32	91.2	0.72	0.04	158	2.25	87.4	50.0	50.0	1.0	76.3	23.7	3.2	230	1.135

INSSEV macrofloc and microfloc multiple regression data set for Tamar estuary experiment 3.

DATE	INSSEV sample	Time BST (hrs)	Estuary	Tide	SPM (mgl^{-1})	TSS (Nm^{-2})	G (s^{-1})	Kolmogorov eddy size (μm)	Ws_{macro} (mms^{-1})	Ws_{macro} error bar (±)	ρs_{macro} (kgm^{-3})	nf_{macro}	$Porosity_{macro}$ (%)	We_{macro} (mms^{-1})	We_{micro} error bar (±)	ρs_{micro} (kgm^{-3})	nf_{micro}	$Porosity_{micro}$ (%)	SPM_{macro} (%)	SPM_{micro} (%)	SPM ratio	MSF_{macro} (%)	MSF_{micro} (%)	MSF ratio	MSF ($mg.m^{-2}s^{-1}$)	Q_c value
150998	4	16:11	Tamar	neap	10	0.04	1.20	931	0.71	0.04	62	2.14	95.0	0.30	0.02	432	2.46	85.6	47.0	53.0	0.9	67.7	32.3	2.1	5	1.061
150998	5	16:33	Tamar	neap	24	0.09	2.02	717	1.00	0.05	52	2.13	95.8	0.54	0.03	63	2.06	95.0	64.0	36.0	1.8	76.8	23.2	3.3	20	0.940
150998	6	16:41	Tamar	neap	32	0.14	2.81	609	1.44	0.07	80	2.21	93.7	0.60	0.03	49	1.88	96.1	59.3	40.7	1.5	77.7	22.3	3.5	36	0.954
150998	7	16:57	Tamar	neap	115	0.17	3.21	569	2.05	0.10	58	2.16	95.4	0.70	0.04	111	2.13	91.2	69.0	31.0	2.2	86.7	13.3	6.5	188	0.964
150998	8	17:08	Tamar	neap	271	0.27	4.60	475	2.29	0.11	77	2.24	93.8	0.87	0.04	134	2.20	89.4	77.4	22.6	3.4	90.0	10.0	9.0	534	1.102
150998	9	17:31	Tamar	neap	80	0.25	4.28	493	1.83	0.09	79	2.24	93.7	0.97	0.05	172	2.29	88.3	72.0	28.0	2.6	82.9	17.1	4.9	127	1.160
160998	2	11:22	Tamar	neap	20	0.15	2.97	592	1.34	0.07	67	2.20	94.6	0.64	0.03	127	2.18	89.9	59.9	40.1	1.5	75.8	24.2	3.1	21	1.470
160998	3	12:12	Tamar	neap	92	0.16	3.13	577	1.87	0.09	95	2.27	92.4	0.80	0.04	258	2.45	79.4	66.0	34.0	1.9	81.9	18.1	4.5	138	0.867
160998	4	12:15	Tamar	neap	94	0.20	3.70	530	2.22	0.11	93	2.26	92.6	0.73	0.04	186	2.26	85.2	59.0	41.0	1.4	81.3	18.7	4.4	151	1.309
160998	5	13:05	Tamar	neap	68	0.16	3.09	581	2.01	0.10	85	2.25	93.2	0.67	0.03	158	2.23	87.4	74.5	25.5	2.9	89.6	10.2	8.8	113	1.214
160998	6	13:39	Tamar	neap	21	0.07	1.71	780	1.25	0.06	66	2.19	94.7	0.58	0.03	121	2.17	90.4	48.0	52.0	0.9	66.6	33.4	2.0	19	1.113
160998	9	13:54	Tamar	neap	16	0.07	1.61	805	1.31	0.07	50	2.14	96.0	0.48	0.02	102	2.13	91.9	64.0	36.0	1.8	82.8	17.2	4.8	16	1.159
160998	10	14:06	Tamar	neap	13	0.05	1.40	863	0.95	0.05	49	2.12	96.1	0.38	0.02	79	2.04	93.7	53.9	46.1	1.2	74.5	25.5	2.9	9	1.109
160998	11	14:21	Tamar	neap	12	0.07	1.65	794	1.10	0.06	43	2.11	47.4	0.42	0.02	82	1.94	93.5	48.5	51.5	0.9	71.2	28.8	2.5	9	1.299
160998	18	17:28	Tamar	neap	34	0.09	1.99	723	1.40	0.07	43	2.16	96.6	0.56	0.03	447	2.45	64.4	47.4	52.6	0.9	69.3	30.7	2.3	32	0.791
160998	19	17:40	Tamar	neap	34	0.11	2.37	682	1.38	0.07	108	2.29	91.4	0.65	0.03	28	1.65	97.8	45.0	55.0	0.8	63.4	36.6	1.7	33	0.879
170998	1	13:21	Tamar	neap	498	0.60	8.39	352	1.44	0.07	65	2.24	93.2	0.89	0.04	208	2.31	83.4	66.8	33.2	2.0	76.5	23.5	3.3	626	0.902
170998	2	13:35	Tamar	neap	368	0.57	8.02	360	2.13	0.11	112	2.31	91.1	0.80	0.04	145	2.21	88.5	64.2	35.8	1.8	82.6	17.4	4.8	606	1.155
170998	3	13:45	Tamar	neap	588	0.34	5.45	437	3.30	0.17	130	2.38	89.6	0.94	0.05	150	2.19	88.0	61.6	38.4	1.6	84.9	15.1	5.6	1408	0.881
170998	5	14:08	Tamar	neap	434	0.27	4.58	476	2.48	0.12	51	2.23	95.9	0.92	0.05	194	2.43	84.5	82.0	18.0	4.6	92.5	7.5	12.3	954	0.986
170998	6	14:23	Tamar	neap	266	0.23	4.14	501	2.00	0.10	62	2.18	95.0	0.81	0.04	108	2.21	91.4	55.8	44.2	1.3	75.7	24.3	3.1	392	0.810
170998	7	14:57	Tamar	neap	82	0.12	2.52	642	2.00	0.10	134	2.33	89.3	0.64	0.03	294	2.33	76.6	47.0	53.0	0.9	73.5	26.5	2.8	105	1.049
170998	8	15:05	Tamar	neap	47	0.13	2.84	627	1.90	0.09	89	2.21	94.5	0.67	0.03	72	2.09	94.3	42.5	57.5	0.7	67.7	32.3	2.1	56	1.263
170998	9	15:12	Tamar	neap	38	0.11	2.39	659	1.18	0.06	49	2.13	96.1	0.49	0.02	106	2.14	91.5	49.0	51.0	1.0	69.9	30.1	2.3	31	1.198
170998	10	15:24	Tamar	neap	40	0.15	2.90	599	1.69	0.08	70	2.20	94.5	0.57	0.03	119	2.15	90.5	45.0	55.0	0.8	70.7	29.3	2.4	43	1.332
210998	1	12:26	Tamar	spring	3071	0.53	7.60	370	3.64	0.18	79	2.27	93.7	0.83	0.04	142	2.24	88.7	90.0	10.0	9.0	97.5	2.5	39.6	10314	1.293
210998	2	12:41	Tamar	spring	2771	0.52	7.52	372	3.37	0.17	86	2.29	93.2	0.69	0.04	111	2.10	91.2	89.2	10.8	8.3	96.9	3.1	31.2	8606	1.258
210998	3	13:04	Tamar	spring	2114	0.58	8.18	357	3.35	0.17	75	2.27	94.0	0.88	0.04	115	2.15	90.8	84.2	15.8	5.3	95.3	4.7	20.3	6257	1.448
210998	4	13:15	Tamar	spring	1974	0.66	9.24	335	2.19	0.11	78	2.23	93.8	0.51	0.03	86	2.00	93.2	82.5	17.5	4.7	95.3	4.7	20.4	3740	1.078
210998	5	14:59	Tamar	spring	1142	0.42	6.43	402	2.79	0.14	139	2.36	88.9	1.26	0.06	236	2.36	81.2	68.4	31.6	2.2	82.8	17.2	4.8	2838	1.402
210998	6	15:10	Tamar	spring	928	0.46	6.92	388	2.69	0.13	116	2.32	90.8	1.09	0.05	178	2.25	85.8	66.0	34.0	1.9	82.7	17.3	4.8	1995	0.835
210998	7	15:56	Tamar	spring	4500	0.33	6.65	396	4.70	0.24	88	2.36	92.2	1.07	0.05	93	2.04	92.6	94.2	5.8	16.2	98.6	1.4	71.0	20198	0.929
220998	3	11:44	Tamar	spring	1700	0.29	4.82	464	3.14	0.16	241	2.46	80.8	1.21	0.06	208	2.33	83.5	73.2	26.8	2.7	87.6	12.4	7.1	4461	0.845
220998	4	12:07	Tamar	spring	2380	0.55	7.82	365	2.55	0.13	104	2.31	91.7	0.85	0.04	175	2.26	88.1	82.6	17.4	4.7	93.4	6.6	14.2	5366	1.092
220998	5	12:18	Tamar	spring	2643	0.69	9.33	334	1.97	0.10	102	2.29	91.9	0.58	0.03	217	2.33	82.7	86.5	13.5	6.4	95.6	4.4	21.8	4701	0.946
220998	6	12:34	Tamar	spring	2337	0.70	9.44	332	2.33	0.12	121	2.33	90.4	0.68	0.03	244	2.44	80.5	82.6	17.4	4.7	94.2	5.8	16.3	4779	0.826
220998	7	16:10	Tamar	spring	858	0.44	6.63	396	3.00	0.15	168	2.44	86.6	1.00	0.05	305	2.44	75.7	73.4	26.6	2.8	89.2	10.8	8.3	2118	1.027
220998	9	17:30	Tamar	spring	8558	0.29	4.80	466	5.80	0.29	73	2.32	94.2	0.94	0.05	170	2.22	88.4	92.3	7.7	12.0	98.7	1.3	74.0	46434	0.900
220998	11	17:49	Tamar	spring	4221	0.24	4.22	497	4.22	0.21	65	2.28	94.8	0.85	0.04	119	2.22	90.5	90.9	9.1	10.0	98.0	2.0	49.7	18520	0.971
220998	12	17:56	Tamar	spring	3592	0.20	3.71	529	3.00	0.15	92	2.29	92.7	0.80	0.04	233	2.35	81.4	91.0	9.0	10.1	97.4	2.6	37.9	10085	0.912
220998	13	18:04	Tamar	spring	3130	0.19	3.51	544	3.40	0.17	83	2.25	93.4	0.73	0.04	161	2.23	87.1	85.4	14.6	5.8	96.5	3.5	27.3	9421	0.844
220998	14	18:08	Tamar	spring	2734	0.22	3.95	513	3.30	0.17	98	2.28	92.2	0.89	0.04	183	2.26	85.5	82.0	18.0	4.6	94.4	5.6	16.9	7836	0.785
230998	1	11:12	Tamar	spring	769	0.51	7.48	373	2.68	0.13	89	2.30	92.9	0.95	0.05	182	2.30	85.5	65.6	34.4	1.9	84.3	15.7	5.4	1604	0.879
230998	2	11:24	Tamar	spring	925	0.53	7.64	369	2.30	0.12	88	2.22	94.6	0.77	0.04	139	2.21	88.9	59.7	40.3	1.5	81.6	18.4	4.4	1557	0.903
230998	3	11:41	Tamar	spring	1234	0.60	8.39	352	2.10	0.11	72	2.24	94.3	0.72	0.04	151	2.23	87.9	66.0	34.0	1.9	84.9	15.1	5.6	2014	0.883
230998	4	11:56	Tamar	spring	1910	0.53	7.64	369	2.54	0.13	61	2.23	95.1	1.11	0.06	211	2.36	83.2	78.0	22.0	3.5	89.0	11.0	8.1	4254	1.152
230998	5	12:14	Tamar	spring	4850	0.58	8.13	358	4.00	0.20	91	2.30	92.7	0.97	0.05	80	2.03	95.2	95.9	4.2	23.1	99.0	1.0	95.2	18790	0.712
230998	6	12:29	Tamar	spring	4394	0.40	6.18	410	4.15	0.21	95	2.33	92.4	1.10	0.06	95	2.07	92.4	95.3	4.7	20.3	98.7	1.3	78.5	17605	0.966
230998	7	12:44	Tamar	spring	3150	0.37	5.80	423	4.00	0.20	94	2.35	92.5	1.06	0.05	194	2.33	84.5	93.0	7.0	13.3	98.0	2.0	50.1	11952	1.037
230998	8	12:54	Tamar	spring	3400	0.26	4.48	462	3.86	0.19	94	2.35	92.5	0.72	0.04	147	2.25	88.3	88.0	12.0	7.3	97.5	2.5	39.4	11842	0.884

Appendix II – *IN-SITU Macrofloc and microfloc multiple regression data sets (continued).*

INSSEV macrofloc and microfloc multiple regression data set for Gironde estuary SWAMGIR1 experiment.

DATE	INSSEV sample	Time BST (hrs)	Estuary	Tide	SPM (mgl^{-1})	TSS (Nm^{-2})	G (s^{-1})	Kolmogorov eddy size (μm)	Ws_{macro} (mms^{-1})	Ws_{macro} error bar (±)	ρB_{macro} (kgm^{-3})	nf_{macro}	$Porosity_{macro}$ (%)	Ws_{micro} (mms^{-1})	Ws_{micro} error bar (±)	ρB_{micro} (kgm^{-3})	nf_{micro}	$Porosity_{micro}$ (%)	SPM_{micro} (%)	SPM_{micro} (%)	SPM ratio	MSF_{macro} (%)	MSF_{micro} (%)	MSF ratio	MSF ($mg.m^{-2}s^{-1}$)	Q_s value
230699	3	10:58	Gironde	neap	81	0.43	8.56	398	2.10	0.11	78	2.19	94.8	0.50	0.03	120	2.16	90.4	21.0	79.4	0.3	52.0	48.0	1.1	211	1.286
230699	4	11:17	Gironde	neap	101	0.52	7.55	371	1.84	0.09	79	2.23	93.7	0.49	0.02	100	2.12	92.0	43.2	56.8	0.8	73.9	26.1	2.8	235	1.045
230699	5	11:29	Gironde	neap	103	0.45	6.75	393	2.16	0.11	112	2.31	91.1	0.57	0.03	123	2.18	90.2	26.6	73.4	0.4	57.9	42.2	1.4	282	0.907
230699	6	11:40	Gironde	neap	107	0.46	6.87	389	2.14	0.11	65	2.18	95.2	0.42	0.02	139	2.14	89.0	48.3	51.7	0.9	82.9	17.1	4.8	274	0.701
230699	7	11:55	Gironde	neap	112	0.47	6.97	388	2.00	0.10	55	2.14	95.8	0.53	0.03	135	2.20	89.2	37.5	62.5	0.8	56.3	43.7	1.3	295	1.051
230699	8	12:18	Gironde	neap	139	0.49	6.84	390	2.35	0.12	64	2.10	96.0	0.61	0.03	147	2.21	89.3	35.2	64.8	0.5	65.7	34.3	1.9	412	0.791
230699	9	12:45	Gironde	neap	78	0.39	6.06	414	1.94	0.10	101	2.28	92.0	0.54	0.03	137	2.20	89.1	56.1	43.9	1.3	82.2	17.8	4.6	193	1.125
230699	10	13:04	Gironde	neap	68	0.43	6.55	398	1.98	0.10	70	2.25	94.4	0.54	0.03	115	2.18	90.8	42.8	57.2	0.7	73.3	26.7	2.8	172	0.932
230699	11	13:19	Gironde	neap	59	0.33	5.40	439	2.20	0.11	103	2.24	93.7	0.61	0.03	155	2.23	87.6	27.8	72.2	0.4	53.3	46.7	1.1	168	0.766
230699	12	13:30	Gironde	neap	56	0.22	3.69	517	2.60	0.13	85	2.28	93.2	0.55	0.03	121	2.11	90.3	53.1	46.9	1.1	85.3	14.7	5.8	177	0.841
230699	13	13:49	Gironde	neap	39	0.18	3.17	572	1.84	0.09	137	2.30	89.1	0.61	0.03	164	2.22	86.9	46.0	54.0	0.9	72.1	27.9	2.6	98	0.881
230699	14	14:04	Gironde	neap	36	0.12	2.43	654	1.98	0.10	91	2.29	92.7	0.68	0.03	144	2.24	88.5	47.4	52.6	0.9	72.3	27.7	2.6	98	0.874
230699	15	14:12	Gironde	neap	23	0.11	2.31	671	1.81	0.09	93	2.26	92.8	0.44	0.02	122	2.15	90.3	47.8	52.2	0.9	79.0	21.0	3.8	52	0.711
230699	16	14:27	Gironde	neap	27	0.09	1.87	745	1.40	0.07	60	2.19	95.2	0.67	0.03	124	2.19	90.1	50.9	49.1	1.0	68.4	31.6	2.2	56	1.321
230699	17	14:46	Gironde	neap	18	0.09	1.83	754	1.52	0.08	90	2.24	92.8	0.73	0.04	180	2.26	85.7	40.5	59.5	0.7	58.7	41.3	1.4	40	0.809
230699	18	14:57	Gironde	neap	17	0.09	1.41	880	1.20	0.06	85	2.26	93.2	0.52	0.03	129	2.17	89.7	50.5	49.5	1.0	77.4	22.6	3.4	28	0.917
230699	19	15:13	Gironde	neap	9	0.06	1.50	834	2.45	0.12	92	2.31	92.8	0.81	0.03	115	2.19	90.8	34.3	65.7	0.5	67.9	32.1	2.1	28	0.975
230699	20	15:24	Gironde	neap	5	0.18	3.06	583	1.60	0.08	124	2.23	91.2	0.41	0.02	140	2.14	88.8	26.7	73.3	0.4	49.0	51.0	1.0	10	0.945
230699	21	15:32	Gironde	neap	6	0.18	3.38	564	1.80	0.09	99	2.22	92.1	0.40	0.02	116	2.10	90.7	31.3	68.7	0.5	58.7	41.3	1.4	14	1.828

Appendix III – LEGI *Macrofloc and microfloc multiple regression data set.*

Macrofloc and microfloc multiple regression data set for LEGI experimental series (natural muds only).

Experiment number	Floc sample	Sampling position	SPM (mgl^{-1})	TSS (Nm^{-2})	G (s^{-1})	Kolmogorov eddy size (μm)	Ws_{macro} (mms^{-1})	Ws_{micro} (mms^{-1})	SPM ratio	MSF ratio
1	tam200-A	A	0.209	1.49	16.55	251	0.60	0.59	1.2	1.4
1	tam200-B	B	0.206	0.75	9.90	324	0.93	0.74	2.5	3.0
1	tam200-C	C	0.210	0.53	7.67	368	1.80	0.74	1.7	3.9
1	tam600-A	A	0.630	1.27	14.75	266	0.77	0.96	1.3	1.1
1	tam600-B	B	0.620	0.69	9.33	334	1.29	1.10	4.0	4.4
1	tam600-C	C	0.585	0.38	5.96	418	2.40	0.67	5.6	18.2
1	tam1000-A	A	1.048	1.17	13.83	274	0.92	0.66	4.0	3.2
1	tam1000-B	B	1.039	0.47	7.00	385	2.30	1.11	9.3	15.7
1	tam1000-C	C	1.045	0.37	5.86	421	3.15	0.94	11.8	38.2
1	tam5000-A	A	8.650	0.88	11.20	305	3.40	0.71	12.5	54.6
1	tam5000-B	B	8.242	0.43	6.52	399	5.74	0.80	40.7	221.2
1	tam5000-C	C	3.096	0.35	5.65	429	3.60	0.56	24.0	124.0
2	gir200-A	A	0.208	1.49	16.55	251	1.26	0.78	0.4	0.6
2	gir200-B	B	0.210	0.75	9.90	324	1.33	1.15	0.6	0.5
2	gir200-C	C	0.206	0.53	7.67	368	2.25	0.71	0.2	1.6
2	gir600-A	A	0.630	1.27	14.75	266	1.14	0.79	7.8	9.8
2	gir600-B	B	0.609	0.69	9.33	334	1.18	1.12	0.6	0.6
2	gir600-C	C	0.625	0.38	5.96	418	2.38	0.84	1.9	5.2
2	gir1800-A	A	1.811	1.17	13.83	274	1.04	0.69	3.7	5.5
2	gir1800-B	B	1.754	0.47	7.00	385	2.65	0.75	4.6	14.4
2	gir1800-C	C	1.766	0.37	5.86	421	3.25	0.69	4.7	20.3

INSSEV *mean* and *MAX6* floc data set for Tamar estuary experiments 1 and 2.

DATE	INSSEV sample	Time BST (hrs)	Estuary	Tide	SPM (mgl^{-1})	TSS (Nm^{-2})	G (s^{-1})	Kolmogorov eddy size (μm)	D_{mean} (μm)	ρe_{mean} (kgm^{-3})	Ws_{mean} (mms^{-1})	D_{MAX6} (μm)	ρe_{MAX6} (kgm^{-3})	Ws_{MAX6} (mms^{-1})	D_{macro} (μm)	D_{micro} (μm)	Q_c value
240698	1	12:13	Tamar	spring	971	0.53	7.64	369	255.0	245	2.00	1255.0	43	16.00	410.2	138.6	1.082
240698	2	12:35	Tamar	spring	885	0.47	6.95	387	244.5	170	2.40	569.0	43	5.50	307.0	116.7	1.088
240698	3	13:00	Tamar	spring	675	0.21	3.75	527	181.3	154	1.55	384.8	65	3.80	222.1	113.1	1.145
240698	4	13:12	Tamar	spring	615	0.21	3.87	518	182.9	166	1.58	400.4	59	3.71	268.6	98.0	1.242
240698	5	13:34	Tamar	spring	487	0.14	2.82	608	121.0	141	0.78	304.5	76	2.43	209.0	95.7	1.183
240698	6	15:10	Tamar	spring	690	0.47	6.98	386	167.9	239	2.03	440.2	65	4.72	264.6	106.4	1.269
240698	7	15:30	Tamar	spring	2637	0.59	8.23	355	240.0	149	1.95	645.9	43	6.95	334.2	112.8	1.177
240698	8	15:41	Tamar	spring	4501	0.43	6.53	399	345.0	179	3.00	1598.5	31	16.58	439.3	123.7	0.965
240698	9	15:59	Tamar	spring	5571	0.36	5.67	428	322.0	152	3.11	898.0	49	15.50	418.7	115.8	0.802
240698	10	16:17	Tamar	spring	4227	0.28	4.74	469	387.0	90	2.87	897.3	36	11.24	507.5	77.7	0.782
240698	11	16:37	Tamar	spring	2579	0.26	4.43	485	215.3	163	2.12	526.5	55	5.91	287.9	102.1	0.861
40898	1	15:19	Tamar	neap	53	0.15	2.97	592	259.4	61	1.20	388.4	42	2.15	270.1	149.8	0.964
40898	2	15:28	Tamar	neap	48	0.13	2.63	629	256.6	57	0.85	477.4	21	1.81	332.5	115.8	0.989
40898	3	15:39	Tamar	neap	38	0.10	2.23	683	190.5	85	0.84	361.7	38	1.92	291.3	102.6	0.859
40898	4	16:00	Tamar	neap	34	0.07	1.61	804	213.4	89	0.94	322.1	39	1.54	257.2	116.2	0.796
40898	5	16:20	Tamar	neap	26	0.04	1.10	972	132.9	90	0.61	224.6	67	1.33	212.2	91.7	0.885
40898	6	16:37	Tamar	neap	25	0.11	2.33	669	277.0	59	1.26	541.0	42	3.72	449.0	117.9	0.895
50898	1	10:42	Tamar	neap	136	0.36	5.67	428	142.0	183	1.09	321.9	41	1.58	234.4	108.2	0.938
50898	2	10:53	Tamar	neap	131	0.32	5.26	445	132.2	147	0.95	280.0	62	3.00	213.8	108.3	0.765
50898	3	11:11	Tamar	neap	122	0.25	4.40	486	111.7	148	0.72	213.1	84	1.53	192.1	101.6	0.866
50898	4	11:28	Tamar	neap	120	0.15	3.03	586	151.0	137	1.08	382.7	66	3.78	236.7	97.0	1.054
50898	5	11:44	Tamar	neap	102	0.12	2.58	635	157.0	96	0.80	255.6	55	1.39	211.2	116.5	0.876
50898	6	12:14	Tamar	neap	78	0.08	1.85	750	120.2	139	0.71	226.6	80	1.48	194.9	97.1	1.186
50898	7	12:46	Tamar	neap	96	0.07	1.60	807	91.6	161	0.39	199.0	53	1.00	196.3	79.0	0.934
50898	8	13:04	Tamar	neap	138	0.18	3.34	558	179.8	154	1.21	376.8	49	2.59	249.5	114.5	0.850
50898	9	13:25	Tamar	neap	262	0.22	4.01	510	226.1	129	1.50	433.0	53	3.90	255.3	114.1	1.005
50898	10	13:46	Tamar	neap	492	0.39	6.01	416	426.9	90	2.12	736.4	28	6.00	446.8	141.2	0.787
50898	11	14:41	Tamar	neap	223	0.16	3.17	573	168.3	145	1.14	274.6	56	1.80	209.9	119.7	0.857
50898	12	15:06	Tamar	neap	107	0.11	2.29	675	203.8	78	1.04	363.9	34	1.69	235.0	123.3	0.808
50898	13	15:25	Tamar	neap	91	0.10	2.19	689	227.1	63	1.14	398.6	49	3.07	258.6	130.2	0.859
50898	14	15:43	Tamar	neap	38	0.13	2.69	622	321.8	60	1.44	504.8	26	2.61	353.1	119.8	1.307
50898	15	15:56	Tamar	neap	32	0.09	2.05	713	215.7	79	1.14	339.5	47	2.29	260.0	103.3	0.875
60898	1	10:32	Tamar	neap	388	0.55	7.89	363	230.5	213	1.45	644.0	44	6.70	268.4	119.2	0.915
60898	2	11:02	Tamar	neap	328	0.53	7.65	369	207.6	150	1.25	395.2	70	4.21	274.3	133.8	1.139
60898	3	11:15	Tamar	neap	310	0.57	8.02	360	188.3	112	1.10	317.2	87	3.30	236.2	131.0	1.197
60898	4	11:30	Tamar	neap	291	0.56	7.91	363	150.8	142	1.24	293.2	75	2.64	227.5	109.0	1.037
60898	5	11:53	Tamar	neap	313	0.37	5.78	424	168.8	156	1.45	301.1	76	2.50	217.6	117.5	1.144
60898	6	12:06	Tamar	neap	325	0.35	5.60	431	146.2	159	1.18	258.8	51	2.60	203.6	114.7	1.089
60898	7	12:19	Tamar	neap	295	0.34	5.48	436	150.3	173	1.22	317.9	53	2.87	222.9	110.8	0.893
60898	8	12:30	Tamar	neap	256	0.28	4.74	469	143.9	143	1.09	279.0	62	2.66	217.9	93.4	0.938
60898	9	12:50	Tamar	neap	152	0.20	3.62	536	162.9	138	1.37	314.8	83	3.23	235.6	111.7	1.135

INSSEV *mean* and *MAX6* floc data set for Tamar estuary experiment 3.

DATE	INSSEV sample	Time BST (hrs)	Estuary	Tide	SPM (mgl^{-1})	TSS (Nm^{-2})	G (s^{-1})	Kolmogorov eddy size (μm)	D_{mean} (μm)	ρe_{mean} (kgm^{-3})	Ws_{mean} (mms^{-1})	D_{MAX6} (μm)	ρe_{MAX6} (kgm^{-3})	Ws_{MAX6} (mms^{-1})	D_{macro} (μm)	D_{micro} (μm)	Q_c value
150998	4	16:11	Tamar	neap	10	0.04	1.20	931	119.3	180	0.60	163.0	408	3.01	172.0	111.6	1.061
150998	5	16:33	Tamar	neap	24	0.09	2.02	717	204.8	54	0.70	238.2	59	1.34	217.6	143.7	0.940
150998	6	16:41	Tamar	neap	32	0.14	2.81	609	181.3	67	0.84	268.3	68	1.58	227.2	117.2	0.954
150998	7	16:57	Tamar	neap	115	0.17	3.21	569	282.5	73	1.44	722.1	28	6.30	343.2	126.8	0.964
150998	8	17:08	Tamar	neap	271	0.27	4.60	475	246.0	90	1.78	567.6	40	4.96	281.0	126.0	1.102
150998	9	17:31	Tamar	neap	80	0.25	4.28	493	205.8	109	1.24	351.2	72	3.29	247.0	121.0	1.160
160998	2	11:22	Tamar	neap	20	0.15	2.97	592	147.7	109	0.80	228.5	69	1.26	238.9	108.3	1.470
160998	3	12:12	Tamar	neap	92	0.16	3.13	577	181.1	150	1.23	256.1	67	1.70	212.4	120.1	0.867
160998	4	12:15	Tamar	neap	94	0.20	3.70	530	149.3	146	1.13	247.0	98	2.34	209.3	103.3	1.309
160998	5	13:05	Tamar	neap	68	0.16	3.09	581	228.4	104	1.57	425.1	59	3.76	268.5	111.2	1.214
160998	8	13:39	Tamar	neap	21	0.07	1.71	780	169.1	97	0.84	238.1	66	1.36	226.7	123.2	1.113
160998	9	13:54	Tamar	neap	16	0.07	1.61	805	193.3	76	0.80	276.4	50	1.42	276.4	111.1	1.159
160998	10	14:06	Tamar	neap	13	0.05	1.40	863	156.4	67	0.60	249.0	43	1.06	225.4	113.4	1.109
160998	11	14:21	Tamar	neap	12	0.07	1.65	794	158.5	65	0.60	260.9	39	1.19	251.1	79.6	1.299
160998	18	17:28	Tamar	neap	34	0.09	1.99	723	115.9	385	0.84	196.3	113	1.58	289.2	84.4	0.791
160998	19	17:40	Tamar	neap	34	0.11	2.37	662	175.6	102	1.02	190.2	86	1.49	182.7	80.2	0.879
170998	1	13:21	Tamar	neap	498	0.60	8.39	352	159.9	150	1.15	334.6	52	2.20	215.1	110.9	0.902
170998	2	13:35	Tamar	neap	366	0.57	8.02	360	197.1	123	1.70	464.0	47	3.67	230.4	128.6	1.155
170998	3	13:45	Tamar	neap	588	0.34	5.45	437	206.3	137	2.30	492.5	64	6.03	267.4	97.7	0.881
170998	5	14:08	Tamar	neap	434	0.27	4.58	476	459.8	52	1.70	742.8	30	6.44	460.8	159.6	0.986
170998	6	14:23	Tamar	neap	266	0.23	4.14	501	253.7	64	1.41	340.7	34	2.35	258.5	128.2	0.810
170998	7	14:57	Tamar	neap	82	0.12	2.52	642	206.6	193	1.44	367.7	73	4.11	254.0	125.1	1.049
170998	8	15:05	Tamar	neap	47	0.13	2.64	627	233.2	70	1.25	366.2	53	2.80	268.9	136.2	1.263
170998	9	15:12	Tamar	neap	38	0.11	2.39	659	208.1	66	0.74	318.5	44	1.66	250.6	109.8	1.198
170998	10	15:24	Tamar	neap	40	0.15	2.90	599	183.5	90	1.00	329.9	62	2.60	234.7	111.0	1.332
210998	1	12:26	Tamar	spring	3071	0.53	7.60	370	329.2	85	2.00	738.3	28	5.86	350.2	119.9	1.293
210998	2	12:41	Tamar	spring	2771	0.52	7.52	372	326.2	89	2.20	808.5	21	5.46	352.1	112.6	1.258
210998	3	13:04	Tamar	spring	2114	0.58	8.18	357	316.7	79	2.15	571.0	40	5.06	339.5	116.0	1.446
210998	4	13:15	Tamar	spring	1974	0.68	9.24	335	263.8	79	1.50	696.3	26	4.83	288.3	113.7	1.078
210998	5	14:59	Tamar	spring	1142	0.42	6.43	402	204.6	170	1.68	513.3	53	5.46	243.7	119.8	1.402
210998	6	15:10	Tamar	spring	928	0.46	6.92	388	189.8	145	1.78	379.2	113	6.30	243.8	129.5	0.835
210998	7	15:56	Tamar	spring	4500	0.33	6.65	396	420.9	97	3.02	1035.9	21	8.88	441.4	90.3	0.929
220998	3	11:44	Tamar	spring	1700	0.29	4.82	464	136.9	215	1.67	271.2	42	3.47	200.0	117.2	0.845
220998	4	12:07	Tamar	spring	2380	0.55	7.82	365	156.3	152	1.33	334.0	76	3.32	254.2	110.5	1.082
220998	5	12:18	Tamar	spring	2643	0.69	9.33	334	152.8	169	1.15	368.2	69	3.66	226.9	100.2	0.946
220998	6	12:34	Tamar	spring	2337	0.70	9.44	332	202.5	156	1.70	290.9	102	3.37	230.4	131.9	0.826
220998	7	16:10	Tamar	spring	858	0.44	6.63	396	234.7	205	2.00	491.1	83	7.76	275.6	121.8	1.027
220998	9	17:30	Tamar	spring	8558	0.29	4.80	466	345.4	98	3.10	639.4	45	7.15	428.1	99.0	0.900
220998	11	17:49	Tamar	spring	4221	0.24	4.22	497	304.8	83	2.59	613.6	26	4.98	395.8	121.3	0.971
220998	12	17:56	Tamar	spring	3592	0.20	3.71	529	238.9	122	2.00	494.0	51	4.84	276.4	102.7	0.912
220998	13	18:04	Tamar	spring	3130	0.19	3.51	544	153.4	135	1.03	407.3	23	3.55	252.6	103.0	0.844
220998	14	18:08	Tamar	spring	2734	0.22	3.95	513	142.1	157	1.06	288.3	91	3.42	221.3	106.9	0.785
230998	1	11:12	Tamar	spring	769	0.51	7.48	373	229.8	121	2.09	468.3	52	4.42	289.1	117.0	0.879
230998	2	11:24	Tamar	spring	925	0.53	7.64	369	230.0	97	1.43	893.0	26	5.82	312.7	107.3	0.903
230998	3	11:41	Tamar	spring	1234	0.60	8.39	352	148.0	129	1.01	288.3	63	2.25	251.9	108.3	0.883
230998	4	11:56	Tamar	spring	1910	0.53	7.64	369	314.7	109	1.89	840.6	17	4.55	404.1	122.6	1.152
230998	5	12:14	Tamar	spring	4850	0.58	8.13	358	272.3	90	2.25	440.5	42	4.29	276.4	151.9	0.712
230998	6	12:29	Tamar	spring	4394	0.40	6.18	410	330.6	95	2.89	452.2	64	5.12	341.2	97.8	0.966
230998	7	12:44	Tamar	spring	3150	0.37	5.80	423	408.0	99	3.00	633.2	64	9.96	425.2	103.8	1.037
230998	8	12:54	Tamar	spring	3400	0.26	4.48	482	353.6	98	2.78	737.2	30	6.14	368.2	114.4	0.864

INSSEV *mean* and *MAX6* floc data set for Gironde estuary SWAMGIR1 experiment.

DATE	INSSEV sample	Time BST (hrs)	Estuary	Tide	SPM (mgl^{-1})	TSS (Nm^{-2})	G (s^{-1})	Kolmogorov eddy size (μm)		D_{mean} (μm)	ρe_{mean} (kgm^{-3})	Ws_{mean} (mms^{-1})		D_{MAX6} (μm)	ρe_{MAX6} (kgm^{-3})	Ws_{MAX6} (mms^{-1})		D_{macro} (μm)	D_{micro} (μm)		Q_c value
230699	3	10:58	Gironde	neap	81	0.43	6.56	398		105.6	120	0.63		217	72	2.45		248	101.7		1.286
230699	4	11:17	Gironde	neap	101	0.52	7.55	371		134.1	101	0.72		329	50	2.19		258	111.9		1.045
230699	5	11:29	Gironde	neap	103	0.45	6.75	393		121.7	123	0.76		255	99	2.48		227	111.0		0.807
230699	6	11:40	Gironde	neap	107	0.46	6.87	389		130.0	140	0.88		275	55	2.33		255	99.7		0.701
230699	7	11:55	Gironde	neap	112	0.47	6.97	386		124.8	124	0.69		317	43	2.21		265	107.7		1.051
230699	8	12:18	Gironde	neap	139	0.46	6.84	390		119.5	142	0.81		302	56	2.40		252	104.9		0.791
230699	9	12:45	Gironde	neap	78	0.39	6.06	414		135.0	136	0.92		322	47	1.99		249	101.3		1.125
230699	10	13:04	Gironde	neap	68	0.43	6.55	398		140.2	109	0.81		313	56	2.10		278	109.5		0.827
230699	11	13:19	Gironde	neap	59	0.33	5.40	439		112.8	156	0.73		235	90	2.40		215	104.3		0.766
230699	12	13:30	Gironde	neap	56	0.22	3.89	517		136.5	116	0.91		346	57	3.03		282	103.5		0.841
230699	13	13:49	Gironde	neap	39	0.16	3.17	572		122.0	170	0.93		209	95	1.97		192	102.0		0.881
230699	14	14:04	Gironde	neap	36	0.12	2.43	654		137.7	130	0.96		250	80	1.99		235	110.6		0.874
230699	15	14:12	Gironde	neap	23	0.11	2.31	671		132.3	142	0.80		221	93	1.93		228	107.3		0.711
230699	16	14:27	Gironde	neap	27	0.08	1.87	745		144.7	105	0.79		309	47	1.76		258	112.1		1.321
230699	17	14:46	Gironde	neap	18	0.08	1.83	754		129.1	174	0.93		210	92	1.60		204	106.5		0.809
230699	18	14:57	Gironde	neap	17	0.06	1.41	860		130.5	120	0.79		239	81	1.70		190	100.9		0.977
230699	19	15:13	Gironde	neap	9	0.06	1.50	834		131.4	103	0.82		183	92	2.62		253	113.6		0.975
230699	20	15:24	Gironde	neap	5	0.16	3.06	583		90.9	127	0.44		171	108	1.63		168	82.9		0.945
230699	21	15:32	Gironde	neap	6	0.18	3.38	554		101.7	120	0.45		182	79	1.90		183	98.9		1.826

Appendix V – POST sensor calibration examples.

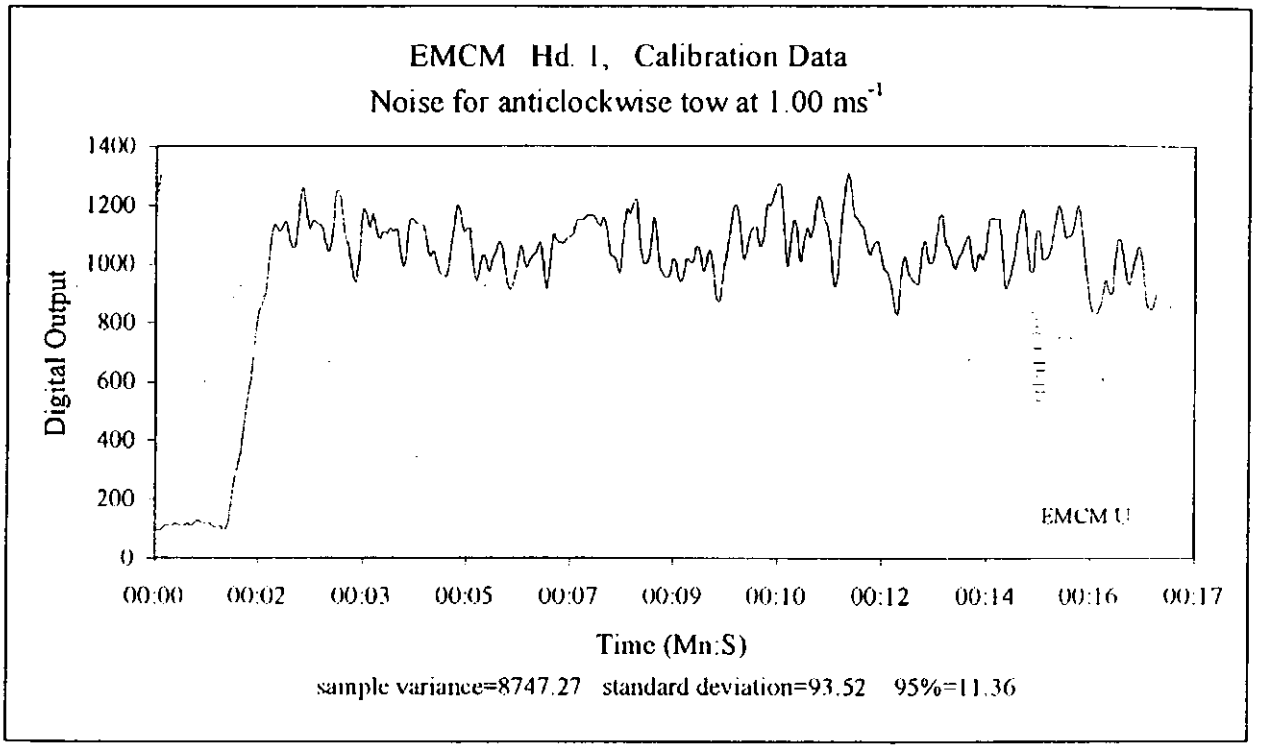

Figure V-1 A time series of a typical POST EMCM sensor calibration response whilst being towed in an annular flume at a speed of 1 ms^{-1} (from Christie, 1997).

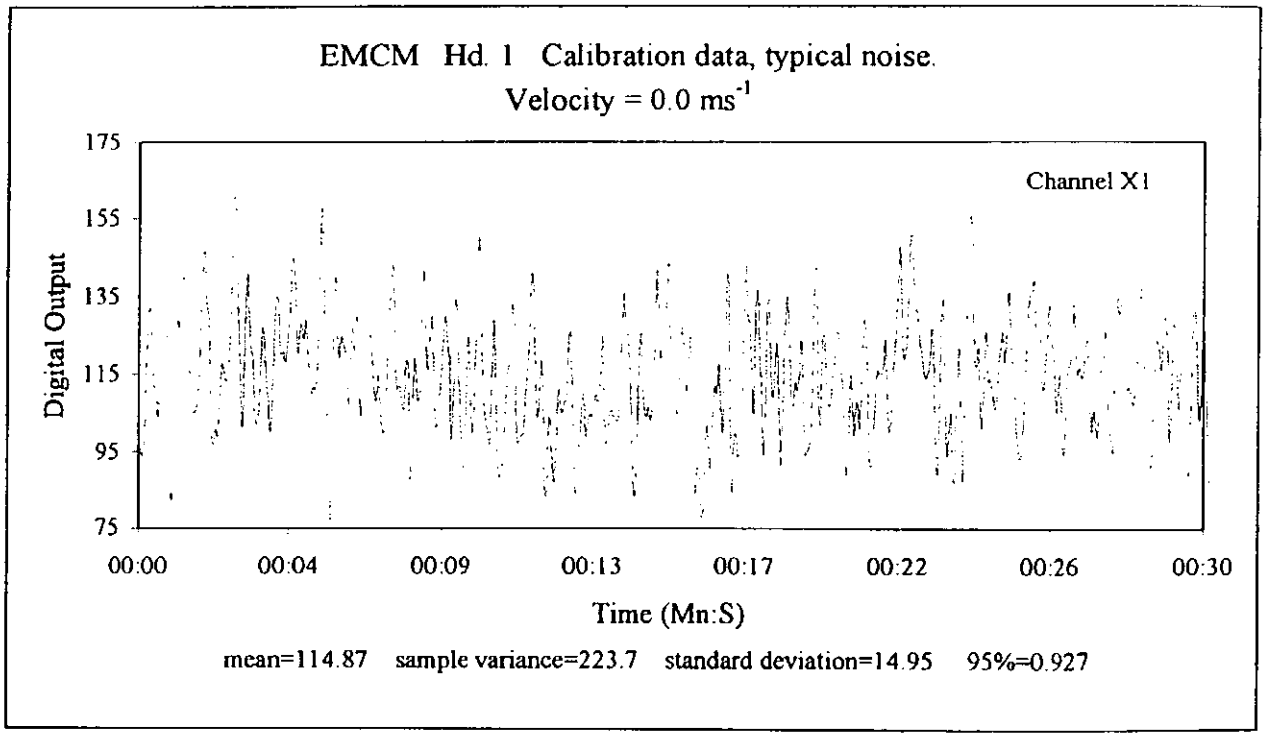

Figure V-2 A time series of a typical POST EMCM sensor calibration response whilst being immersed in still water(from Christie, 1997).

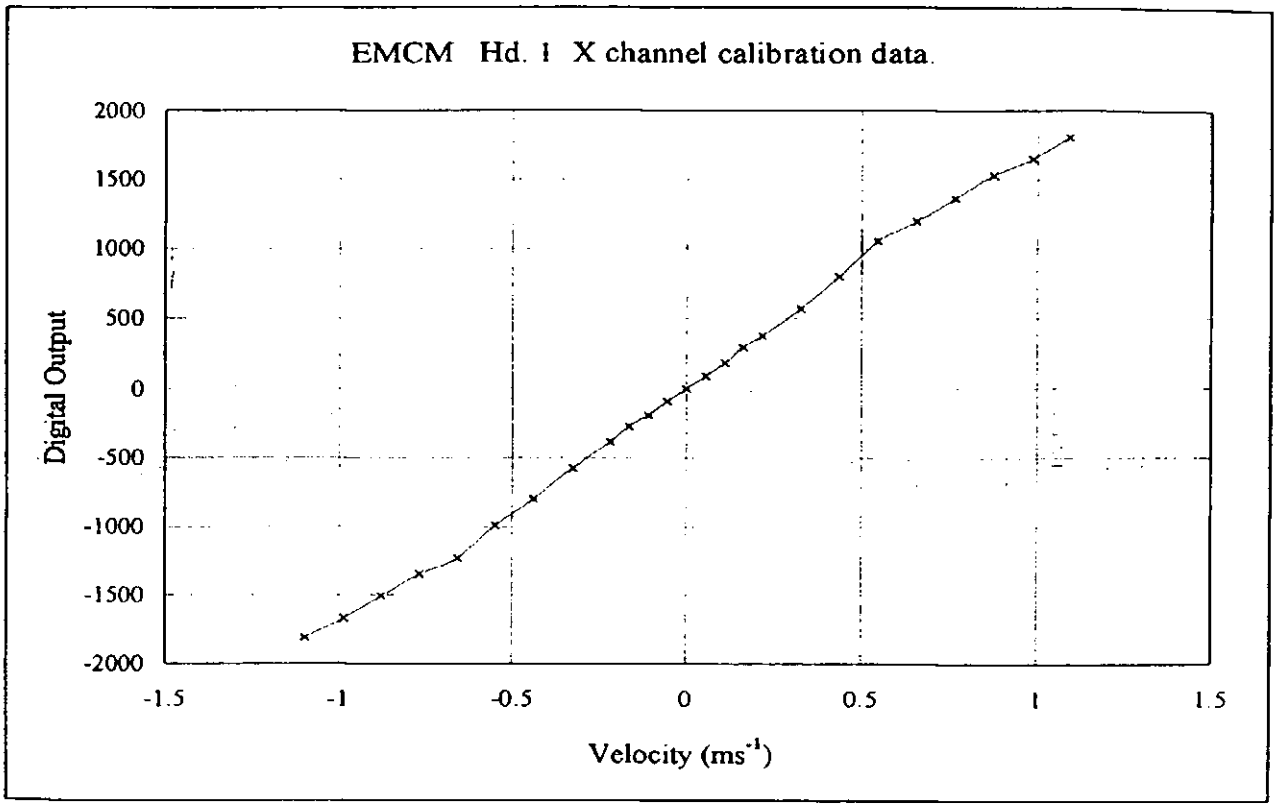

Figure V-3 A typical POST EMCM sensor calibration (from Christie, 1997).

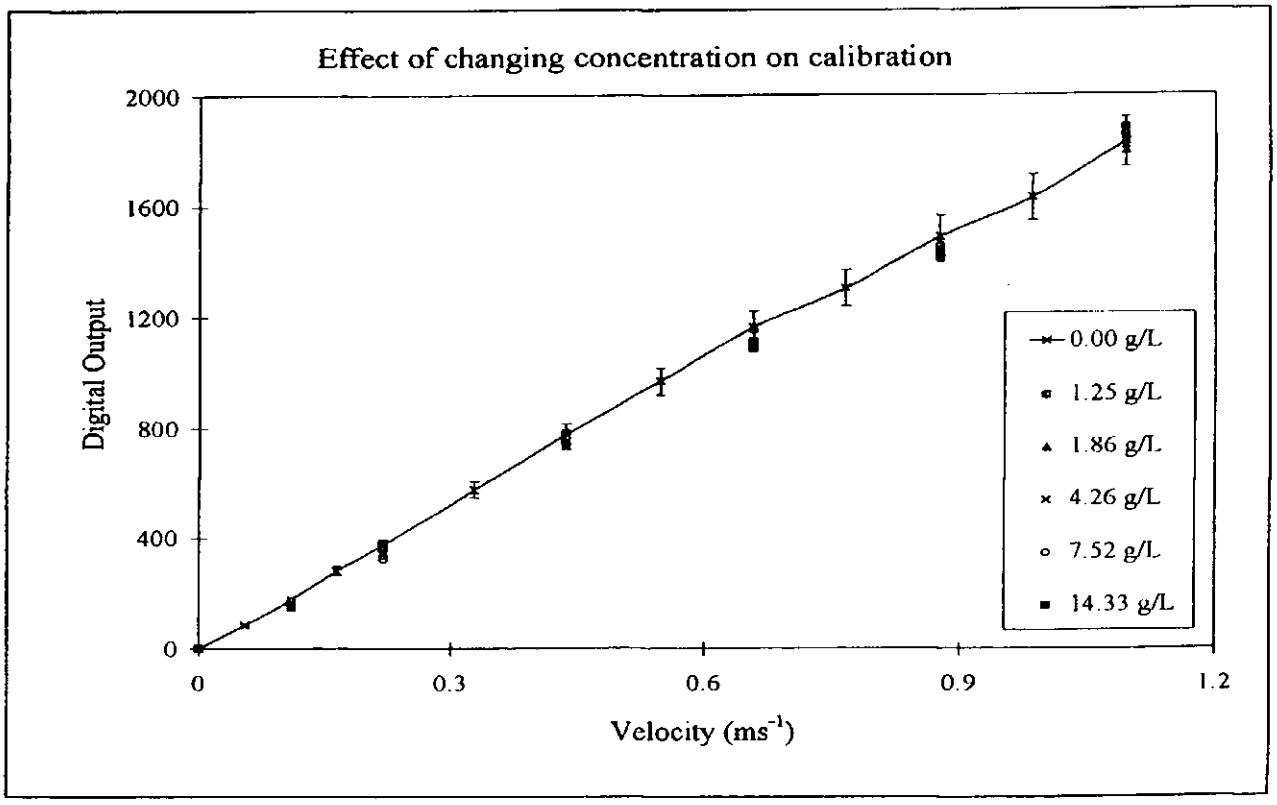

Figure V-4 A typical POST EMCM sensor calibration curve illustrating the effect of increasing SPM concentrations (from Christie, 1997).

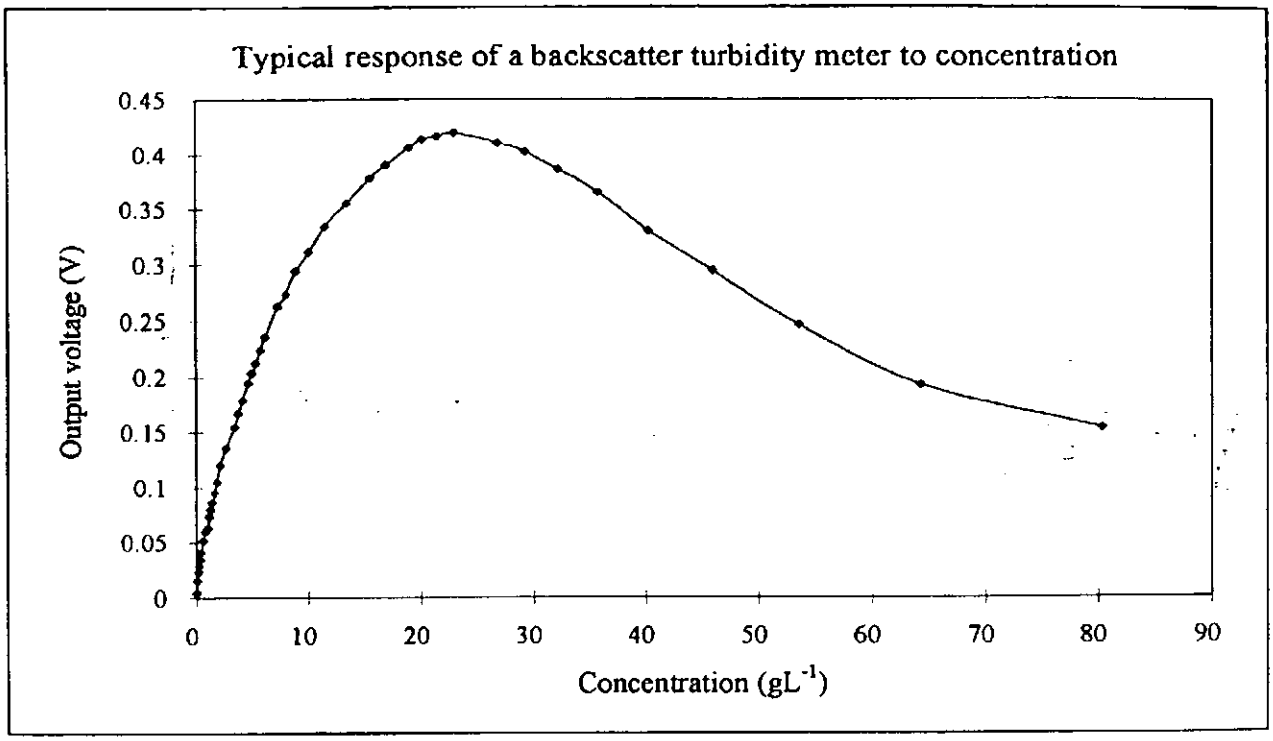

Figure V-5 A typical POST OBS sensor calibration (from Christie, 1997).

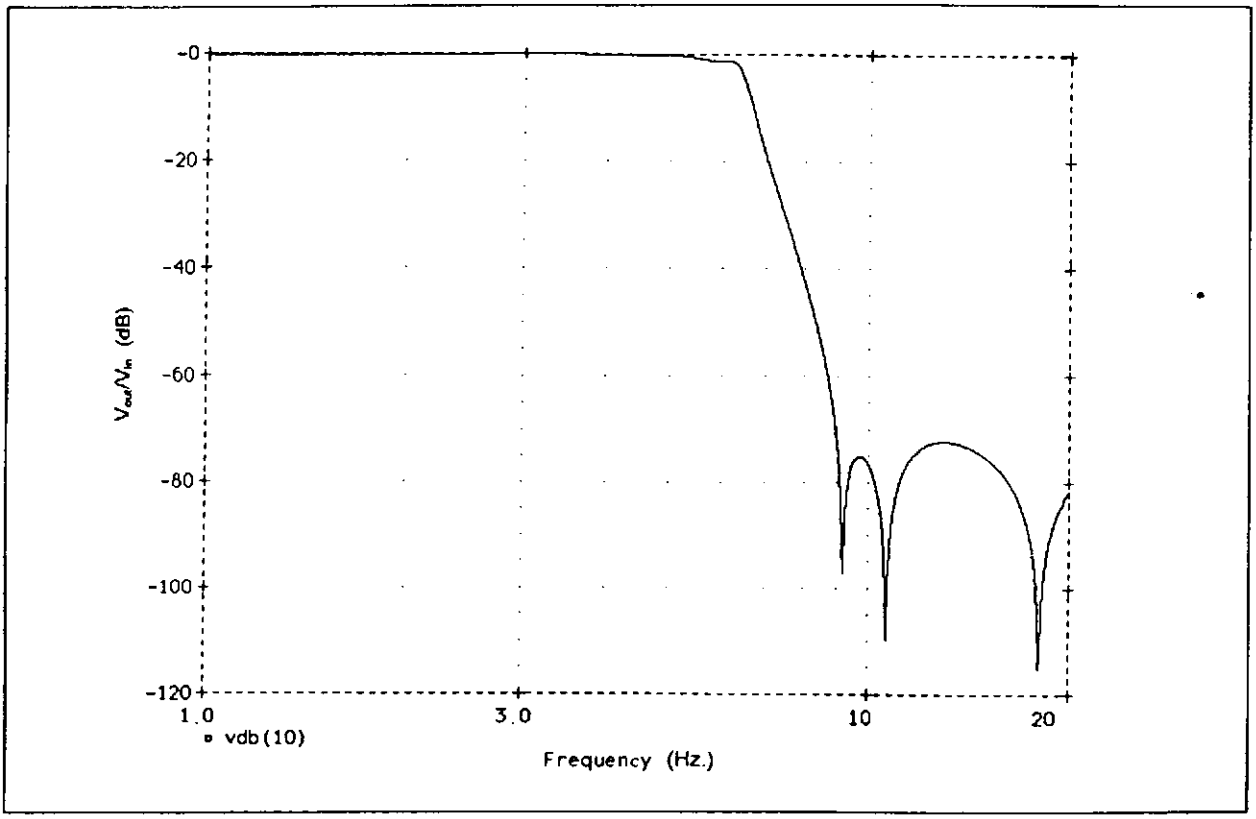

Figure V-6 The characteristic shape of the POST low pass (anti-alaising) filters (from Christie, 1997).

Appendix VI – List of Symbols and Abbreviations.

This appendix lists the most commonly used symbols and abbreviations used within this thesis.

A = absorbence.

A/D = analogue to digital.

ADCP = acoustic Doppler current profiler.

ADV = acoustic Doppler velocimeter.

C = concentration (as SPM).

CBS = Concentrated Benthic Suspension.

CCU = camera control unit.

$C_{filtered}$ = SPM concentration determined from gravimetric analysis.

C/H/N = carbon/hydrogen/nitrogen.

C_{INSSEV} = SPM concentration determined from flocs measured by INSSEV.

$C_{INSSEVcal}$ = calibrated INSSEV SPM concentration.

$_{CM}$ = subscript denoting *conceptual model* parameters.

COSINUS = Prediction of COhesive Sediment transport and bed dynamics in estuaries and coastal zones with Integrated NUmerical Simulation models.

D = floc spherically equivalent diameter.

d = individual particle diameter.

DGPS = differential global positioning system.

D_{mean} = mean floc spherically equivalent diameter.

D_p = primary particle diameter.

Dx = floc diameter perpendicular to the direction of settling.

Dy = floc diameter in the direction of settling.

E = turbulent kinetic energy (as TKE).

EC = European Commission.

EMCM = electromagnetic current meter.

EPS = extra-cellular polymetric substance.

F = momentum flux across the horizontal parallel to the flow direction.

G = root mean square of the gradient in turbulent velocity fluctuations (i.e. turbulent shear).

g = acceleration due to gravity.

GC = gas chromatograph.

GPS = global positioning system.

HR, HRW = Hydraulics Research Wallingford.

hr = hour.

HW = high water.

INSSEV = IN-Situ SEttling Velocity.

K = collision frequency function.

k = Boltzmann's constant.

l = integral lengthscale.

LED = light emitting diode.

LEGI = Laboratoire des Ecoulements Geophysiques et Industriels.

MAX6 = mean floc characteristics determined from the six largest flocs from a specific sample.

$M_{f\,dry}$ = uncorrected dry mass of an individual floc.

$M_{f\,dry\,c}$ = corrected dry mass of an individual floc.

MSF = mass settling flux.

N = total number of particles in a fractal aggregate.

N = number of particle collisions.

nf = fractal dimension.

OBS = optical backscatter sensor.

P = turbulent energy production rate.

PC = personal computer.

P_f = floc porosity.

PML = Plymouth Marine Laboratory.

POST = Profile Of Sediment Transport.

Q_c = INSSEV floc sample quality factor.

Ri_g = gradient Richardson number.

SB = size band.

SPM = suspended particulate matter.

$SPM\%_{macro}$ = percentage of total suspended particulate matter constituting the macroflocs.

$SPM\%_{micro}$ = percentage of total suspended particulate matter constituting the microflocs.

SPM_{ratio} = ratio of SPM constituting the macroflocs divided by the respective microfloc fraction.

SW = south west.

SWAMIEE = Sediment and WAter Movement in Industrialised Estuarine Environments.

T = absolute temperature.

T_F = flocculation time.

TKE = turbulent kinetic energy (as E).

TM = turbidity maximum.

TMR = Training and Mobility of Researchers.

TP = tide pole.

Tsd = INSSEV slide door open-time duration.

TSS = turbulent shear stress.

U = total streamwise flow velocity (orthogonal x-axis).

u = streamwise mean flow velocity component.

u' = streamwise fluctuating (turbulent) flow velocity component.

U_* = frictional velocity.

UJF = Universite Joseph Fourier.

U_o = amplitude of tidal oscillation in longitudinal velocity.

UO = University of Oxford.

UOP = University of Plymouth.

UR = University of Rouen.

U_T = streamwise tidal flow velocity component.

UV/Vis = ultraviolet/visible.

UWB = University of Wales Bangor.

V = total vertical flow velocity (orthogonal y-axis).

v = vertical mean flow velocity component.

v' = vertical fluctuating (turbulent) flow velocity component.

V_A = attractive forces (London-van de Waals force).

VCR = video cassette recorder.

V_f = floc volume.

$V_{filtrate}$ = volume of filtrate.

VIL = Video In Laboratory.

VIS = Video In-Situ.

V_{iw} = volume of interstitial water.

V_{meth} = volume of methanol.

V_R = repulsive forces (electrostatic Coulombic forces).

V_T = vertical tidal flow velocity component.

V_{vs} = INSSEV video object plane sample volume.

W = total cross-stream flow velocity (orthogonal z-axis).

w = cross-stream mean flow velocity component.

w' = cross-stream fluctuating (turbulent) flow velocity component.

Ws = settling velocity.

W_{50} = median settling velocity.

Ws_{macro} = sample mean macrofloc mean settling velocity.

Ws_{mean} = arithmetic mean settling velocity.

Ws_{micro} = sample mean microfloc mean settling velocity.

W_{so} = reference settling velocity.

W_T = cross-stream tidal flow velocity component.

z_0 = bed roughness length.

Greek symbols

α', α = collision efficiency factor.

ε = turbulent energy dissipation rate.

η = the size of dissipating eddies in a turbulent flow as defined by the Kolmogorov microscale.

κ = von Karman's constant.

μ = dynamic viscosity.

ν = kinematic viscosity.

ρ = water density.

ρ_e = corrected ambient floc effective density.

$\rho_{e\ column}$ = floc effective density in relation to the INSSEV settling column.

$\rho_{e\ np}$ = the mean effective density for solid (non-porous) aggregates.

$\rho_{e\ Oseen}$ = Oseen modified ambient floc effective density.

ρ_f = floc bulk density.

ρ_{mo} = the mean dry density of the primary particles.

ρ_{sed} = sediment density.

ρ_w = density of sediment laden water.

$\rho_{w\ column}$ = density of water within the INSSEV settling column.

$\rho_{w\ difference}$ = difference between the INSSEV settling column and ambient water density.

τ = turbulent shear stress (as TSS).

τ_b = bed shear stress.

ϕ = total volume of sediment per unit volume.

Appendix VII

Selected INSSEV video image floc stills.

This appendix contains a selection of floc images from the various experiments reviewed in chapters three through to seven in this thesis. The images presented are illustrative of the most common floc variants which appear during the various local ambient estuarine conditions experienced. The plate groupings presented are as follows:

- Plates VII-1 to VII-10 are illustrative of flocs sampled from the Tamar estuary on 24th June 1998 during spring tides.
- Plates VII-11 to VII-18 are illustrative of flocs sampled from the Tamar estuary on 21st September 1998 during spring tides.
- Plates VII-19 to VII-25 are illustrative of flocs sampled from the Tamar estuary on 5th August 1998 during neap tides.
- Plates VII-26 to VII-33 are illustrative of flocs sampled from the Gironde estuary on 23rd June 1999 during neap tides.

It must be noted that the original monochrome INSSEV images were recorded on analogue S-VHS video cassette tape, and the floc images presented were obtained by digitisation via a PC "video image capture card". This produced an uncompressed windows bitmap (.BMP) file format with a resolution of 720 x 576 pixels. This digitisation process, together with the pausing action of the moving floc images has resulted in a partial "smearing" and "softening" of the images printed in this appendix. Original INSSEV video recordings have a greater clarity and can display much finer floc detailing.

Flocs sampled from the Tamar estuary on 24th June 1998 during spring tides.

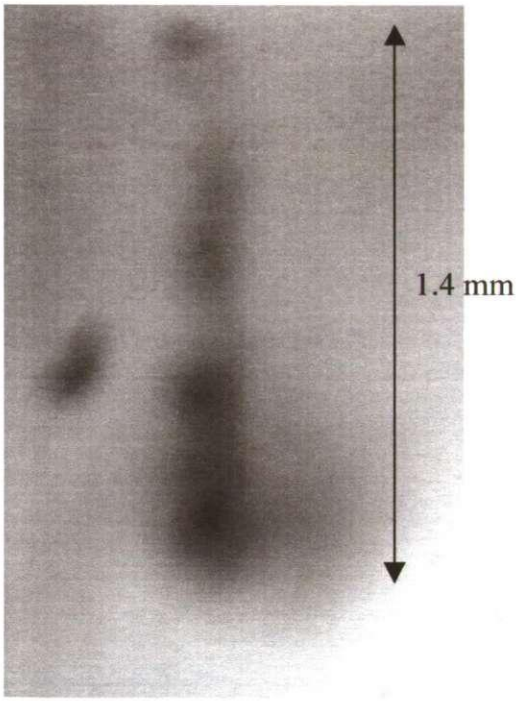

Plate VII-1 "String of pearls" type stringer (24-1, frame 935)

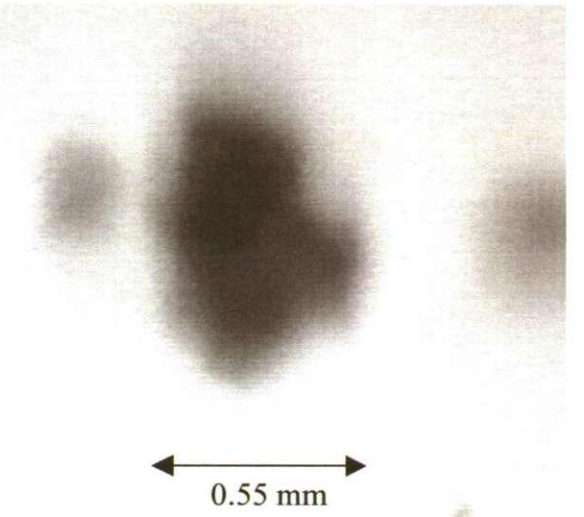

Plate VII-2 Clustered type macrofloc (24-1, frame 1015)

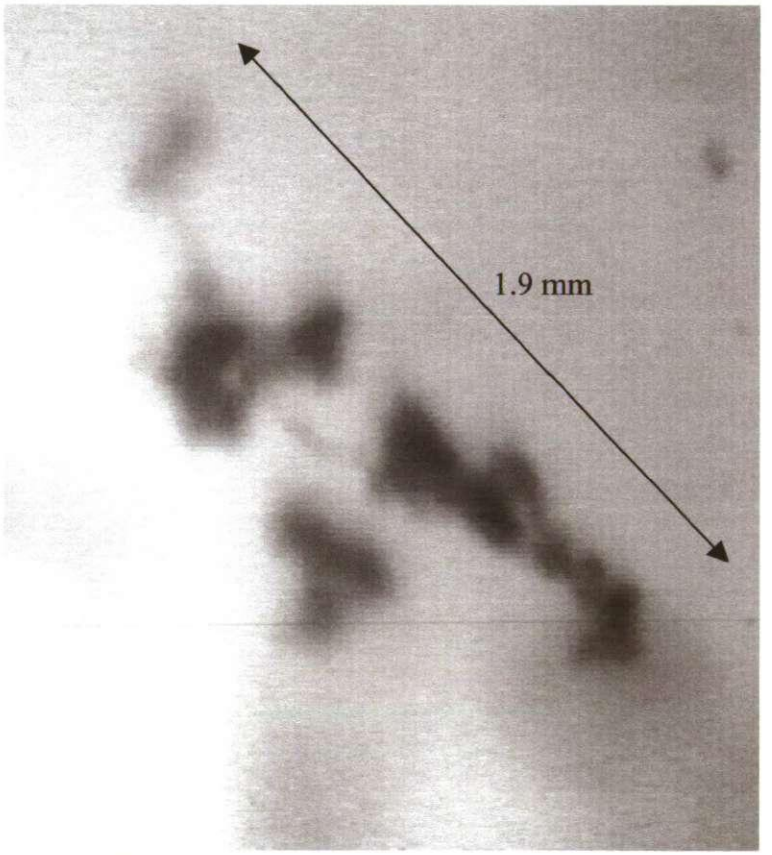

Plate VII-3 Long interlinked stringer comprising two clustered macroflocs (24-2, frame 1258)

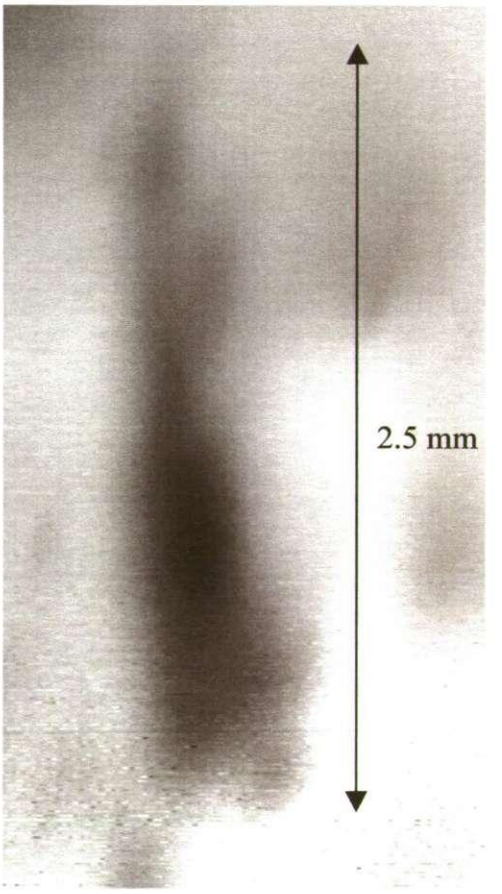

Plate VII-4 Long comet-shaped stringer (24-1, frame 745)

Flocs sampled from the Tamar estuary on 24th June 1998 during spring tides.

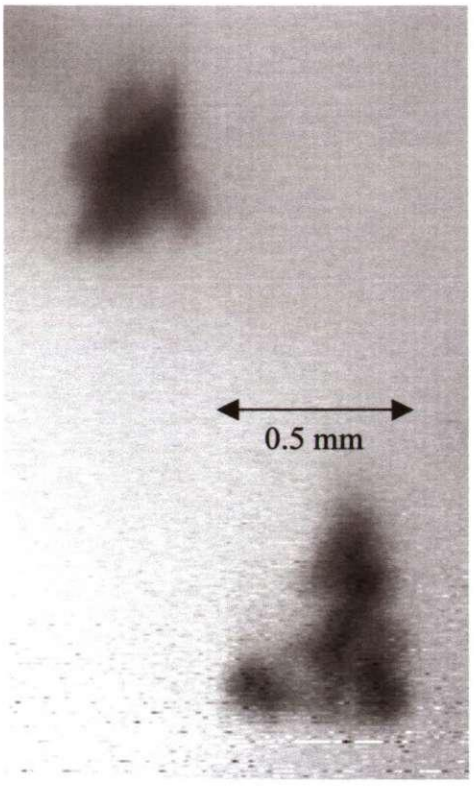

Plate VII-5 Two clustered macroflocs (24-6, frame 795)

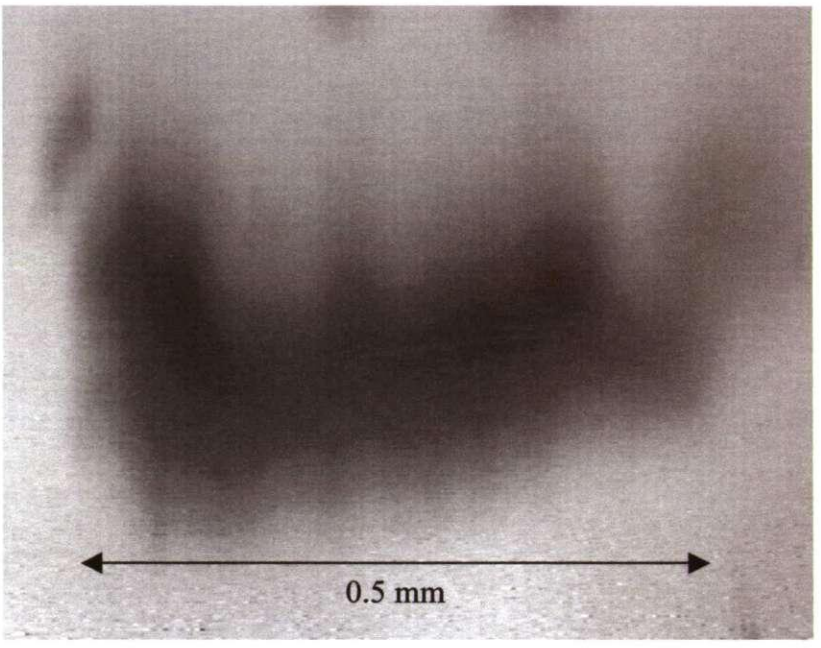

Plate VII-6 Large macrofloc flatened from non-destructive inter-macrofloc contacts possibly occurring within the CBS layer (24-9, frame 477)

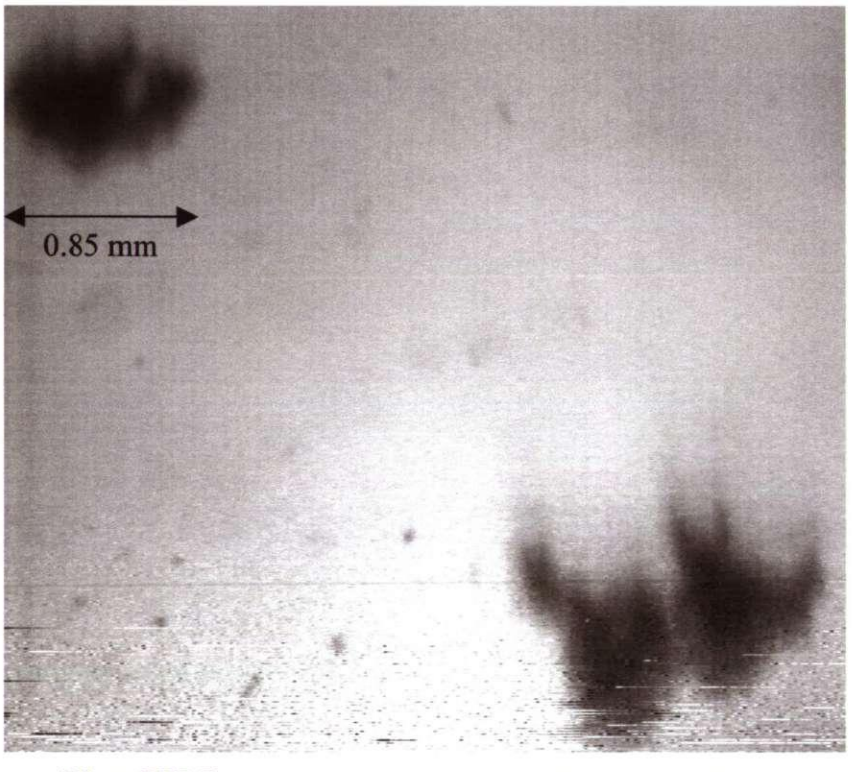

Plate VII-7 Ragged macroflocs settling (24-9, frame 419)

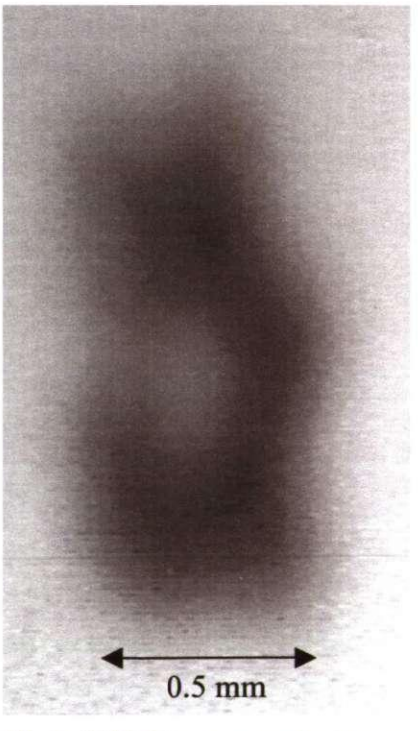

Plate VII-8 Long curved stringer (24-7, frame 550)

Flocs sampled from the Tamar estuary on 24th June 1998 during spring tides.

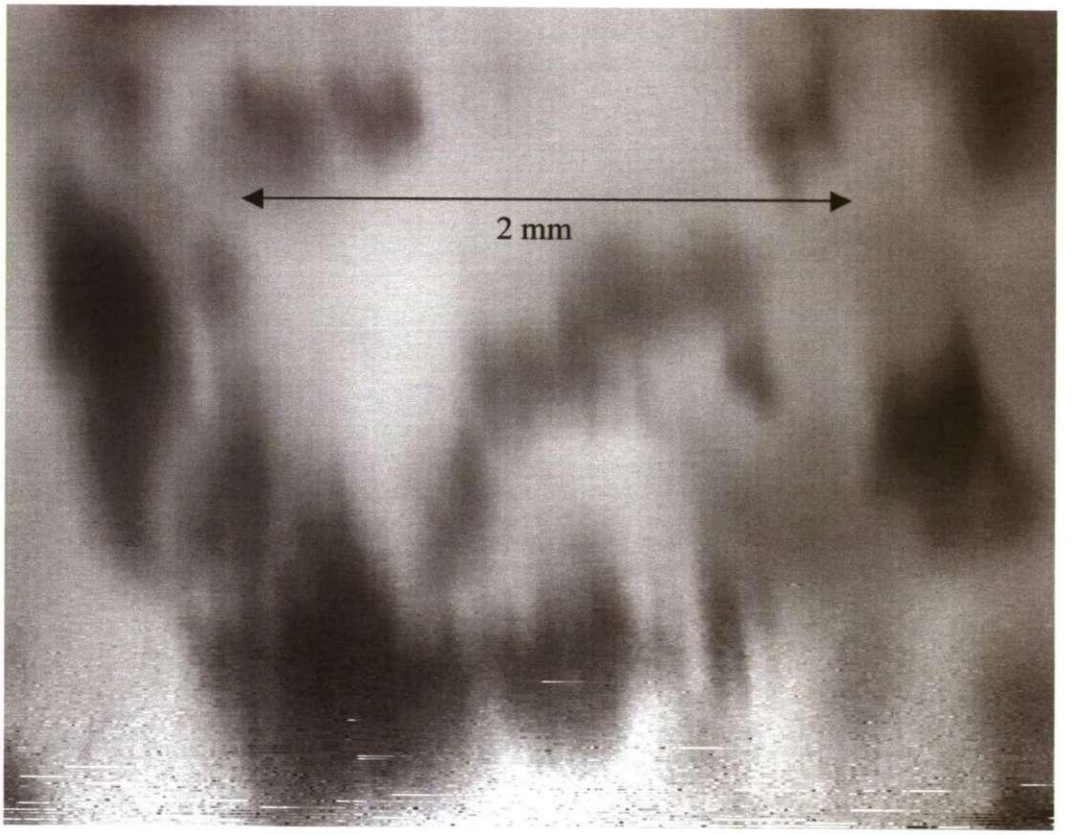

Plate VII-9 Numerous clustered macroflocs settling early in the record of a CBS sample (24-9, frame 509)

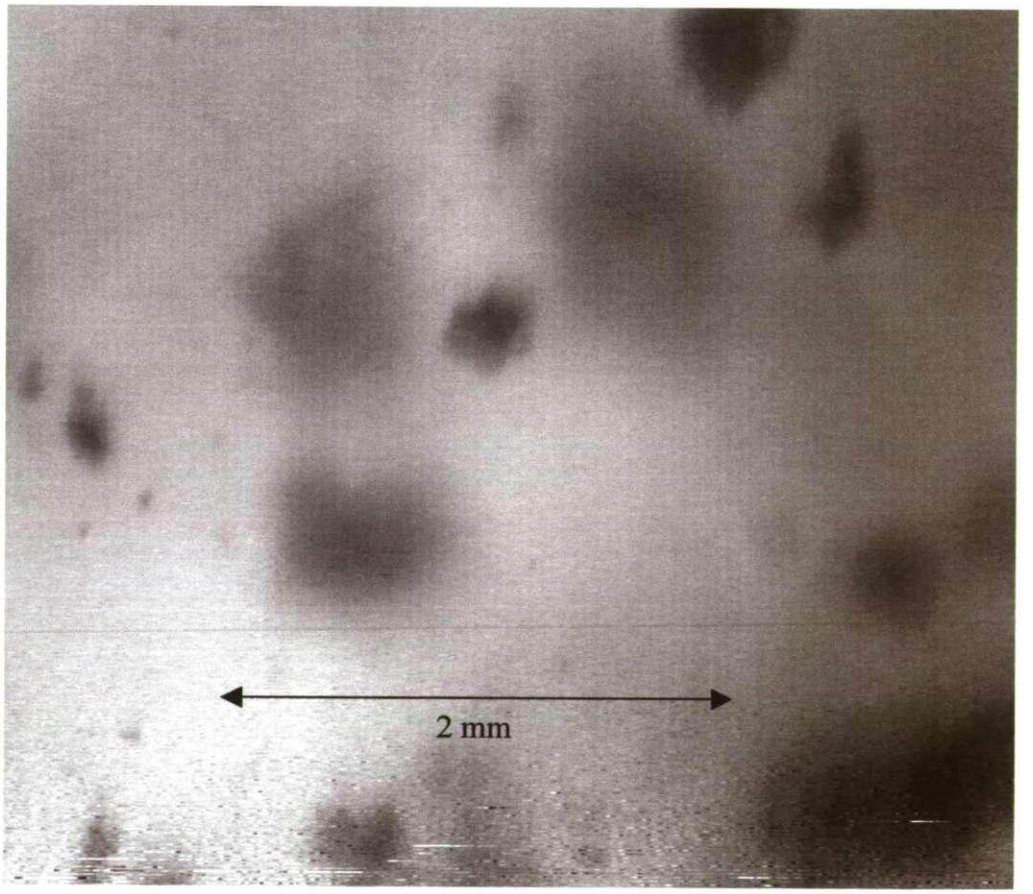

Plate VII-10 A variety of floc sizes settling slightly latter in the CBS sample record (24-9, frame 676)

Flocs sampled from the Tamar estuary on 21st September 1998 during spring tides.

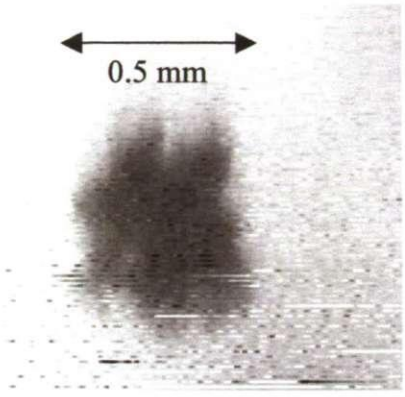

Plate VII-11 An example of a ragged macroflocs formed during high SPM concentration levels and moderately high turbulence (21-2, frame 561)

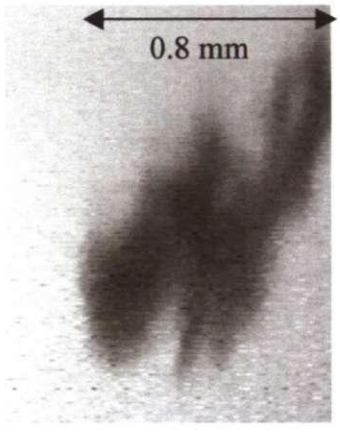

Plate VII-12 Ragged stringer type macroflocs (21-2, frame 603)

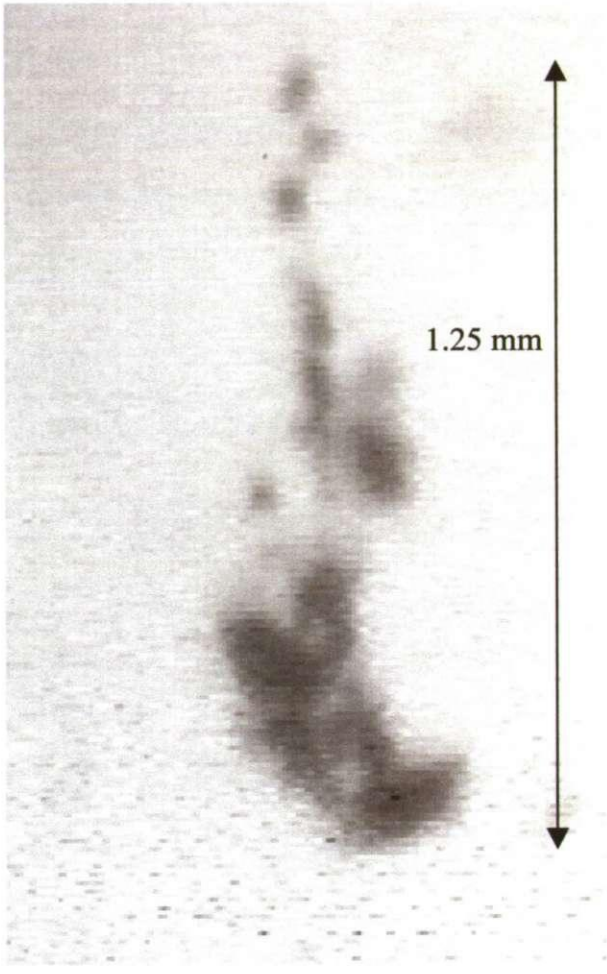

Plate VII-13 Long stringer composed of a large macrofloc sinker with trailing microfloc & smaller macroflocs interconnected by fine organic thread-like materials (21-5,

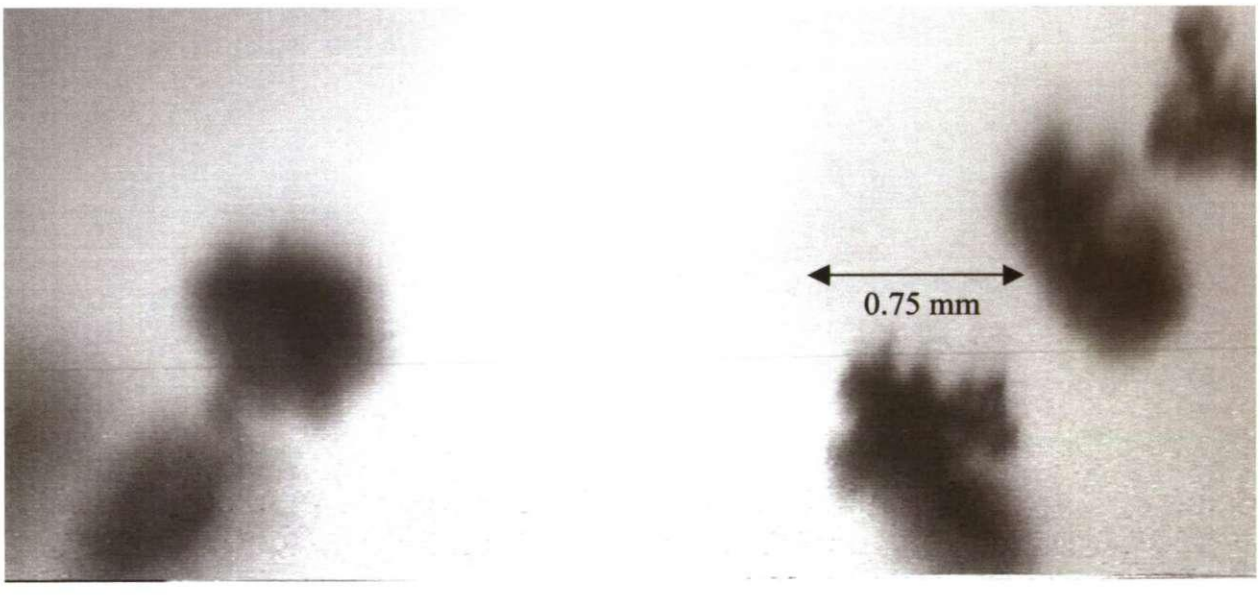

Plate VII-14 A group of settling cluster-type macroflocs (21-2, frame 716)

Flocs sampled from the Tamar estuary on 21st September 1998 during spring tides.

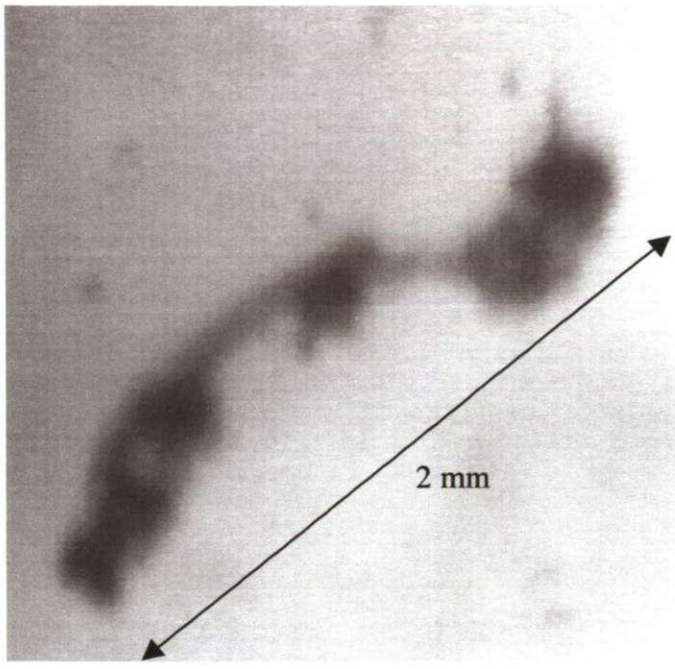

Plate VII-15 An example of a "string of pearls" type macrofloc (21-5, frame 1052)

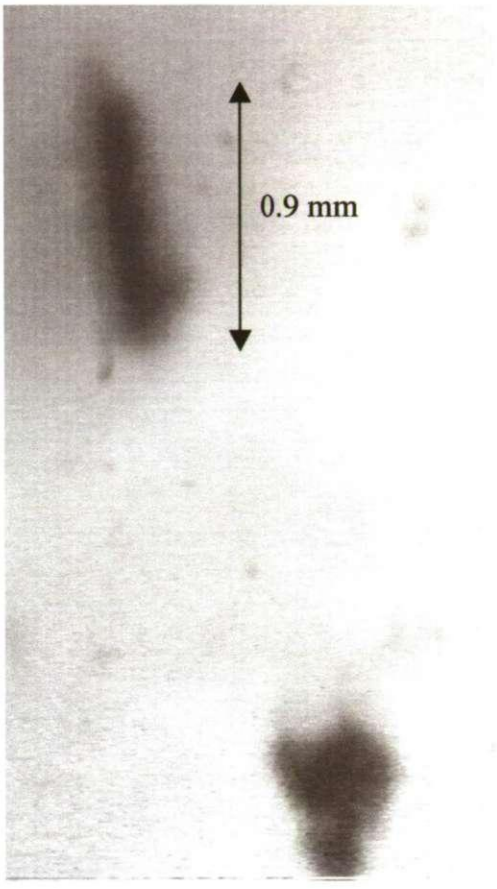

Plate VII-16 A comet-shaped macrofloc (top) and a cluster macrofloc (bottom) (21-5, frame 1213)

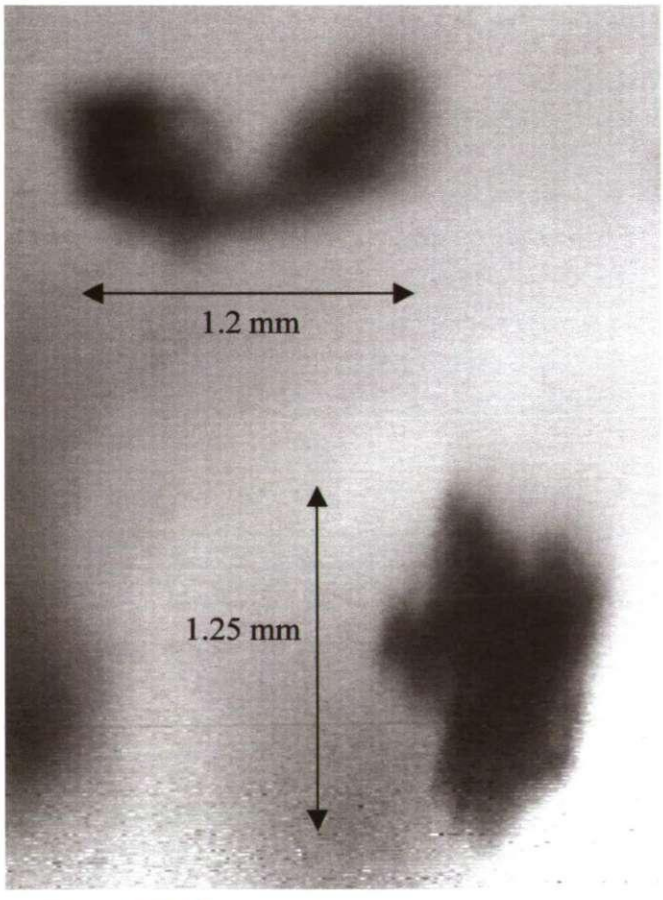

Plate VII-17 A simple stringer composed of two macroflocs interlinked by organic fibres (top) and a more ragged cluster-type macrofloc (bottom; 21-5, frame 769)

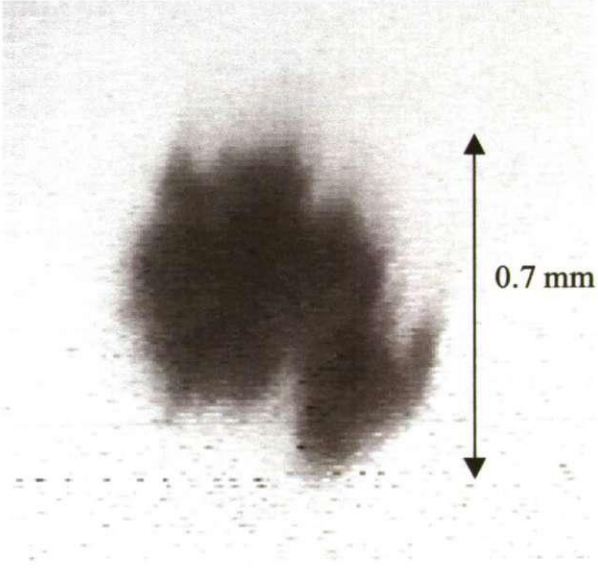

Plate VII-18 A ragged clustered macrofloc (21-2, frame 753)

Flocs sampled from the Tamar estuary on 5th August 1998 during neap tides.

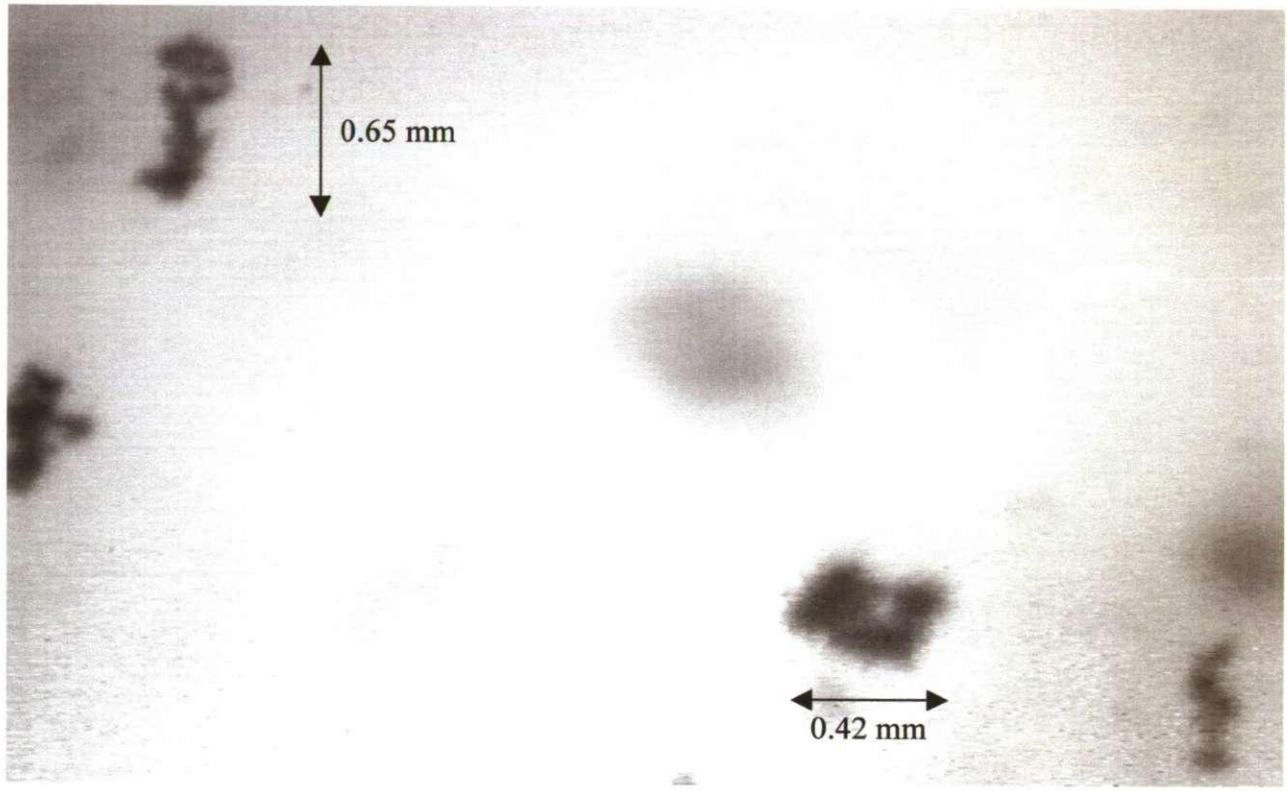

Plate VII-19 A ragged clustered macrofloc (right) and small stringers (left and far right; 05-9, frame 3440)

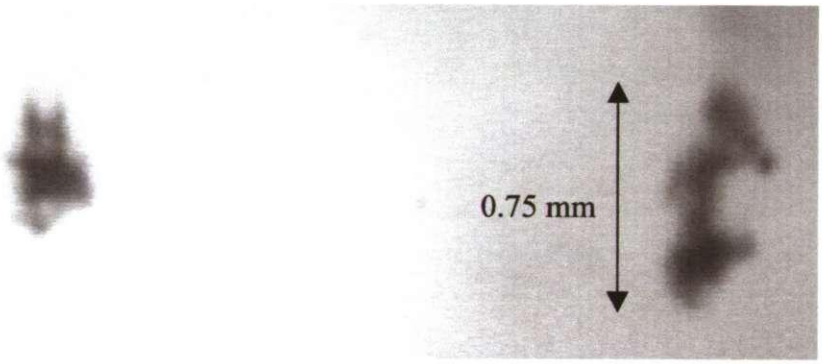

Plate VII-20 A loosely structured ragged macrofloc (left) and a moderately long stringer (right; 05-9, frame 2387)

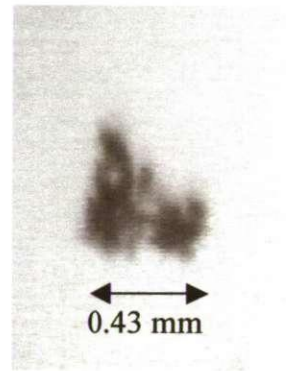

Plate VII-21 A loosely structured macrofloc (05-8, frame 2114)

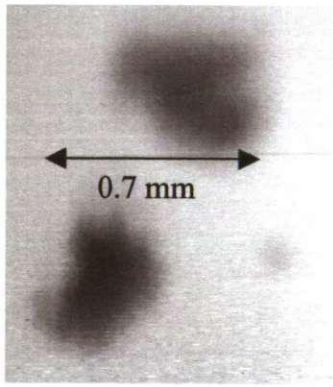

Plate VII-22 Two clustered macroflocs (05-9, frame 1116)

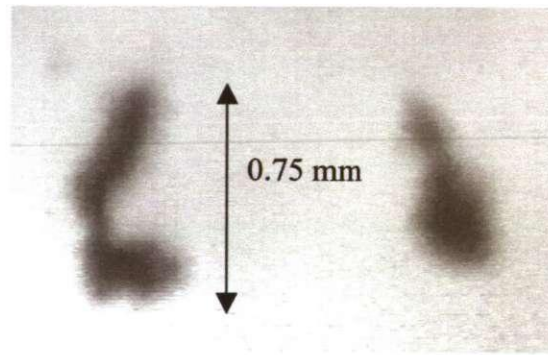

Plate VII-23 A moderately long stringer composed of a single macrofloc with a trailing organic tail (left), and a shorter "comet-shaped" macrofloc (right; 05-9, frame 2032)

Flocs sampled from the Tamar estuary on 5th August 1998 during neap tides.

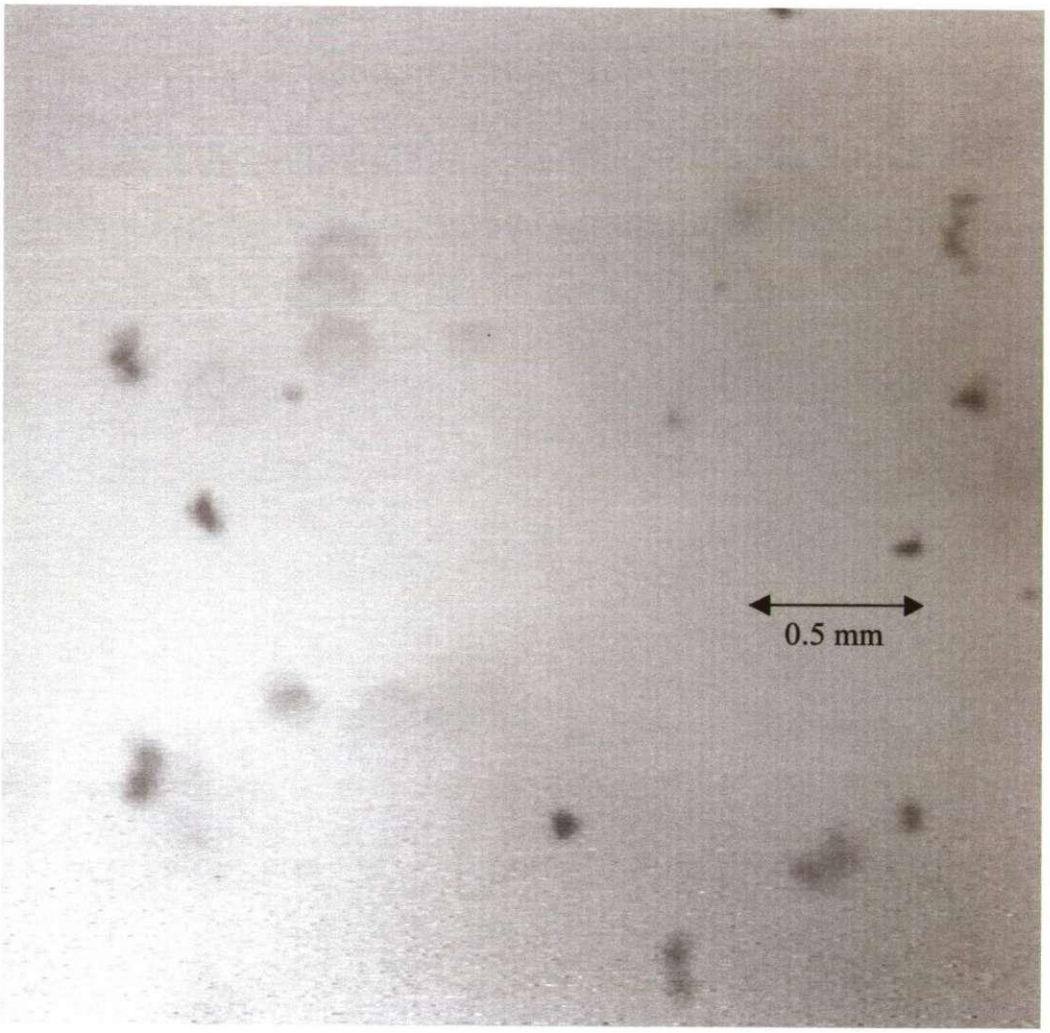

Plate VII-24 A selection of small slow settling microflocs, some of which are probably the result of macrofloc fracturing during a turbulent event which exceeded the original macrofloc structural integrity threshold (05-8, frame 11603)

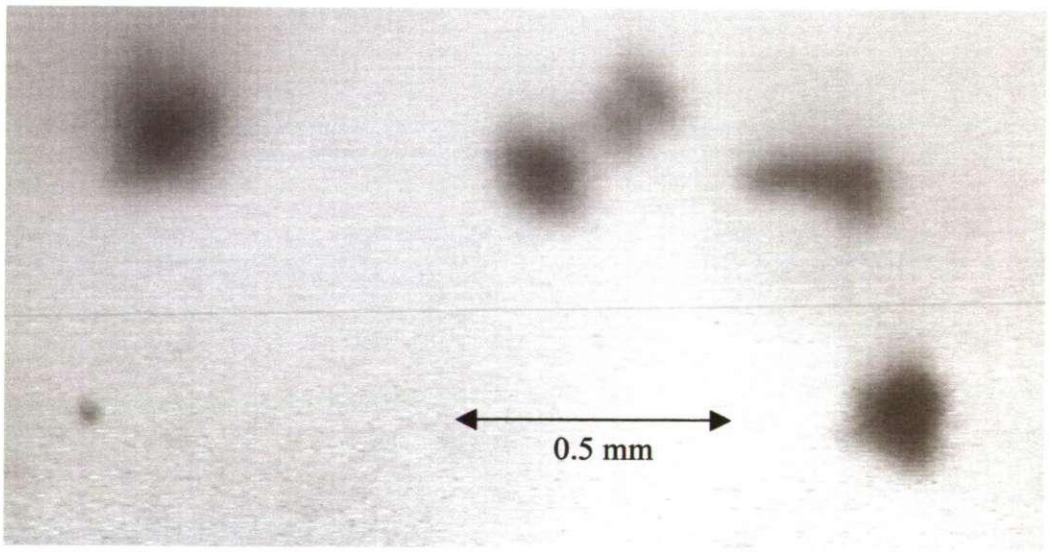

Plate VII-25 A selection of small, slow settling, low density macroflocs (05-9, frame 2323)

Flocs sampled from the Gironde estuary on 23rd June 1999 during neap tides.

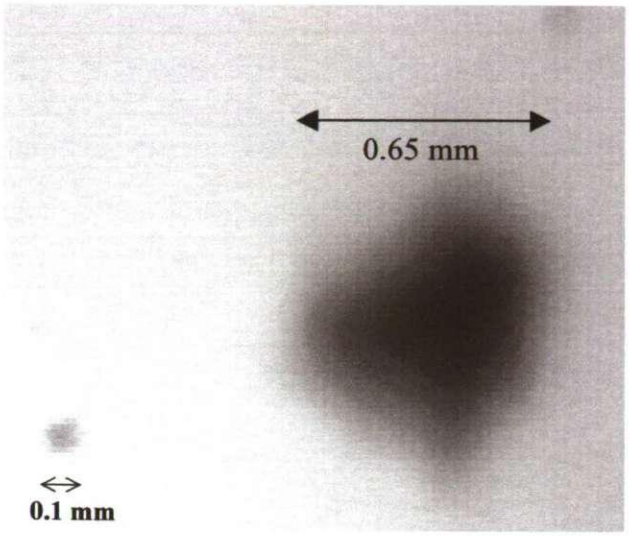

Plate VII-26 A fast settling macrofloc (right) and a small fast settling dense non-cohesive aggregate (left; 23G-4, frame 850)

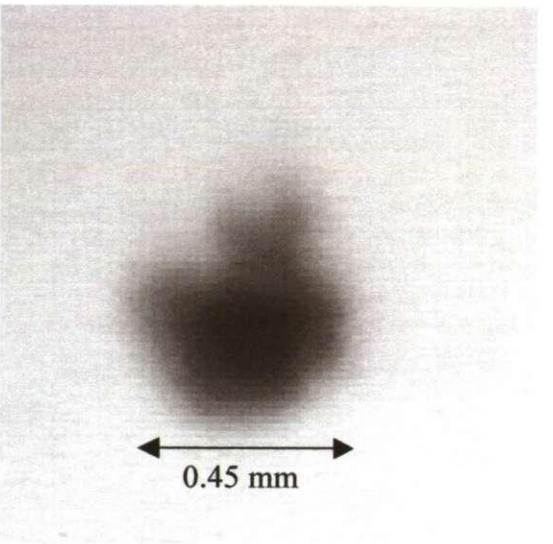

Plate VII-27 A medium sized clustered macrofloc with a short organic tail (23G-10, frame 1323)

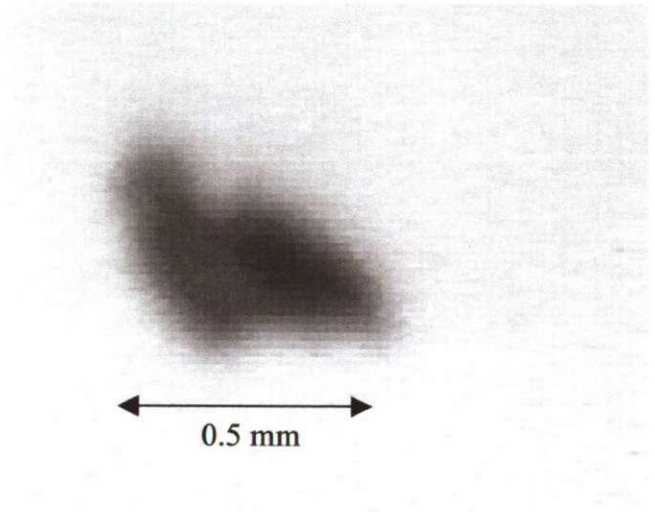

Plate VII-28 An angular shaped macrofloc (23G-9, frame 1880)

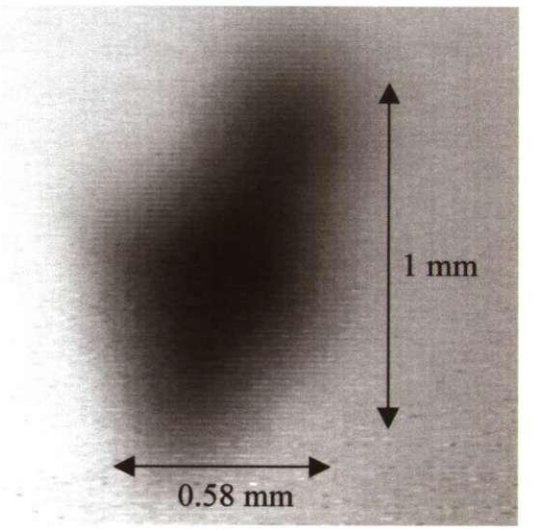

Plate VII-29 A large low density "comet-shaped" macroflocs (23G-7, frame 1977)

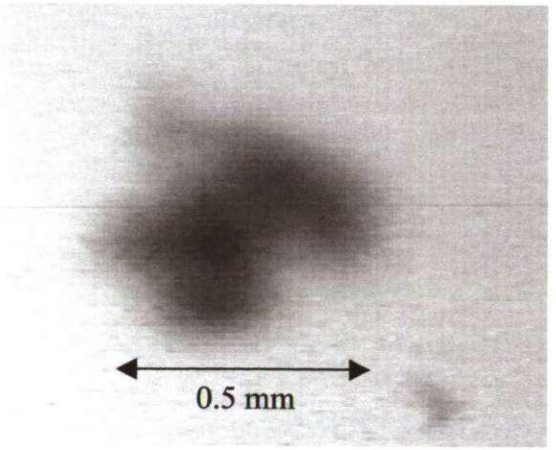

Plate VII-30 A loosely clustered, irregular shaped macrofloc (23G-9, frame 2230)

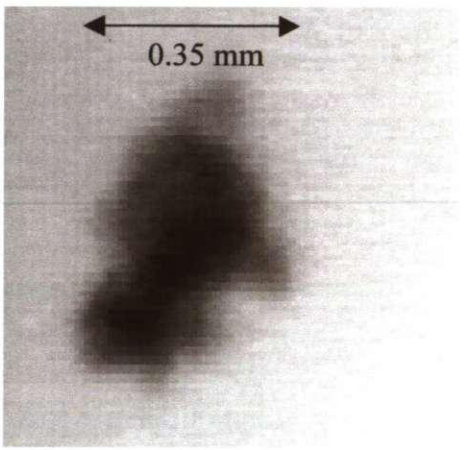

Plate VII-31 A selection of small, slow settling, low density macroflocs (23G-4, frame 2900)

Flocs sampled from the Gironde estuary on 23rd June 1999 during neap tides.

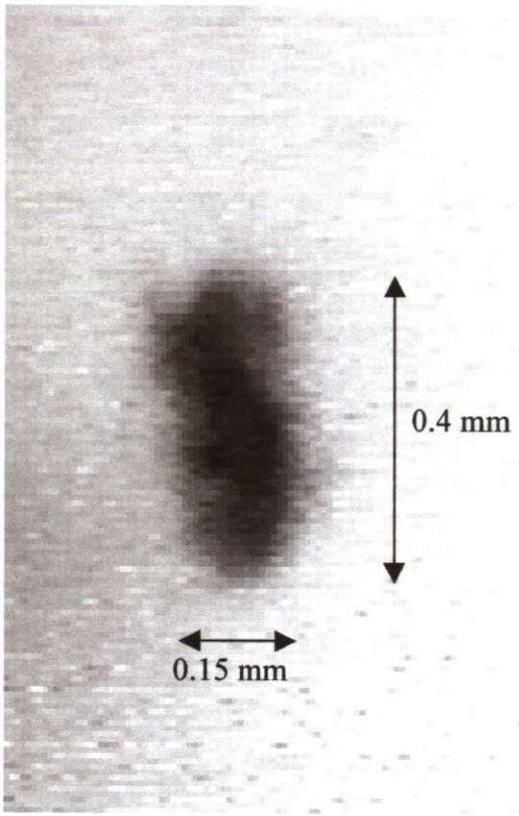

Plate VII-32 A slender, slow settling, low density "comet-shaped" macrofloc (23G-6, frame 3137)

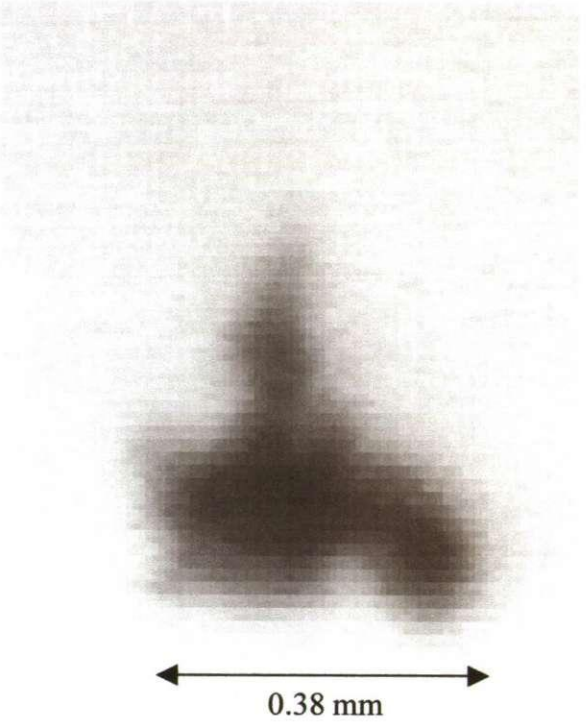

Plate VII-33 An irregular shaped, small / medium sized , slow settling, low density macrofloc (23G-6, frame 3443)